



Spherical Agglomeration for Intensified Pharmaceutical Manufacturing: Evaluating the Influence of Bridging Liquid Miscibility

Jonathan Daniel Tew

A THESIS SUBMITTED FOR THE DEGREE OF DOCTOR OF PHILOSOPHY

DEPARTMENT OF CHEMICAL AND BIOLOGICAL ENGINEERING

THE UNIVERSITY OF SHEFFIELD

DECEMBER 2020

Declaration of Authenticity

This thesis describes work undertaken at the Department of Chemical and Biological Engineering at The University of Sheffield, for the degree of Doctor of Philosophy. The complete works within are all original and of my own doing, except where explicitly stated within the text. This work does not contain any material which has been submitted for any prior degree, diploma or other qualification at any other university.

Jonathan Daniel Tew

Department of Chemical and Biological Engineering

The University of Sheffield

December 2020

Peer Reviewed Publications

Pitt, K., Peña, R., **Tew, J.D.**, Pal, K., Smith, R., Nagy, Z.K., Litster, J.D. Particle design via spherical agglomeration: A critical review of controlling parameters, rate processes and modelling. *Powder Technology*, **2018**, 326, 327-343 <https://doi.org/10.1016/j.powtec.2017.11.052>

Arjmandi-Tash, O., **Tew, J.D.**, Pitt, K., Smith, R., Litster, J.D. A new mathematical model for nucleation of spherical agglomerates by the immersion mechanism. *Chemical Engineering Science X*, **2019**, 115258. <https://doi.org/10.1016/j.ces.2019.115258>

Publications in Preparation

Tew, J.D., Pitt, K., Smith, R., Litster, J.D. True bridging liquid to solid ratio (TBSR): Redefining a critical process parameter in spherical agglomeration.

Conference Proceedings

Tew, J.D., Pitt, K., Smith, R. and Litster, J.D., 2020, November. True Bridging Liquid-Solid Ratio (TBSR): Redefining a Critical Process Parameter in Spherical Agglomeration. In *8th World Congress on Particle Technology*. In *2020 AIChE Annual Meeting*. AIChE.

Tew, J.D., Pitt, K., Ahmed, B., Smith, R. and Litster, J.D., 2020, September. A mechanistic study of wetting and nucleation in spherical agglomeration. In *2019 Continuous Manufacturing and Crystallisation Symposium*. CMAC, University of Strathclyde.

Arjmandi-Tash, O., **Tew, J.D.**, Yusoff, F., Pitt, K., Smith, R.M. and Litster, J.D., 2019. Mechanistic modeling of spherical agglomeration for continuous manufacturing of pharmaceuticals. In *4th International Symposium on Continuous Manufacturing of Pharmaceuticals*.

Arjmandi-Tash, O., **Tew, J.D.**, Yusoff, S.N.M., Pitt, K., Litster, J.D. and Smith, R.M., 2019, November. Spherical Agglomeration Process: Mechanistic Understanding and Mathematical Modelling. In *2019 AIChE Annual Meeting*. AIChE.

Tew, J.D., Arjmandi-Tash, O., Pitt, K., Smith, R. and Litster, J.D., 2018, April. A Mechanistic Approach to Developing Spherical Agglomeration for Process Intensification in Pharmaceutical Manufacturing. In *8th World Congress on Particle Technology*. AIChE.

Acknowledgements

I wish to extend a massive personal thank you to Professor Jim Litster & Dr Rachel Smith. Your support throughout my studies has been invaluable. Whenever I needed something, both your doors have always been open. Your advice has been instrumental from day one, helping me to shape my project, think critically, challenge myself and do something I have thoroughly enjoyed.

Dr Kathryn Pitt, thanks for being so generous with your time. As someone once said, *“It’s all fun and games”*. Thanks for listening to all the rants throughout the years; it has definitely helped me hold on to a very thin thread of sanity. Dr Bilal Ahmed, thank you for encouraging me to pursue a career in academia and get those applications sent in.

I would also like to express my gratitude to the rest of the Particle Technology Group, former and current. Thank you for all the great times we have had on socials, food trips and the academic discussion. A massive thank you for all your help and support during my first year of study. Good luck to all of you.

A thanks is also in order for all the team at University of Strathclyde – Ian and Cameron to name a few, as well as the SPA99 CORE Project Industry team. Your academic input has been fantastic and undoubtedly made me see things from a different perspective.

CBE PGR students, past and present, thanks for all the laughs on Fridays in The Red Deer. We’ve all probably single-handedly kept them in business, but that is a story for another day. To all the folks in the workshop and lab techs in C10 – sorry I have made such a nuisance of myself over the last four years – I will raise a beer (or two, or three...) to you guys very soon.

To my long-suffering family – thank you, thank you, thank you. To my Mum and Gran, I cannot express how grateful I am - thank you for everything. Mat, you will still always be better than me at Crash Bandicoot – I guess that’s something. To you all, thank you for always supporting me, despite often making questionable life choices. I appreciate it all so much. Love to you all.

Abstract

Spherical agglomeration is a size enlargement technique which is highly suited to high value products with problematic morphologies. The addition of a partially immiscible bridging liquid to a suspension allows the formation of dense, spherical agglomerates with superior properties, *i.e.* flowability and compressibility. These products reduce further downstream processing requirements, and thus, the associated energy, time, and cost.

Currently, the mechanistic understanding of the process is limited, and few studies specifically investigate and elucidate these mechanisms to further a wider understanding as a whole. Conversely, the current literature provides a detailed account of the influence of process and formulation parameters on the final agglomerate properties. One such parameter is the bridging liquid-solid ratio, of which an optimal range can be found. Within the range, superior agglomerates are formed. However, these are specific and change for each system under consideration, due to failure to account for bridging liquid miscibility.

To address this, a new parameter is defined – the true bridging liquid-solid ratio (TBSR), which is defined as the volume of the bridging liquid rich phase divided by the volume of solid product. To evaluate miscibility between the bridging liquid and solvent, a ternary phase diagram is required. Here the phase diagram is determined through a novel combined approach using both experimental and computational studies. Analysis of these diagrams and computation allows the volume of the bridging liquid-rich phase to be calculated. This dimensionless parameter allows easy comparison across a variety of systems. The new definition has been partially validated through a rigorous experimental plan. The extent of agglomeration, and agglomerate size distribution is measured for salicylic acid (crystals) in several acetone-water solvent systems with three different bridging liquids at a solids loading of 3%. The results showed much closer alignment between the agglomerate profiles across different systems when TBSR is used to measure the required amount of bridging liquid.

A kinetic study of spherical agglomeration of paracetamol using immersion nucleation was performed. An optimal TBSR range of 0.7 – 0.8 was found. Five distinct operational zones were found: Zone A, insufficient bridging liquid for complete agglomeration; Zone B and C, high quality, well controlled agglomerates were formed; Zone D and E, poorer quality agglomerates were formed and the time to paste was short. These zones were found to be independent of the solid loading used. Experimental results were compared to a previously developed mathematical model, which correctly predicts the experimental trends. The model predicts results which are quantitatively very different in timescale, compared to experimental observations.

Contents

Declaration of Authenticity	ii
Peer Reviewed Publications	iii
Publications in Preparation	iii
Conference Proceedings.....	iii
Acknowledgements	iv
Abstract	v
Contents	vi
Table of Figures	ix
Table of Tables.....	xiv
Nomenclature.....	xv
CHAPTER 1: INTRODUCTION	1
1.1 The Pharmaceutical Industry.....	2
1.2 Background to the Research	2
1.3 Thesis Structure.....	6
CHAPTER 2: LITERATURE REVIEW.....	8
2.1 Introduction.....	9
2.2 Spherical Crystallisation Techniques	10
2.2.1 Ammonia Diffusion	11
2.2.2 Quasi-Emulsion Solvent Diffusion	12
2.2.3 Spherical Agglomeration.....	14
2.2.4 Comparison of Spherical Crystallisation Techniques.....	15
2.3 Current Kinetic & Mechanistic Understanding of Spherical Agglomeration	16
2.3.1 Wetting & Nucleation	17
2.3.2 Growth & Consolidation.....	18
2.3.3 Breakage & Attrition	20
2.3.4 Analogies to Wet Granulation	20
2.4 The Factors Affecting Spherical Agglomeration	22
2.4.1 Solvent Composition of the System	23
2.4.2 The Bridging Liquid	28
2.4.3 Shear Force through Agitation.....	44
2.4.4 Residence Time	46
2.5 Current Modelling in Spherical Agglomeration.....	48
2.5.1 Models of Agglomeration in Suspension Systems.....	48
2.5.2 Models of Simultaneous Crystallisation and Agglomeration Systems	54
2.6 Further Applications of Spherical Crystallisation	55
2.6.1 Co-agglomeration of Crystals and Additives.....	55
2.6.2 Continuous Spherical Crystallisation	57
2.7 Critical Summary	59

2.8	Research Objectives	61
CHAPTER 3:	MATERIALS & METHODS	63
3.1	Introduction.....	64
3.2	Materials.....	65
3.2.1	<i>Characterisation of Materials</i>	<i>66</i>
3.3	Hypothesis of the True Bridging Liquid-Solid Ratio.....	69
3.4	Determination of Ternary Phase Diagrams.....	72
3.4.1	<i>Experimental Approach & Methodology.....</i>	<i>72</i>
3.4.2	<i>Simulation Approach & Methodology.....</i>	<i>74</i>
3.5	TBSR Validation Methodologies	74
3.5.1	<i>Agglomeration Methodology.....</i>	<i>75</i>
3.5.2	<i>Characterisation of Agglomerates</i>	<i>76</i>
3.6	Kinetic Study of Spherical Agglomeration Processes	76
3.6.1	<i>Experimental Methodology.....</i>	<i>76</i>
3.6.2	<i>Imaging Methods.....</i>	<i>77</i>
3.6.3	<i>Process Parameters Study.....</i>	<i>77</i>
3.6.4	<i>Agglomerate Formation Kinetics</i>	<i>78</i>
3.6.5	<i>Percentage Agglomeration</i>	<i>78</i>
3.6.6	<i>Agglomerate Size & Sphericity</i>	<i>78</i>
3.6.7	<i>Agglomerate Density</i>	<i>79</i>
CHAPTER 4:	THE TRUE BRIDGING LIQUID TO SOLID RATIO – THEORY	80
4.1	Introduction.....	81
4.2	Agglomeration Systems.....	82
4.2.1	<i>Development of Theoretical Systems.....</i>	<i>82</i>
4.2.2	<i>Verification of Acceptable Error.....</i>	<i>83</i>
4.3	Results & Discussion.....	84
4.3.1	<i>Ternary Phase Diagrams: Experimental Results</i>	<i>84</i>
4.3.2	<i>Ternary Phase Diagrams: Modelling Results</i>	<i>86</i>
4.3.3	<i>Comparison of BSR and TBSR for All Systems</i>	<i>86</i>
4.4	Conclusions.....	92
CHAPTER 5:	VALIDATION OF THE TRUE BRIDGING LIQUID-SOLID RATIO	93
5.1	Introduction.....	94
5.2	Equipment and Methodology Validation	94
5.3	Experimental Design.....	97
5.4	Results & Discussion.....	100
5.4.1	<i>The TBSR as a Comparison Tool.....</i>	<i>100</i>
5.4.2	<i>Effect of Bridging Liquid on Agglomerate Size Distribution</i>	<i>103</i>
5.4.3	<i>Bulk Solution Compositions.....</i>	<i>107</i>
5.5	Conclusions.....	107
CHAPTER 6:	A KINETIC STUDY OF SPHERICAL AGGLOMERATION PROCESSES	109
6.1	Introduction.....	110
6.2	Results & Discussion.....	111

6.2.1	<i>Influence of True Bridging Liquid-Solid Ratio</i>	112
6.2.2	<i>Influence of Solid Loading</i>	119
6.2.3	<i>Influence of Impeller Speed</i>	122
6.2.4	<i>Agglomerate Structure Development</i>	124
6.2.5	<i>Mathematical Theory</i>	130
6.2.6	<i>Model Parameters & Assumptions</i>	133
6.2.7	<i>Model Prediction: Analysis & Discussion</i>	135
6.2.8	<i>Experimental vs Modelling Observations</i>	138
6.3	Conclusions	139
CHAPTER 7: CONCLUSIONS & FUTURE WORK		141
7.1	Conclusions	142
7.2	Future Work	143
Bibliography		144
	Figure Acknowledgements	152
Appendix A. The TBSR Theory		154
	Titration Data	155
	Aspen Data	165
	TBSR Calculation	181
	An Exemplar TBSR Calculation	181
Appendix B. Validation of the TBSR		186
	Common Properties of Agglomerates	187
Appendix C. Kinetic Studies of Paracetamol		190
	TBSR Influence on Agglomerate Properties	191
	Agglomerate Structure Development	193

Table of Figures

Figure 1.1. A simplified flowsheet for the traditional manufacturing of pharmaceutical products.	4
Figure 1.2. A simplified schematic for the spherical agglomeration process. Adapted from Pitt et al [7].	5
Figure 1.3. A proposed flowsheet for pharmaceutical manufacturing with spherical crystallisation.	6
Figure 2.1. a) Primary particles of salicylic acid prior to addition of a bridging liquid, b) dense, spherical agglomerates of salicylic acid post addition of bridging liquid. Reproduced from Kawashima et al., [10]. Scale bars are 200 μm and 10 mm for a) and b) respectively.	10
Figure 2.2. Mechanism for the ammonia diffusion method of spherical crystallisation. Ammonia-water droplets are indicated by blue circles. Immiscible solvent is represented by red circles. The crystals of interest are shown as grey rectangles. Adapted from Ueda et al., [25].	12
Figure 2.3. Spherical agglomerates produced via the ammonia diffusion method. Note the individual constituent crystals at the agglomerate surface. Reproduced from Ueda et al., [25].	12
Figure 2.4. Mechanism for quasi-emulsion solvent diffusion method of spherical crystallisation. The anti-solvent is indicated by red circles, solvent by blue circles, and crystals by grey rectangles. Adapted from Nocent et al., and Peña & Nagy [31,32].	13
Figure 2.5. Agglomerates as formed through the quasi-emulsion solvent diffusion method. Note the much more porous structure of agglomerates and absence of constituent crystals. Reproduced from Nocent et al., [31].	13
Figure 2.6. Mechanism for the spherical agglomeration method of spherical crystallisation. The bridging liquid is indicated by blue circles and crystals of interest by grey rectangles. Note, the solvent and anti-solvent are not shown in this schematic. Adapted from Mahanty et al., [36].	14
Figure 2.7. The proposed distribution mechanism for spherical agglomeration. Adapted from Subero-Couroyer et al., [42].	17
Figure 2.8. The proposed immersion mechanism for spherical agglomeration. Adapted from Subero-Couroyer et al., [42].	18
Figure 2.9. Four types of liquid-particle interactions structures. Reproduced from Iveson et al., [5].	19
Figure 2.10. The proposed nucleation regime map in wet granulation. Reproduced from Hapgood et al., [5,56].	22
Figure 2.11. A proposed framework for identifying ternary solvent systems. The framework accounts for the influence of Lifshitz-van der Waals and Lewis acid-base parameters. Reproduced from Chen et al., [77].	25
Figure 2.12. An example of a ternary phase diagram for a spherical agglomeration system. Tie-lines are shown as dashed blue lines. The line of miscibility is indicated by a solid blue line. Component X represents the anti-solvent, Component Y the solvent, and Component Z the bridging liquid.	26
Figure 2.13. The influence of feeding rate on the benzoic acid agglomerate size distribution. Reproduced from Thati & Rasmuson, [46].	28
Figure 2.14. Displacement of a non-wetting liquid, or bulk solution, by a wetting liquid, or the bridging liquid, in a thin capillary. Reproduced from Arjmandi-Tash et al., [12].	30
Figure 2.15. The influence of a BSR value below the critical range on the distribution mechanism in spherical agglomeration. Adapted from Petela [87] and Peña & Nagy, [32].	32
Figure 2.16. The influence of a BSR value below the critical range on the immersion mechanism in spherical agglomeration. Adapted from Petela [87] and Peña & Nagy, [32].	32
Figure 2.17. The influence of a BSR value within the critical range on the distribution mechanism in spherical agglomeration. Adapted from Petela [87] and Peña & Nagy, [32].	32
Figure 2.18. The influence of a BSR value within a critical range on the immersion mechanism in spherical agglomeration. Adapted from Petela [87] and Peña & Nagy, [32].	32

Figure 2.19. The influence of a BSR value above the critical range on the distribution mechanism in spherical agglomeration. Adapted from Petela [87] and Peña & Nagy, [32].	33
Figure 2.20. The influence of a BSR value above the critical range on the immersion mechanism in spherical agglomeration. Adapted from Petela [87] and Peña & Nagy, [32].	33
Figure 2.21. The effect of liquid saturation on the mean granule size for different binders. Reproduced from Iveson et al., [5,90].	35
Figure 2.22. Agglomerate size as a function of BSR for different agglomerate systems: ○ CaCO ₃ -kerosene; △ salicylic acid-chloroform; x benzoic acid-toluene; ◇ lobenzarit-hexane; + atorvastatin calcium-dichloromethane [21,45,46,91,92].	35
Figure 2.23. In-situ visualisation of chloroform-salicylic acid initial interactions. Scale bar is the same for all images. Reproduced from Subero-Couroyer et al., [42].	37
Figure 2.24. a) The initial formation of a particle shell around a bridging liquid droplet, b) prior to their movement into the droplet itself. Reproduced from Madec et al., [93].	38
Figure 2.25. (a-d) The evolution of salicylic acid flocs during the injection of chloroform as a bridging liquid. Note the compaction of flocs during this process across an unknown time period. Reproduced from Subero-Couroyer et al., [42].	39
Figure 2.26. The quantification of critical packing volume (ϕ_{cp}) of a unit cell in spherical agglomeration processes. Adapted from Arjmandi-Tash et al., [12].	41
Figure 2.27. A bridging liquid-solid ratio a) below the critical range, b) within the critical range, and c) above the critical range, for the distribution mechanism of spherical agglomeration.	42
Figure 2.28. A bridging liquid-solid ratio a) below the critical range, b) within the critical range, and c) above the critical range, for the immersion mechanism of spherical agglomeration.	42
Figure 2.29. The influence of agitation speed on the size distribution of spherical agglomerates of cefotaxime sodium. Adapted from Zhang et al., [99].	44
Figure 2.30. The relationship between friability of buccillamine agglomerates and the residence time of agglomerates: (○) 30 minutes; (△) 60 minutes; (□) 120 minutes. Here, X represents the pulverised fraction of agglomerates. Reproduced from Morishima et al., [47].	47
Figure 2.31. The relationship between experimental growth curves as a function of a) particle concentration and b) agitation speed during bridging liquid injection. Reproduced from Bemer [49].	49
Figure 2.32. The comparison between experimental and modelling results for a) mean diameter and porosity, and the number particle size distribution at agglomeration times of b) 200 secs, c) 2880 secs and d) 11390 secs. Reproduced from Blandin et al., [50].	53
Figure 3.1. An overview of the methodologies conducted within this research and their order within this thesis.	64
Figure 3.2. The particle size distributions of commercial salicylic acid and prepared, sub 45 µm salicylic acid particles.	66
Figure 3.3. The experimental set-up of the goniometer system used for contact angle measurements.	67
Figure 3.4. The die and press used to form tablets for contact angle analysis.	67
Figure 3.5. The contact angle measurements of chloroform on a salicylic acid tablet, with a) chloroform droplet prior to measurement and b) the next frame showing perfect wetting.	68
Figure 3.6. The contact angle measurements of MIBK on a salicylic acid tablet, with a) MIBK droplet prior to measurement, b) the next frame with a contact angle of 33 degrees and c) the subsequent frame showing perfect wetting.	68
Figure 3.7. The contact angle measurements of <i>n</i> -butyl acetate on a salicylic acid tablet, with a) <i>n</i> -butyl acetate droplet prior to measurement and b) the next frame showing perfect wetting.	69
Figure 3.8. Contact angle of water, approximately 42°, on a micronised paracetamol tablet.	69

Figure 3.9. An example of a ternary phase diagram where X is the anti-solvent, Y is the solvent and Z is the bridging liquid. The cross represents a system of interest, and the circles the immiscible phase compositions. Values represent an exemplar of the inverse lever rule.	71
Figure 3.10. Agglomerator set-up.	75
Figure 3.11. The experimental set-up of the Luminera Infinity 3 camera with 12 x zoom lens and LED light dome diffuser.	77
Figure 4.1 Ternary phase diagrams (% w/w) for water-acetone-bridging liquid systems. Red crosses represent experimental data points; a) heptane; b) toluene; c) chloroform; d) <i>n</i> -butyl acetate; e) MIBK.	85
Figure 4.2. Ternary phase diagrams (mass fraction) of water-acetone-bridging liquid systems featuring experimental data and Aspen prediction overlays; a) heptane UNIFAC prediction; b) toluene UNIQUAC prediction; c) chloroform UNIF-LL prediction; d) <i>n</i> -butyl acetate UNIQUAC prediction; e) MIBK UNIQUAC prediction.	87
Figure 4.3. Agglomerate size for different spherical agglomeration systems: o kerosene/CaCO ₃ [91]; Δ chloroform/salicylic acid [45]; × toluene/benzoic acid [46]; – hexane/lobenzarit disodium [21]; + dichloromethane/atorvastatin calcium [92] as a function of a) BSR (Source: Pitt et al. [7]) and b) TBSR. Here the TBSR values are for illustrative purposes only.	88
Figure 4.4. True bridging liquid volume available to agglomerate solid particles as a function of BSR, for water-acetone-bridging liquid systems a) heptane; b) toluene; c) chloroform; d) MIBK; e)	89
Figure 4.5. Comparison between a solid loading of a) 1 % w/w and b) 5 % w/w for water-acetone-chloroform systems.	91
Figure 4.6. Increasing the bridging liquid volume addition causes the system to move further into the immiscible region, shown here for four exemplar bulk solution conditions.	92
Figure 5.1. Testing of closed reactor experimental set-up for a) evaporation and b) dissolution and precipitation during spherical agglomeration experiments. Conditions replicating those of the validation experimental methodology were used here.	96
Figure 5.2. The identified agglomeration systems for three different bridging liquids with the same initial bulk solution composition (90 % w/w water, 10 % w/w acetone).	99
Figure 5.3. The identified agglomeration systems for three different bridging liquids with the same initial bulk solution composition (95 % w/w water, 5 % w/w acetone).	99
Figure 5.4. The identified agglomeration systems for chloroform with three different bulk solution concentrations.	100
Figure 5.5. The relationship between critical packing bridging liquid volume (ϕ_{cp}) and the predicted minimum TBSR value, as developed by Arjmandi-Tash et al., [12].	101
Figure 5.6. The relationship between the BSR and the percentage of fines observed for the systems investigated, including different bulk solutions, and bridging liquids.	102
Figure 5.7. The relationship between the TBSR and the percentage of fines observed for the systems investigated, including different bulk solutions, and bridging liquids.	102
Figure 5.8. The relationship between the BSR and the agglomerate mean size for different bridging liquids and bulk solutions.	104
Figure 5.9. The relationship between the TBSR and the agglomerate mean size for different bridging liquids and bulk solutions.	104
Figure 5.10. Agglomerate size distribution for salicylic acid-bridging liquid systems, a) chloroform, b) MIBK and c) <i>n</i> -butyl acetate, with an initial bulk solution of 90 % w/w water and 10 % w/w acetone. Error bars represent standard error of a least three repeats.	106
Figure 5.11. Agglomerate size distribution for salicylic acid-chloroform systems with an initial bulk solution of a) 85 % w/w water and 15 % w/w acetone, and b) 95 % w/w water and 5 % w/w acetone. Error bars represent standard error of a least three repeats.	108

Figure 6.1. Agglomerates sampled at a) 20 minutes, b) 40 minutes, c) 60 minutes and d) 80 minutes with an Acid Red IV dyed bridging liquid (TBSR = 0.75; solids loading = 5 % w/w).	111
Figure 6.2. TBSR 0.2 produced agglomerates sampled at a) 60 minutes, b) 120 minutes, c) 180 minutes and d) 240 minutes.	113
Figure 6.3. TBSR 0.5 produced agglomerates sampled at a) 60 minutes, b) 120 minutes, c) 180 minutes and d) 240 minutes.	113
Figure 6.4. Agglomerates at 75 minutes after bridging liquid addition (TBSR = 0.7) with a) and b) isolated from the reactor and c) and d) filtered and dried.	114
Figure 6.5. Agglomerates at 75 minutes after bridging liquid addition (TBSR = 0.8) with a) and b) isolated from the reactor and c) and d) filtered and dried.	115
Figure 6.6. Agglomerates at 56 minutes after bridging liquid addition (TBSR = 1.0) with a) and b) isolated from the reactor and c) and d) filtered and dried.	115
Figure 6.7. Agglomerates at 35 minutes after bridging liquid addition (TBSR = 1.5) with a) and b) isolated from the reactor and c) and d) filtered and dried.	116
Figure 6.8. Agglomerates at 25 minutes after bridging liquid addition (TBSR = 2) with a) and b) isolated from the reactor and c) and d) filtered and dried.	117
Figure 6.9. Agglomerates at 15 minutes after bridging liquid addition (TBSR = 3) with a) and b) isolated from the reactor and c) and d) filtered and dried.	117
Figure 6.10. The influence of the TBSR value on the time required for paste formation in paracetamol-heptane-water spherical agglomeration experiments.	119
Figure 6.11. The influence of the TBSR value on the time required for paste formation in different solid loading conditions.	120
Figure 6.12. The mean size (a) and size distribution (b) of agglomerates as a function of solid loading, at a TBSR of 0.7. The recovery times are 100 mins for 1 % w/w loading, 160 mins for 5 % w/w loading and 320 mins for 9 % w/w loading.	121
Figure 6.13. Agglomerate porosity as a function of solid loading. Error bars represent standard error of 20 measurements.	121
Figure 6.14. The influence of impeller speed on agglomerate size and morphology, at a TBSR of 0.75 with a 5 % solid loading. Conditions at a) 300 rpm, b) 500 rpm and c) 700 rpm.	123
Figure 6.15. The influence of impeller speed on agglomerate size distribution at a TBSR of 0.75 with a 5 % solid loading.	123
Figure 6.16. The influence of impeller speed on agglomerate porosity at a TBSR of 0.75 with a 5 % solid loading.	124
Figure 6.17. Observations of spherical agglomerate nuclei and paracetamol flocs 20 minutes after bridging liquid addition.	124
Figure 6.18. Observations of spherical agglomerates, nuclei and paracetamol flocs formed 40 minutes after bridging liquid addition.	125
Figure 6.19. Observations of spherical agglomerates, and paracetamol flocs formed 60 minutes after bridging liquid addition.	125
Figure 6.20. Observations of spherical agglomerates and fragments formed 80 minutes after bridging liquid addition.	125
Figure 6.21. Observations of spherical agglomerates and fragments formed 100 minutes after bridging liquid addition.	126
Figure 6.22. Observations of spherical agglomerates and fragments formed 120 minutes after bridging liquid addition.	126

Figure 6.23. The influence of residence time on the percentage of initial solid incorporated into agglomerates. A BSR of 0.75, 5 % w/w solid loading, and 500 rpm shear rate was used. Error bars represent standard error of three measurements.	127
Figure 6.24. The influence of residence time on the agglomerate size distribution. A BSR of 0.75, 5 % w/w solid loading, and 500 rpm shear rate was used.	128
Figure 6.25. The influence of residence time on the agglomerate mean size and sphericity. Standard error bars represent standard deviation of two experiments.....	129
Figure 6.26. The influence of residence time on the agglomerate density. A BSR of 0.75, 5 % w/w solid loading and 500 rpm shear rate was used here. and	130
Figure 6.27. Bridging liquid droplet and particle interaction which defines the target efficiency. Reproduced from Arjmandi-Tash et al., [12].....	133
Figure 6.28. The time evolution of solid fraction within the bulk solution for the immersion rate limited regime, with variations in TBSR shown.....	136
Figure 6.29. The time evolution of solid fraction within the bulk solution for the collision rate limited regime, with variations in TBSR shown.....	136
Figure 6.30. The time evolution of solid fraction within the bulk solution for the immersion rate limited regime, with variations in solid loading shown.	137
Figure 6.31. The time evolution of solid fraction within the bulk solution for the collision rate limited regime, with variations in solid loading shown.	138

Table of Tables

Table 2.1. Summary of solvents utilised in different spherical crystallisation techniques. Note the greater flexibility of SA processes.	15
Table 2.2. A summary of rate process studies in both experimental (E) and modelling (M) contexts.	21
Table 2.3. The four suggested groups for spherical crystallisation solvent selection by Chow & Leung [58].	23
Table 2.4. A selection of spherical agglomeration systems within the literature.	24
Table 2.5. A summary of the bridging liquid to solid ratio critical range for a variety of different bridging liquids and primary particles.	34
Table 2.6. Nomenclature for Equation 2.18 through to Equation 2.23 [50].	53
Table 2.7. Summary of the effects of process parameters on spherical agglomeration processes and products.	61
Table 3.1. Standard properties of solvents used at 1 atmosphere and 25 °C [76].	65
Table 3.2. Standard properties of solids used at 1 atmosphere and 20 °C [76].	65
Table 3.3. A review of experimental data for the interfacial tension (dyne cm ⁻¹) of bridging liquids in water. ...	72
Table 3.4. Water titrations into various bridging liquid-acetone solutions for experimental determination of the binodal curves.	73
Table 3.5. Bridging liquid titrations into various water-acetone solutions for experimental determination of the binodal curves.	73
Table 3.6. Geometry of reactor and impeller used within validation experiments.	75
Table 3.7. Geometry of reactor and impeller used within kinetic experiments.	76
Table 4.1. Standard properties of solvents used at 1 atmosphere and 25 °C [76].	82
Table 4.2. Experimental data for the interfacial tension (dyne cm ⁻¹) of bridging liquids in water.	84
Table 5.1. The bridging liquid addition volumes, BSR, TBSR and compositions (% w/w) of the bulk solutions, used in agglomeration validation experiments, prior to solid addition.	98
Table 6.1. Calculated energy dissipations rates.	122
Table 6.2. Summary of parameters and values used for sensitivity analysis of a mechanistic model.	134

Nomenclature

Symbol(s)	Definition	Units
A	Pre-exponential factor (constant)	-
A_p	Proportionality constant	-
C	Concentration	mol m^{-3}
C_i	Volume percentage of binding agent in the agglomerate i	-
D	Diameter	m
def^{max}	Contact surface radius	m
$eff(i, j, t)$	Agglomeration efficiency	-
$F_{adh}(i, j, t)$	Adhesion force	N
F_{bridge}	Force exerted by a liquid bridge between two elementary particles	N
$F_{sep}(i, j, t)$	Shear-induced disruptive force	N
$f(i, j, t)$	Product of the meeting probability	-
G	Gibb's free energy, Growth rate of agglomerates	kJ mol^{-1}
G_S	Surface energy	kJ mol^{-1}
G_V	Volume energy	kJ mol^{-1}
h	Covered distance in time t	kJ mol^{-1}
$i ; j$	The size of a particle, or average of a class of particles	-
J	Nucleation rate	$\text{m}^{-3} \text{s}^{-1}$
k	Boltzmann constant	J K^{-1}
k_{ak}	Agglomeration rate constant of k -type (Brownian, laminar or turbulent)	Dependent on k
$K(i, j, t)$	Agglomeration kernel	-
M	Marchal's relative size function	-
m	Mass	kg
n	Number	-
N	Agitation speed	s^{-1}
$N_i(t); N_j(t)$	Concentration of agglomerating particles, i and j with time	nb m^{-3}
P	Dissipated power per unit mass	W kg^{-1}
r_c	Critical radius	m
R_A	Rate distribution of agglomeration	$\text{m}^{-4} \text{s}^{-1}$
$r_{agg}(l, t)$	Agglomeration rate of particles of rank l at time t	$\text{nb m}^{-3} \text{m}^{-1}$
$S_i ; S_j$	Size of agglomerates, or particle, under consideration	m
S_{inner}	Inner section of the bed	m^2

S_{final}	Final agglomerate size	m
S_R	Supersaturation ratio	-
t	Time	s
T	Temperature	K
u	Collision velocity of particles or droplets	$m\ s^{-2}$
ν	Kinematic Viscosity	$m^2\ s^{-1}$

Greek Letters	Definition	Units
$\alpha(i, j, t)$	Target efficiency of the process	-
$\mathcal{P}(t)$	Mean porosity of the agglomerates	-
ρ_{susp}	Density of suspension	$Kg\ m^{-3}$
ε	Specific stirring power	$W\ kg^{-1}$
ρ	Density	$kg\ m^{-3}$
Δ	Difference	-
ω	Molecular volume	
φ	Porosity	-
σ	Relative supersaturation	-
γ	Surface energy, also referred to as interfacial tension	$J\ m^{-2}$
μ	Viscosity	$N\ s\ m^{-2}$
θ	Wetting angle	-
τ	Tortuosity	-
δ	Weight coefficient of solid particles	-
δ_l	Weight coefficient of liquid particles	-
λ_c	Taylor microscale	-
$\beta_{i,j,t}$	Agglomeration constant of k-type, between particles of classes j and i	$m\ s^{-1}$
ψ	Number density function	$nb\ m^{-1}\ m^{-3}$
Ψ	Sphericity	-

Abbreviations	Definition	Units
<i>AD</i>	<i>Ammonia diffusion</i>	-
<i>AgNu</i>	<i>Agglomerate nucleation number</i>	-
<i>BSR</i>	<i>Bridging liquid-solid ratio</i>	-
<i>MSMPR</i>	<i>Mixed-suspension mixed-product removal</i>	-
<i>PBM</i>	<i>Population balance modelling</i>	-
<i>QESD</i>	<i>Quasi-emulsion solvent diffusion</i>	-
<i>SA</i>	<i>Spherical agglomeration</i>	-
<i>TBSR</i>	<i>True bridging liquid-solid ratio</i>	-

CHAPTER 1:

INTRODUCTION

1.1 The Pharmaceutical Industry

The global markets for prescription and over-the-counter medications in 2017 are valued at around \$1tn and \$140bn (USD) respectively [1]. However, despite improvements in technology in recent years, the number of new drugs reaching the market is steadily declining. This is mainly due to more rigorous and stringent requirements, designed by regulatory bodies to enhance patient safety [2]. A direct consequence of this is that batch-to-batch variability must be minimised to ensure consistent performance and quality of the product. These requirements have further implications on the production of such products, as they limit the design space and require processes to operate within a narrow operating window. This often means production processes become complex, energy-intensive and have a reduced through-put which increases the time to market.

To negate these issues, a switch from batch to continuous processes could be highly beneficial [3]. Continuously operated processes have an increased throughput, allow reductions in production equipment size, reduce the footprint of facilities, and almost guarantee a consistent product through steady-state operation. Whilst the starting capital for such facilities is reduced, the operating capital is increased as operations run continuously. However, this is negated by the decrease in the time to market as a continuous stream of final product is manufactured and packaged.

Whilst other industries, predominantly those dealing with natural raw materials, have successfully transitioned to continuous manufacturing, the pharmaceutical industry is only part way there. There are several problematic processes in production which have not been successfully adapted to be operated continuously [3].

There is a key requirement for processes to have predictable performance, as being able to operate within the design space is a key requirement of regulatory bodies. The modelling of processes is vital as it allows engineers to be able to adapt to different situations, have a better understanding of the process, and identify issues as they arise.

1.2 Background to the Research

Crystallisation is a widely used process within the pharmaceutical industry. It is primarily used for the isolation and/or purification of target molecules. Crystallisation is often one of the initial

downstream operations used to separate target particles from solution. At this crucial stage in the manufacturing process, the properties of crystals directly influence the amount of further processing required [4]. Additionally, the target properties should be strictly controlled to ensure predictable shelf life and *in vivo* performance. Beneficially tailoring such properties here, prior to further downstream processing, can create redundancy in the manufacturing process and thus rapidly intensify the process.

Control of the wide range of these properties is paramount to ensuring pharmaceutical production does not encounter issues. The crystal size, size distribution and crystal morphology are all key properties. For oral solid dosages, particles within a specified size range may be required to achieve the desired performance or regulatory approval. In this instance, granulation may be used to increase the crystal size prior to tableting [5]. Problems can arise however, especially if the binder formulation is incorrect: granules become excessive in size. In these instances, milling is required to reduce granule size and recycle the product. These unit operations, as well as drying, are energy and cost intensive. As granulation and milling are usually used in tandem, they also increase the time to market. A traditional process such as this is presented in a simplified format in [Figure 1.1](#).

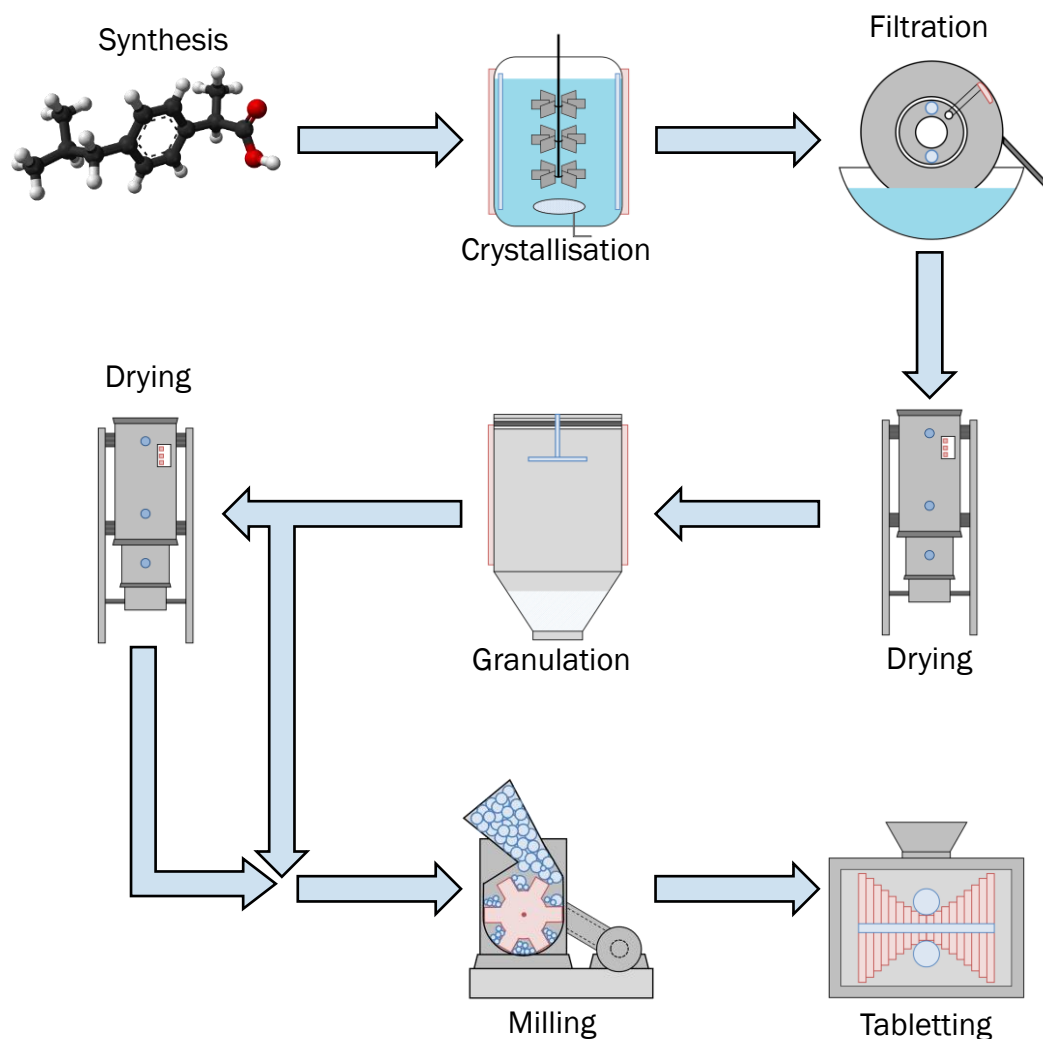


Figure 1.1. A simplified flowsheet for the traditional manufacturing of pharmaceutical products.

Spherical agglomeration provides a unique opportunity to improve and tailor these properties through the precipitation and agglomeration of initial crystals. These steps can be achieved simultaneously, or in sequence [6]. The method is reliant upon the relative solubilities of different solvents in each other, and the interactions between these solvents and the target molecule. Generally, an anti-solvent crystallisation causes uniform crystals of the drug to form. A third solvent is then used to agglomerate the crystalline particles together, as shown in [Figure 1.2](#).

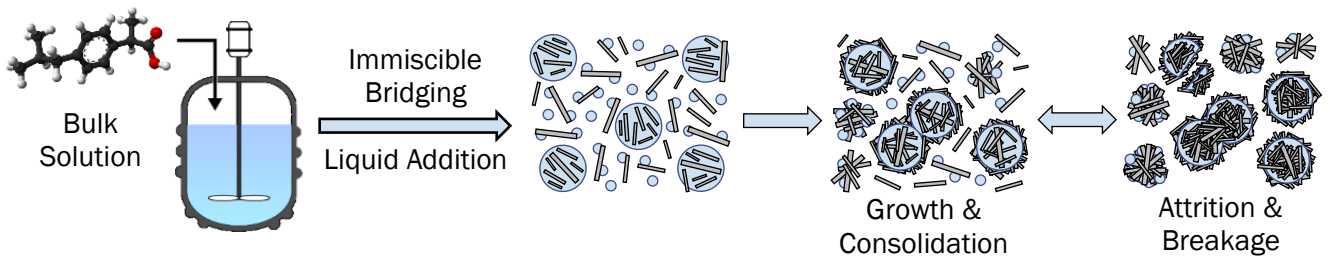


Figure 1.2. A simplified schematic for the spherical agglomeration process. Adapted from Pitt et al [7].

There are three major mechanisms, all of which are analogous to wet granulation: wetting and nucleation; growth and consolidation; breakage and attrition. The degree of agglomeration can be directly controlled, allowing tailoring of the size and porosity of agglomerates, both of which are important for the required bioavailability of the drug product [8]. These properties in turn infer the tableability of the particles, with the potential for agglomerates to be directly compressed into a tablet form [9]. Narrow size distributions can be achieved immediately or through direct sieving, which removes the need for product recycling. In addition, the sphericity of agglomerates tends to be high, which vastly improves the handling of crystal particles, especially those that are acicular in nature [10]. Thus, spherical agglomeration has the potential to create redundancy in the manufacturing of oral solid dosages, as detailed in Figure 1.3.

Generally, the key focus of research has been geared towards improving a wide range of particle properties through modification of experimental procedures and parameters [11]. Causal relationships between these have been identified for a wide range of crystalline particles. However, there is a lack of literature which explores the mechanisms in detail, especially those which directly underpin the process itself. The few models which do exist are often based around the theory of granulation and its mechanisms [12]. Others are reliant on coalescence kernels and/or fitting parameters. Critically, many models fail to incorporate terms for all the mechanisms within the process itself. As such, none of these models can be relied upon for the accurate and robust prediction of process performance.

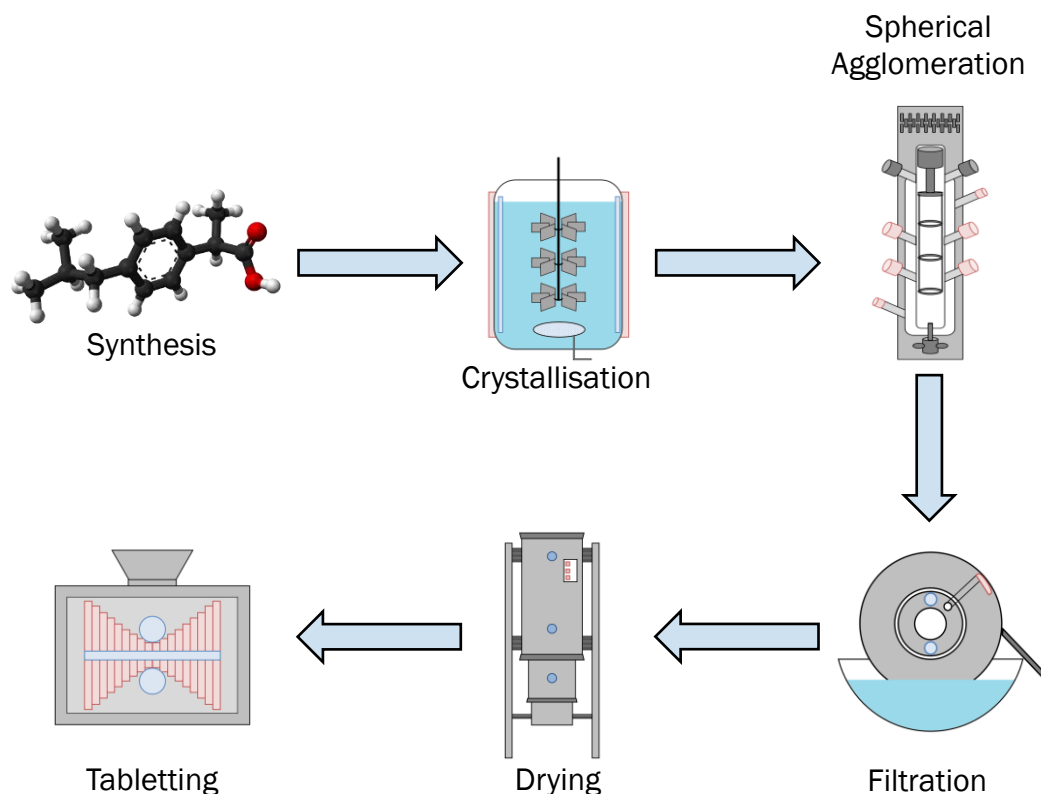


Figure 1.3. A proposed flowsheet for pharmaceutical manufacturing with spherical crystallisation.

1.3 Thesis Structure

Chapter 2 of this thesis presents a review of existing literature within spherical agglomeration. There are two specific areas of the literature which are given a stronger emphasis: the current mechanistic understanding of the process and the influence of the bridging liquid in spherical agglomeration processes. Within this chapter, the current gaps within the broader existing knowledge are also presented. The thesis objectives are listed at the end of the chapter.

Chapter 3 provides a detailed account of the materials used within the experimental work of this thesis. The methodologies used to perform experiments and characterise the outputs are also provided. Sections are also provided to detail the simulation and theoretical works presented.

Chapter 4 presents the theory behind a new definition, the true bridging liquid-solid ratio. This includes development of the theory from both an experimental and simulation approach. A variety of bridging liquids are investigated to highlight the influence of solvent miscibility in spherical agglomeration processes.

Chapter 5 presents the experimental validation of the true bridging-liquid to solid ratio. This includes the selection of several systems of interest to investigate whether the definition can be used over multiple bridging liquids and bulk solution compositions. Salicylic acid is used as the compound of interest.

Chapter 6 details the results from a novel study into the immersion nucleation wetting mechanism using paracetamol. Kinetic studies were performed to further elucidate the mechanisms of agglomerate growth. These results are framed in the context of mathematical studies, as a means of an initial validation step.

Finally, recommendations for future work are presented alongside the overall conclusions of this work.

CHAPTER 2: LITERATURE

REVIEW

2.1 Introduction

Crystallisation is a common processing method which, is utilised in a variety of different industries, including pharmaceutical, bulk chemicals and food processing. The process can be used for both the synthesis and purification of products. The crystallisation operation is usually the first instance in which the product is initially separated from a solid-liquid mixture. This provides engineers with the opportunity to produce crystals with desired attributes such as size and shape [13].

Crystallisation can be used to improve crystal properties, ensuring stable polymorphs, controlling crystal size and morphology *etc.* The size distribution of the crystals is also important. These properties directly relate to the functional properties of the product, including the flowability and compressibility, reactivity, and dissolution profile. These are all particularly important, especially within the pharmaceutical industry, as they dictate product performance. If these functional properties are not as desired, it may be extremely difficult to further process the product. This leads to product recycling or waste. Thus, improving product properties at this stage would include the vast reduction of downstream processing, which reduces operating expenditures, equipment costs and the time to market. Thus, exploring alternative techniques may be highly beneficial for the industry as a whole.

Spherical crystallisation is a group of such techniques, which provides the opportunity to beneficially tailor the key properties of crystal products, prior to further downstream processing. These techniques use binders, or bridging liquids, to agglomerate particles either during or after their precipitation. There are three main techniques which are discussed in more detail in [Section 2.2](#): ammonia diffusion; quasi-emulsion solvent diffusion; spherical agglomeration. All the techniques involve the agglomeration of particles to form dense, spherical agglomerates, through the use of a solvent known as a bridging liquid. Spherical crystallisation techniques have already been successfully applied to some of these industries, especially those handling raw and/or bulk materials. Within the literature, the agglomeration of calcium carbonate, graphite, coal, heavy metals and sand has been reported previously [14–18]. Additionally, spherical crystallisation has also been used successfully in the food processing and biochemical industries [19,20]. Thus, spherical crystallisation has applications in other industries which use granulation, including the bulk chemicals and detergents industries [4].

Within the pharmaceutical context especially, there has been more intensive research in the use of spherical crystallisation, and more specifically spherical agglomeration, despite a lack of industrial adoption. Spherical agglomeration processes have been investigated as a means of improving the properties of a variety of drugs, including lobenzarit disodium, mebendazole and

aceclofenac, amongst others [21–23]. The process has also been used for biopharmaceuticals, including bovine serum albumin [20]. The first paper exploring the spherical agglomeration of pharmaceuticals was in 1982 [10]. There, the authors demonstrated the full capability of the method, turning problematic needle-like salicylic acid crystals into dense, distinct, spherical agglomerates with improved mechanical properties (see Figure 2.1) [10]. The precipitated crystals alone would be unsuitable to be used in the formation of tablets, due to the brittle nature of their morphology. Thus, agglomerating the crystals into spherical, dense agglomerates, which have high flowability, vastly simplifies the downstream processing of the product.

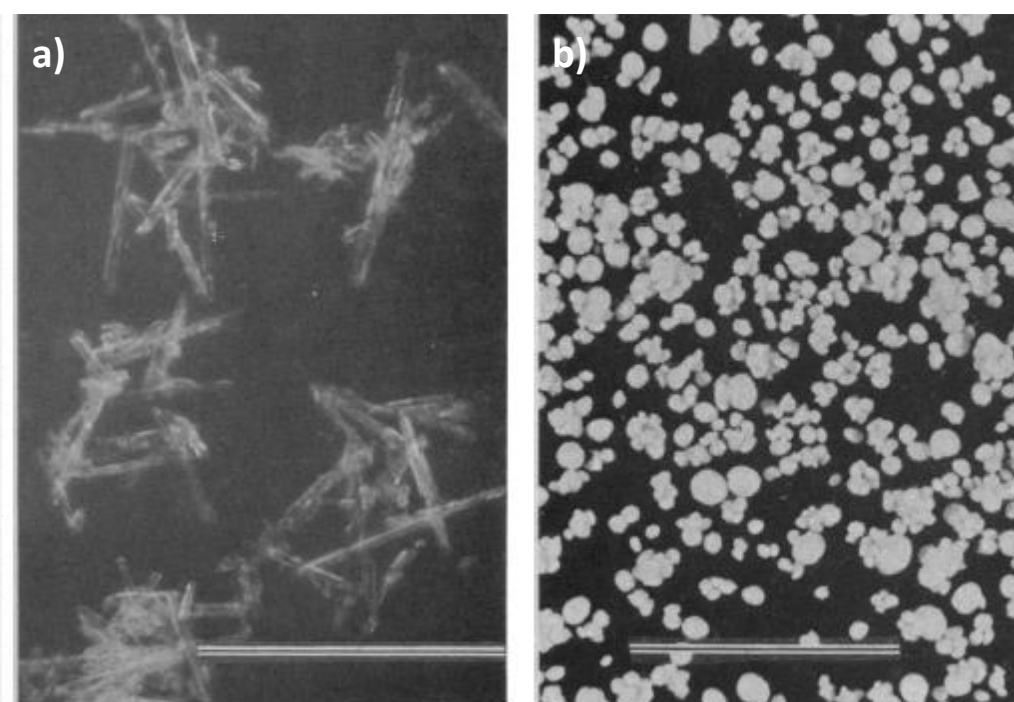


Figure 2.1. a) Primary particles of salicylic acid prior to addition of a bridging liquid, b) dense, spherical agglomerates of salicylic acid post addition of bridging liquid. Reproduced from Kawashima et al., [10]. Scale bars are 200 μm and 10 mm for a) and b) respectively.

2.2 Spherical Crystallisation Techniques

There are three common methods through which spherical crystallisation can be achieved: ammonia diffusion; quasi-emulsion solvent diffusion; spherical agglomeration. These are discussed individually in the following sub-sections. All the methods rely on the relative solubilities of the solid of interest in different solvents. The bridging liquid is a key solvent, which the solid of interest is partially soluble in. Upon drying of agglomerates, liquid bridges solidify between drug molecules, increasing the strength of agglomerates. The process of spherical crystallisation is directly dictated by numerous factors. Several of these are directly related to the solutions from which crystal particles are

precipitated. Thermodynamic mechanisms play an important role, including the solubility of the drug in different solvents, the interfacial tension level at the solid-liquid interface, and the temperature of the system [11]. These properties directly affect the kinetics of such systems, including the level of supersaturation and the metastable zone width of crystallisation. If agglomeration occurs post-crystallisation, these kinetic properties directly dictate the formation of agglomerates. The influence of molecular interactions, including hydrogen bonds and non-covalent bonding, should also be considered. Thus, it is imperative that suitable solvents are identified and utilised based on these properties.

2.2.1 Ammonia Diffusion

The ammonia diffusion (AD) method consists of an ammonia solution which must be able to dissolve the crystal of interest. In this method, the initial solvent is also the bridging liquid [24]. An anti-solvent is also used in this method, which must have high miscibility with the aqueous ammonia solution [11]. An additional solvent is required which is water-immiscible *i.e.* dichloromethane [25]. When the solutions are added together, the anti-solvent droplets become enveloped within the ammonia solution droplets. As a result, the drug is effectively forced out of the droplet and precipitates [25]. A second mechanism is also apparent in which droplets of ammonia are liberated by the immiscible solvent. This process is important as reducing the ammonia concentration around the crystals of interest reduces the amount of bridging liquid available, thus directly affecting the level of agglomeration [26]. Ammonia diffusion, unlike the other two common methods, can be used to agglomerate amphoteric solutes [26]. The method was first used in 1990 for the agglomeration of the drug enoxacin [25].

A schematic of the process is presented in [Figure 2.2](#). Ammonia-water droplets (blue circles) contain the dissolved crystal of interest (grey rectangles). Immiscible solvent droplets (red circles) diffuse into the ammonia droplets causing the precipitation of the crystals of interest in and around the droplet (see [Figure 2.2a](#)). Ammonia is effectively expelled from the droplets, aiding the formation of liquid bridges (see [Figure 2.2b](#)). Over-time, further compaction of agglomerate nuclei allows dense agglomerates to form (see [Figure 2.2c](#)).

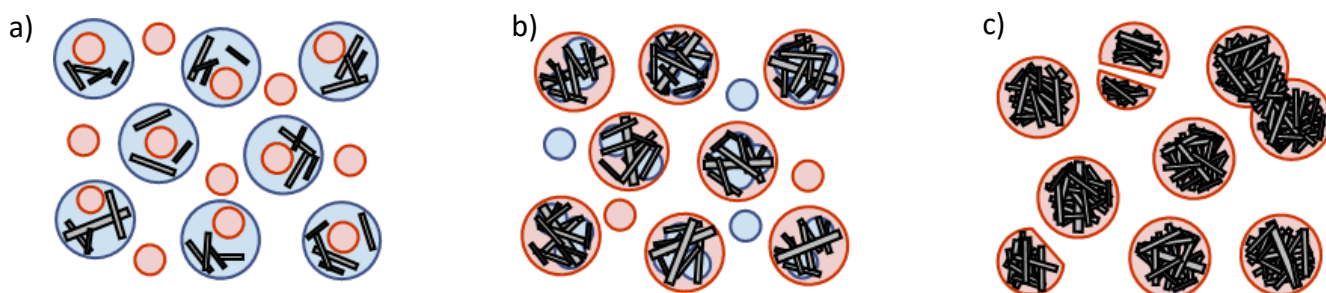


Figure 2.2. Mechanism for the ammonia diffusion method of spherical crystallisation. Ammonia-water droplets are indicated by blue circles. Immiscible solvent is represented by red circles. The crystals of interest are shown as grey rectangles. Adapted from Ueda et al., [25].

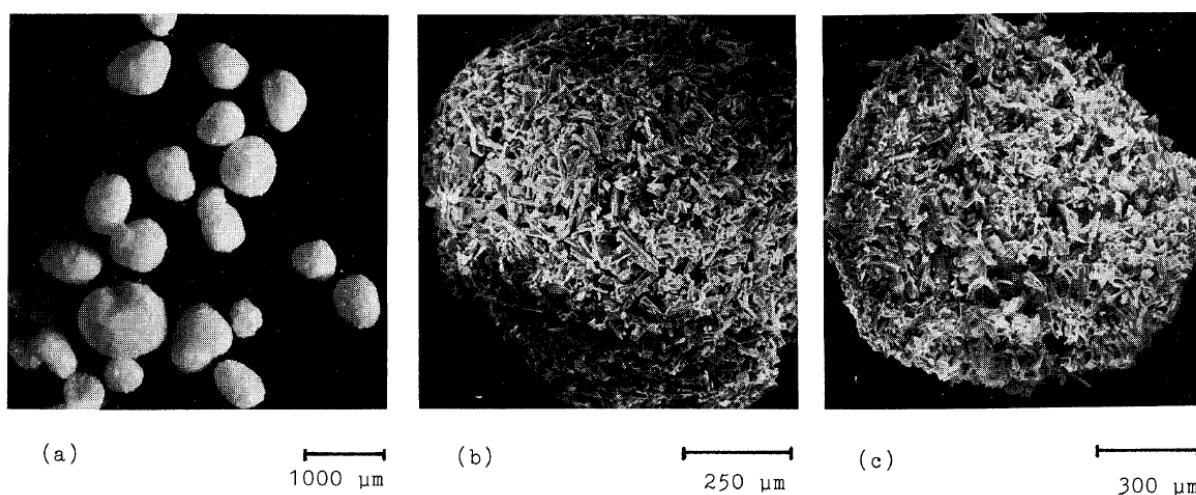


Figure 2.3. Spherical agglomerates produced via the ammonia diffusion method. Note the individual constituent crystals at the agglomerate surface. Reproduced from Ueda et al., [25].

2.2.2 Quasi-Emulsion Solvent Diffusion

Quasi-emulsion solvent diffusion (QESD) was first documented in 1989 [27]. The method also requires the drug of interest to be dissolved in a solvent, this solution is then added to the anti-solvent. Critically, the interactions between the dissolved crystal and the solvent it is dissolved in must be stronger than those between that solvent and the anti-solvent [28]. This principle accounts for the formation of quasi-emulsion droplets. Over time, the solvent from the emulsion transfers into the bulk solution of the anti-solvent. This, in turn, allows the anti-solvent to diffuse into the droplets [29]. As the dissolved crystals are insoluble in this solution, the anti-solvent reduces the solubility of the crystals inside the droplet, eventually causing precipitation inside the droplets. The crystals are then agglomerated within the droplets by the original solvent, which also acts as the bridging liquid in this instance.

A schematic of the process is presented in Figure 2.4. The anti-solvent (red circles) and solvent (blue circles) are added together (see Figure 2.4a). The dissolving solvent contains the dissolved drug of interest. The anti-solvent diffuses into the droplets of the other solvent, effectively a solvent exchange mechanism. As this occurs, the drug solubility is reduced which causes initial precipitation and crystallisation (see Figure 2.4b). The remaining dissolving solvent acts as a bridging liquid causing crystalline bridges to form between agglomerates (see Figure 2.4c). It has been reported within the literature the difficulty in ensuring the system remains emulsified to allow the diffusion of the two solvents [30].

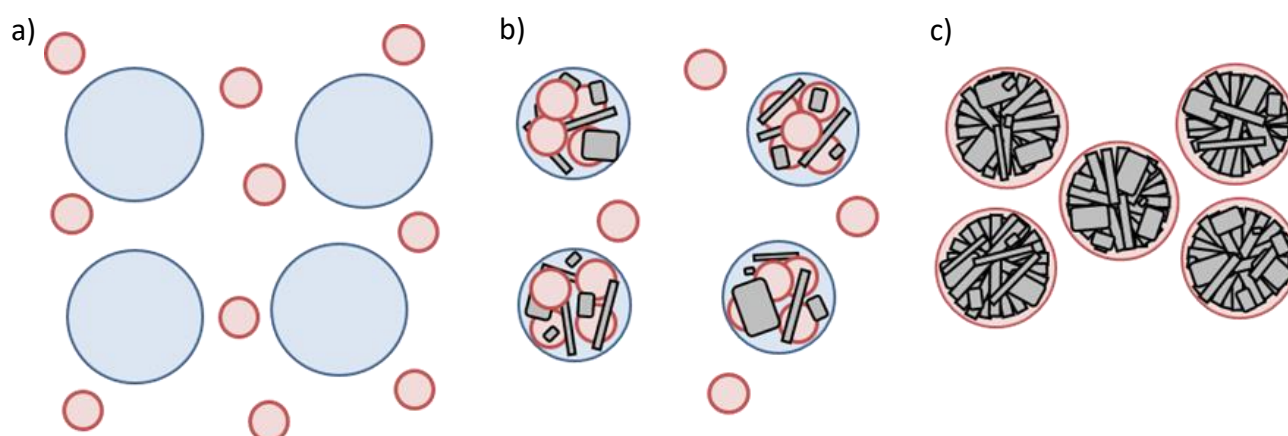
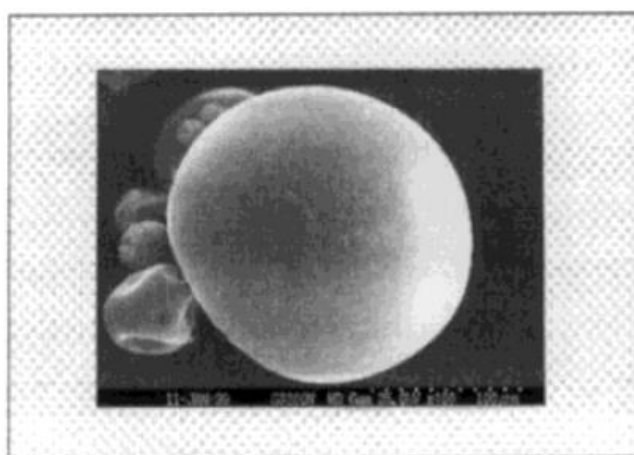
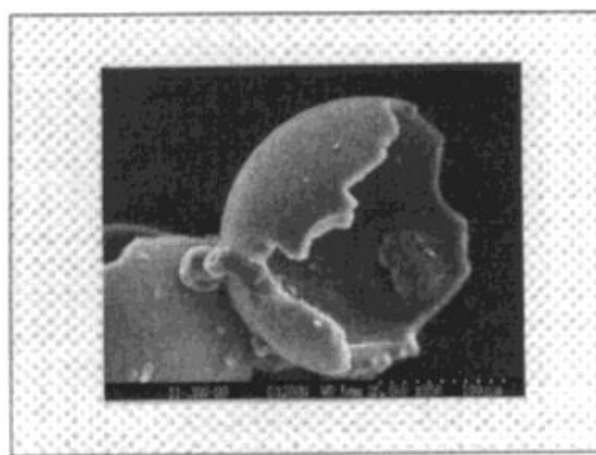


Figure 2.4. Mechanism for quasi-emulsion solvent diffusion method of spherical crystallisation. The anti-solvent is indicated by red circles, solvent by blue circles, and crystals by grey rectangles. Adapted from Nocent et al., and Peña & Nagy [31,32].



00503 Zone A grandissement 400



Zone C grandissement 350

Figure 2.5. Agglomerates as formed through the quasi-emulsion solvent diffusion method. Note the much more porous structure of agglomerates and absence of constituent crystals. Reproduced from Nocent et al., [31].

2.2.3 Spherical Agglomeration

Spherical agglomeration was first documented in the 1960s [33]. This technique also involves the crystal of interest being dissolved in a solvent and this solution added to the anti-solvent. The solvent and anti-solvent must be miscible with each other to allow the subsequent precipitation and crystallisation of the solute crystals. However, the addition of the partially immiscible bridging liquid makes such systems ternary, as opposed to the binary nature of AD and QESD. The bridging liquid must have a high affinity for the solute, as it is directly responsible for the agglomeration of the precipitated solid [11]. The strength of liquid bridges formed by the bridging liquid has been found to be *'proportional to the interfacial tension between the bridging liquid and the medium'* [34]. These bridges, when wet, effectively hold the agglomerate together through both interfacial tension and capillary forces [35]. It is worth noting that much of the research in spherical crystallisation has specifically focussed on this method; these studies are evaluated in [Section 2.4](#).

A schematic of the process is presented in [Figure 2.6](#). The schematic shows crystals and bridging liquid droplets only. In this example, crystals with varied sizes and aspect ratios are used. It is possible for all crystals to have the same morphology, and/or a comparable size, and spherical agglomeration be successful. Initially, the solvent containing dissolved crystals and the anti-solvent are generally, added together. Upon mixing, the precipitation of crystals occurs. Three distinct rate processes then follow. The addition of bridging liquid allows a dispersed phase to form. These droplets wet the particles of interest: wetting and nucleation (see [Figure 2.6a](#)). These nuclei densify and grow and incorporate other wetted particles, to form spherical agglomerates via drop-drop and drop-particle collisions: growth and consolidation. (see [Figure 2.6b](#)). At longer residence times, particles can be sheared from the surface of agglomerates and agglomerates may fracture: attrition and breakage (see [Figure 2.6c](#)). These rate processes are discussed in more detail in [Section 2.3](#).



Figure 2.6. Mechanism for the spherical agglomeration method of spherical crystallisation. The bridging liquid is indicated by blue circles and crystals of interest by grey rectangles. Note, the solvent and anti-solvent are not shown in this schematic. Adapted from Mahanty et al., [36].

2.2.4 Comparison of Spherical Crystallisation Techniques

The three separate methods of spherical crystallisation discussed share some similarities, including the required knowledge of the properties of the solvents used during agglomeration, as well as the influence of operational parameters on the end-product (*e.g.* agitation speed, residence time, solids concentration). Table 2.1 displays a summary of the solvents used in different spherical crystallisation techniques.

Quasi-emulsion solvent diffusion (QESD) and spherical agglomeration (SA) techniques are the two techniques which have been investigated in the literature the most, due to the much higher likelihood of agglomeration success (compared to ammonia diffusion). Whilst the former of these is generally considered as a favoured technique, due to the simpler process operation, difficulties have been reported within the literature. A major issue is ensuring that the system itself remains as an emulsion, as if this does not occur, the efficiency of solvent exchange is drastically reduced [30]. Several authors have reported that this issue can be negated through the use of an emulsifier [31,37]. Spherical agglomeration is sometimes favoured due to the potential for simultaneous crystallisation and agglomeration [38]. In this sense, the technique is more flexible, and allows the end-product properties to be controlled to a greater degree. It is worth noting however, the difficulties in the initial establishment of the solvent system. Considerations must also be given for the potential of residual bridging liquid to remain in the agglomerates post-drying. A summary of solvents used in spherical crystallisation techniques is presented within Table 2.1.

Table 2.1. Summary of solvents utilised in different spherical crystallisation techniques. Note the greater flexibility of SA processes.

Technique	Solvent	Anti-solvent	Bridging Liquid
AD	Ammonia-water	Acetone	-
QESD	Water	Oil <i>e.g.</i> cyclohexane	-
SA	Organic Solvent <i>e.g.</i> ethanol	Water	Immiscible <i>e.g.</i> 1-pentanol

Whilst there is a lack of studies which have explicitly compared spherical crystallisation methods for the same crystal loaded system, some do exist. These studies tend to identify changes in the end-product between different spherical crystallisation techniques. Sano et al., investigated the

differences in the morphological and structural properties [37]. In the tolbutamide agglomerates formed by QESD, with a fatty acid ester emulsifier, the agglomerates were noted to be extremely dense which correlated with high mechanical strength. The authors also noted the highly spherical shape of agglomerates, resulting in excellent flowability. Whilst the agglomerates made via SA were not as dense, and therefore weaker, their structure was found to be more porous with a high specific surface area of constituent crystals. As a result, these agglomerates had superior dissolution properties.

To explain this phenomenon, the authors proposed that slightly different mechanisms of QESD and SA were responsible [37,39]. In QESD, quasi-emulsion droplets slowly become agglomerate nuclei through crystallisation. This is thought to be the reason why agglomerates formed by this method tend to be very dense and spherical in nature, with a smooth surface. In SA, agglomerates are formed over time through compaction and coalescence. As a result, the end-product usually has a lower density and can be covered at the surface by constituent crystal particles. These differences have also been noted by another study, where agglomerates produced by QESD were found to be much harder due to a higher level of plastic deformation [40].

Most studies recognise that each spherical crystallisation technique has both advantages and disadvantages. These are often most apparent in the end-product properties, which further highlights the need for well-established performance criteria of solid dosage formats. It may be beneficial for formulators to identify the most critical of these, and thus find the product property which is most significant. However, spherical agglomeration is the most well rounded of the techniques. Whilst the operational space for the desired agglomerate properties is narrow, overall a wider range of systems can be investigated, meaning the technique is more broadly applicable to different particles. For this involving crystallisation, it is possible to directly control crystal properties, and thus, the end agglomerate properties yielded.

2.3 Current Kinetic & Mechanistic Understanding of Spherical Agglomeration

Much of the spherical agglomeration literature is devoted to how the process parameters influence the agglomerates formed. These studies link the particulate properties of agglomerates (*e.g.* size, size distribution, sphericity) to their subsequent functional properties (*e.g.* flowability, compressibility, strength, solubility). These studies are discussed in more detail in [Section 2.4](#). Most of these studies do not aim to improve mechanistic understanding of the process, and it is unclear which

rate processes control the properties previously mentioned. This knowledge is imperative to accurately predict the performance, as well as control the process in its entirety.

2.3.1 Wetting & Nucleation

A critical part of this mechanistic understanding for spherical agglomeration is when the primary particles first interact with the bridging liquid, often referred to as the wetting phase. A previous study has suggested two mechanisms which arise during wetting [21]. These mechanisms are differentiated by the size ratio of the bridging liquid droplets and particles of interest:

- i. Bridging liquid droplets are *smaller*: distribution mechanism occurs in which droplets coat particles prior to agglomeration, as shown in [Figure 2.7](#), resulting in particles ‘sticking’ together. Through further compaction, bridging liquid becomes available. Crystalline bridges form upon agglomerate drying.
- ii. Bridging liquid droplets are *larger*: immersion mechanism occurs in which droplets envelop particles prior to agglomeration, as shown in [Figure 2.8](#), with the agglomerate forming within the droplet initially. Particles also adhere to the droplet surface before the bridging liquid is removed through further compaction.

These mechanisms have also been observed when agglomerating limestone with kerosene, and are comparable to nucleation mechanisms during granulation [5,41].

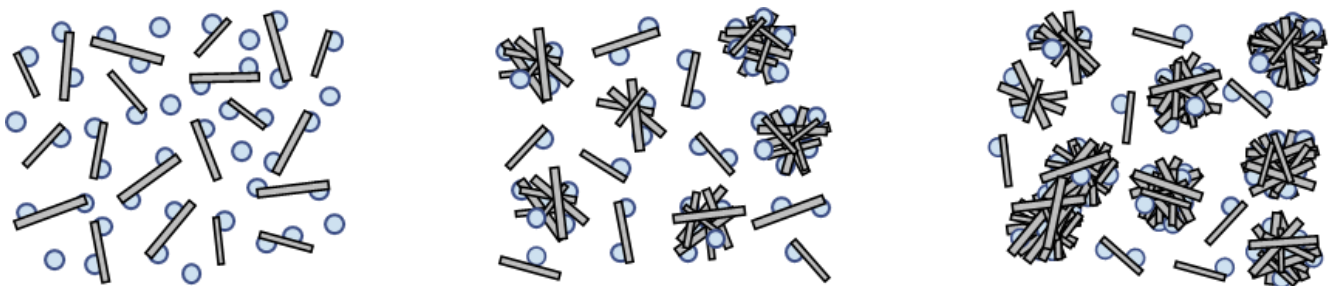


Figure 2.7. The proposed distribution mechanism for spherical agglomeration. Adapted from Subero-Couroyer et al., [42].

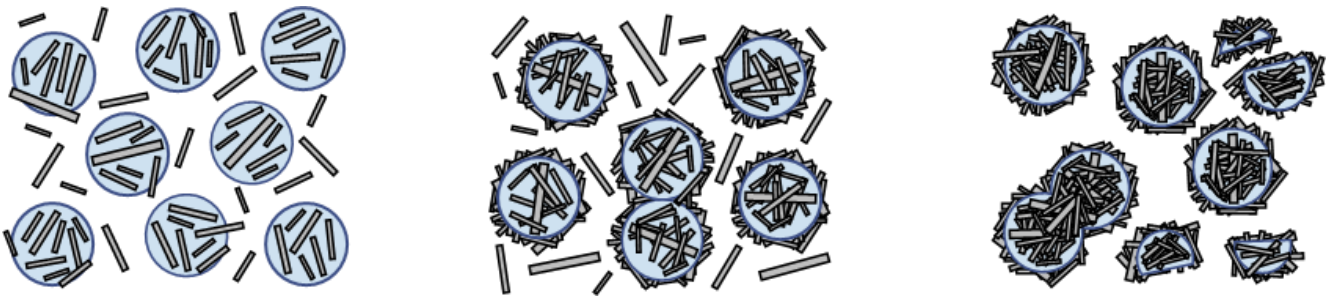


Figure 2.8. The proposed immersion mechanism for spherical agglomeration. Adapted from Subero-Couroyer et al., [42].

The wetting phase has also been visualised using image analysis employing a visualisation cell and a microscope [42]. The droplets were prepared to be much larger than the particles and the immersion mechanism was clearly observed. The same study also found that the droplets were more well dispersed at an increased agitation rate, noted by the smaller size of bridging liquid droplets; their surface area to volume ratio increased. The small size of the primary crystals, 5 μm , meant that there was a strong tendency for the formation of flocs. The authors noted the presence of some bridging liquid droplets amongst the flocs, as well as the penetration of some flocs into the bridging liquid droplets. The authors cited several key challenges with the experiment, including the difficulty in recognising droplets and particles and the analysis probe becoming obscured by particles. Post-experiment, agglomerates were found to increase in size with the square of the bridging liquid-solid ratio.

The formation of bridges between precipitated crystals has also been observed using a microscale study to assess the bridging geometry and strength [43,44]. Glass ballotini beads were agglomerated using silicone oil and then submerged in liquid. The authors found that the force exerted by the liquid bridges could be accurately predicted through the variation in pressure in the liquid-bridge interface, verified experimentally.

2.3.2 Growth & Consolidation

Shear forces are responsible for the compaction and coalescence mechanisms which are thought to occur during agglomeration. Building on previous work, novel imaging has been used to observe spherical agglomeration in-situ, in combination with off-line characterisation [45]. During agglomeration, agglomerate size was found to decrease during the compaction of flocs. This occurs post-wetting. Agglomerates were found to reach a minimum size before coalescence occurs, mirrored

by a decrease in the number of agglomerates. The growth is found to be rapid initially, before slowing and the size distribution becoming narrow. The kinetics of fines was found to be much higher than that of larger agglomerates; fines are incorporated much more rapidly than agglomerate-agglomerate coalescence. Other mechanisms have been previously suggested, including a '*compaction and rearrangement*' mechanism in which primary particles are organised in a compact manner to form spherical agglomerates, and an '*adhesion*' mechanism in which layered growth arises and is delimited by porous zones [45]. The latter of these has been verified experimentally.

The growth of agglomerates has also been compared to some of the mechanisms of wet granulation [4]. Capillary forces have been found to be responsible for increasing agglomerate size, as particles become bound to those with high amounts of bridging liquid [46]. Microcrystals have also been thought to form initial, loose agglomerates held together by the funicular state. With time, the shear force allows agglomerates to reach the capillary state through increased wetting by the bridging liquid [47]. These mechanisms are shown in Figure 2.9. Layering mechanisms have also been speculated to exist through analysis of agglomerate samples [46,48].

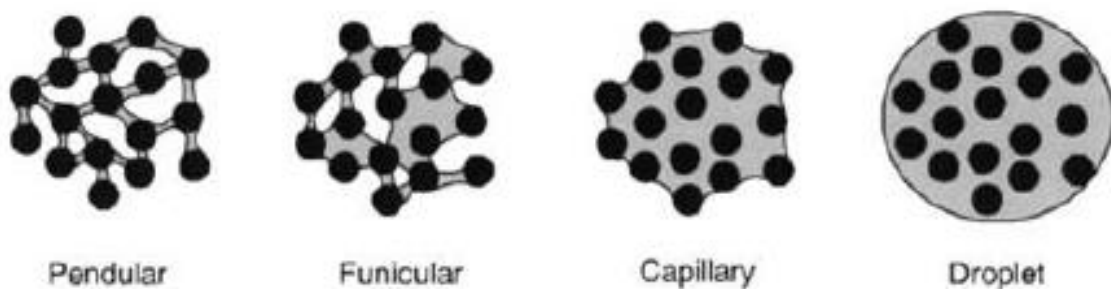


Figure 2.9. Four types of liquid-particle interactions structures. Reproduced from Iveson et al., [5].

The earliest work on spherical agglomeration mechanisms was conducted in 1979 and found that different growth regimes were present during the agglomeration of powdered glass [49]. The first regime, flocculation, is the formation of loose interconnected flocs of particles. The zero-growth regime immediately follows in which a reduction in the available bridging liquid limits growth. The fast growth regime is when the flocs are consolidated to form agglomerates. Further growth in size occurs as bridging liquid moves to the surface of the agglomerates. Eventually, an equilibrium occurs in which the size of agglomerates remains constant.

2.3.3 Breakage & Attrition

Breakage mechanisms have also been speculated as being a part of the overall process, with shear forces splitting agglomerates into smaller particles, which then may be incorporated into remaining agglomerates. However, these mechanisms are traditionally not regarded as being part of the process, partly due to the deformable nature of early agglomerates; instead, disruptive forces to coalescence are more likely to occur [50]. It has also been found that agglomerates are significantly stronger after they have been allowed to dry, as a result of the bridging liquid evaporating and solid crystalline liquid bridges forming [45,51]. There has been no specific visual observations in-situ.

2.3.4 Analogies to Wet Granulation

For spherical agglomeration processes to be controlled accurately to achieve the desired end-product properties, it is imperative that the mechanisms involved are well understood. Understanding of some of these mechanisms, or rate processes, were developed as interest in spherical agglomeration increased [49]. Later studies draw analogies between spherical agglomeration and wet granulation mechanisms, including initial wetting [35], agglomerate growth [42] and agglomerate breakage [46]. Such comparisons are useful, as they allow development of the mechanistic knowledge of the process, as well as insights into the influence of such mechanisms on the agglomerates yielded.

As in wet granulation, the wetting mechanism is dictated by the size ratio between the bridging liquid droplets and crystal particles [52]. This is discussed in more detail in [Section 2.3.1](#). As the process progresses, nuclei are subjected to continued shear which promotes their consolidation; this arises through either agglomerate-equipment or agglomerate-agglomerate collisions [10]. Due to this mechanism, there is generally a decrease in the mean size of the agglomerates as well as a reduction in the average porosity. Immediately preceding this, there is a lack of available bridging liquid for growth, and thus this phase is often referred to as the 'zero-growth' regime [49].

As agglomerates continue to compact and collide, eventually some of the bridging liquid is thought to be '*squeezed out*', and thus becomes available for particle adhesion via coalescence. Both mechanisms can involve either individual crystal particles or formed agglomerate nuclei [45]. It is assumed that due to the collisions within the vessel, as well as the shear rate imparted on agglomerates, breakage and attrition must also occur. This mechanism occurs most likely in combination with the growth mechanisms previously discussed. Whilst generally breakage and

attrition will shift the agglomerate size distribution to the left, *i.e.* reducing the overall size. It is believed that fines and smaller agglomerates produced in these processes can be reincorporated into agglomerates. Over time, an equilibrium between these competing growth and breakage mechanisms is reached and, thus, no major changes in agglomerate size are observed. A summary of the rate processes studied in both an experimental and modelling context is given in Table 2.2. The studies presented in are discussed in more detail in [Section 2.4](#) and [Section 2.5](#).

Table 2.2. A summary of rate process studies in both experimental (E) and modelling (M) contexts.

Rate Process Investigated					Ref
Formation	Consolidation	Growth		Breakage	
		Coalescence	Layering		
E + M		E + M		E + M	[49]
E + M	E + M			E + M	[53]
	E	E			[47]
E	E				[41]
	E	E	E		[45]
	E + M			E + M	[44]
	E + M	E + M			[50]
E					[42]
	E	E	E	E	[46]
E + M		E + M	E + M	E + M	[54]
M	M				[55]

Hapgood et al. performed a critical study of understanding of nucleation and wetting rate processes in wet granulation [56]. Of particular note in that study is the proposal for a nucleation regime map. The proposed map uses a combination of dimensionless groups: dimensionless drop penetration time which accounts for formulation parameters; dimensionless spray flux which accounts for process parameters. Similar work was also performed by Iveson & Litster [57], with a dimensionless group defined for the maximum pore saturation of agglomerates. This group, combined with an increasing deformation number group, was used to construct a regime map for growth of wet granulation systems. The use of dimensionless groups here, means the work can be applied to a wide variety of different wet granulation systems. This is exceptionally useful for engineers as it provides a robust and quick method to easily understand their process. The regime map itself has three separate

regimes within it: droplet controlled; intermediate; mechanical dispersion. The proposed map is displayed in Figure 2.10.

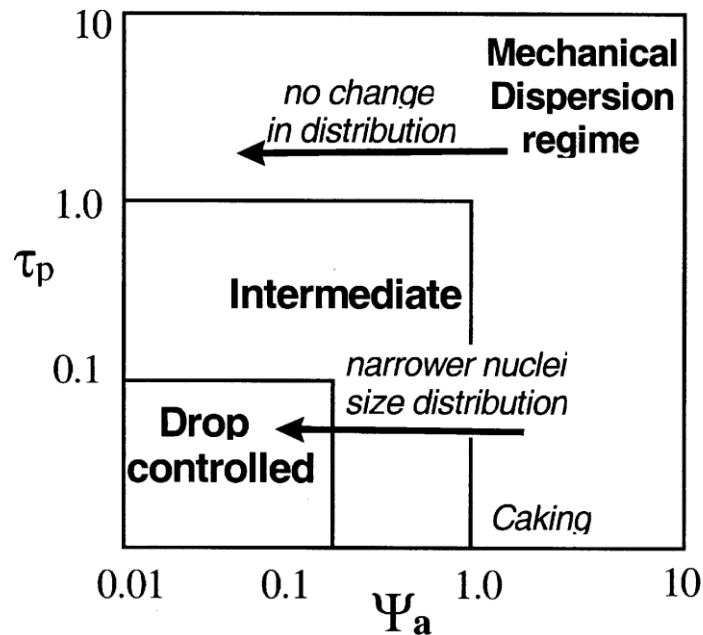


Figure 2.10. The proposed nucleation regime map in wet granulation. Reproduced from Hapgood et al., [5,56].

If a regime map could be developed in a similar way for spherical agglomeration, as indeed there are some analogous mechanisms, although these are yet to be fully explained, then this would provide an excellent tool for improving the overall mechanistic understanding of the process. This is because relevant process parameters, whose influence is relatively well understood, can be incorporated, as well as the specific formulation parameters which may be of interest. This could allow distinct regions on the map to be developed for each wetting and nucleation mechanism. In turn, this could guide engineers in finding a spherical agglomeration process with the desired final-product characteristics.

2.4 The Factors Affecting Spherical Agglomeration

For the most part, currently published literature on spherical agglomeration specifically investigates the influence of process parameters on the formation of spherical agglomerates. The key studies for each of these is discussed in the following sub-sections.

2.4.1 Solvent Composition of the System

The use of three solvents and varying crystal properties can create challenges when selecting solvents. However, several systems have been identified and used with a variety of different drugs. Some general rules have also been proposed to aid in the selection of different solvents and are briefly stated in Table 2.3 [58]. Table 2.4 provides an overview of solid-solvent systems which have been successfully used in spherical agglomeration processes. Note, that all systems identified within Table 2.4 fall within Group 2 or Group 3 from Table 2.3, as suggested by Chow & Leung [58]. Here, the bridging liquid is not immiscible in the solvent system as described, and thus some bridging liquid will be “lost” to the bulk solution. As a result, the volume of the bridging liquid phase to agglomerate the particles is unknown. This is discussed in more detail in Section 2.4.2.

Table 2.3. The four suggested groups for spherical crystallisation solvent selection by Chow & Leung [58].

Group	Drug Solubility ¹	Bridging Liquid	Anti-Solvent
1	Water	Salt solutions of high concentration <i>e.g.</i> 20 % CaCl ₂	Water-miscible organic solvent <i>e.g.</i> cyclohexane
2	Organic solvents <i>e.g.</i> chloroform.	Water-miscible organic solvent <i>e.g.</i> chloroform	Water
3	Water-miscible solvents <i>e.g.</i> ethanol, methanol	Ethanol-Chloroform solution	Water
4	Not sufficiently soluble in the above solvents: binding agent required, <i>e.g.</i> PEG	Salt solutions of high concentration <i>e.g.</i> 20 % CaCl ₂	Water-immiscible organic solvent <i>e.g.</i> dichloromethane

¹ Drug solubility refers to the good solvent which is used to dissolve the particles of interest. Note - relative quantities of solvents are listed in the publication.

Table 2.4. A selection of spherical agglomeration systems within the literature.

Solid	Solvent System		Bridging Liquid	Immiscible ^a	Ref
	Solvent	Anti-Solvent			
Aspartic acid	Water	Ethyl acetate	Chloroform	x	[59]
Aceclofenac	Acetone	Water	Dichloromethane	x	[60]
Aminophylline	Ethanol	Chloroform	Water	x	[61]
Benzoic acid	Ethanol	Water	Toluene	x	[62]
Carbamazepine	Ethanol	Water	Chloroform	x	[63]
Celecoxib	Acetone	Water	Chloroform	x	[64]
Cycloserine	Water	1-Butanol	Ethyl acetate	x	[65]
Fenbufen	THF ^b	Water	Isopropyl acetate	x	[66]
Flurbiprofen	Acetone	Water	Hexane	x	[67]
Glibenclamide	Dichloromethane	Water	Benzene	x	[68]
Glipizide	Benzene	Toluene	Chloroform	x	[69]
Indomethacin	DMF ^c	Water	Chloroform	x	[70]
Nabumetone	Ethanol	Water	Cyclohexane	x	[71]
Naproxen	Ethanol/acetone	Water	Chloroform	x	[72]
Propyphenazone	Ethanol	Water	Isopropyl acetate	x	[73]
Salicylic acid	Ethanol	Water	Chloroform	x	[74]
Tranilast	Ethanol	Acetone	Water	x	[75]

^a Immiscibility data from CRC [76]. ^b Tetrahydrofuran. ^c Dimethylformamide.

Other studies have taken a more theoretical approach, including evaluating the influence of Lifshitz-van der Waals forces and Lewis acid-base interactions in combination [77]. The authors noted the superiority of both this and ternary phase diagram approaches in developing spherical agglomeration processes [77,78]. The latter of these is discussed in more detail in [Section 2.4.1.1](#). The authors summarised that both approaches were useful in selecting which three solvents to utilise, whereas evaluation of solubility of the drug of interest can promote the use of binary systems. A proposed framework for solvent selection also produced successful ternary solvent systems for the agglomeration of cefotaxime sodium particles (see [Figure 2.11](#)). Unfortunately, the authors did require a verification step in their work, which involved conducting a spherical agglomeration experiment. Thus, full prediction of a ternary solvent system without experimental work was not possible.

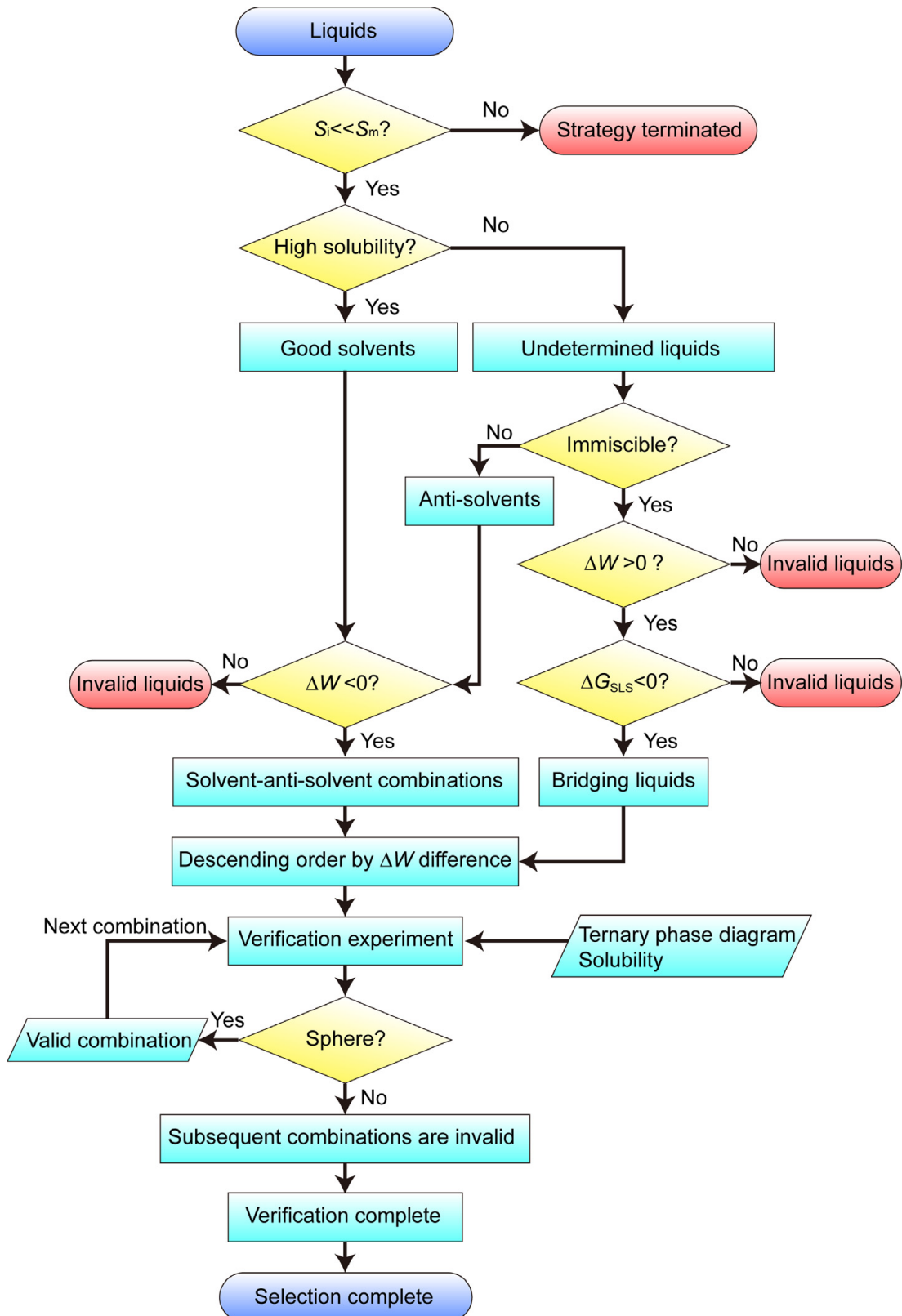


Figure 2.11. A proposed framework for identifying ternary solvent systems. The framework accounts for the influence of Lifshitz-van der Waals and Lewis acid-base parameters. Reproduced from Chen et al., [77].

2.4.1.1 Ternary Phase Diagrams

The solvent system for spherical agglomeration has a direct influence on the level of crystallisation which can be achieved, as well as the extent of agglomeration. This is a result of the level of supersaturation, discussed previously, and the agglomeration kinetics.

To aid in the selection of solvent concentrations for each of the three solvents, ternary phase diagrams can be utilised, an example of which is shown in Figure 2.12. Each axis represents the relative fraction of that component within the solution identified. Here, component X is the anti-solvent, component Y is the solvent, and component Z is the bridging liquid.

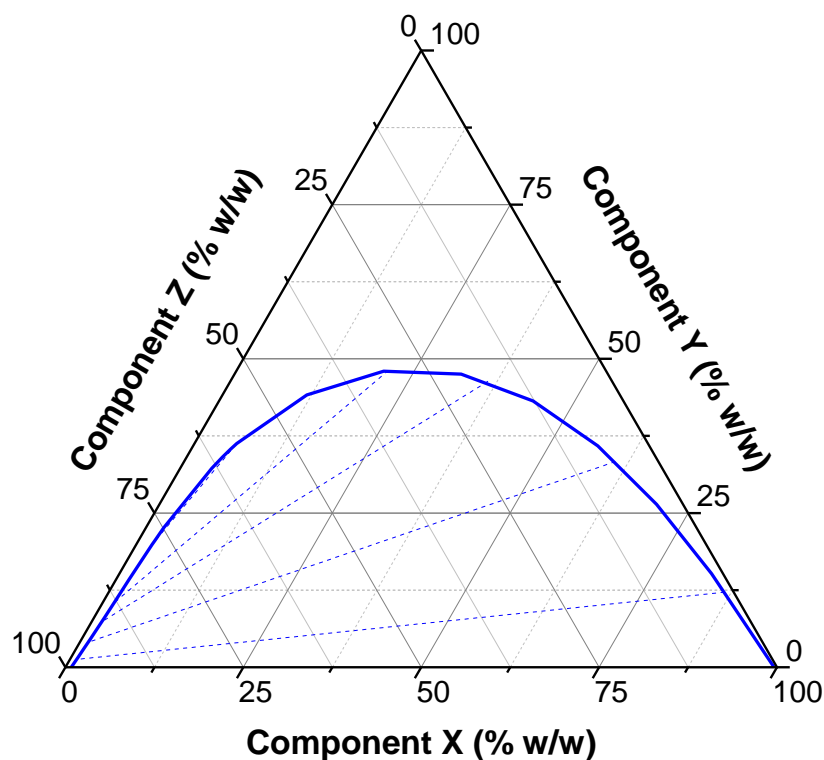


Figure 2.12. An example of a ternary phase diagram for a spherical agglomeration system. Tie-lines are shown as dashed blue lines. The line of miscibility is indicated by a solid blue line. Component X represents the anti-solvent, Component Y the solvent, and Component Z the bridging liquid.

Crucially, there is a boundary line of equilibrium. This line separates the miscible and immiscible regions. Tie-lines on the diagram also show lines of equilibrium and can be used to calculate the compositions of each immiscible phase. Along a single tie-line, the immiscible phase compositions remain the same, only the mass fraction of each phase changes.

The first documented use of this was in 1982 [10]. A ternary phase diagram for the solubility of an ethanol-water-chloroform system was used for the spherical agglomeration of salicylic acid. A

recent study has also utilised this method prior to the agglomeration of the drug etodolac [79]. A variety of other crystals have been agglomerated through the determination of ternary phase diagrams, including tolbutamide, acebutolol hydrochloride, fenbufen and ketoprofen [9,46,66,80,81]. Generally, these studies have encouraged the use of the ternary phase diagram as it allows identification of a system where agglomeration can be optimised within the immiscible region.

The ternary phase diagram has been used previously by several studies to identify a region of operation for agglomeration processes [46,66,79,80,82]. Such regions are always within the immiscible region of the diagram, where two distinct liquid phases are present. In these studies, the solubility of bridging liquid in the bulk solution is exceeded to allow formation of a distinct bridging liquid phase. However, no studies have evaluated the influence of solvent system miscibility, nor the influence of this phenomenon on the bridging liquid volume available to agglomerate the particles of interest. As such, the traditional BSR value only provides an indication of the volume of bridging liquid available to agglomerate particles.

Different approaches have been used to select the solvents for spherical agglomeration. For instance, the relative solubilities of the crystals of interest can be evaluated in a variety of different solvents [83]. The authors also investigated miscibility, partitioning, and the vapour pressures of the solvents in an initial screening. Interestingly, this study reports the co-crystallisation of two different crystal species. The level of supersaturation, which is dictated by the solvent composition of the system, was found to directly influence which polymorph formed [83]. These considerations must be accounted for when designing spherical agglomeration systems. The choice of selecting a bridging liquid is detailed in [Section 2.4.2.1](#).

The solvent addition method will directly affect the level of supersaturation within the system. The first study to investigate this process parameter used continuous spherical agglomeration for the agglomeration of sulfamethoxale crystals [84]. The study found that increasing the feed rate of the bridging liquid led to an exponential increase in the average diameter of agglomerates [84]. This is to be expected, as increasing the amount of bridging liquid increases the level of agglomeration. Conversely, increasing the feed rate of the suspension, containing all other solvents and the dissolved crystals, led to a decrease in the average diameter of agglomerates, as shown in [Figure 2.13](#) [84].

The suspension feed rate results were later verified by another study. Here, increasing the addition rate of the solution of benzoic acid, solvent and bridging liquid to the anti-solvent yielded agglomerates with a smaller size [46]. The authors did, however, note that the strength of these smaller

agglomerates was higher than when the bridging liquid was added alone. This was identified through measurements of the fracture stress [46].

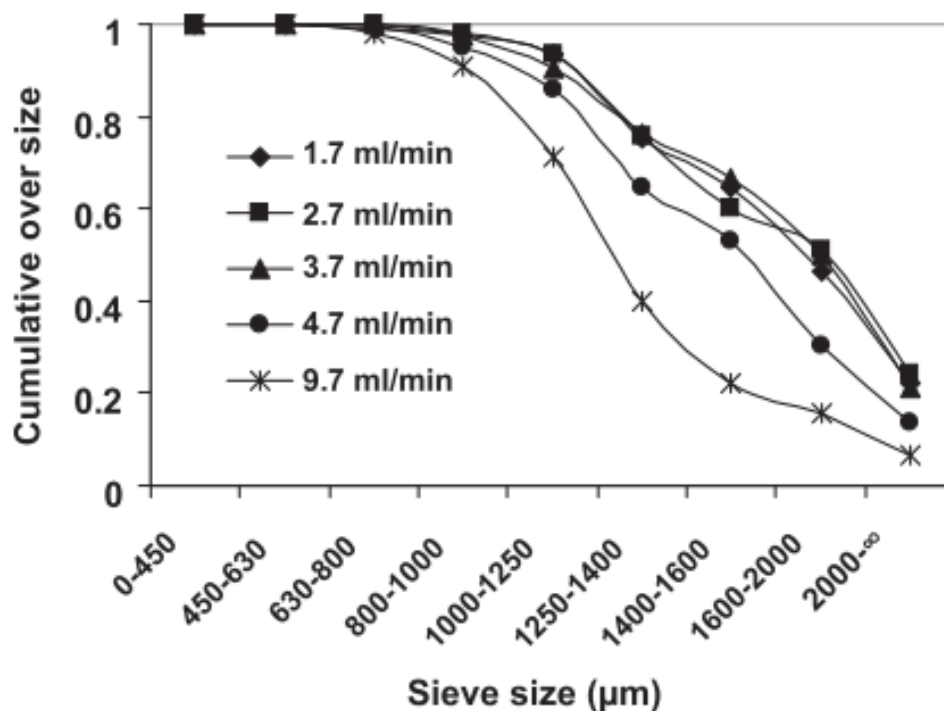


Figure 2.13. The influence of feeding rate on the benzoic acid agglomerate size distribution. Reproduced from Thati & Rasmuson, [46].

2.4.2 The Bridging Liquid

The bridging liquid solvent is perhaps one of the single most important parameters to consider when designing spherical agglomeration experiments [7]. Crucially, it must be immiscible in the anti-solvent. The properties of the liquid itself, as well as how much bridging liquid is added, has a major influence on the product properties. Thus, there are several considerations which must be made when considering bridging liquid addition methods.

2.4.2.1 Choice of Bridging Liquid

The choice of the bridging liquid will directly influence the amount of agglomeration and, therefore, influence the morphology and mechanical properties of agglomerates. Several studies have investigated a variety of different solvents as the bridging liquid. One of these studies evaluated the wettability of the drug particles by different solvents [21]. This was achieved through the Washburn's test, which relies upon capillary action. The Washburn's equation is given as:

$$\frac{h^2}{t} = \frac{\gamma \bar{r} \tau}{2\eta} \cos\theta \quad \text{Equation 2.1}$$

where h is the covered distance in time t , γ is the interfacial tension, η the viscosity of the liquid, \bar{r} the mean of constant radius, τ tortuosity and θ the wetting angle of the liquid [85]. The authors measured changes in the weight variation of a bed of lobenzarit disodium particles. To do this, the weight of the liquid within the bed was related to the liquid front height:

$$m = \phi \rho S_{inner} h \quad \text{Equation 2.2}$$

where m is the mass, ϕ the porosity of the packed powder bed, ρ the density of the fluid and S_{inner} is the inner section of the bed. Finally, Equation 2.1 and Equation 2.2 are combined to measure the variation in weight with time:

$$\frac{m^2}{t} = \frac{\gamma \rho^2 (S_{inner} \phi)^2}{\eta} \frac{\tau \bar{r} \cos\theta}{2} \quad \text{Equation 2.3}$$

The study also compared a ‘perfect’ wetting agent, where they assumed the contact angle to be zero, to the bridging liquid solvent to be tested which had an unknown contact angle. The bridging liquids were then tested experimentally [21]. The solvent with the highest wettability of lobenzarit disodium, n-hexane, was found to have the lowest contact angle and, indeed, produced agglomerates which were denser, larger and had high sphericity [21]. These results suggest the Washburn’s test may be a suitable method for the selection of a bridging liquid.

A similar study has been performed more recently, although the wettability data of different bridging liquid solvents was not provided [86]. The authors used the sessile drop-method to calculate the wettability of these solvents to aid selection of an appropriate bridging liquid. The study did highlight that the bridging liquid solvent has a pivotal role in producing the desired agglomerates. The authors concluded that the different solvents can directly influence the yield of agglomerates as well as their strength. Morphological changes were also observed: size, size distribution and sphericity [86].

The interfacial tension of the bridging liquid in water can provide insights into how suitable a solvent is for agglomeration procedures. It has been suggested that the interfacial tension between the bridging liquid and the anti-solvent should also be high, although the authors fail to provide quantitative data for this [86]. Bridging liquids with higher interfacial tensions in water provide a larger immiscible region to work with; that is, immiscible systems form with lower quantities of bridging liquid. In effect, this provides a wider range of experimental systems which may be used when

designing agglomeration procedures.

Previously, the interfacial tension has been considered as an important parameter in the displacement of a non-wetting liquid (*i.e.* mother solution) by a wetting fluid (*i.e.* bridging liquid) within a thin capillary. The velocity profile of a wetting fluid can be expressed as follows:

$$u(r) = \left(\frac{1}{4\mu_d} \left| \frac{dP}{dz} \right| \right) (R^2 - r^2) \quad \text{Equation 2.4}$$

where R represents the radius of a cylindrical pipe, r is the radial co-ordinate, μ_d is the viscosity of the liquid, and $\left| \frac{dP}{dz} \right|$ is the pressure gradient for the flow. The flow rate q can thus be expressed as follows, which then allows the average flux of the flow, Q to be calculated:

$$q = \left(\frac{\pi}{8\mu_d} \left| \frac{dP}{dz} \right| \right) R^4 \quad \text{Equation 2.5}$$

$$Q = \frac{q}{\pi R^2} = \left(\frac{1}{8\mu_d} \left| \frac{dP}{dz} \right| \right) R^2 \quad \text{Equation 2.6}$$

From here, the authors calculated the rate of displacement of a non-wetting liquid, such as the mother solution, by a wetting liquid, such as the bridging liquid. A schematic of this is shown in [Figure 2.14](#). The authors used these calculations as a basis for two separate models for the immersion mechanism. These are discussed in more detail in [Section 2.5](#).

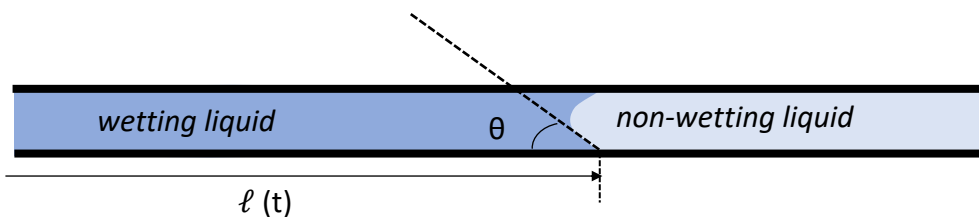


Figure 2.14. Displacement of a non-wetting liquid, or bulk solution, by a wetting liquid, or the bridging liquid, in a thin capillary. Reproduced from Arjmandi-Tash et al., [12].

2.4.2.2 Bridging Liquid-Solid Ratio (BSR)

The bridging liquid-solid ratio is defined as the ratio between the volume of bridging liquid (V_z) and the volume of the solid, or crystals, to be agglomerated (V_s), as defined in [Equation 2.7](#):

$$BSR = \frac{V_z}{V_s} \quad \text{Equation 2.7}$$

The ratio is critical to the agglomeration rate. Many studies are in agreement in that if the ratio is too low, there is an insufficient level of agglomeration, whereas if the ratio is too high, a paste-like product is formed [21,45,46]. Many of these studies recognise a 'critical range' in which the ratio is suitable for agglomeration. Increasing the ratio from the lower to the upper limit, promotes an increasing agglomerate size [50,86]. The critical range has been previously determined for select salicylic acid (0.35 – 0.47) and benzoic acid (0.47 – 1.16) systems [50,86].

The effect of BSR may be described in further detail. When the BSR is below the critical range, agglomerates may form, but crystals will remain in solution. Increasing the BSR in the critical range increases the agglomerate size, as the remaining crystals in solution become agglomerated [50,86]. Above the critical range, a bridging liquid layer forms around the agglomerates and, above this, the layer grows to its maximum level. Residual bridging liquid remains as droplets within the suspension before subsequent increases promote the formation of soft, paste-like agglomerates as previously discussed [50,86]. These relationships are detailed in [Figure 2.15](#) through to [Figure 2.20](#) for various levels of bridging liquid, for both the distribution and immersion mechanisms, as shown in [Figure 2.7](#) and [Figure 2.8](#) respectively.

In [Figure 2.15](#) and [Figure 2.16](#), the level of bridging liquid is too low. In the immersion mechanism, not all crystals can enter droplets, due to the lack of bridging liquid. In the distribution mechanism, not all crystals will be wetted by the bridging liquid droplets. Growth and consolidation occurs as usual, but many crystals may be left in solution due to not being wetted. Agglomerates formed tend to have weak mechanical properties, making them more prone to breakage and attrition.

In [Figure 2.17](#) and [Figure 2.18](#), the level of bridging liquid is ideal. In the distribution mechanism all crystals are sufficiently wetted by the bridging liquid droplets. In the immersion mechanism the droplets are effectively 'saturated' with crystals. Compaction occurs as usual and all nuclei begin to form agglomerates, which densify over time. The resultant agglomerates are highly spherical and have the desired mechanical properties.

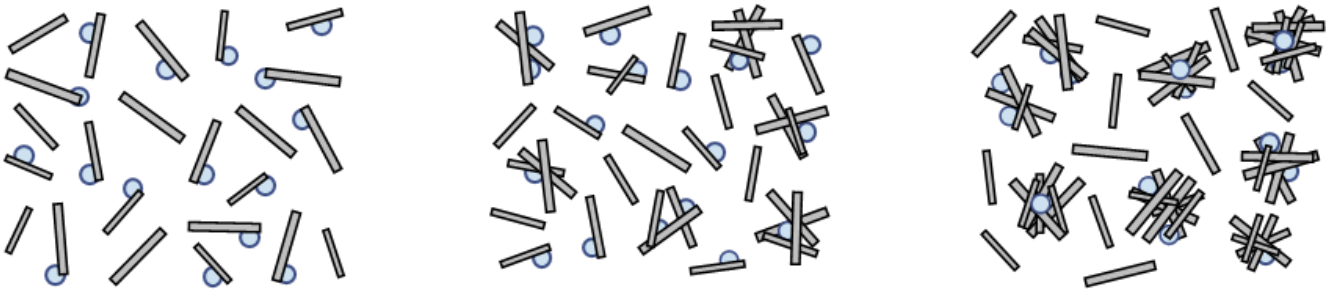


Figure 2.15. The influence of a BSR value below the critical range on the distribution mechanism in spherical agglomeration. Adapted from Petela [87] and Peña & Nagy, [32].

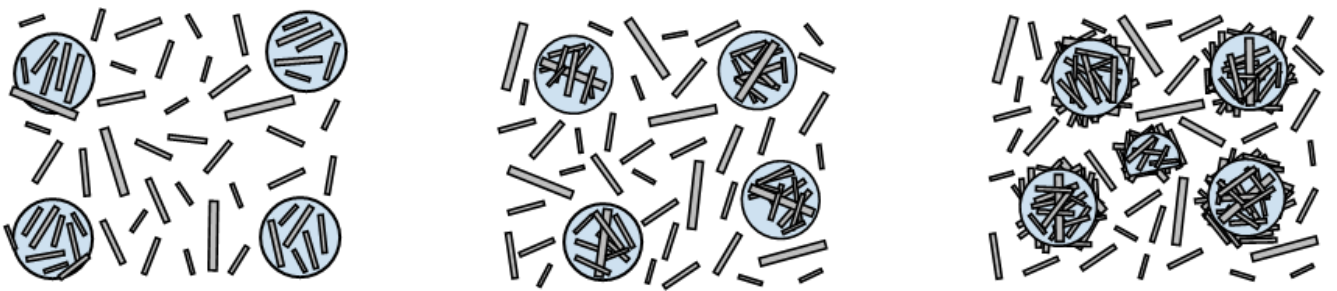


Figure 2.16. The influence of a BSR value below the critical range on the immersion mechanism in spherical agglomeration. Adapted from Petela [87] and Peña & Nagy, [32].

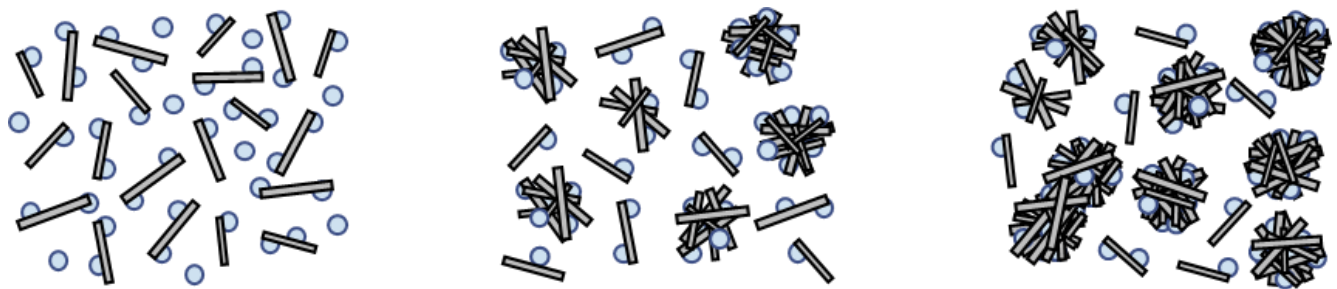


Figure 2.17. The influence of a BSR value within the critical range on the distribution mechanism in spherical agglomeration. Adapted from Petela [87] and Peña & Nagy, [32].

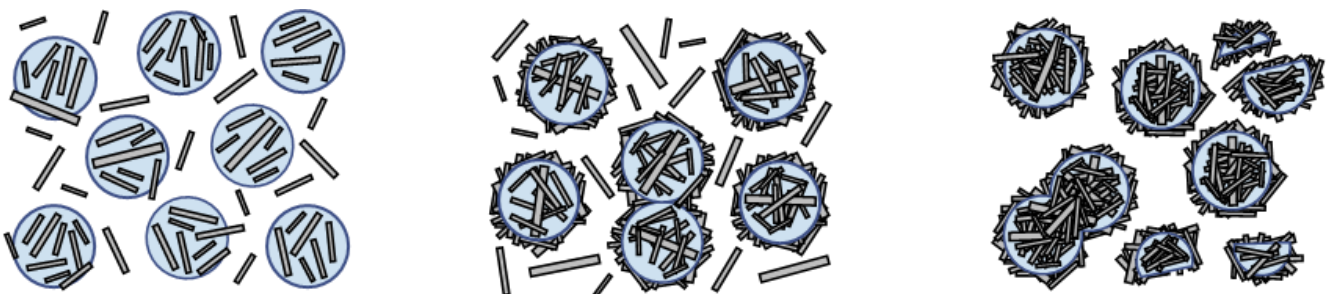


Figure 2.18. The influence of a BSR value within a critical range on the immersion mechanism in spherical agglomeration. Adapted from Petela [87] and Peña & Nagy, [32].

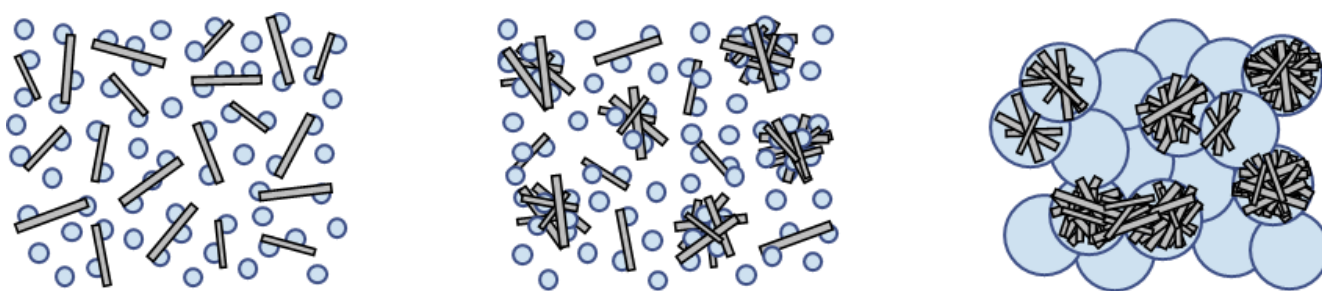


Figure 2.19. The influence of a BSR value above the critical range on the distribution mechanism in spherical agglomeration. Adapted from Petela [87] and Peña & Nagy, [32].

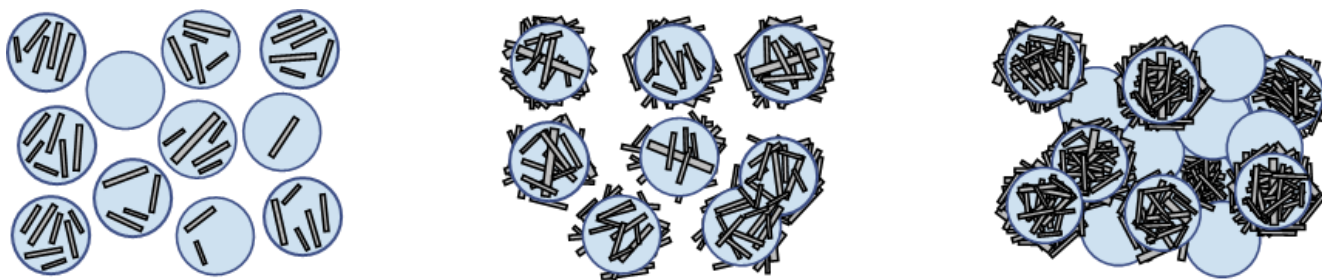


Figure 2.20. The influence of a BSR value above the critical range on the immersion mechanism in spherical agglomeration. Adapted from Petela [87] and Peña & Nagy, [32].

In Figure 2.19 and Figure 2.20, the level of bridging liquid is too high. In the immersion mechanism, not all droplets will contain crystals, and the volume of crystals will vary. In the distribution mechanism, the excess bridging liquid causes excess wetting of crystals. The final agglomerates form a paste-like material, which has poor mechanical properties. Over time, agglomerates begin to form through compaction and consolidation with the excess bridging liquid.

It has been suggested that increasing the BSR within the critical range leads to an increase in the deformability of agglomerates, which means there is an increased amount of energy dissipation. This, in turn, leads to an improvement in the efficiency of agglomeration and an increase in agglomerate size. Other studies have recognised that increasing the BSR within the critical range also leads to a reduction in the size distribution of agglomerates [42,48].

Furthermore, there are a lack of studies which have compared different crystals of interest within the same solvent system. In these instances, it remains unclear whether the critical range identified is consistent across compounds. Studies have shown that changes in one of three solvents used causes changes in the critical range value, as highlighted within Table 2.5 [21,45,46,86]. In practice, the solvent species changed is almost always the bridging liquid. However, process optimisation may require one of the other two solvents to be changed, for example, to improve the crystallisation yield of the product. Such studies have currently not been performed in the context of SA. Table 2.5 shows that the critical range for BSR is strongly system dependent. There is no general

method for determining the correct range of BSR a priori, only by extensive experimental studies for each new system. Thus, predictive design of spherical agglomeration is, at present, impossible. These issues create complex challenges for engineers, hampering process development and industrial adoption, as the critical range is crucial for accurate control of the process.

Table 2.5. A summary of the bridging liquid to solid ratio critical range for a variety of different bridging liquids and primary particles.

Anti-Solvent/Solvent	Bridging Liquid	Primary Particles	Critical BSR Range	Ref
Sulfuric Acid/-*	Chloroform	Salicylic acid	0.35 – 0.50	[45]
Water/Ethanol	Chloroform	Salicylic Acid	0.72	[10]
Water/Ethanol	Chloroform	Benzoic Acid	0.47 – 1.16	[88]
Water/Acetone	Hexane	Benzoic Acid	1.08 – 1.43	[21]
Water/Ethanol	Heptane	Benzoic Acid	0.72 – 1.23	[86]
Water/Ethanol	Toluene	Benzoic Acid	0.47 – 1.16	[46]
Water/Ethanol	Toluene	Benzoic Acid	0.80	[89]
Water/Acetone	DCM	Aceclofenac	0.88	[23]

* *N.B. binary system used.*

The influence of BSR could be compared to the influence of the binder-solid ratio parameter in granulation. The observations noted are much the same: inadequate levels of binder results in a lack of granulation, whilst excessive levels lead to the formation of a slurry. Within this critical range, increases also lead to increases in the binder level, as with spherical agglomeration. The pore saturation is an imperative factor in this manner [90]. This factor represents the level of intra-granular voids filled with binder liquid. Figure 2.21 shows the calcium hydrogen phosphate growth rates with a variety of different binders – all of which collapse onto a single curve, regardless of the binder used.

Figure 2.22 shows similar trends for the growth in agglomerate size as a function of BSR within the critical range for a variety of different spherical agglomeration systems. All these curves, though qualitatively similar, are quantitatively different and, therefore, prevent a major obstacle in predictive design. Here, the relationship between agglomerate size and BSR cannot be established for a given system. The data does follow a similar exponential trend as identified in Figure 2.21, suggesting that it may be in fact possible to collapse the data onto a single line. For this to be achieved, standardisation across the BSR value should be achieved, along with other experimental parameters. This could be achieved using dimensionless parameters or groups, like those well established for wet granulation.

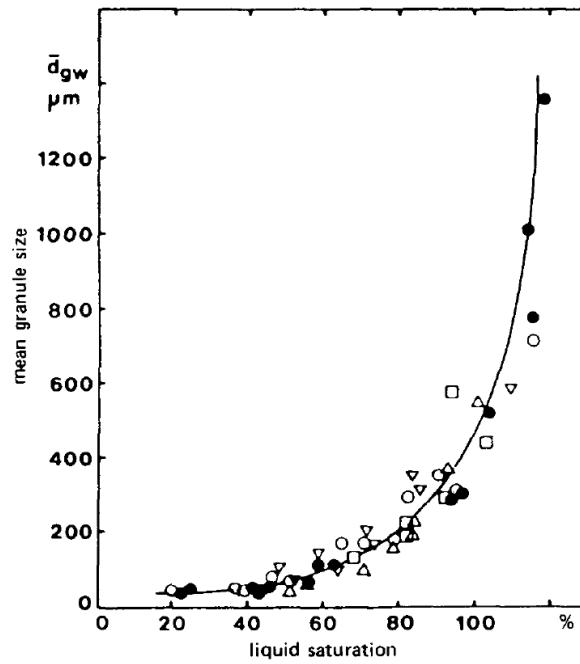


Figure 2.21. The effect of liquid saturation on the mean granule size for different binders. Reproduced from Iveson et al., [5,90].

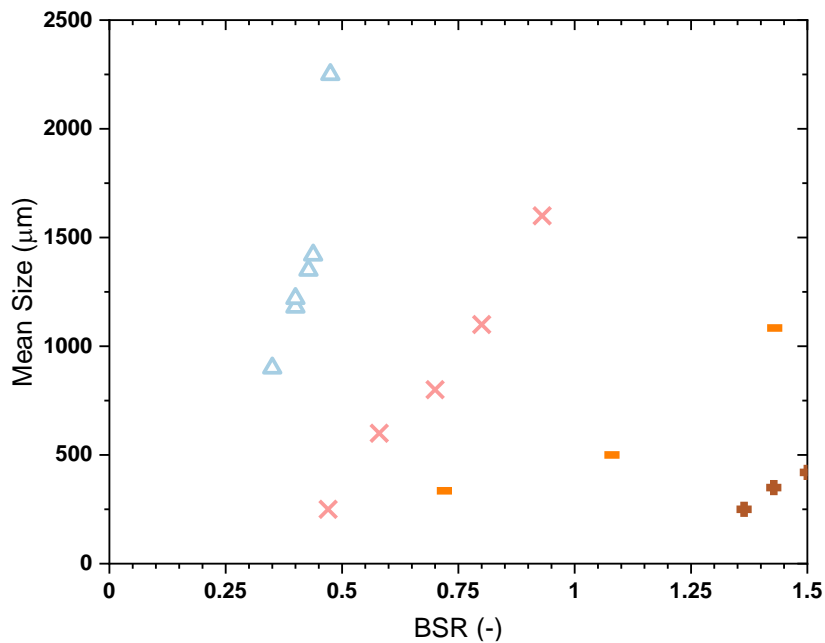


Figure 2.22. Agglomerate size as a function of BSR for different agglomerate systems: \circ CaCO_3 -kerosene; \triangle salicylic acid-chloroform; \times benzoic acid-toluene; \diamond lobenzarit-hexane; $+$ atorvastatin calcium-dichloromethane [21,45,46,91,92].

There is one respect in which predicting BSR in spherical agglomeration is more complex than predicting liquid to solid ratio for wet granulation. In wet granulation, the continuous fluid is air and there is complete immiscibility between the air and the liquid binder. For spherical agglomeration, however, the continuous fluid is a solvent and there is partial miscibility between the continuous phase solvent, and dispersed phase bridging liquid. Furthermore, the extent of miscibility is not constant, but depends on the operating position on the ternary phase diagram (Figure 2.12). By using the actual bridging liquid volume accounting for partial miscibility, it may be possible collapse data from many systems onto a single curve. In this instance, it may be possible to predict both the mean size of agglomerates, and thus infer the level of fines in solution, when considering a different bridging liquid volume quantification method. This approach uses the “true bridging liquid to solid ratio” (TBSR) rather than the BSR. This approach has not previously been proposed or tested in the literature.

2.4.2.3 Bridging Liquid Addition Method

A key study has investigated the influence of two different addition methods on the formation of spherical agglomerates of salicylic acid [35]. In the first method, an ethanol solution containing salicylic acid was placed in the reactor prior to the addition of water, the anti-solvent, to crystallise salicylic acid particles [35]. The bridging liquid, chloroform, was added last. In the second method, the reverse process occurred – the bridging liquid and water were added to the reactor, before the ethanol solution was added [35]. The agglomerates formed through the latter method were found to be both more compact and spherical, although an explanation was not proposed for this observation [35].

A later study reported an increase in the number of spherical agglomerates when the bridging liquid is initially mixed into the solvent system prior to precipitation, as opposed to addition after precipitation [88]. These results were later verified for atorvastatin calcium crystals, where simultaneous precipitation and agglomeration occurred when the bridging liquid was initially mixed into the solution [92]. The authors also noted the improved flowability and compressibility of agglomerates formed in this way, as opposed to adding the bridging liquid post-precipitation [92]. This could be due to immediate agglomeration, which reduced the likelihood of polymorph transformation. Injecting the same level of bridging liquid over a shorter period of time has been found to decrease the overall agglomerate size [42]. The authors state that this is due to increased dispersion of bridging liquid into many more, smaller droplets, which subsequently increases the number of agglomerate nuclei.

2.4.2.4 Bridging Liquid Droplet Size: Immersion vs Distribution Mechanism

As previously noted in [Section 2.3.1](#), the size ratio between the bridging liquid droplets and the particles of interest dictates which wetting mechanism occurs. This subsequently affects agglomerate growth and consolidation and may also influence the degree of breakage. This is due to the generally higher friability of agglomerate nuclei formed by the distribution mechanism. The bridging liquid droplet size is almost always overlooked. There are many practical difficulties in observing, tracking, and characterising bridging liquid droplets within stirred tank reactors. This means it is difficult to understand the balance of droplet coalescence and breakage processes, as well as their influence upon agglomerate size distributions.

Only one study to date has looked at both droplet and particle size control parameters together [42]. The authors visualised the in-situ wetting of salicylic acid particles. This involved creating a droplet of the bridging liquid (chloroform) of approximately 240 μm using a microcapillary. A suspension of salicylic acid was pumped through the visualisation zone. This allowed the authors to visualise the initial interactions between the bridging liquid droplet and the particles of interest. In this study, the particle size was controlled and found to be approximately 30 μm ; thus, the initial wetting occurs by the immersion mechanism. This can be seen in [Figure 2.23](#).

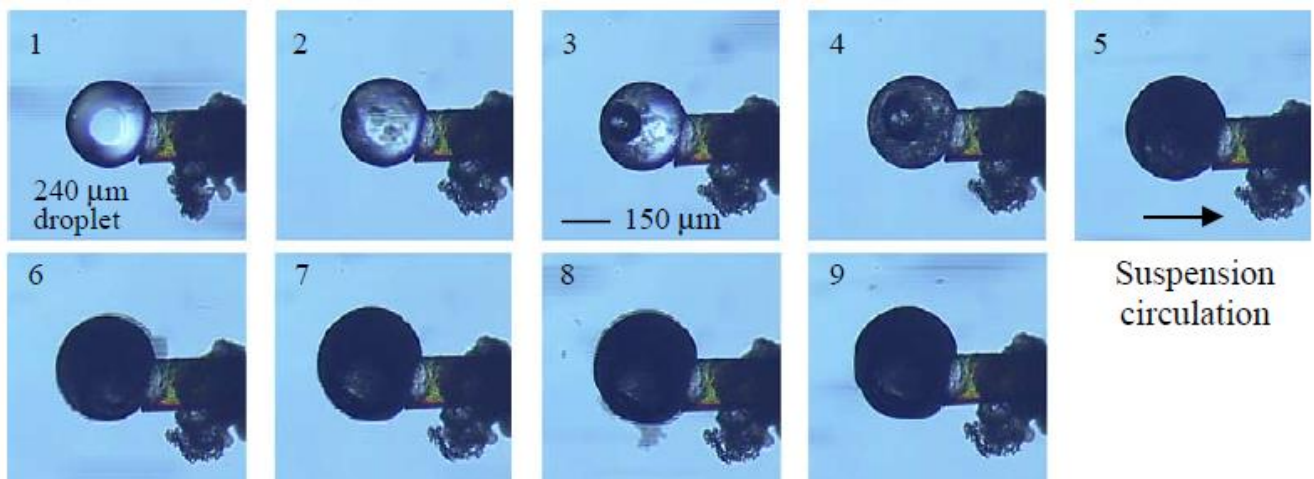


Figure 2.23. In-situ visualisation of chloroform-salicylic acid initial interactions. Scale bar is the same for all images. Reproduced from Subero-Couroyer et al., [42].

The authors also noted the contrast in the immersion mechanism as previously identified by Madec et al., [93]. In this study, the authors noted that a particle shell formed around the bridging liquid droplet, and through shear, particles began to migrate towards the core of the droplet over time. This frees up bridging liquid at the droplet surface for further particles to interact, as shown in [Figure 2.24](#). Madec et al., also noted that immersion in this manner prevented droplet coalescence. This suggests that pre-nucleation (*i.e.* allowing a “*protective layer*” of droplets to form), could be advantageous as a method of controlling bridging liquid droplet sizes.

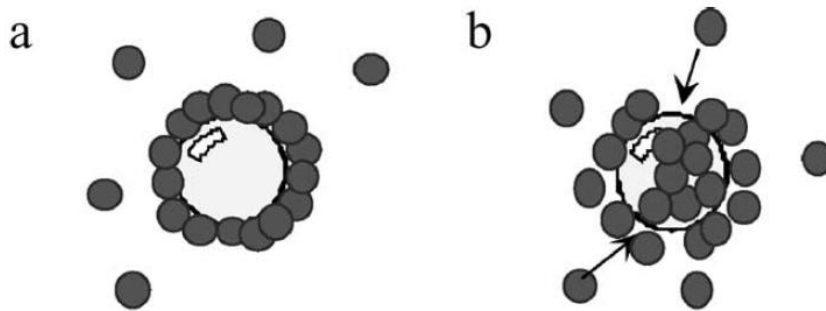


Figure 2.24. a) The initial formation of a particle shell around a bridging liquid droplet, b) prior to their movement into the droplet itself. Reproduced from Madec et al., [93].

Indeed, the prior study also managed to observe wetting and nucleation in-situ of a stirred agglomeration vessel. It can be seen from the images obtained by the authors that the wetting & nucleation, and growth & consolidation, were consistent with the distribution mechanism. These results are shown in [Figure 2.25](#). Whilst the qualitative results of the mechanism are sufficient, the quantitative results which underpin the mechanism need further study. This secondary result from the same study highlights the need for accurate control of the bridging liquid droplet sizes. It is unclear whether the authors achieved this during the agglomeration process and, if so, how it was achieved. The control of initial particle size is challenging but possible through the use of techniques such as recrystallisation, milling *etc.* However, the control of bridging liquid droplets is much more difficult. This could be achieved through microfluidic systems, which would provide droplets at a pre-determined size. Whether these droplets coalesce or break during agglomeration process remains unclear but could be investigated using a stabilisation method as described by Madec et al., [93].

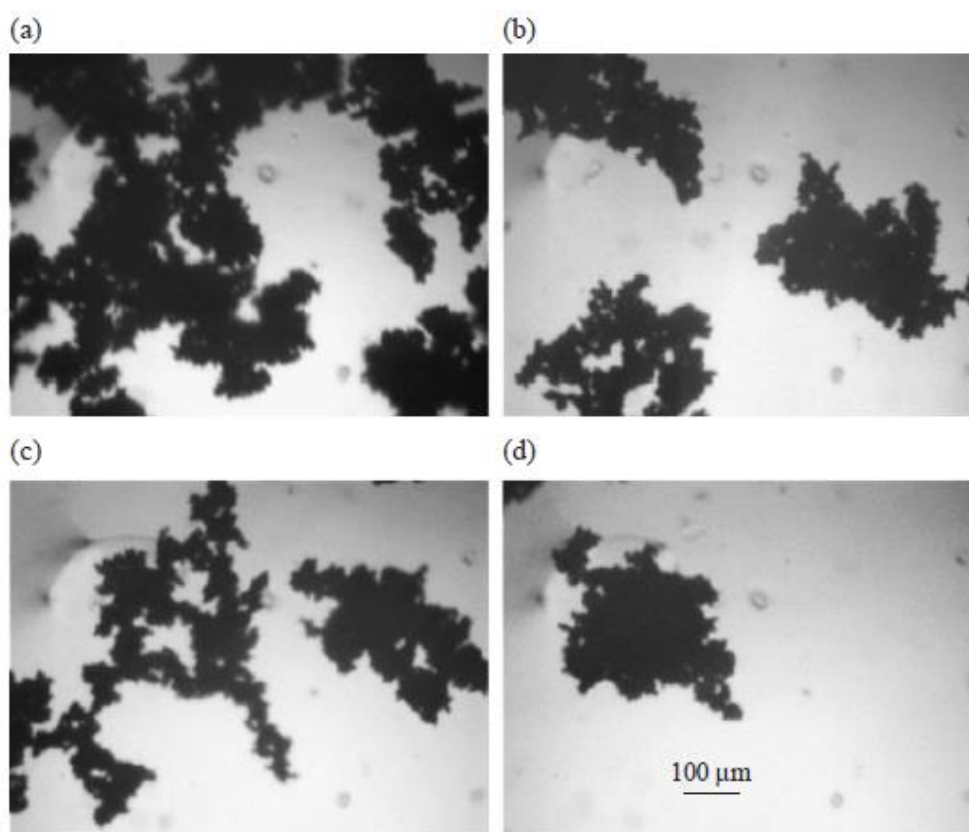


Figure 2.25. (a-d) The evolution of salicylic acid flocs during the injection of chloroform as a bridging liquid. Note the compaction of flocs during this process across an unknown time period. Reproduced from Subero-Couroyer et al., [42].

Building on these works, the mean size of spherical agglomerates has also been directly controlled through the bridging liquid droplet size [94]. Here, the authors used variations in the bridging liquid droplet size and investigated how this affected the mean agglomerate size. The bridging liquid (toluene) was infused into the suspension at a controlled flow rate using a microfluidic capillary. Whilst direct visualisation and measurement of the droplets was not feasible, the droplet size was estimated using mathematical relationships rooted in the forces acting upon forming droplets at the capillary tip. These were estimated at between 750 and 1000 μm depending upon the experimental conditions, *i.e.* impeller speed, capillary geometries. The benzoic acid primary particles had a mean size of approximately 12 μm . This ensured the immersion mechanism of wetting occurred. The authors found that the final agglomerate size was approximately one and a half times that of the initial droplet size. This study highlights the possibility of tuning bridging liquid droplet sizes to control the final size of agglomerates, and the importance of their size on agglomerate wetting & nucleation and growth & consolidation.

2.4.2.5 Prediction of Bridging Liquid Volume Requirements

PA modelling study has investigated the influence of the critical packing volume during immersion nucleation driven, spherical agglomeration processes [12]. There, a new definition of the true bridging liquid solid ratio was introduced (TBSR), although the supporting theory and validation of this was not provided. This definition accounts for miscibility of the bridging liquid in other solvents. The authors also used a bridging liquid which was completely immiscible in the one-component suspension and, thus, remained as a distinct phase within their simulations. In such scenarios, the TBSR and BSR are considered to be mathematically equal as there is no solvent miscibility. The authors were able to predict the TBSR optimal range from estimations of the critical packing volume, as shown in

Equation 2.8:

$$TBSR_{opt} = \frac{\varphi_{cp}}{1 - \varphi_{cp}} \quad \text{Equation 2.8}$$

where φ_{cp} is the critical packing liquid volume fraction within the agglomerate nuclei. This parameter quantifies the amount of bridging liquid contained within an agglomerate nucleus. When $\varphi_{cp} = 1$, the nucleus is filled with bridging liquid and no crystals are present. Conversely, if $\varphi_{cp} = 0$, the nuclei are filled with crystals and no bridging liquid is present. Eventually, the bridging liquid droplet is occupied by a maximum fraction of particles, *i.e.* the critical packing volume is reached. A schematic of this is shown in [Figure 2.26](#).

However, in practice, most particulates suited to the spherical agglomeration process are not perfectly spherical. As a result, the critical packing may be considerably different and, thus, the calculations used within this study would produce undesirable results. DEM studies have previously demonstrated the significant influence of aspect ratio and particle size on the critical packing of particles [95]. In practice, identifying the value in-situ during experiments may be incredibly difficult, especially if crystallisation steps are included. This is due to the potential breakage of primary particles, as well as increases in their size through secondary nucleation.

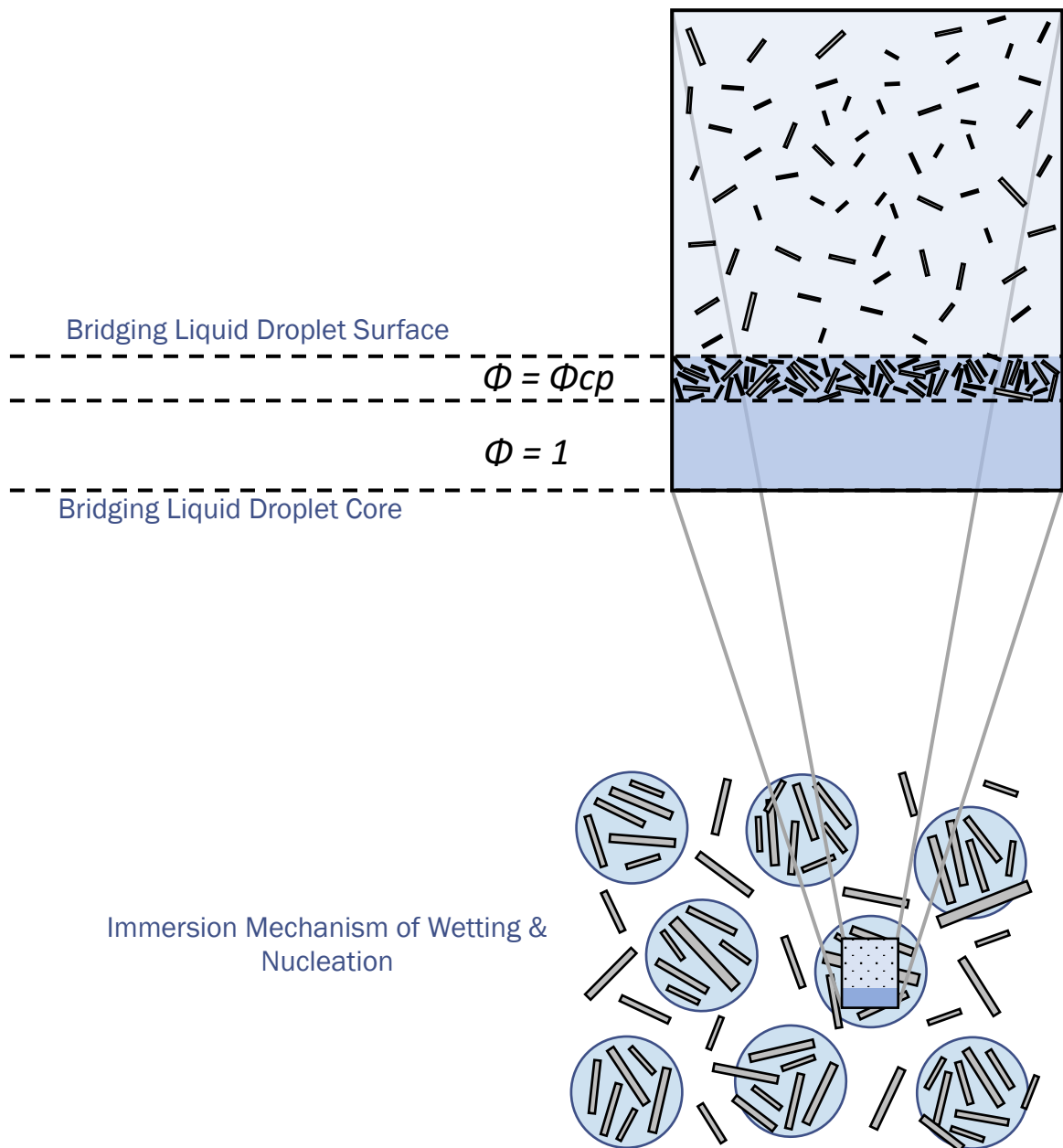


Figure 2.26. The quantification of critical packing volume (ϕ_{cp}) of a unit cell in spherical agglomeration processes. Adapted from Arjmandi-Tash et al., [12].

2.4.2.6 Bridging Liquid Miscibility

Within spherical agglomeration literature, a critical range for BSR is often recognised. Below the critical range, the volume of bridging liquid added to the system is too low to form agglomerates suitable for direct compression. This is usually indicated by the presence of un-agglomerated crystals within the bulk solution and low agglomerate yields. Many studies have found such agglomerates to have poor mechanical properties namely, high friability and porosity. This condition is shown for the distribution and immersion mechanisms below (Figure 2.27a and Figure 2.28a respectively).

The second of these conditions considers a system with a BSR above that of the critical range, where the volume of bridging liquid added to the system is too high. In these processes, agglomerates often form a paste which is impossible to recover and characterise. This condition is shown for the distribution and immersion mechanisms below (Figure 2.27c and Figure 2.28c respectively).

The final condition is a spherical agglomerate process which operates within the critical range. Here, enough bridging liquid is available to incorporate a high percentage of primary crystals, without the formation of a paste. As such, agglomerates are good candidates for direct compression due to their mechanical robustness. This condition is shown for the distribution and immersion mechanisms below (Figure 2.27b and Figure 2.28b respectively).

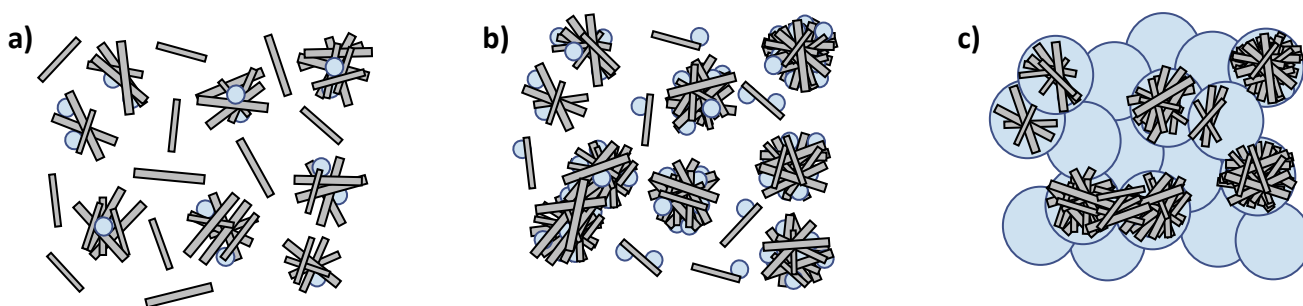


Figure 2.27. A bridging liquid-solid ratio a) below the critical range, b) within the critical range, and c) above the critical range, for the distribution mechanism of spherical agglomeration.

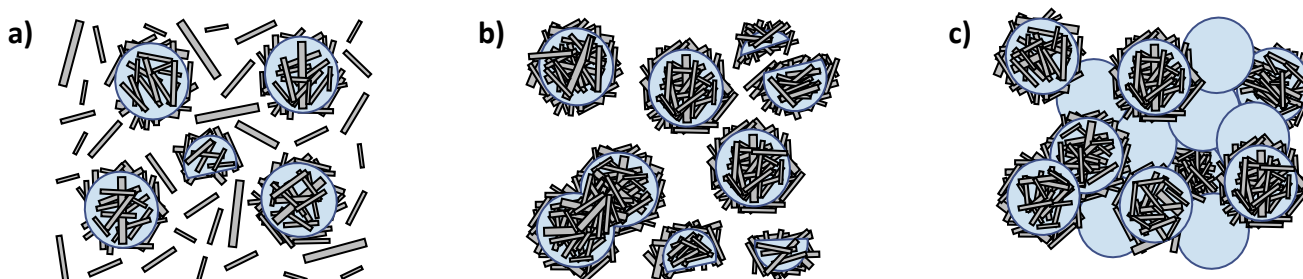


Figure 2.28. A bridging liquid-solid ratio a) below the critical range, b) within the critical range, and c) above the critical range, for the immersion mechanism of spherical agglomeration.

All spherical agglomeration processes should, ideally, operate within the critical range as this maximises product recovery and drastically enhances the likelihood of improvements in the micromeritic properties of bulk crystal powders, which ultimately controls the likelihood of successful tablet formation. This range has previously been identified for a variety of solvent-crystal systems, but there is not a clear methodology for determining this *a priori* [21,45,46,86]. All these studies have relied upon time and cost intensive trial and error experimental work. In the case of developing the process for a newly discovered compound, often, only small quantities are available, meaning such trial-and-error experimental determination is likely to be impossible to complete.

Figure 2.22 shows that the best range of BSR for any given system is very narrow but also very system dependent. This is indicated by a range varying from 0.1 to 1.6 for the six systems shown in Figure 2.22. By contrast, for an analogous wet granulation process the optimum range of binder to solid ratio is largely system *independent* when expressed as the liquid saturation of the granules (Figure 2.21). If the BSR for spherical agglomeration is correctly defined, it too should be largely system independent as well.

The current BSR definition is based upon the volumes of both the bridging liquid and solid of interest introduced to the process. As such, two assumptions are made: a) that there is no solubility of the solid within the system; b) there is complete immiscibility between the bridging liquid and the other two solvents utilised. These assumptions have separate ramifications: a) all crystals are available to be agglomerated; b) all the bridging liquid is available to agglomerate the crystals.

The first assumption is acceptable as, most often, crystals are precipitated through an anti-solvent crystallisation. As such, under the same process conditions, the volume of crystals available to be agglomerated should remain constant across different runs. However, the true volume of bridging liquid available ultimately depends upon the other two solvents used. Most often in pharmaceutical applications, water is used as an anti-solvent, and an organic compound as the solvent, for example acetone or ethanol [10,46,79,86,96]. These solvents are completely miscible to allow precipitation of the crystals of interest. Ideally, the bridging liquid exists as a distinct phase within the agglomeration process as this promotes the immersion mechanism and therefore greater control. For this to occur, either the bridging liquid must be completely immiscible with the bulk solution or the bridging liquid solubility in the bulk solution must be exceeded. The former of these conditions is often impractical to achieve. Here, the ternary phase diagram is imperative to identifying the relative solubility of the bridging liquid in the bulk solution (see Figure 2.12).

Although the relative compositions of each immiscible phase differ significantly, they still contain all three solvent components. The variation in the compositions of these phases is attributed to two phenomena: the transfer of some of the bridging liquid to the bulk solution phase and the transfer of some of the bulk solution to the bridging liquid phase. The bulk solution phase can be referred to as bridging liquid poor as the bridging liquid only forms a small percentage of the phase. The bridging liquid phase can be referred to as bridging liquid rich as, here, the bridging liquid forms the vast majority of the phase, with small quantities of bulk solution present. This is shown in.

2.4.3 Shear Force through Agitation

The agitation speed can directly affect the magnitude of hydrodynamic forces within the agglomeration vessel, especially the shear force. As a result, an increase in agitation speed leads to an increase in the frequency of particle-particle collisions and particle-equipment collisions, which may induce the breakage of particles or agglomerates. However, mixing must be sufficient to promote the formation of a flow profile which allows for adequate liquid-particle collisions. Most studies report an increased particle size with agitation rate. This could be attributed to increased levels of agglomerate nuclei coalescence at higher agitation rates. Further increases in the speed reduce the agglomerate size as high agitation rates have the potential to fragment weaker agglomerates that have already formed [88,97]. This has been reported within a wide range of studies [6,10,23,45,98].

Increases in the size of agglomerates has been reported across a range of low agitation speeds [97]. Similarly, the size distribution of agglomerates becomes larger, whilst a reduction of fines can be observed, as shown in Figure 2.29 [99]. This could be attributed to a shorter contact time between particles and the bridging liquid, meaning agglomerates do not grow uniformly. The average size was found to decrease from 96 μm at 500 rpm to 64 μm at 800 rpm.

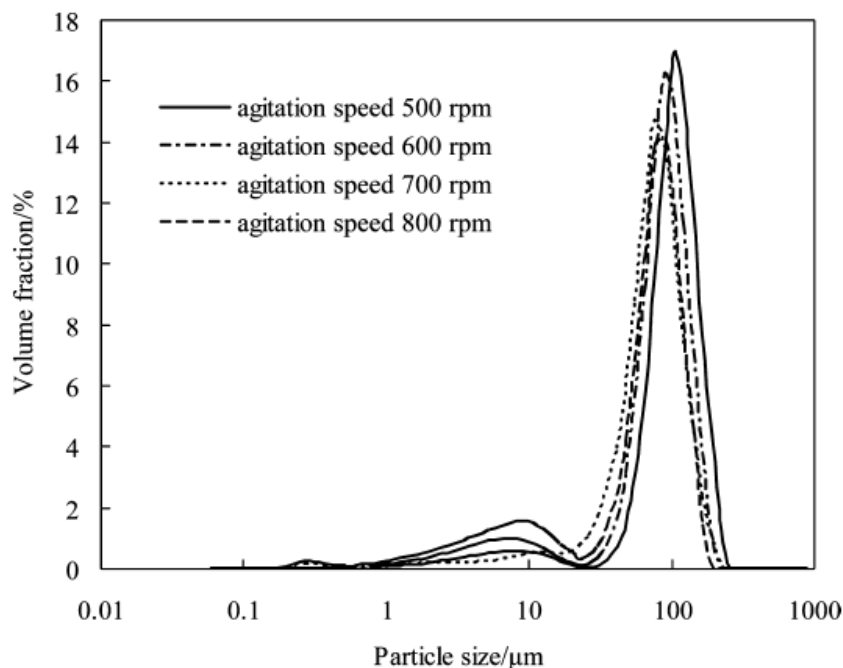


Figure 2.29. The influence of agitation speed on the size distribution of spherical agglomerates of cefotaxime sodium. Adapted from Zhang et al., [99].

The speed of agitation directly influences the nucleation and subsequent crystal growth of primary particles, with increasing speeds promoting nucleation and, thus, decreases in crystal size [100]. Furthermore, the agitation speed also affects the dispersion of the bridging liquid. This has been documented through a reduction in the lower limit of the BSR at higher agitation speeds as the liquid becomes more well-distributed within the system [92]. Higher agitation speeds also favour smaller particles and a faster rate of agglomeration [42]. Agglomeration should be easier at a higher speed, as the likelihood of bridging liquid-primary particle collisions is increased.

The influence of the agitation rate on the mechanical properties of agglomerates has also been reported. The porosity of agglomerates was found to decrease with agitation speed, yielding agglomerates which were more dense and, thus, had a higher compressive strength [45]. These agglomerates were also found to have improved sphericity and flowability [23]. This has been previously attributed to the increased shear forces causing agglomerates to become more compact during growth [6]. These trends have been recognised to lead to reductions in the size of agglomerates [99].

Unfortunately, most studies provide the degree of shear rates as a revolution per minute value only. Whilst this is adequate for a quick comparison between different systems, the unit fails to account for variations in impeller diameters and suspensions volumes. A standardised definition, such as the energy dissipation rate ($\text{m}^{-2} \text{s}^{-3}$), could be used to help alleviate this issue and allow instant comparison across different systems. This parameter is defined as follows:

$$\varepsilon = 0.6 D_{imp} \times \frac{N^3}{V_{susp}} \quad \text{Equation 2.9}$$

where ε is the energy dissipation rate, D_{imp} is the diameter of the impeller, N is the speed of the impeller in revolutions per minute, and V_{susp} is the suspension volume. A definition such as this therefore allows comparisons of different reactors on different scales, and is common in mixing studies as a result, and is thus recommended for the future work in the area. The shear rate clearly affects agglomerate size and size distribution to a degree, although the overall influence of this parameter seems low. Crucially, enough shear must be provided to ensure that particles are adequately suspended, and that the system as a whole remains well-mixed.

2.4.4 Residence Time

The residence time, or the duration of agitation, of particles can also have significant effects on the properties of agglomerates. This is assumed to be as a result of increasing the relative portion of time for processes such as growth and consolidation. Ultimately, a steady-state equilibrium is reached between the rate of both agglomerate growth and breakage. As this equilibrium time is ultimately dictated by other process parameters, it is important to identify when this occurs. The size of the agglomerates produced by spherical agglomeration can be effectively controlled through variations in the residence time of agglomerates. For example, aminophylline agglomerates were found to increase in size over longer residence times, from a mean of approximately 200 μm at 1 hour to 250 μm at 4 hours, until the equilibrium point was reached (approximately 500 μm) [101]. This supports previous studies performed by the same group [18]. This growth can be attributed to the growth rate processes being much higher than the breakage processes initially before the two processes become approximately equal, *i.e.* steady-state is reached.

The size distribution profile of salicylic acid agglomerates has also been shown to be affected over a variety of residence times [35]. The authors found that increases in the residence time created a wider overall size distribution. As more primary particles are incorporated into agglomerates, the size distribution should theoretically narrow. This result was obtained, in contrast, by a theoretical study using population balance models [102]. Some of these are discussed in more detail in [Section 2.5](#). Experimental studies have also reported these findings more recently and attributed these increases as a result of the continued coalescence of particles within the system [47].

Other studies have found that increased residence times also encourage the integration of a higher level of primary particles into spherical agglomerates [98]. This was also found to be directly related to the median diameter of spherical agglomerates of a steroid compound. The same trends were found regardless of the other process parameters which were changed, including temperature and agitation speed. The authors did, however, find that lower residence times are needed when higher speeds are employed. These findings were supported by increases in the weight of agglomerates over time.

The intrinsic mechanical properties of agglomerates are also reported to change with the residence time. One of the first studies to investigate the influence of residence time found that agglomerate porosity decreased with increasing experimental time, even up to a period of two hours [18]. This was attributed to an increased time for the consolidation of agglomerates, resulting in decreasing associated porosity.

One study has investigated such properties in high detail. The authors found a direct relationship between increases in the size and density of spherical agglomerates as the residence time was increased [47]. The same authors also reported that the friability of agglomerates decreases with an increasing residence time, as shown in Figure 2.30. This was also supported by an increase in the crushing strength of agglomerates, as reported elsewhere in the literature [45,86]. Agglomerates formed over two hours were approximately twice as strong as those formed over one hour and four times stronger than those formed over thirty minutes. Interestingly, this relationship is relatively linear over a wide range of particle sizes, suggesting the agglomerate formation was relatively uniform.

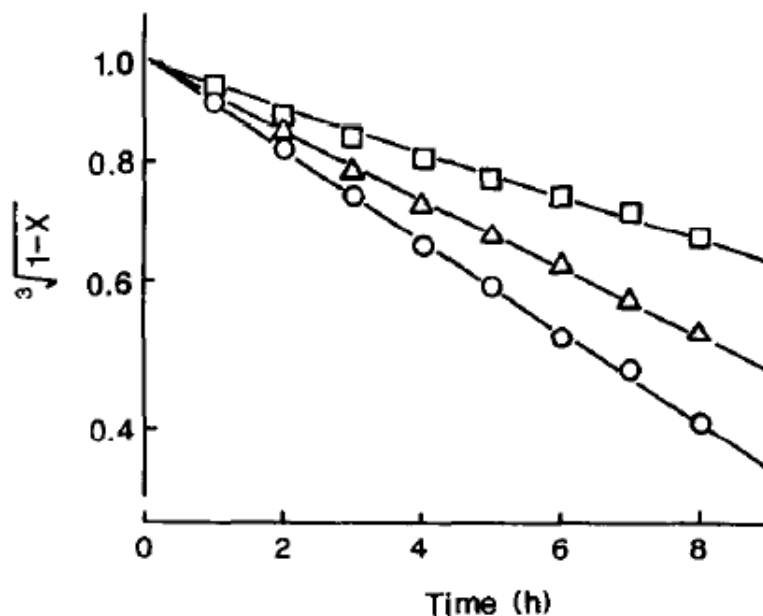


Figure 2.30. The relationship between friability of buccillamine agglomerates and the residence time of agglomerates: (○) 30 minutes; (△) 60 minutes; (□) 120 minutes. Here, X represents the pulverised fraction of agglomerates. Reproduced from Morishima et al., [47].

Residence time of agglomerates is shown to directly influence the end product properties obtained and should be considered as a means of optimising the performance of spherical agglomeration processes. The kinetics associated with the residence time, such as wetting and growth, are intrinsically linked to the agglomerate properties, and thus should be studied in further detail as a means of understanding and developing these relationships further. This is emphasised by a lack of studies which track agglomerate populations and their properties over a range of residence times.

2.5 Current Modelling in Spherical Agglomeration

2.5.1 Models of Agglomeration in Suspension Systems

The modelling of spherical agglomeration is complex, especially without a full understanding of the mechanisms which drive the process. Some modelling work has been undertaken, however. A population balance model (PBM) was developed to predict any changes in the agglomerate size distribution [49]. This work included terms for both coalescence and breakage as well as growth. The model was found to be useful for predicting the agglomerate size distribution at steady state. The study did not focus on the nucleation and growth of crystals but purely their agglomeration.

Initially this was solved using an agglomeration rate kernel which could account for additional factors, including particle concentrations, supersaturation and crystal size, amongst others [53]. A multi-layer agglomeration model was then developed which accounted for the efficiency of agglomeration based upon the collision mechanisms, Brownian *brow*, laminar *lam*, or turbulent *turb* [103,104]. These are represented respectively in Equation 2.10 through to Equation 2.12. As the particle size increases through agglomeration, the collision mechanism changes from Brownian to laminar, and finally to turbulent.

$$\beta_{i,j,b} = k_{A,brow} G_{agg} \frac{(S_i + S_j)^2}{S_i S_j} \quad \text{Equation 2.10}$$

$$\beta_{i,j,l} = k_{A,lam} G_{agg} (S_i + S_j)^3 \left(\frac{P}{\nu}\right)^{\frac{1}{2}} \quad \text{Equation 2.11}$$

$$\beta_{i,j,t} = k_{A,turb} G_{agg} \frac{(S_i + S_j)^2}{S_j} M\left(\frac{S_i}{S_j}\right) ND \left(1 - \frac{(S_i + S_j)^2}{\lambda_c^2}\right) \quad \text{Equation 2.12}$$

where k_A is the agglomeration rate constant, G_{agg} is the growth rate of agglomerates, S_i and S_j refer to the size of particles i and j , P is the dissipated power per unit mass, ν is the kinematic viscosity, M is Marchal's relative size function, N is the agitation speed, D is particle diffusivity and λ_c is the Taylor microscale.

It is worth noting that these kernels apply directly to crystallisation processes in which agglomeration arises, not agglomeration in suspension systems. However, the effects of hydrodynamics, particle size and concentration have been verified experimentally as relevant to both

(see Figure 2.31)[49]. The kernels developed incorporated the supersaturation level and temperature of the system within the growth rate term; supersaturation increases promote strengthening of the liquid bridges, which, in turn, increases the efficiency of the process [105].

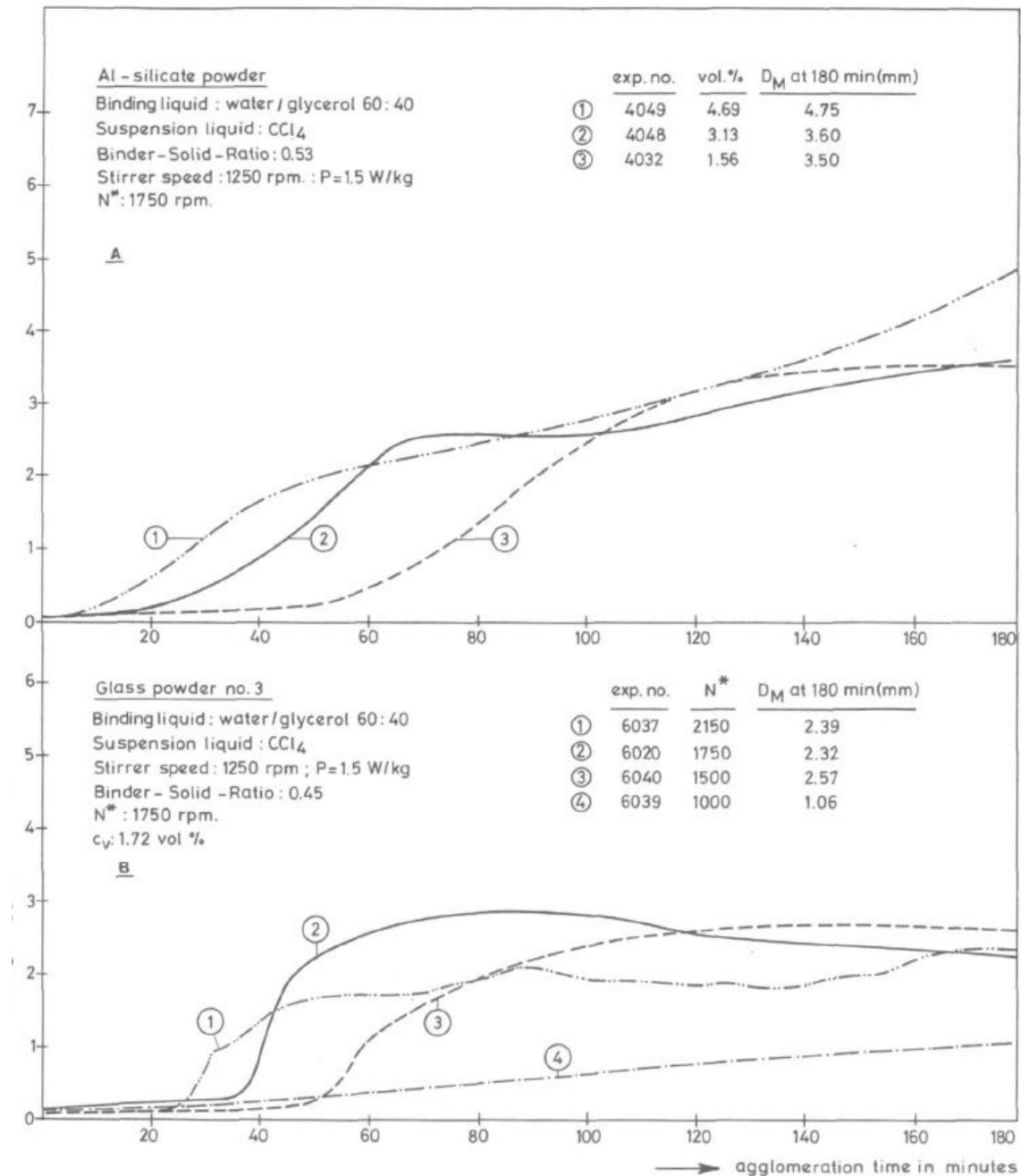


Figure 2.31. The relationship between experimental growth curves as a function of a) particle concentration and b) agitation speed during bridging liquid injection. Reproduced from Bemer [49].

Other work has investigated the Monte Carlo approach to solve multi-dimensional kernels designed for agglomeration in suspension [102]. The bridging liquid composition was included in these kernels. The bridging liquid is a critical parameter in forming spherical agglomerates.

$$\beta = \beta_0(S_i^3 + S_j^3) \left((c_i + c_j)^\alpha \left(100 - \frac{c_i + c_j}{2} \right)^\delta \right)^A \quad \text{Equation 2.13}$$

$$c_i = \frac{\text{volume of liquid}}{\text{volume of the agglomerate}} \times 100 \quad \text{Equation 2.14}$$

$$\delta = \left(\frac{1 - c_{opt}}{c_{opt}} \right) \delta_l \quad \text{Equation 2.15}$$

where c_i is the volume percentage of the binding agent, defined in Equation 2.14, δ is the weight coefficient of solid particles and δ_l is the weight coefficient of liquid particles. This composition function, Equation 2.14, is derived to account for the level of bridging liquid present within agglomerates; those with too much bridging liquid, or not enough, will not form agglomerates. Equation 2.15 accounts for both the amount of bridging liquid and the weight coefficients of both solids and droplets, ensuring that agglomeration cannot occur without sufficient wetting. This serves as an efficiency term by which the agglomeration processes reach an equilibrium. These kernels could more accurately predict the agglomeration size distribution, improving upon the previous work [49].

Other work has also looked into the modelling of the growth period of agglomerates [45,50]. A combination of experimental and modelling work was performed once the most significant characteristics of the process were identified, building on previous work [49]. The authors concluded that four mechanisms are present during the agglomeration process [45]:

- i. Bridging liquid droplets form and engulf solid particles; agglomerate nuclei form within these droplets.
- ii. The collisions of droplets cause a decrease in the size of agglomerate nuclei through a compaction mechanism.
- iii. The process conditions dictate the level of growth and consolidation of agglomerates, *i.e.* agitation speed, amount of bridging liquid.

- iv. Compaction mechanism no longer occurs; agglomeration ends and there is no further growth in size.

The authors found the relative relationship between the bridging liquid-solid ratio, particle solid concentration and agitation rate of the system studied, [Equation 2.16](#). Through experimental observations, a ‘*growth only*’ agglomeration model was then established, [Equation 2.17](#):

$$S_{final} = A_p \cdot C_S^{0.3} \cdot N^{-0.6} \cdot BSR^{2.1} \quad \text{Equation 2.16}$$

$$\frac{\delta\psi(S, t)}{\delta t} = R_A(S, t) \quad \text{Equation 2.17}$$

where S_{final} is the final agglomerate size, A_p is a proportionality constant, C_S is the solid concentration of particles and BSR is as defined previously in [Equation 2.7](#). In [Equation 2.17](#), ψ is the number density function, t is the agglomeration time and R_A is the agglomeration rate distribution. This final parameter can be separated into the agglomeration rate of rank $r_{agg}(l, t)$, agglomeration kernel K , the probability of two particles meeting f , and the efficiency of agglomeration, eff , as shown in [Equation 2.18](#) through to [Equation 2.21](#) respectively:

$$r_{agg}(l, t) = K(i, j, t) N_i(t) N_j(t) \quad \text{Equation 2.18}$$

$$K(i, j, t) = f(i, j, t) \text{eff}(i, j, t) \quad \text{Equation 2.19}$$

$$f(i, j, t) = C_{coll} \alpha(i, j, t) \left(\frac{\pi}{4}\right) (S_i + S_j)^2 \left[\overline{u(S_i)^2} + \overline{u(S_j)^2}\right]^{0.5} \quad \text{Equation 2.20}$$

$$\left\{ \begin{array}{ll} \text{eff}(i, j, t) = \frac{f_{adh}(i, j, t)}{f_{sep}(i, j, t)} - 1 & \text{if } f_{adh}(i, j, t) \geq f_{sep}(i, j, t) \\ \text{eff}(i, j, t) = 0 & \text{otherwise} \end{array} \right. \quad \text{Equation 2.21}$$

The target efficiency, $\alpha(i, j, t)$, accounts for the densities of both agglomerates and fluids, as well as the fluid viscosity. Collision velocities are calculated from the relative velocity of particles and fluids as a function of energy dissipation. The agglomeration efficiency is the ratio of adhesive forces to disruptive forces. The former, $F_{adh}(i, j, t)$, accounts for deformation energies and collision energies.

The deformation energy is related to the strength of agglomerates and is influenced by porosity and BSR. The adhesion forces equation is given in [Equation 2.22](#). The collision energies are related to the particle size as well as its interfacial energy and binding force. The latter, $F_{sep}(i, j, t)$, is a function of shear stress and dissipation energies. The separation force is given in [Equation 2.23](#). The notation for [Equation 2.18](#) to [Equation 2.23](#) is displayed in [Table 2.6](#).

$$F_{adh}(i, j, t) \propto \left[\frac{def^{\max(i, j, t)}}{D_p/2} \right]^2 (1 - \mathcal{P}(t)) F_{bridge} \left(\frac{S_i^2 + S_j^2}{S_i^3 + S_j^3} \right) \quad \text{Equation 2.22}$$

$$F_{sep}(i, j, t) \propto \rho_{susp} [\varepsilon(S_i + S_j)]^{\frac{2}{3}} \cdot (S_i)^2 \quad (S_i < S_j) \quad \text{Equation 2.23}$$

All the previously discussed models agreed with the experimental data, as shown in [Figure 2.32](#). The key difference between these two papers is that the latter ignores breakage and fragmentation due to the experimental observations of deformation and compaction during collisions [49,50]. The work to date on modelling has used experimental results and observations to improve the models which describe the critical mechanisms of the agglomeration process. Different growth regimes in the formation of agglomerates were observed and a model developed to combine coalescence and breakage to aid the prediction of these [49].

Differences in agglomeration with fluid flow regimes and particle sizes allowed the development of models with multilayer agglomeration kernels [103]. These models were improved upon further through the addition of terms which account for the bridging liquid composition [45]. Finally, the most comprehensive model to date has been established, which accounts for both mechanistic phenomena and the operating conditions of spherical agglomeration [50].

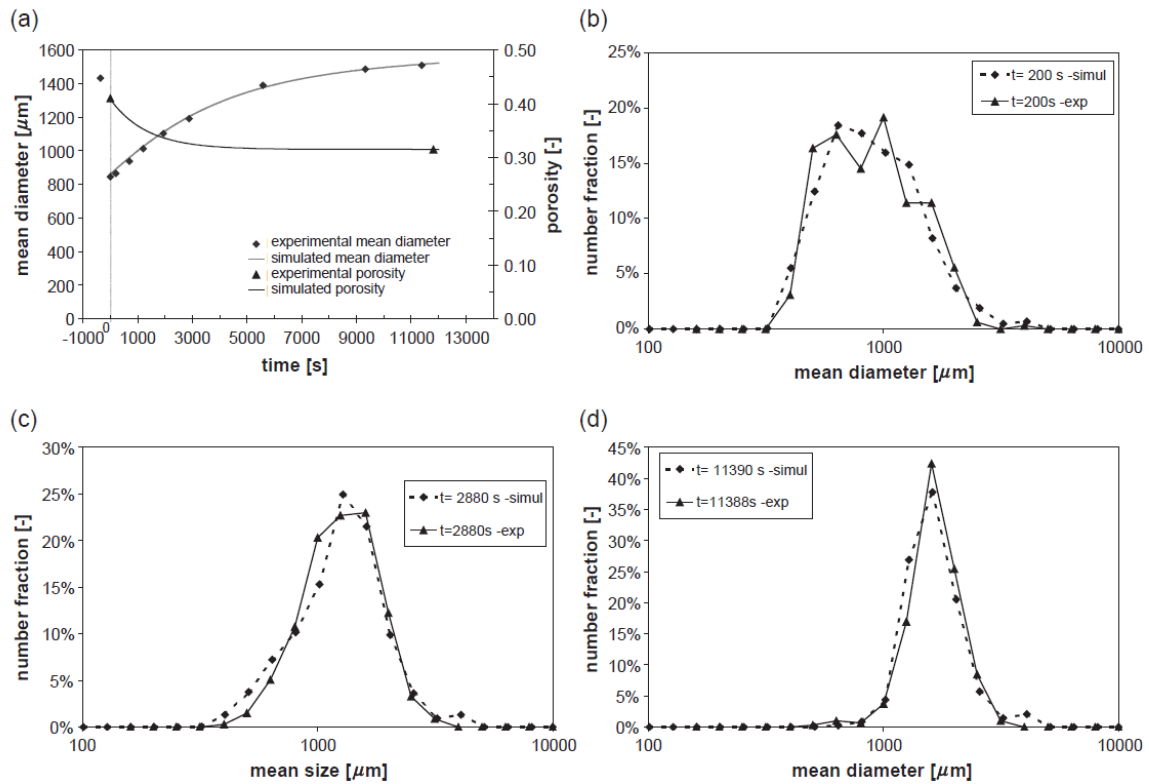


Figure 2.32. The comparison between experimental and modelling results for a) mean diameter and porosity, and the number particle size distribution at agglomeration times of b) 200 secs, c) 2880 secs and d) 11390 secs. Reproduced from Blandin et al., [50].

Table 2.6. Nomenclature for Equation 2.18 through to Equation 2.23 [50].

Nomenclature	Definition	Units
$r_{agg}(l, t)$	Agglomeration rate of rank $l = l(i, j)$ at time t	$\text{nb m}^{-3} \text{s}^{-1}$
$K(i, j, t)$	Agglomeration kernel, function of time and particles i and j	-
$N_i(t); N_j(t)$	Concentration of agglomerating particles, i and j with time	nb m^{-3}
$f(i, j, t)$	Product of the meeting probability	-
$\text{eff}(i, j, t)$	Agglomeration efficiency	-
C_{coll}	Kinetic parameter; matched on agglomeration experiments	-
$\alpha(i, j, t)$	Target efficiency of the process	-
$S_i; S_j$	Size of agglomerates under consideration	m
u	Collision velocity of particles	m s^{-2}
$F_{adh}(i, j, t)$	Adhesion force	N
$F_{sep}(i, j, t)$	Shear-induced disruptive force	N
def^{max}	Contact surface radius	m
D_p	Primary particle diameter	m
$\mathcal{P}(t)$	Mean porosity of the agglomerates	-
F_{bridge}	Force exerted by a liquid bridge between two elementary particles	N
ρ_{susp}	Density of suspension	Kg m^{-3}
ε	Specific stirring power	W kg^{-1}

2.5.2 Models of Simultaneous Crystallisation and Agglomeration Systems

Whilst these studies show the progression of models over time, there is still scope for further improvements to accurately predict and control spherical agglomeration processes. There has been a tendency for studies to separate the agglomeration process, either investigating crystallisation systems which exhibit agglomeration [53], or the agglomeration of particles which have been pre-suspended in solution [49]. However, some studies have investigated crystallisation and agglomeration in the same process [46,86]. Here, the authors investigated whether the addition of bridging liquid was preferential during or after crystallization. They concluded that the bridging liquid itself, and thus, the agglomeration step, was much more critical in the formation of dense spherical agglomerates, when compared to the anti-solvent crystallization. To increase understanding within these processes, it is important to use experimental knowledge surrounding the nucleation, growth and agglomeration mechanisms which govern the process. The changes of the primary particles themselves should also be considered [106], despite the difficulty in this observation. This is reflected in the challenges of identifying when rate processes occur, their duration, and their dependence upon one another.

Other modelling work has investigated the use of a coupled PBM framework to evaluate the agglomeration of needle-like crystals [106]. This framework features a 2D population balance equation to describe the two-dimensional growth of crystals. This method allowed a kernel to be developed which accounted for both the lengths of crystals during agglomeration, as well as their specific orientation.

The authors also identified five key issues which are current barriers to filling the knowledge gap in the modelling of spherical agglomeration processes [106]. These are as follows:

1. *'Experimental tools that allow for the measurement of both shape and degree of agglomeration simultaneously.'*
2. *'Require a suitable modelling framework that enables description of entire crystallisation procedures with a high level of accuracy.'*
3. *'Obtain a better grasp of the roles of both fluid dynamics and mixing.'*
4. *'The use of adequate models to describe the collision frequency and the agglomeration efficiency of non-equant crystals, considering their rotational anisotropy.'*
5. *'Instructive ways of analysing experiments and comparing them to models, to inform of us of shortcomings and to improve predictions.'*

The modelling of the process is challenging but ultimately relies upon a key understanding of the mechanisms which drive the process. Without considering all these mechanisms, and in sufficient detail, models will fail to accurately predict the agglomeration process.

2.6 Further Applications of Spherical Crystallisation

The applications of spherical crystallisation are wide and varied, with the process itself being applied in a variety of industries which deal with fine particulate materials. As mentioned in [Section 2.1](#), this includes the agglomeration of graphite, coal and sand in the bulk chemicals industries [14–16]. Further to this, there is the application of the technique for the co-agglomeration of particles and excipients prior to tableting, as well as the continuous operation of the process as a whole. Both applications are discussed in more detail in [Section 2.6.1](#) and [Section 2.6.2](#) respectively.

2.6.1 Co-agglomeration of Crystals and Additives

The co-agglomeration of particles with suitable additives is a further route to vastly improving the efficiency of manufacturing processes for solid dosage formats within the pharmaceuticals industry. Co-agglomeration potentially allows the removal of downstream blending and formulation unit operations, allowing agglomerates to be directly tableted and packaged. Additives previously investigated in spherical crystallisation include polymers to improve the physicochemical properties of the agglomerates themselves, and disintegrants to improve the *in vivo* dissolution profile of the drug. This is possible due to high polymorph stability of compounds [107,108].

Carbamazepine-saccharine cocrystals have previously been agglomerated with a variety of different bridging liquids [6,83]. The role of sodium starch glycolate on agglomerate properties has been investigated [6]. The disintegrant was found to vastly improve the dissolution profile of sodium starch glycolate agglomerates compared to the pure agglomerates. The authors did note, however, a significant reduction in the recovery yield of the cocrystals. Sodium starch glycolate was insoluble other than in the dissolving solvent, which led to sedimentation within the system overall. The influence of mannitol, a disintegrant, in the co-agglomeration of bovine serum albumin has also been investigated, with the dissolution profile of the drug also significantly improved [20].

The influence of polymers on spherical agglomerate properties has also been investigated. An improved dissolution rate has been found for agglomerates of mefenamic acid which were co-

agglomerated with hydroxypropyl methyl cellulose (HPMC) [71]. The inclusion of a surfactant in tolbutamide spherical agglomerates found similar results, with the dissolution rate improvements being attributed to the increased wettability of the agglomerates [80].

In a separate study, the incorporation of HPMC into aceclofenac agglomerates led to an increase in agglomerate size [23]. The authors also noted that increasing concentrations of HPMC led to subsequent increases in the agglomerate size. This was attributed to an increased level of particle-particles interactions during agglomerate formation, which promoted bridging liquid “squeezing out”. As a result, more bridging liquid was available for agglomerate growth. Whilst the aceclofenac-HPMC agglomerates had a higher porosity compared to agglomerates formed without HPMC, increasing concentrations of HPMC were found to decrease their porosity. This could be explained by an increase in the layering mechanism of growth and, thus, a subsequent decrease in the degree of consolidation.

Two studies by Kawashima et al., investigated the influence of the addition of polyethylene glycol (PEG) into agglomerates of phenytoin [109,110]. The authors discovered that the co-agglomeration of phenytoin with PEG led to dramatic improvements in the mechanical strength of agglomerates compared to pure agglomerates of phenytoin. Upon further characterisation of agglomerate structure, it was noted that the PEG was able to form solid bridges between phenytoin crystals, which promoted the observed strength increase. Furthermore, the authors noted the significantly smoother surface of agglomerates. In one of these studies, PEG was found to increase the rate of dissolution of the agglomerates in water, most likely as a result of the hydrophobic tendency of PEG [109]. In the second study, increasing the concentration of PEG during the co-agglomeration procedure led to a decrease in the overall mean size of agglomerates [110]. The authors also stipulated that the introduction of PEG led to an overall reduction in the cohesive force necessary for particles to agglomerate, through a reduction in the interfacial tension and wettability of the bridging liquid.

As the physicochemical properties of agglomerates can be altered through the incorporation of additives, it is feasible that such properties could be directly tailored through a combination of polymer additions, including hydroxypropyl cellulose (HPC). This has been successfully achieved in one study, where the sphericity and dissolution profiles of agglomerates could be accurately tailored [79]. The authors noted that co-agglomerating etodolac with a specific polymer blend (HPMC-PEG-HPC) resulted in a superior product with improved flowability and dissolution.

Co-agglomeration could provide a viable option for simplifying the manufacturing process, specifically formulation and blending unit operations, required for oral solid dosages prior to tableting. Whilst the product quality of agglomerates can be improved directly in this nature, care must be taken

to ensure no adverse effects persist. This includes whether the addition of polymers affects the solvent system itself, namely the solubility of components in each other, the overall viscosity of the system, and the interfacial tensions of the system components themselves. Ultimately, this can disturb and disrupt the overall agglomeration process.

2.6.2 Continuous Spherical Crystallisation

As previously discussed, spherical agglomeration can drastically improve the micromeritic properties of crystal particles, especially those with a naturally acicular morphology. The enhancement in the size and shape of particles is mirrored in their dynamic powder properties, namely their flowability and tableability. As a result, the downstream processing of such particles is significantly simplified through the reduction in the required number of unit operations. A stream-lined process such as this not only decreases the equipment costs of manufacturing but further benefits in terms of energy and time intensity. This in turn increases throughput, which would allow comparably more product to be delivered to market in the same period of time.

Continuous manufacturing processes can further improve product quality and process efficiency, all whilst retaining robust and predictable performance [3]. The transition from batch to continuous manufacturing processes has already been successful in a variety of different chemical engineering sectors: petrochemicals and fine chemicals [111]; pharmaceuticals [112]; foods [113]. The benefits of continuous manufacturing have been highlighted in a plethora of peer-reviewed papers. These include reductions in the energy and cost requirements as well as a reduction in the quantity of waste produced [3]. Whilst regulatory issues have previously been a cause for concern, especially for governing and executive bodies, improvements to in-line monitoring using process analytical tools (PAT) have allowed the Food & Drug Administration (FDA) to approve continuous manufacturing processes [114].

The earliest recorded work for continuous operation of spherical agglomeration was performed in 1982, observing the preparation of sulfamethoxazole wax matrices [84]. A single-stage continuous mixed suspension mixed product removal (MSMPR) crystalliser was used to investigate agglomeration mechanisms. The authors, along with others, have noted the presence of different mechanisms in the size enlargement regime when compared to batch spherical agglomeration [91].

In continuous spherical agglomeration, a fast growth period persists prior to a decrease in the overall mean size of agglomerates. There is some residual growth in the system before finally, the mean

size plateaus at a relatively constant value [91]. In contrast, batch systems usually follow a period of zero growth in agglomerate size, succeeded by a fast growth period prior to the mean size plateau [49,91]. The initial fast growth period in continuous spherical agglomeration has previously been attributed to a reduced slurry density and poor bridging liquid dispersion. Both factors occur due to the MSMPR not reaching continuous steady state prior to the addition of crystalline particles. As both the bridging liquid droplets and crystalline particles are not evenly distributed throughout the MSMPR, flocculation tends to dominate rather than agglomeration. As these flocs compact, larger than normal agglomerates are produced. As the MSMPR reaches continuous steady state, the slurry density increases, and the dispersion of bridging liquid and crystalline particles becomes almost uniform. As a result, agglomerate nuclei form more evenly throughout the reactor and are more uniform in size but critically, smaller than the agglomerates produced prior to continuous steady state (size reduction period). It is worth noting however, that between both batch and continuous processes, the same overall trends can be drawn between the final physicochemical properties of agglomerates as a function of operating conditions. The role of operational conditions is discussed in more detail in [Section 2.5](#).

The work by Kawashima et al., and Bos & Zuiderweg was extended by using a two-stage continuous MSMPR [32]. The use of a two-stage system allowed the authors to isolate the crystallisation and agglomeration phenomena, permitting a more in-depth study of the mechanisms of each: first stage for crystal nucleation and subsequent growth of individual crystals and the second stage for crystal agglomeration. In the first stage, the crystals are dissolved in a solvent and then precipitated with an anti-solvent. The crystal population could be controlled through the solvent to anti-solvent ratio (SASR), the amount of shear applied to particles and their residence time within the crystalliser. In the second stage, the solution of crystals is infused along with the bridging liquid, promoting the agglomeration of crystals. As before, the shear rates and residence time could be accurately controlled, as well as the bridging liquid to solid ratio (BSR). Because the operational parameters of both stages can be controlled independently, it is possible to directly tailor both the crystallisation and agglomeration stages to produce spherical agglomerates with the desired final properties.

The authors went on to extend their work further through the use of an oscillatory baffled crystalliser (OBC) [115]. This plug-flow configuration crystalliser has many benefits over a traditional crystalliser. For instance, both the primary particle and agglomeration size distributions can be accurately controlled through the process parameters. Due to the nature of the reactor, the

temperature profile through the crystalliser could be controlled accurately, as well as the as solvent streams, crystal solution and bridging liquid solution. As a result, the crystallisation and agglomeration mechanisms can be separated and studied independently despite the process occurring in a single-stage. The authors noted the high level of autonomy of the system and improved consistency over their prior work. Their work highlighted how continuous spherical agglomeration can produce spherical agglomerates with the desired properties through fine control of the system process.

Other studies have investigated the influence of continuous operation of emulsion solvent diffusion (ESD) [116]. In their study, a single-stage continuous MSMPR crystalliser was used. Whilst ESD does differ from spherical agglomeration, the authors did find trends in the operating parameters and final agglomerate properties. These trends align with those for batch systems, which are discussed in more detail in [Section 2.5](#). The authors also made use of a reservoir in the experimental set-up, which allowed solvent to be recycled back into the reactor. Subsequently, crystalline particles have more bridging liquid available for the formation of agglomerate nuclei, leading to an improved yield overall. This system could be incorporated into spherical agglomeration systems which utilise a single-stage continuous MSMPR crystallisers. It is worth noting however, that continuous MSMPRs only operate at a single point in the ternary phase diagram which reduces the overall yield of agglomerates.

2.7 Critical Summary

The available literature surrounding spherical crystallisation, generally, is wide and varied. Many studies have concentrated on spherical agglomeration, specifically investigating the process using drug compounds such as salicylic acid, an active metabolite of aspirin. Most of these studies have offered major insights into the influence of process parameters on the agglomeration process itself, and the agglomerates produced. This has included the influence of temperature, agitation speed and solid loading, amongst others. These studies have been successful and provide general relationships between process parameters and the critical quality attributes of drug molecules, including size, porosity, and mechanical strength. Some of these studies are summarised in [Table 2.7](#).

Additionally, the spherical agglomeration modelling is currently under-developed. There are a limited amount of studies which directly address modelling the entirety of the process. Also, there is a lack of studies which attempt to clearly define the rate processes which govern spherical agglomeration. Whilst some models have been developed for the process, and their performance has been verified experimentally for the model system used, it remains to be seen whether these models

can be applied universally. Finally, a full model which incorporates all rate processes is not currently available. This is primarily due to studies focussing on different elements of spherical agglomeration, with some models failing to account for other influential rate processes as discussed.

The vast majority of the literature covers spherical agglomeration in batch operation only. For the continuous operation of oral solid dosages to be successful, from initial molecule synthesis through to the end-stage packaging, all processes must be fully modelled in a way which offers predictable performance. This performance must persist, regardless of the operational parameters, or indeed the drug molecule itself. The development of such models would vastly improve both the macro-scale production of final formulations, as well as the micro-scale production of new research and development molecules.

From the presented literature, a key gap in the currently available knowledge has been identified. The relationships identified between process parameters and product properties should be underpinned directly by relevant rate parameters, which should also be validated experimentally. Here, the analogies between spherical agglomeration and wet granulation have been qualitatively recognised within the literature.

However, the quantitative approaches for wet granulation, including key dimensionless groups and regime maps for engineering design, have not been applied to spherical agglomeration. Additionally, there are a lack of mechanistic studies which investigate the role of the bridging liquid-solid ratio on the rate processes of spherical agglomeration, despite its recognition as a key process parameter. This makes current prediction difficult, with the impact of miscibility between the binder and solvent not being fully recognised. Here, approaches from wet granulation can be used, but the impact of bridging liquid miscibility, which is not an issue in wet granulation, must be included. Hence, a new definition is required to evaluate the effect of bridging liquid miscibility on overall agglomerate properties. Such parameters are key to the success of developing robust models which can address the industrial challenges discussed. As such, there is the potential to rapidly intensify the production of both new and existing drug molecules.

Table 2.7. Summary of the effects of process parameters on spherical agglomeration processes and products.

Parameter	Influence
Solvent Addition Method	Good solvent with crystal of interest added to poor solvent-bridging liquid mixture found to produce more compact and spherical agglomerates [38] Rate of bridging liquid infusion produces unclear effects [42,84] Simultaneous precipitation and agglomeration produces more agglomerates, improved flowability and compressibility [88,92]
Bridging Liquid	High wettability leads to large, dense spherical agglomerates [21] High vapor pressure of bridging liquid drives supersaturation [83]
Original BSR Value	Must be in the critical range for successful agglomeration, with increases in this range producing larger agglomerates [45,86] Too low – little, if any, agglomeration [21,46] Too high – paste product forms with poor flowability [21,46]
Temperature	Initial increases in temperature decrease agglomerate size. Further increases lead to larger agglomerates being formed [38] Bulk density and sphericity found to decrease with increases [6] Constituent crystal size increases [38]
Agitation Speed	Low speed increases promotes increases in agglomerate size [97] High speeds decreases the agglomerate size [6,23,45] Agglomerate size distribution was also found to broaden at higher speeds [99] Increases can reduce level of bridging liquid required [92] Porosity increases with speed, whilst strength, sphericity and flowability decrease [23,45]
Residence Time	Increased agglomerate size with residence time [101] Sphericity and strength increase also [45,86] Porosity decreases / agglomerate density increases [45,47]

2.8 Research Objectives

This thesis aims to develop and further the mechanistic understanding of spherical agglomeration processes in order to aid in the development of robust and predictive models. This research will specifically identify and investigate parameters which influence wetting and nucleation rate processes as ultimately these dictate the subsequent rate processes and the overall unit operation. Here, a combination of theoretical, simulation and experimental elements are combined. Within the literature, no studies account for the role of solvent miscibility, especially that of the bridging liquid. Furthermore, it is not clear whether studies have focussed on the operation within the immiscible region of ternary solvent systems, where process control is much greater. The main objectives of this thesis are to:

- 1. Identify and quantify the influence of bridging liquid miscibility on the binder liquid volume available in spherical agglomeration processes, including the effects of different bridging liquids, solid loading levels and bulk solution compositions.*
- 2. Experimentally validate this theory, with the aim of standardising bridging liquid volume reporting within future literature.*
- 3. Investigate the immersion nucleation mechanism and associated kinetics using a model compound, comparing the results with mathematical models previously developed.*

CHAPTER 3: MATERIALS & METHODS

3.1 Introduction

This chapter outlines the materials and methodologies used within this research. Figure 3.1 displays a workflow of the described methodologies undertaken. First, titration experiments and Aspen simulations used for ternary phase diagram construction are described. An analysis was performed in which further examination of the bridging liquid-solid ratio, allowed the true bridging liquid-solid ratio to be defined. The results are presented within Chapter 4. The experimental validation of the definition is then described, including agglomeration and characterisation methodologies. These results are presented within Chapter 5. Finally, the methods are described for a study into the agglomeration kinetics of paracetamol, with results presented within Chapter 6.

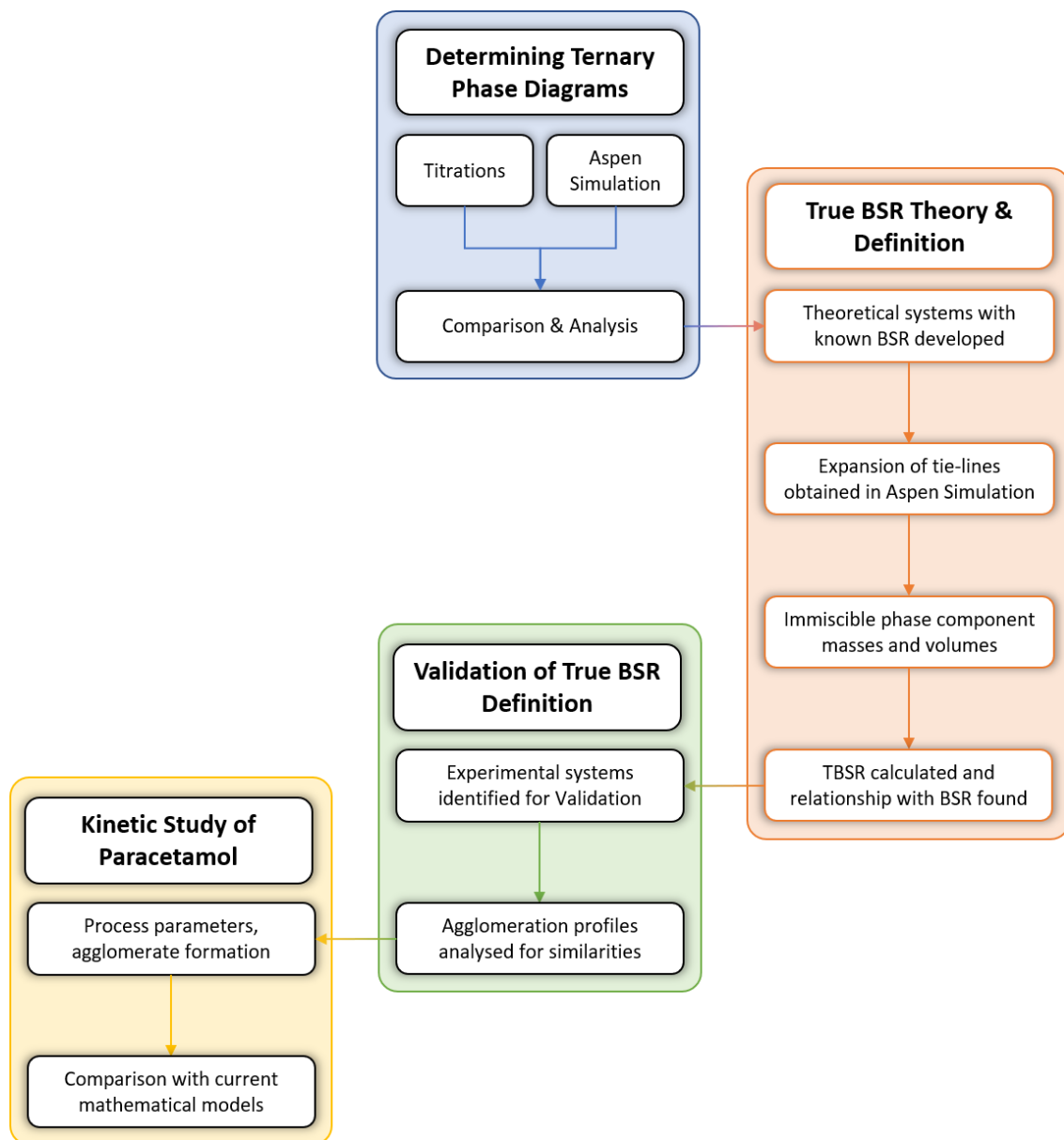


Figure 3.1. An overview of the methodologies conducted within this research and their order within this thesis.

3.2 Materials

The following solvents were purchased from Sigma-Aldrich (UK) for use as a bridging liquid: chloroform (99+ %), heptane (99 %), toluene (99.8 %). The following solvents were purchased from Acros Organics (UK) for use as a bridging liquid: 4-methylpentan-2-one (MIBK, 99 %), butyl-acetate (99+ %). Acetone (≥ 99.8 %) was used as a solvent and purchased from Sigma-Aldrich. Distilled water was used in all experimental work. The properties of these solvents are given in Table 3.1. Salicylic acid was purchased from Sigma-Aldrich. Paracetamol was kindly prepared and provided by Dr N Rajoub of the University of Strathclyde. Table 3.2 provides common properties of these solids.

Table 3.1. Standard properties of solvents used at 1 atmosphere and 25 °C [76].

Chemical Species	Molecular Formula	Molecular Weight (g mol ⁻¹)	Density (g cm ⁻³)
Acetone	C ₃ H ₆ O	58.079	0.7845
Chloroform	CHCl ₃	119.378	1.4788
Heptane	C ₇ H ₁₆	100.202	0.6795
MIBK	C ₆ H ₁₂ O	100.158	0.7965
<i>n</i> -Butyl acetate	C ₆ H ₁₂ O ₂	116.158	0.8825 ^a
Toluene	C ₇ H ₈	92.139	0.8668 ^a
Water	H ₂ O	18.015	0.9970

^a Values at 20 °C

Table 3.2. Standard properties of solids used at 1 atmosphere and 20 °C [76].

Chemical Species	Molecular Formula	Molecular Weight (g mol ⁻¹)	Density (g cm ⁻³)
Paracetamol	C ₈ H ₉ NO ₂	151.163	1.2930
Salicylic Acid	C ₇ H ₆ O ₃	138.121	1.4430

For the determination of ternary phase diagrams, the following solvents were used: water/acetone mixtures as a bulk solution; and chloroform, heptane, MIBK, *n*-butyl acetate or toluene as a bridging liquid. In addition, bridging liquid/acetone mixtures were used as a bulk solution, with water as a third solvent. For the TBSR validation, water/acetone mixtures were used as a bulk solution. Chloroform, MIBK or *n*-butyl acetate were used as bridging liquids. Salicylic acid was used as the solid. For the kinetic study, water was used as a bridging liquid, heptane was used as the suspending liquid and paracetamol is used as a solid.

3.2.1 Characterisation of Materials

3.2.1.1 Salicylic Acid Size Distributions

Salicylic acid particles were sieved at an amplitude of 2.25 mm for 10 minutes on a 45 μm sieve and pan to encourage breakage (Retsch AS200 Sieve Shaker). The sample within the pan was retained and used in subsequent experiments. These samples are referred to as *prepared* from hereon in, with *commercial* samples referring to off the shelf product as purchased. The particle size distribution of samples was measured with a Malvern MasterSizer 3000 (Malvern Instruments Ltd, Malvern, UK). The dry cell was attached and used to feed samples through the instrument. Particles pass through an emitted laser beam, and the beam is scattered, allowing particles between of 0.01 μm and 3500 μm to be measured. During measurements, both the air pressure and feed rate were adjusted as necessary to ensure an obscuration percentage of 1-6 %. This is the recommended region for obtaining reliable measurements. The sample was fed until fifteen separate measurements were obtained. Figure 3.2 shows the averaged results for commercial and prepared salicylic acid.

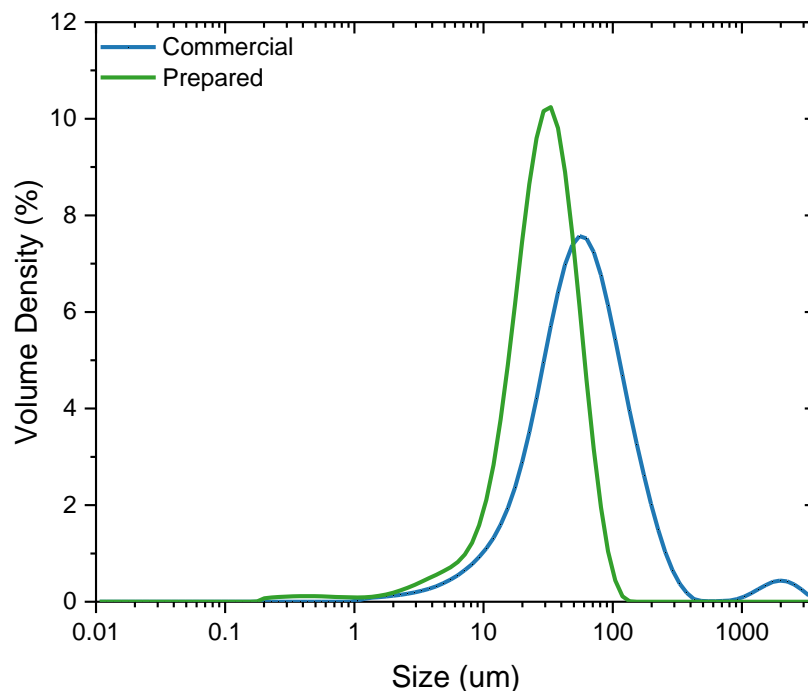


Figure 3.2. The particle size distributions of commercial salicylic acid and prepared, sub 45 μm salicylic acid particles.

3.2.1.2 Static Contact Angles of Bridging Liquid-Solid

The static contact angles of a bridging liquid on the solid were measured using a goniometer (FTÅ200, First Ten Ångstrom, Sweden). Here, the sessile-drop method was used to determine the contact angle of the liquid at the solid-liquid interface in air. The set-up is shown in [Figure 3.3](#). A custom die produced in-house was used to form tablets of the required solid. The die had an internal diameter of 2 cm (see [Figure 3.4](#)). The die was partially filled with the solid before pressure being applied by hand for one minute. The tablet was recovered and mounted on a slide for further analysis.

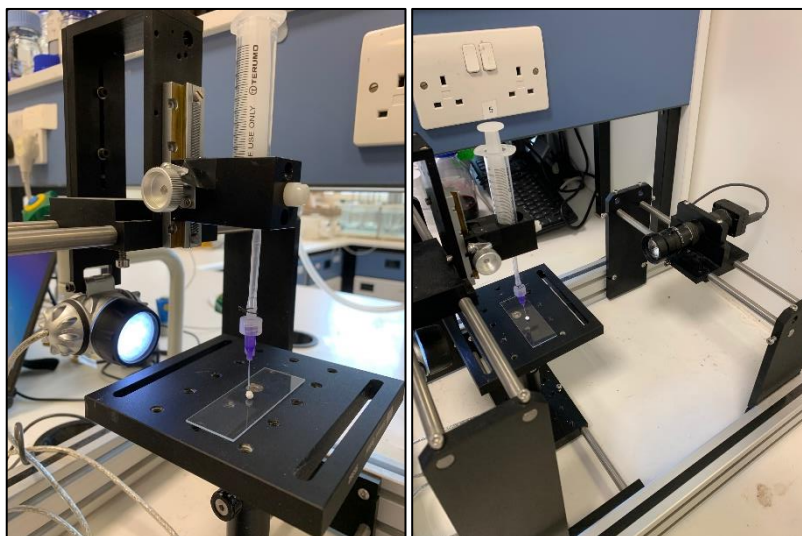


Figure 3.3. The experimental set-up of the goniometer system used for contact angle measurements.



Figure 3.4. The die and press used to form tablets for contact angle analysis.

A syringe with needle tip was positioned directly above the tablet. A droplet of the required solution was allowed to form at the needle tip and dropped directly onto the powder bed. The experiment was recorded using an integrated camera. The video was analysed in FTÅ-32 software (First Ten Ångstrom, Sweden). A minimum of five droplets were observed for each system. The results are displayed in Figure 3.5 through to Figure 3.8. Here, frames are taken one thirtieth of a second apart, the maximum frame rate possible (30 fps). The contact angle was measured as 0° , or perfectly wetting, for chloroform and *n*-butyl acetate. MIBK had a contact angle of approximately 33° after 0.033 of a second. It should be noted that the following frame (0.067 secs) showed a contact angle of 0° , indicating perfect wetting, albeit on a slower scale. This is shown in Figure 3.6.

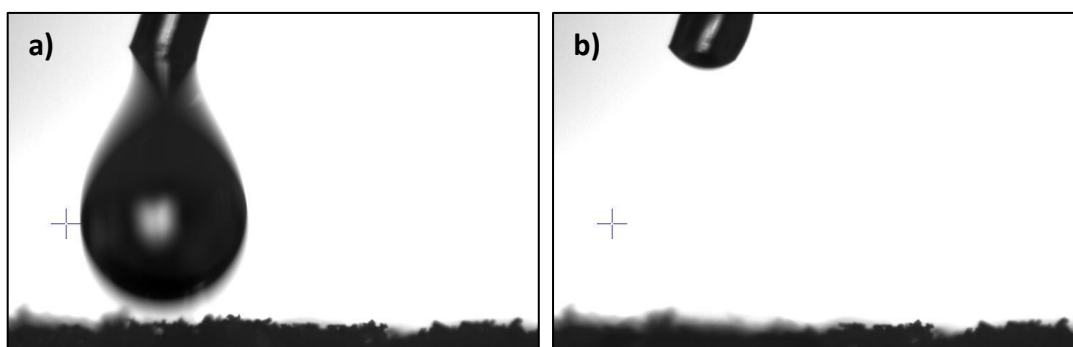


Figure 3.5. The contact angle measurements of chloroform on a salicylic acid tablet, with a) chloroform droplet prior to measurement and b) the next frame showing perfect wetting.

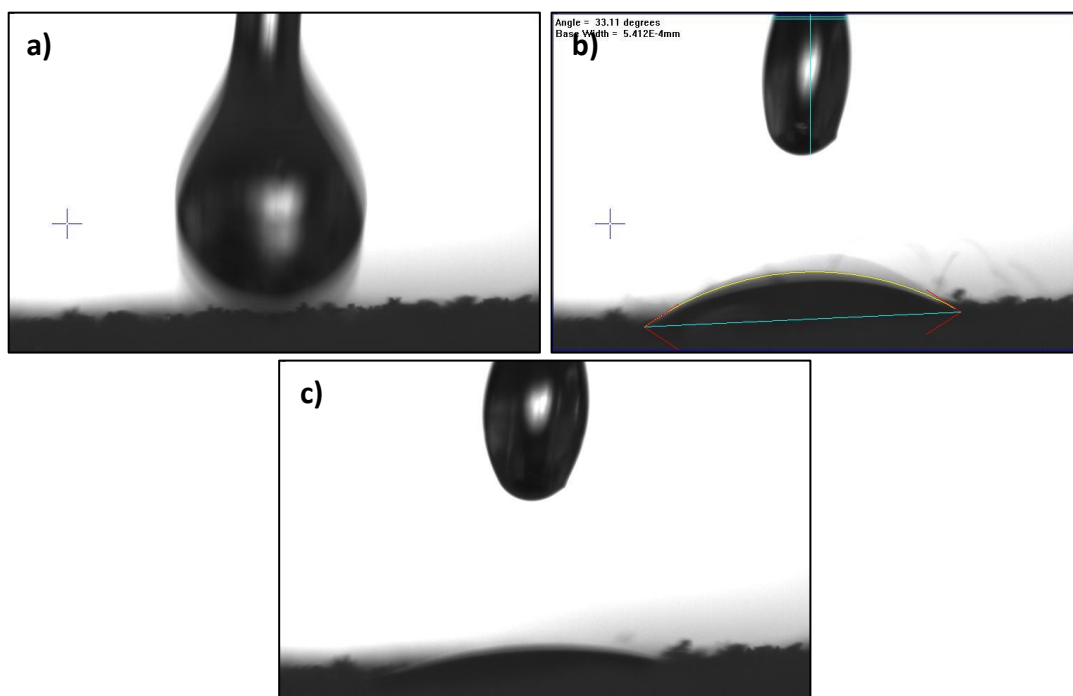


Figure 3.6. The contact angle measurements of MIBK on a salicylic acid tablet, with a) MIBK droplet prior to measurement, b) the next frame with a contact angle of 33 degrees and c) the subsequent frame showing perfect wetting.

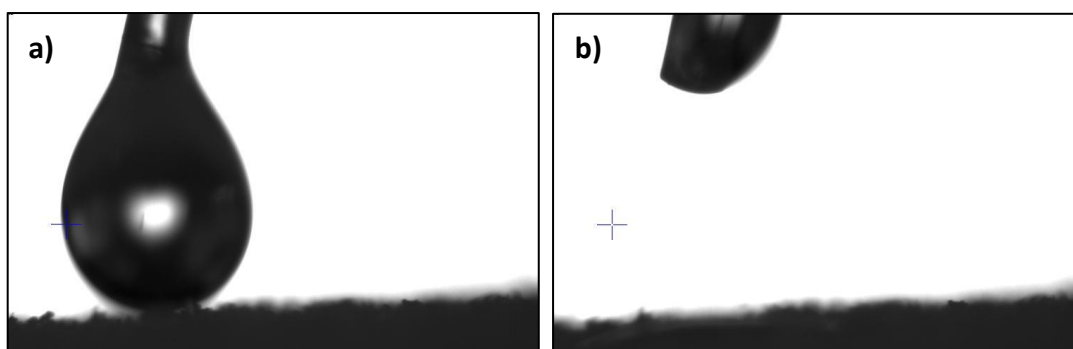


Figure 3.7. The contact angle measurements of *n*-butyl acetate on a salicylic acid tablet, with a) *n*-butyl acetate droplet prior to measurement and b) the next frame showing perfect wetting.

Contact angles measurements were performed using two different liquids on a hand-pressed tablet of paracetamol. This tablet was formed using the method as described previously. The measurements were performed as per the method described previously. The results are displayed in Figure 3.8.

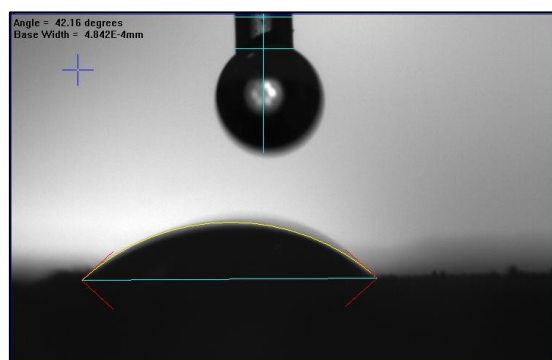


Figure 3.8. Contact angle of water, approximately 42°, on a micronised paracetamol tablet.

3.3 Hypothesis of the True Bridging Liquid-Solid Ratio

As the crystals of interest are preferentially wet by the bridging liquid, only the bridging liquid rich phase is available to agglomerate the crystals of interest. Thus, the volume of this bridging liquid-rich phase should be accurately quantified and reported.

As shown in Figure 3.10, the anti-solvent is denoted X, the solvent Y and the bridging liquid Z. X and Y are fully miscible, whilst Z is selected for its immiscibility with the X-Y mixture. If we plot the X-Y-Z ternary phase diagram, a significant two-phase region exists. Here, a solvent rich continuous phase

and a bridging liquid rich discrete phase form. The definition of the bridging liquid-solid ratio is given as:

$$BSR = \frac{V_Z}{V_S} = \frac{\frac{M_Z}{\rho_Z}}{\frac{M_S}{\rho_S}} \quad \text{Equation 3.1}$$

where the mass of solid within the system is M_S , and the mass of three liquid components in the system, on a solids free basis, is M_X , M_Y and M_Z respectively. The true density of the bridging liquid and solid are represented as ρ_Z and ρ_S respectively. Provided that the masses of each liquid component given, the ternary phase diagram can be used to identify the system conditions. If the system lies within the immiscible two-phase region, the tie-lines can be interpolated to give the composition of the discrete phase and the continuous phase. These can be given as x_X, x_Y, x_Z and y_X, y_Y, y_Z respectively. A mass balance on any of the three liquid components allows the mass fraction of the bridging liquid-rich phase to be calculated:

$$M_Z = x_Z M_D + y_Z (M_T - M_D) \quad \text{Equation 3.2}$$

where M_D represents the mass fraction of the dispersed or bridging liquid-rich phase. M_T represents the total system mass:

$$M_T = M_X + M_Y + M_Z \quad \text{Equation 3.3}$$

The well-known inverse lever rule can be obtained if we rearrange **Equation 3.2**, where M_D is the true amount of the bridging liquid rich phase available to agglomerate the solid (see **Equation 3.2**). This is represented graphically in Figure 3.9.

$$M_D = \frac{M_Z - y_Z M_T}{x_Z - y_Z} \quad \text{Equation 3.4}$$

Thus, the true bridging liquid to solid ratio is given:

$$TBSR = \frac{V_D}{V_S} = \frac{\frac{M_D}{\rho_D}}{\frac{M_S}{\rho_S}} \quad \text{Equation 3.5}$$

Here, M_Z describes the amount of bridging liquid which is lost to the continuous phase, M_C . This relationship is primarily influenced by the interfacial tension, which is in turn, governed by a variety of thermodynamic properties.

$$M_D = M_Z - M_C \tag{Equation 3.6}$$

If the phase is considered to be an ideal solution, ρ_D can be estimated as:

$$\frac{1}{\rho_D} = \sum \left(\frac{x_i}{\rho_i} \right) \tag{Equation 3.7}$$

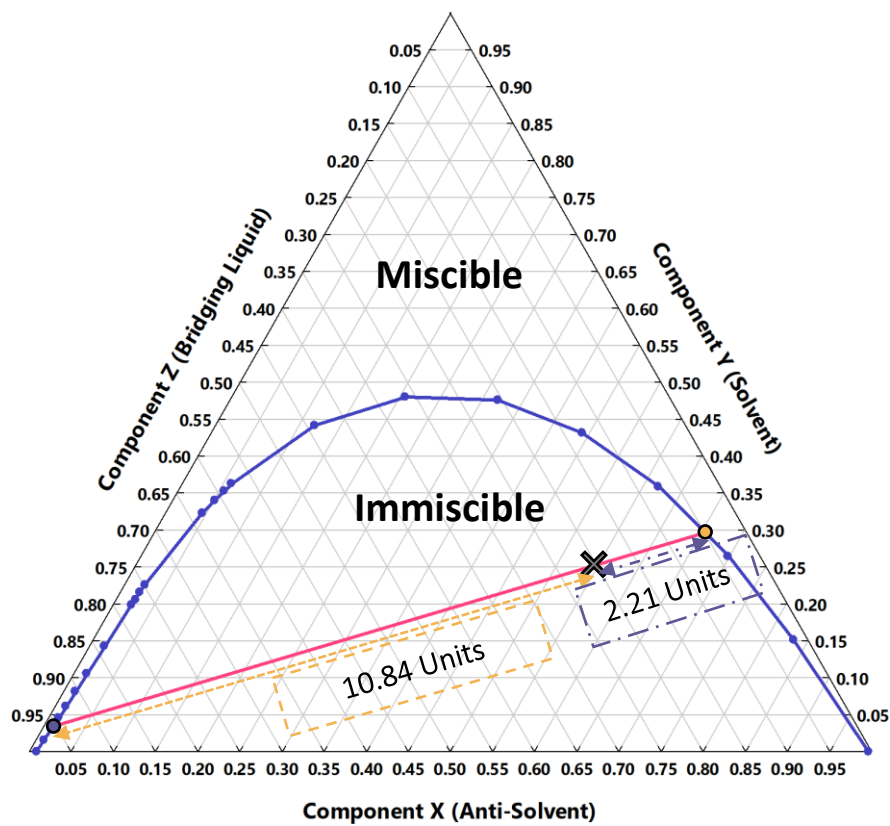


Figure 3.9. An example of a ternary phase diagram where X is the anti-solvent, Y is the solvent and Z is the bridging liquid. The cross represents a system of interest, and the circles the immiscible phase compositions. Values represent an exemplar of the inverse lever rule.

3.4 Determination of Ternary Phase Diagrams

This section details both experimental and simulation approaches for the determination of the ternary phase diagrams. The results are presented and discussed within [Chapter 4](#). The interfacial tensions values of different bridging liquids in water are listed in [Table 3.3](#). These values provide an indication of bridging liquid miscibility, that is, the degree of bridging liquid available to agglomerate the particles of interest.

[Table 3.3](#). A review of experimental data for the interfacial tension (dyne cm^{-1}) of bridging liquids in water.

	Chloroform	Heptane	MIBK	Butyl acetate	Toluene	Ref
Interfacial Tension in Water at 25 °C (dyne cm^{-1})	30.8	50.1	10.4	-	35.4	[117]
	31.6	50.2	-	14.5	36.1	[118]
	32.8 ^a	50.2	10.1	14.5	36.1	[119]
	31.6	50.2	10.1	14.5	36.1	[120]
	31.1	50.1	-	-	35.8	[121]
	-	-	-	15.0 ^b	35.8 ^b	[122]

^a Values at 20 °C; ^b Values at 17 °C.

3.4.1 Experimental Approach & Methodology

The following methodologies describe the titrations used to obtain the binodal curve for ternary phase diagrams. All experiments were conducted within a fume cupboard at 19.5 °C (± 0.5 °C). The bridging liquids used were those identified in [Table 3.3](#). A solution of one of these bridging liquids and acetone was prepared in varying compositions as identified in [Table 3.4](#). The solutions were made to a mass of 20 g in a 50 ml conical flask.

Whilst under vigorous agitation by hand, distilled water was added to the solution dropwise from a burette. Upon the formation of a two-phase solution, the boundary between miscible and immiscible regions is reached. The change is identified visually by a cloudy solution being formed or droplets within the solution forming after agitation is stopped. The mass of water added to reach this state was noted. Two further repeats were also performed. The nineteen conditions specified in [Table 3.4](#) produced fifty-seven data points of the first half of the binodal curve.

The second half of the binodal curve was determined using solutions of water and acetone in varying compositions (see [Table 3.5](#)). These solutions were also made to a mass of 20 g in 50 ml conical flasks. The bridging liquid required was titrated dropwise from a burette, recording the mass added at

the onset of two immiscible phases being formed, as per the method described above. Across nine conditions, triplicates produced a further eighteen data points for the binodal curve. Each triplicate data point was considered individually, and no averages were taken.

Table 3.4. Water titrations into various bridging liquid-acetone solutions for experimental determination of the binodal curves.

Initial Solution Composition (% w/w)	
Bridging Liquid	Acetone
95	5
90	10
85	15
80	20
75	25
70	30
65	35
60	40
55	45
50	50
45	55
40	60
35	65
30	70
25	75
20	80
15	85
10	90
5	95

Table 3.5. Bridging liquid titrations into various water-acetone solutions for experimental determination of the binodal curves.

Initial Solution Composition (% w/w)	
Water	Acetone
40	60
50	50
60	40
70	30
80	20
90	10

The mass of each solvent was known at the end point of each titration, which allowed the final composition (% w/w) of the solution to be calculated. For each bridging liquid, the ternary phase diagram is plotted using Origin Pro.

3.4.2 Simulation Approach & Methodology

The following section describes the methodology to obtain ternary phase diagrams in Aspen software. Tie-lines are lines of equilibrium within the immiscible region of a ternary phase diagram. Provided that the system composition is known, the relative composition of each immiscible phase can be calculated from the tie-lines. The system location along this line also provides the relative mass of each immiscible phase. As such, the full masses of all three components, in both immiscible phases, can be calculated from the tie-lines.

To evaluate the tie-lines of each ternary phase diagram, Aspen Plus was used (v8.4, Aspen Technologies). Here, several thermodynamic models commonly used in liquid-liquid extraction models were used, which incorporate activity coefficients, and the results compared [123]: the Universal Quasi-Chemical, or UNIQUAC, model; the Universal Quasi-Chemical Functional-group Activity Coefficient (UNIFAC) model; the Universal Functional-group Liquid-Liquid (UNIF-LL) model; and the Universal Quasi-Chemical Redlich-Kwong (UNIQU-RK) model. The conditions of the experimental titrations were replicated within Aspen, *i.e.* 19.5 °C and 1.01325 bar. The maximum number of tie-lines was obtained each time (twenty-five). The maximum number of iterations was set to five thousand, with a mole fraction error tolerance of 1×10^{-5} . The data for binodal curves and tie-line values produced in the previous section were analysed in Origin Pro. Using the molecular weights identified in [Table 3.1](#), the mole fractions were converted to masses, and then mass fractions (see [Appendix A](#) for details). These values were then plotted.

3.5 TBSR Validation Methodologies

This section describes the methodologies for validating the TBSR definition. The results obtained from these procedures are detailed in [Chapter 5](#). Here, a 1 L agglomerator and Rushton turbine are used for spherical agglomeration, the geometries of which are displayed in [Table 3.6](#).

Table 3.6. Geometry of reactor and impeller used within validation experiments.

Geometry	Distance (mm)
Agglomerator inner diameter	90
Agglomerator outer diameter	100
Impeller shaft diameter	8
Impeller diameter	30
Impeller blade height	6
Impeller blade width	7.5
Impeller height from agglomerator floor	30

3.5.1 Agglomeration Methodology

For the agglomeration experiments, salicylic acid saturated mother solutions were prepared at the following solvent compositions: 95 % w/w water, 5 % w/w acetone, 90 % w/w water, 10 % w/w acetone; 85 % w/w water, 15 % w/w acetone..

12 g of the sieved salicylic acid was suspended in the saturated mother solution (388 g). This corresponds to a 3 % w/w loading, not accounting for the mass of bridging liquid to be added. The system was agitated for one minute at 750 rpm to disperse the solid within the saturated solution in a 1 L agglomerator, as shown in Figure 3.10. The bridging liquid was then manually added from a measuring cylinder through a funnel in the top of the reactor, corresponding to an infusion time of approximately one second. The funnel was replaced with parafilm to ensure the system remained closed and evaporation was limited.

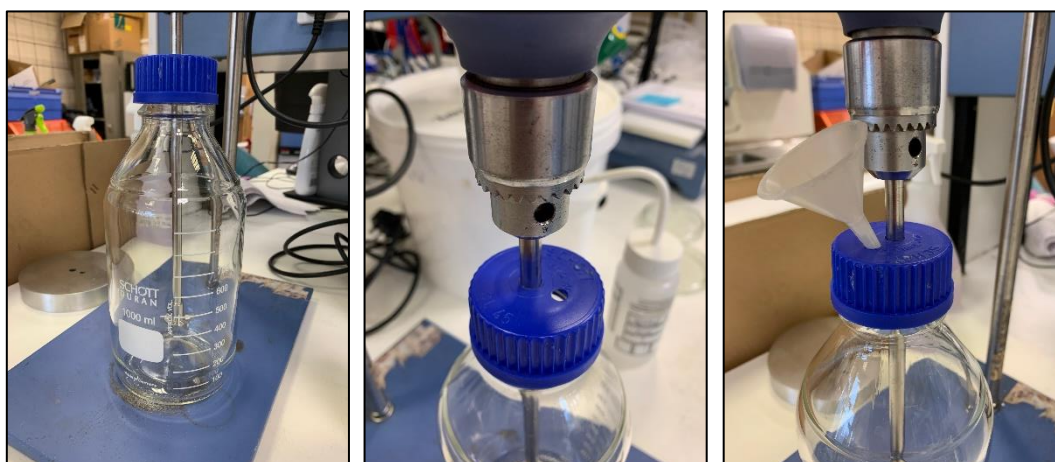


Figure 3.10. Agglomerator set-up.

3.5.2 Characterisation of Agglomerates

To analyse the percentage of crystals agglomerated, the agglomeration suspensions were filtered after 45 minutes, using glass microfibre filter papers with a pore size of 1.2 μm . Agglomerates were washed with distilled water. The retentate was allowed to dry overnight at room temperature. The sample was then sieved using a variety of different sieve meshes on the sieve shaker at an amplitude of 0.40 mm for 30 seconds. The smallest mesh used was 300 μm and the largest mesh used was 8 mm. The agglomerate mass retained in each sieve was noted and a particle size distribution determined for each experiment. Particles which passed through all sieve meshes were recovered from the pan (< 300 μm) and were considered un-agglomerated. These results were used as the basis for a comparison between different agglomeration systems in validation of the TBSR definition.

3.6 Kinetic Study of Spherical Agglomeration Processes

3.6.1 Experimental Methodology

All experiments were conducted at 21 $^{\circ}\text{C}$ (± 0.5 $^{\circ}\text{C}$). There are several common elements across both residence time and TBSR studies undertaken in this work. These are described here, with differences highlighted in the following subsections. Here, a 150 ml agglomerator and three blade-pitched impeller are used for spherical agglomeration, the geometries of which are displayed in [Table 3.7](#).

[Table 3.7. Geometry of reactor and impeller used within kinetic experiments.](#)

Geometry	Distance (mm)
Agglomerator inner diameter	55
Agglomerator outer diameter	60
Impeller shaft diameter	65
Impeller diameter	35
Impeller height from agglomerator floor	20

All systems were agitated at a speed of 500 rpm unless otherwise stated. 47.5 g of heptane was used to suspend 2.5 g of paracetamol, which corresponded to a solid loading of 5 % w/w, unless otherwise stated. Distilled water saturated with paracetamol was used as a bridging liquid in all

experiments. It should be noted that heptane and water are completely immiscible; here, the BSR is equal to the TBSR.

3.6.2 Imaging Methods

Samples were imaged using a Navitar 12 x zoom lens (Image Optics, UK) equipped with a dome diffuser LED light (Model LGT.19.MF2d, Haishu Honyu Opto-Electro Co., Ltd, Ningbo, PR China). A Luminera Infinity 3 camera and Infinity Analyse software was used to capture the images. This is displayed in [Figure 3.11](#). Scale bars were added manually using images of a calibration slide at different zoom levels. Size measurements were performed by importing the images to Pixelink μ Scope software. Within the software, the software was calibrated to ensure measurements performed corresponded to the actual scale of the picture. No further image alteration was performed.



Figure 3.11. The experimental set-up of the Luminera Infinity 3 camera with 12 x zoom lens and LED light dome diffuser.

3.6.3 Process Parameters Study

A variety of TBSR values were investigated in the range of 0.2-8. The bridging liquid was added from a volumetric pipette into a port in the reactor lid. This corresponds to a bridging liquid addition time of approximately 1 second. In some experiments, the bridging liquid was dyed with Acid red IV (Sigma Aldrich, UK). This allowed identification of the bridging liquid. Samples were recovered every five minutes using a Pasteur pipette. These samples were imaged both before and after drying, as per the method discussed in [Section 3.6.2](#). All experiments were repeated using a solid loading of 1 % w/w,

and a solid loading of 9 % w/w. Effect of shear rate experiments were performed at a TBSR of 0.75 and a solid loading of 5 % w/w. The shear rate was adjusted using impeller speeds of 300 rpm, 500 rpm and 700 rpm.

3.6.4 Agglomerate Formation Kinetics

The required bridging liquid volume was dispensed from a volumetric pipette through a port opening in the reactor lid. The TBSR of 0.75 was used at a 5 % solid loading and shear rate of 500 rpm. A second set of experiments used bridging liquid samples dyed with Acid Red IV (Sigma Aldrich) to allow visualisation and identification of bridging liquid as a function of time. The solution was sampled using a Pasteur pipette to recover agglomerates in solution at various time intervals.

3.6.5 Percentage Agglomeration

Individual experiments were performed for each time point investigated: 10 mins through to 120 mins in 10-minute intervals. The TBSR of 0.75 was used at a 5 % solid loading and shear rate of 500 rpm. Once the desired residence time was reached, the experiment was stopped. The solution was poured through a 212 μm sieve (Retsch) positioned directly above a Buchner flask with a 0.7 μm pore sized filter paper. Heptane was used to wash agglomerates. Agglomerates retained on the sieve were dried overnight and weighed. Material retained on the filter paper was also dried overnight and weighed to calculate the percentage agglomerated. Triplicates were performed for each time point.

3.6.6 Agglomerate Size & Sphericity

Individual experiments were performed for each time point investigated. The TBSR of 0.75 was used at a 5 % solid loading and shear rate of 500 rpm. At the desired residence time, the experiment was stopped. A sample of the suspension was isolated in a small petri dish. Imaging of the samples used the method described in [Section 3.6.2](#). Size measurements were performed by importing the images to Pixelink μScope software. The number of agglomerates measured was typically in the range of 500 – 750 individual agglomerates per time interval. The experiments were repeated. The aspect

ratio of agglomerates was used as an indication of their sphericity. This required measurement of the shortest physical dimension and dividing this by the longest physical dimension. This was also performed in Pixelink μ Scope software.

3.6.7 Agglomerate Density

At the required time, a sample of the suspension was removed and placed on a microscope slide. Images were immediately taken, as per [Section 3.6.2](#). The samples were dried overnight at room temperature. Individual agglomerates were weighed using a microbalance (Mettler Toledo, UMT2). Agglomerates were transferred using a small probe or tweezers. Here, only the most spherical agglomerates are used to limit error in the volume calculation. The diameter is measured in both the x and y dimensions. In the instance a small difference between the values was found, an average of the two was taken. This allowed a volume to be estimated and the density calculated, assuming the third dimension to be the same value. A minimum of ten agglomerates were measured for each time interval. The mean density was then calculated. Triplicates of the experiments were performed.

**CHAPTER 4: THE TRUE
BRIDGING LIQUID TO
SOLID RATIO – THEORY**

4.1 Introduction

The literature review presented within **Chapter 2** provided an overview of the current state of the art, with respect to the influence of process parameters and mechanistic understanding of spherical agglomeration. Crucially, the bridging liquid-solid ratio (BSR) was found to be one of the most critical process parameter (**Section 2.4.2**) [35,47,83,84,99]. This parameter can be used to control the overall agglomerate properties, including size, porosity *etc.* The parameter is defined as a dimensionless ratio:

$$BSR = \frac{V_z}{V_s} \quad \text{Equation 4.1}$$

where V_z is the volume of binder liquid added and V_s is the volume of the solid (crystalline) phase in the system. There is consensus in the literature that a critical range of the BSR prevails for all agglomeration systems [21,45]. Within **Section 2.4.2**, the influence of solvent miscibility, including that of the bridging liquid, was mentioned and how this is not accounted for within the current literature. To address this, the following objectives were developed:

- Identify the degree of miscibility within ternary solvent systems, using reproducible and robust methods.
- Analyse results to account for the full bridging liquid volume added, across both immiscible phases.
- Highlight the need for a new definition, using a variety of different exemplar systems.

Here, a new definition is developed and discussed: the true bridging liquid-solid ratio (TBSR). This definition aims to standardise bridging liquid volume reporting by accounting for solvent miscibility of ternary solvent systems. This chapter will highlight the need for the definition by looking at several different agglomeration systems.

4.2 Agglomeration Systems

To evaluate the equations presented, several agglomeration systems were identified. The agglomeration systems were based upon the literature presented within [Chapter 2](#). These components are commonly used within the context of spherical agglomeration: acetone as the solvent; water as an anti-solvent; a partially immiscible bridging liquid. Solid loadings of 1 % w/w, 3 % w/w and 5 % w/w were used, as these were found to be common within the literature. These systems were based upon the ternary phase diagrams determined through titration and computational methods (see [Section 3.3](#)). Common properties of the solvents used within this section are listed below.

Table 4.1. Standard properties of solvents used at 1 atmosphere and 25 °C [76].

Chemical Species	Molecular Formula	Molecular Weight (g mol ⁻¹)	Density (g cm ⁻³)
Acetone	C ₃ H ₆ O	58.079	0.7845
Chloroform	CHCl ₃	119.378	1.4788
Heptane	C ₇ H ₁₆	100.202	0.6795
MIBK	C ₆ H ₁₂ O	100.158	0.7965
<i>n</i> -Butyl acetate	C ₆ H ₁₂ O ₂	116.158	0.8825 ^a
Toluene	C ₇ H ₈	92.139	0.8668 ^a
Water	H ₂ O	18.015	0.9970

^a Values at 20 °C.

4.2.1 Development of Theoretical Systems

For the theoretical systems, a solution of water-acetone was first considered. The first composition contained 5 % w/w water and 95 % w/w acetone. A second solution, containing 10 % w/w water and 90 % w/w acetone was also investigated. A 5 % w/w increment was used for each subsequent composition, the final of which was 95 % w/w water, 5 % w/w acetone. This formed a total of nineteen individual, bulk mother solution compositions. Here, an assumption of a 20 g solution was made. From this, the mass of both water and acetone components could be calculated, as well as the volume, according to the density values given in Table 4.1. It was assumed that salicylic acid particles are completely insoluble in all solvents and, thus, were completely available to be agglomerated.

The first agglomeration system had an addition of 0.02 ml of the bridging liquid across all bulk solutions and bridging liquid variations. The volume and mass fractions of each component, post-addition, were then calculated. As the volume of bridging liquid is constant, and the solid loading remains the same, the BSR is equal across all systems. In this addition, the BSR is approximately 0.05.

A second system was then considered, with the bulk solution composition kept constant. The second system included a bridging liquid addition of 0.04 ml of the required bridging liquid. This corresponding to a BSR of approximately 0.1. The increment of bridging liquid was 0.02 ml for each subsequent system, up to a maximum of a 1 ml addition, corresponding to fifty different theoretical agglomeration systems. This process was repeated, across all bulk solutions, to form nine-hundred and fifty theoretical system across each bridging liquid. The BSRs are equal, regardless of the initial composition or bridging liquid used.

4.2.2 Verification of Acceptable Error

One key parameter to check was whether the system of interest developed in this section was, in fact, within the immiscible region, as identified previously. To do so, the co-ordinates of the binodal curve from Aspen were used first. The co-ordinates closest to the system of interest were identified. First, the acetone mass fraction (y -value) was considered. The value of the theoretical system must be lower than that of the closest co-ordinate identified. This indicates that the system lies below the closest binodal curve co-ordinate. As this does not necessarily indicate that the system is within the immiscible region, the water mass fraction (x -value) was also considered. As all the theoretical systems lie along the y -component axis initially, and move towards the origin, the x -value must be lower than the closest curve co-ordinates, indicating the system lies to the left of the closest co-ordinate. Both these conditions must be satisfied for the theoretical system to be considered as within the immiscible region. Data within the miscible region was identified and discarded. The accuracy of the calculations involving tie-lines were also evaluated.

As the relative compositions of each individual immiscible phase were calculated, along with the masses of each individual component, further checks could be performed. The total mass of the theoretical systems devised in [Section 4.3.1](#) was used here. The calculated values for each individual component in each individual phase were summed and compared. The respective densities of each individual component, as identified in Table 4.1 are used to calculate the volumes here. The volumes can be summed individually, under the assumption that each immiscible phase is an ideal solution when considered as a single entity.

A maximum allowable error of $\pm 5\%$ was implemented, *i.e.* the volume of each component from both phases must be within 5% of the original theoretical system volumes. As the TBSR relies

solely on the bridging liquid rich phase and, indeed, the volume of bridging liquid initially added, a final check was performed. The total error in the volume of the bridging liquid was also not permitted to exceed $\pm 5\%$. This ensured that TBSR calculations were accurate and based upon the volumes originally added in theoretical systems. An example of the calculations utilised in [Section 4.2.1](#) is presented within [Appendix A](#).

4.3 Results & Discussion

4.3.1 Ternary Phase Diagrams: Experimental Results

[Chapter 3](#), [Section 3.3.1](#) provides the methodology for experimental titrations. The experimental titration results are shown in [Figure 4.1](#) for water-acetone-bridging liquid systems. The onset of turbidity during each titration was easily observed, and this is reflected in the high level of reproducibility across all the bridging liquids. The general shape of all systems, regardless of the bridging liquid used, follows a smooth, bell-shaped curve with shallow sides. The height of the curve, as expected, is dictated by the degree of the miscibility of the three solvents, which can be inferred by their interfacial tensions in water (see [Table 4.2](#)). Essentially, less miscible bridging liquids can be identified by a higher peak in the curve, or a greater immiscible region (see [Figure 4.2](#)). For the components investigated as bridging liquids, the results were found to also follow the trend of the interfacial tension in water, *i.e.* higher interfacial tensions produce higher curve peaks, and thus, higher degrees of immiscibility. Heptane displays the highest peak, followed by toluene, chloroform, butyl-acetate, and MIBK, which follows the highest interfacial tension through to the lowest.

[Table 4.2](#). Experimental data for the interfacial tension (dyne cm^{-1}) of bridging liquids in water.

	Heptane	Toluene	Chloroform	Butyl acetate	MIBK	Reference
Interfacial Tension in Water at 25 °C (dyne cm^{-1})	50.1	35.4	30.8	-	10.4	[117]
	50.2	36.1	31.6	14.5	-	[118]
	50.2	36.1	32.8 ^a	14.5	10.1	[119]
	50.2	36.1	31.6	14.5	10.1	[120]
	50.1	35.8	31.1	-	-	[121]
	-	35.8 ^b	-	15.0 ^b	-	[122]

^a Values at 20 °C; ^b Values at 17 °C.

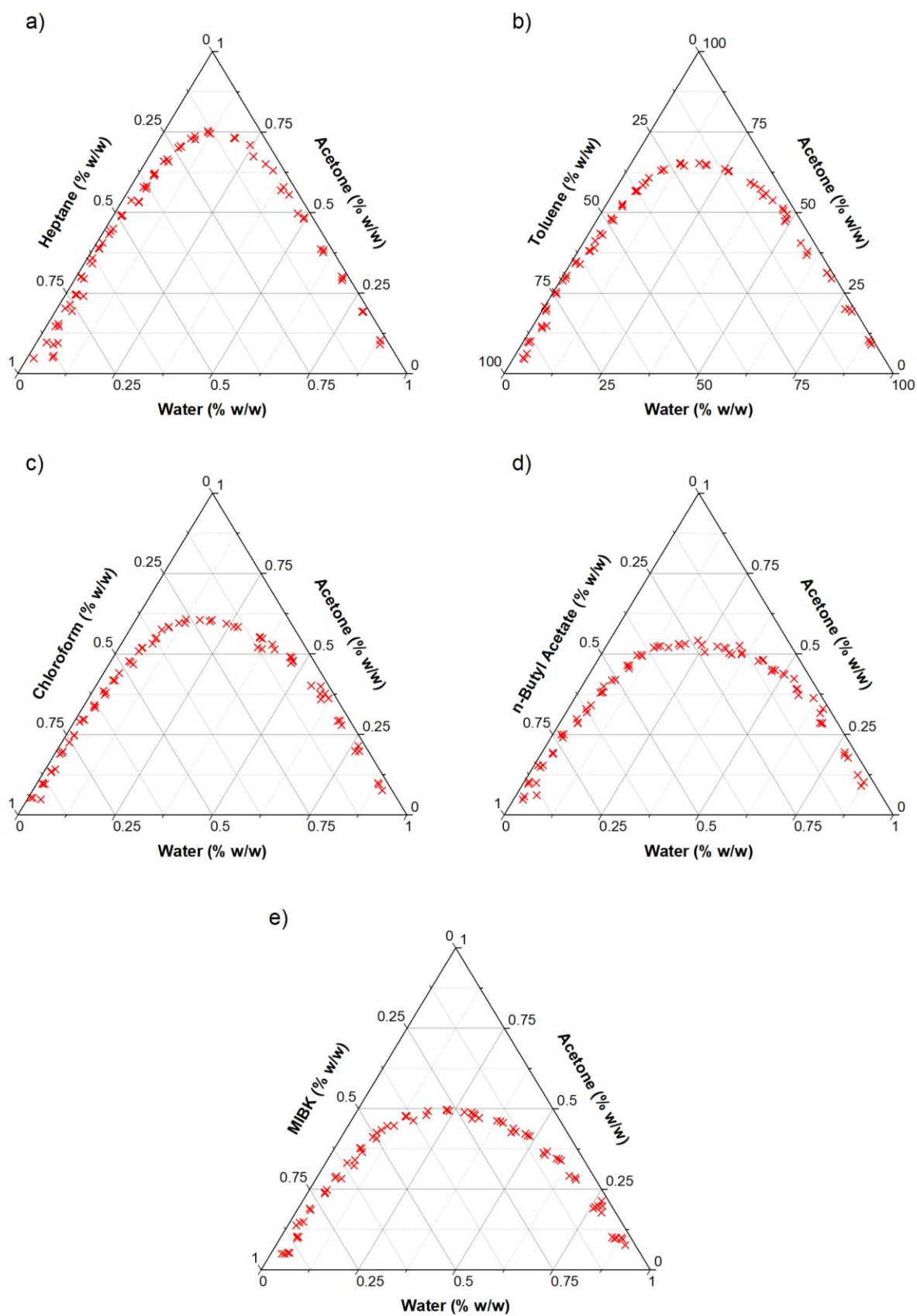


Figure 4.1 Ternary phase diagrams (% w/w) for water-acetone-bridging liquid systems. Red crosses represent experimental data points; a) heptane; b) toluene; c) chloroform; d) *n*-butyl acetate; e) MIBK.

4.3.2 Ternary Phase Diagrams: Modelling Results

Five thermodynamic models were compared to experimental results: UNIQUAC, and its variations UNIFAC, UNIF-LL, UNIQ-RK. Each model was simulated against all five bridging liquids and the results compared. The models with the closest alignment to the experimental results are displayed in Figure 4.2.

UNIF-LL was shown to best predict water-acetone-chloroform systems, whilst UNIFAC best predicted water-acetone-heptane systems. UNIQUAC was found to best predict the behaviour of the remaining systems: butyl acetate; MIBK; toluene. For butyl acetate and MIBK, the interfacial tension in water is relatively low. Subsequently, there is a much higher degree of miscibility, and therefore there are potential difficulties in predicting system behaviour. This could explain why all the models failed to accurately predict the peak location of the binodal curve, as this observation was not noted with the bridging liquids with higher interfacial tensions in water.

4.3.3 Comparison of BSR and TBSR for All Systems

It is hoped that utilisation of the TBSR, rather than the BSR, will increase the comparability of different systems. For the TBSR to be used, the formation of two immiscible phases is required, *i.e.* the solubility of the bridging liquid in the bulk solution must be exceeded. Thus, when the immiscible phases do form, this soluble volume is lost to the bulk solution. A result of this behaviour is that the TBSR is always initially less than the BSR. Prior to this, the system is considered miscible and, as a result, the TBSR is equal to zero, as there is no bridging liquid rich phase but a single homogenous solution. Bulk solutions with a higher initial mass fraction of water were shown to have least deviation from the BSR equals TBSR relationship. This behaviour is to be expected as all the bridging liquids are much less miscible in water compared to acetone.

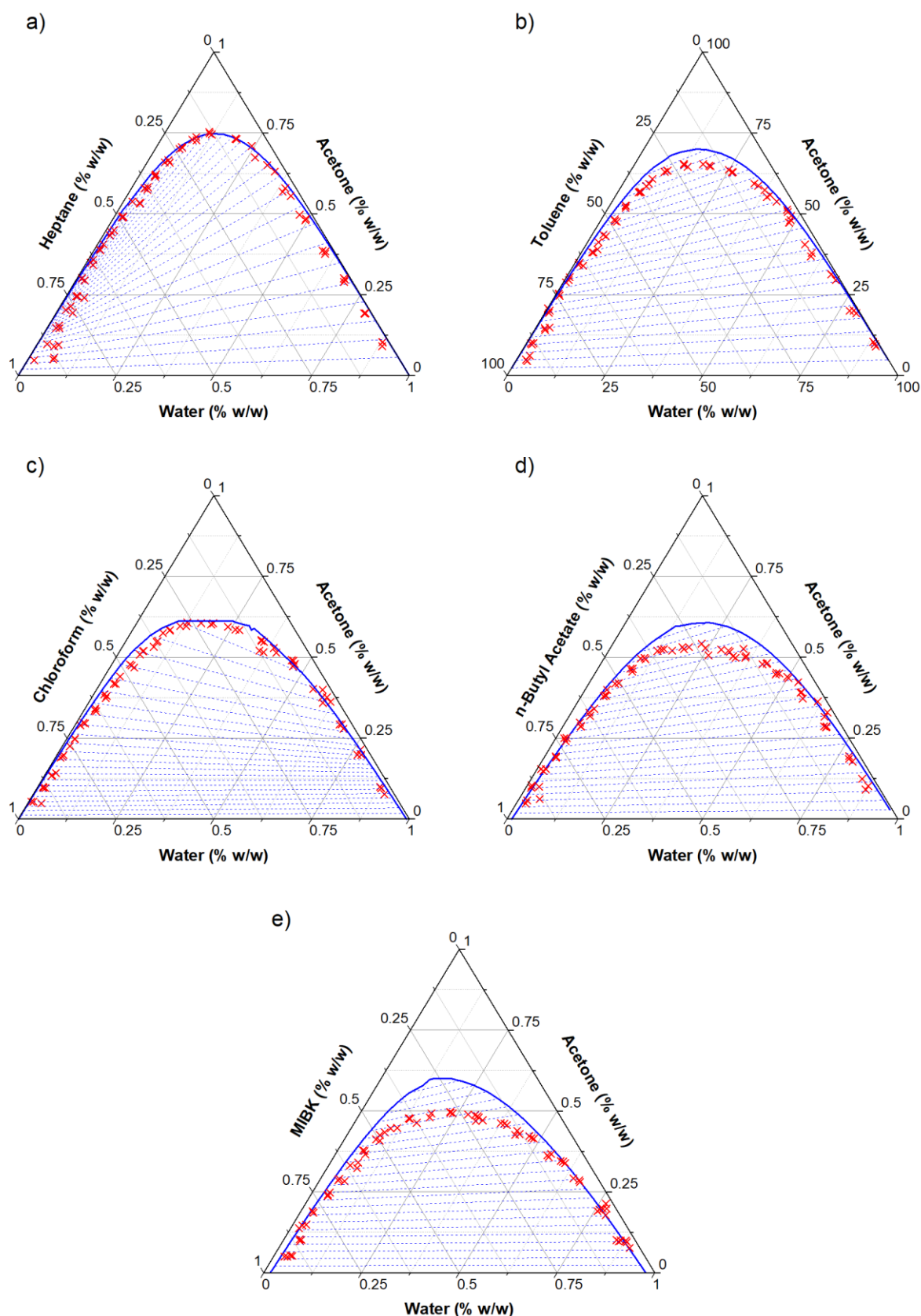


Figure 4.2. Ternary phase diagrams (mass fraction) of water-acetone-bridging liquid systems featuring experimental data and Aspen prediction overlays; a) heptane UNIFAC prediction; b) toluene UNIQUAC prediction; c) chloroform UNIF-LL prediction; d) *n*-butyl acetate UNIQUAC prediction; e) MIBK UNIQUAC prediction.

As the initial mass fraction of acetone is increased, significant deviation of TBSR from the BSR occurs, regardless of the bridging liquid used. As the bridging liquid is more miscible in acetone than water, the solubility is much higher. The BSR is calculated as being high in these systems, whereas the TBSR is low. In the ternary phase diagram, this is reflected by theoretical systems requiring more bridging liquid to cross the binodal curve into the immiscible region of the diagram. Interestingly, and according to the literature presented in [Chapter 2](#), most BSR values used are below a value of 1. However, the optimum BSR value can vary greatly for different systems (see [Figure 2.22](#)). Unfortunately, many studies do not provide detailed enough information to calculate the TBSR accurately.

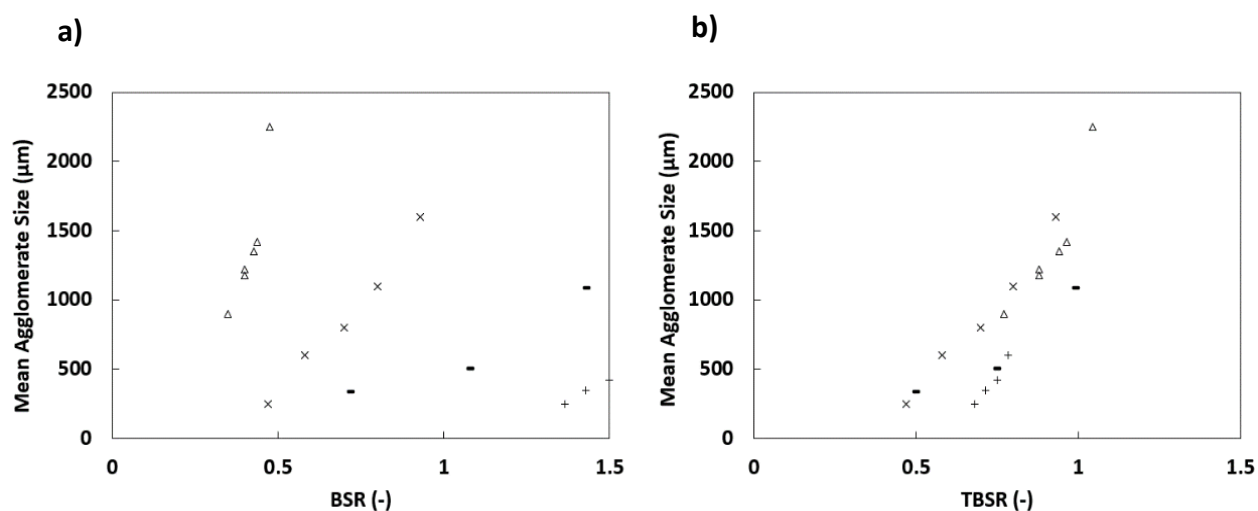


Figure 4.3. Agglomerate size for different spherical agglomeration systems: o kerosene/CaCO₃ [91]; Δ chloroform/salicylic acid [45]; × toluene/benzoic acid [46]; - hexane/lobenzarit disodium [21]; + dichloromethane/atorvastatin calcium [92] as a function of a) BSR (Source: Pitt et al. [7]) and b) TBSR. Here the TBSR values are for illustrative purposes only.

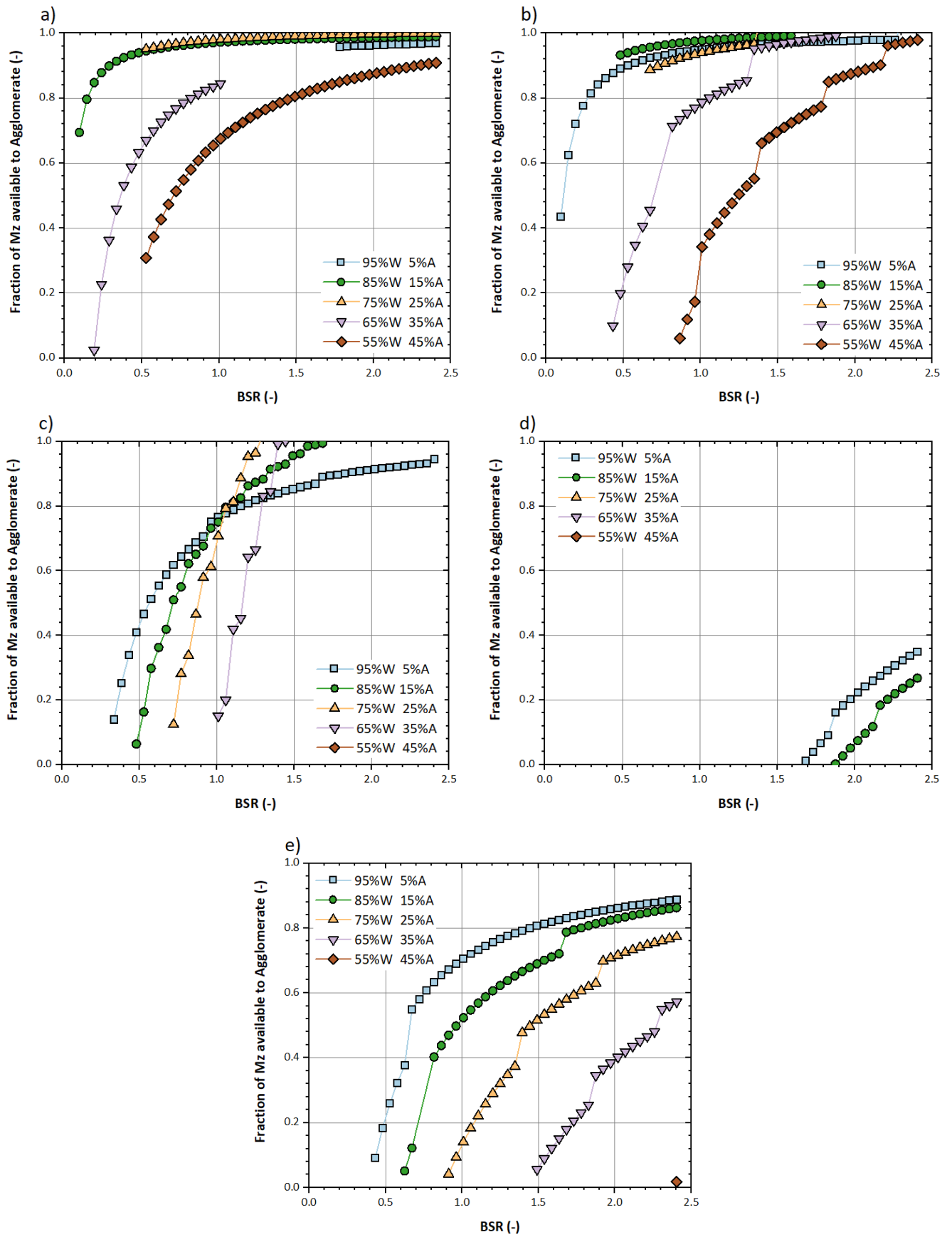


Figure 4.4. True bridging liquid volume available to agglomerate solid particles as a function of BSR, for water-acetone-bridging liquid systems a) heptane; b) toluene; c) chloroform; d) MIBK; e) *n*-butyl acetate.

If the fraction of the bridging liquid addition available to agglomerate particles is plotted as a function of the BSR, powerful relationships can be established. For the agglomeration systems identified, these results are shown in [Figure 4.4](#). For heptane, if a BSR of 1 is considered, approximately 65 % to 95 % of the bridging liquid is available to agglomerate the particles of interest, dependent upon the bulk solution composition (see [Figure 4.4a](#)). These comparisons can also be made for the other bridging liquids; toluene (see [Figure 4.4b](#)): chloroform (see [Figure 4.4c](#)): *n*-butyl acetate (see [Figure 4.4d](#)): MIBK (see [Figure 4.4e](#)). Note that as the initial concentration of acetone increases, more bridging liquid is lost to the bulk solution. In all cases, this results in the initial immediate volume of bridging liquid available to agglomerate particles being reduced. This same relationship is observed for increases in the bridging liquid miscibility (with the bulk solution). Note that here, more bridging liquid is immediately available for bridging liquids which have a higher interfacial tension in water (*i.e.*, less miscible).

For chloroform, the fraction of M_z available becomes greater than 1.0 at a BSR of around 1.25 for some bulk solutions. That is, that the TBSR value becomes larger than the BSR value calculated for the same bridging liquid volume addition. As higher volumes of bridging liquid are added, a greater amount of water and acetone is transferred into the bridging liquid rich phase. As acetone is more miscible in the bridging liquid than the water, more acetone is transferred in these instances. It should be noted that these systems represent unrealistically high BSR values and indeed TBSR values. At these high values, systems are more likely to form pastes upon bridging liquid addition. Note that this only occurs for chloroform and should be attributed to the negative gradient of the tie-lines, as observed in [Figure 4.2](#).

Two further solid loading concentrations were investigated and tested against water-acetone-chloroform systems, as developed in [Section 4.2](#). The same theoretical agglomeration systems were also utilised. Considering a 1 % w/w loading, the initial solid volume is one third that of the system originally investigated. As a result, the BSR value traditionally used would be expected to be three times higher. This holds true. Additionally, the TBSR values were seen to be approximately three times larger. Considering the available volume of M_z to agglomerate particles, at a given BSR, only one third the fraction of that calculated for 3 % solid loading systems is available ([Figure 4.5a](#)). Investigations using a 5 % w/w loading produced results in-line with the above observations, as shown in [Figure 4.5b](#).

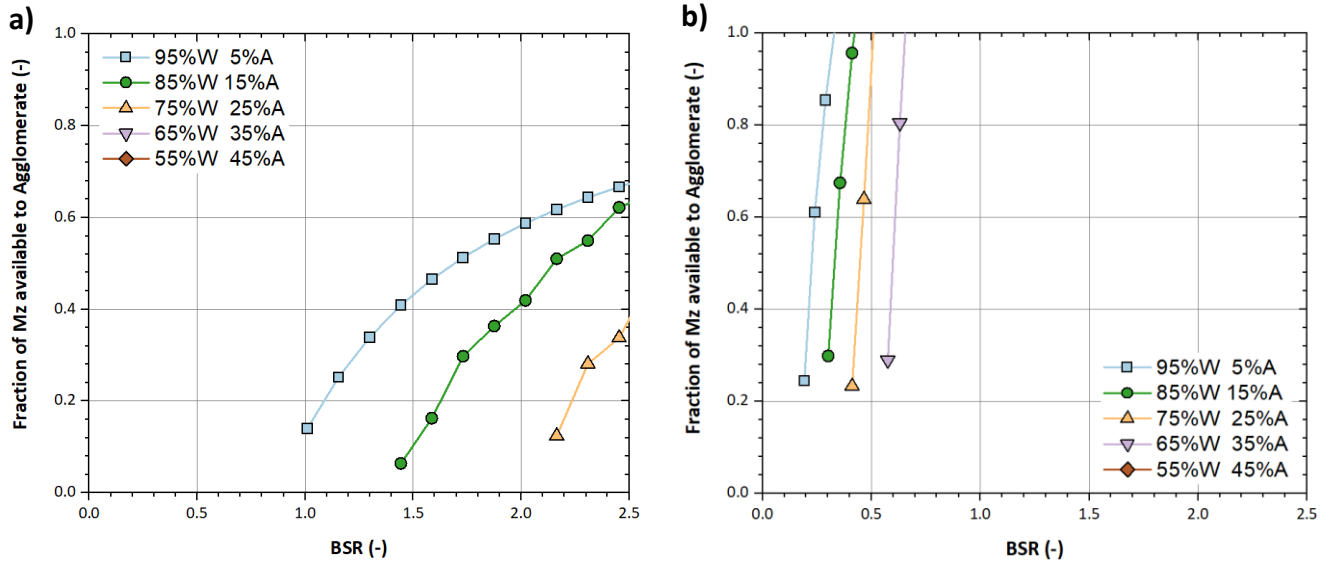


Figure 4.5. Comparison between a solid loading of a) 1 % w/w and b) 5 % w/w for water-acetone-chloroform systems.

These results demonstrate that the solid loading of systems should also be considered carefully in practice, especially when the solid loading is below 3 % w/w. At 1 % w/w, the influence of bridging liquid miscibility within the bulk solution becomes even greater. Increasing the solids content increases the amount of binder liquid added and pushes the operating point further into the immiscible region (see Figure 4.6). If the operating point is very close to the boundary envelope, then a small drop in solids content could cause a dramatic change in performance. The precise value of solids content for this will be system specific and depends also on the BSR, the shape of boundary envelope and the solvent composition. However, it is easily calculated for a given system using the approaches described in this chapter.

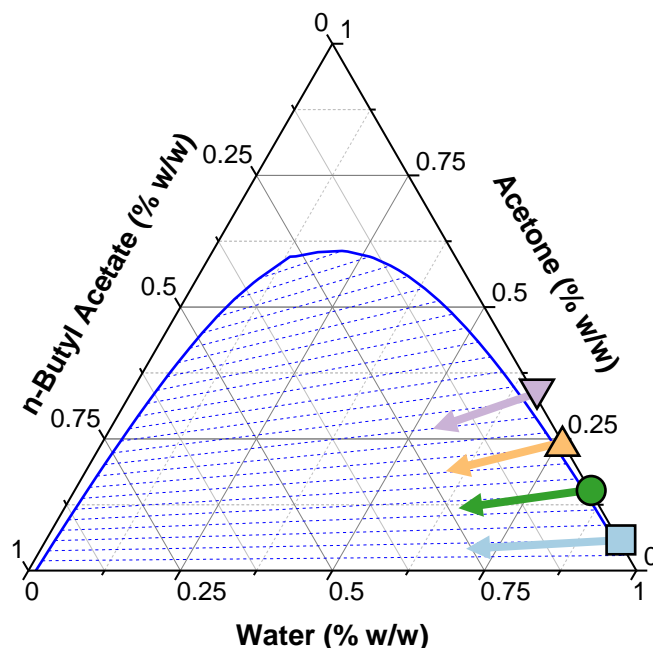


Figure 4.6. Increasing the bridging liquid volume addition causes the system to move further into the immiscible region, shown here for four exemplar bulk solution conditions.

4.4 Conclusions

The traditional bridging liquid to solid ratio (BSR) does not account for the solubility, or miscibility, of the bridging liquid in the bulk solution. This, in turn, directly influences the volume of bridging liquid available for agglomeration of the particles of interest. If any of the three solvents in the process are changed, the amount of available bridging liquid phase changes. This is also true for changes in the solid loading.

Here, the True BSR (TBSR) has been defined. The results demonstrate that this new parameter is a much more accurate measure of the bridging liquid, especially when considering the fraction of the initial bridging liquid added available to agglomerate particles of interest. Under some process conditions, the TBSR can vary dramatically from the BSR, and thus, the bridging liquid fraction available may be exceptionally lower than thought. This is particularly true when the ternary phase diagram features a large miscible region. Highly miscible bridging liquids lead to increased levels of deviation in the TBSR value, when compared to the BSR. The mother solution must also be considered here as increasing the initial acetone mass fraction was shown to produce the same trend. TBSR is generally lower than the BSR, especially upon the formation of two immiscible phases. One exception was found using chloroform as the bridging liquid, where the TBSR exceeded the BSR value at very high values. This is attributed to the negative gradient of the tie-lines within the ternary phase diagram.

CHAPTER 5: VALIDATION OF THE TRUE BRIDGING LIQUID-SOLID RATIO

5.1 Introduction

As detailed in [Chapter 4](#), the current bridging liquid to solid ratio definition fails to account for solvent miscibility. As such, the amount of bridging liquid available to agglomerate particles of interest may be less or, in some cases more, than initially intended. As a result, whilst a critical range for a particular solvent-solid system can be identified, within which agglomeration behaviour is predictable and efficient, this target critical range may not be achieved. Thus, the subsequent agglomeration profile of these systems may be hard to predict and deviation from expected behaviour becomes increasingly likely. The definition also fails if a different ternary solvent system is utilised or the solid of interest changes. This creates a key challenge for producing robust processes which perform as expected.

In this chapter, the TBSR definition is experimentally tested. To do so, the results presented in the previous chapter are utilised to calculate the required volume of bridging liquid to reach a desired TBSR value. The extent of agglomeration is measured at several TBSR values with three different bridging liquids: butyl acetate; chloroform; methyl-isobutyl ketone. These will test the hypothesis that all systems have similar levels of agglomeration at the same TBSR. In addition, three different bulk liquid compositions are investigated: 95 % w/w water, 5 % w/w acetone; 90 % w/w water, 10 % w/w acetone; 85 % w/w water, 15 % w/w acetone.

5.2 Equipment and Methodology Validation

Agglomeration experiments were performed using the equipment and methodology described in [Section 3.4.1](#). In these experiments, the fraction of solids agglomerated, and the size distribution of the agglomerates were measured in batch agglomeration experiments. A residence time of 45 minutes at 750 rpm was used. A Rushton turbine was placed 2.5 cm from the bottom of a sealed 1 L beaker, as shown in [Figure 5.1](#). A solid loading of 3 % w/w corresponding to 12 g of mass of solid, was added to 388 g of saturated bulk solution.

Several tests were designed to evaluate the robustness of the experimental equipment and methodology. The first of these looked exclusively at whether any solvent within the system would evaporate over the 45-minute duration of the experiment. To test the level of evaporation, if any, the system was agitated for the full duration. A mass balance was performed both before and after this time. The highest acetone percentage initial solution was used: 85 % w/w water, 15 % w/w acetone. A

triplicate was performed, and the losses calculated as followed: 0.53 g loss from 400.88 g; 0.29 g loss from 401.89 g; 0.30 g loss from 389.89 g. These values correspond to losses of 0.13 %, 0.07 % and 0.08 % respectively. This reactor design was incorporated into further testing. These results are displayed in [Figure 5.1a](#).

The dissolution of suspended samples, or precipitation, of crystals from the initial solution was considered next. Evaporation was not considered an issue. Thus, the above experiments were repeated using a system with both suspended solids and a bridging liquid of interest. The mass balances were repeated for 85 % w/w water, 15 % w/w acetone, with a bridging liquid corresponding to a TBSR of 0.5. The repeat for chloroform showed a 0.94 g loss from 411.15 g. A second repeat showed a 0.68 g loss from 412.39 g, and a third repeat a 0.78 g loss from 412.19 g. These values correspond to 0.23 % w/w, 0.16 % w/w and 0.19 % w/w respectively (see [Figure 5.1b](#)). Assuming that the evaporation of the bulk solution remained consistent, only slight increases in losses are present when using a system with suspended solid and bridging liquid, compared to without. These losses were deemed reasonable.

Dissolution of agglomerates is also possible during the washing procedure. To evaluate this, suspended and agitated retentates, with no added binder liquid were washed with either water or water saturated with salicylic acid. The recovered samples were left to dry overnight in an oven, with samples separated from the filter paper and weighed. The mass balance for both conditions was in the order of less than 0.01 % when considering the initial mass suspended.

Crystal aggregation, due to the hydrophobicity of salicylic acid, could also be occurring. In these scenarios, it is possible that false readings would be obtained for the agglomeration profiles, despite no agglomerates actually being formed. To evaluate the influence of this, a TBSR of 0.00 (no added bridging liquid) was implemented as a control across all initial solutions. The recovery and characterisation followed the procedure described in [Section 3.4.2](#). As no bridging liquid was added, a 0 % agglomeration profile would be expected, *i.e.* all aggregates pass through the 300 μm sieve, and no agglomerates are present. Triplicates used the 90 % w/w water, 10 % w/w acetone bulk solution. The results for the agglomeration profiles showed that agglomeration was less than 1 % of the original solid mass.

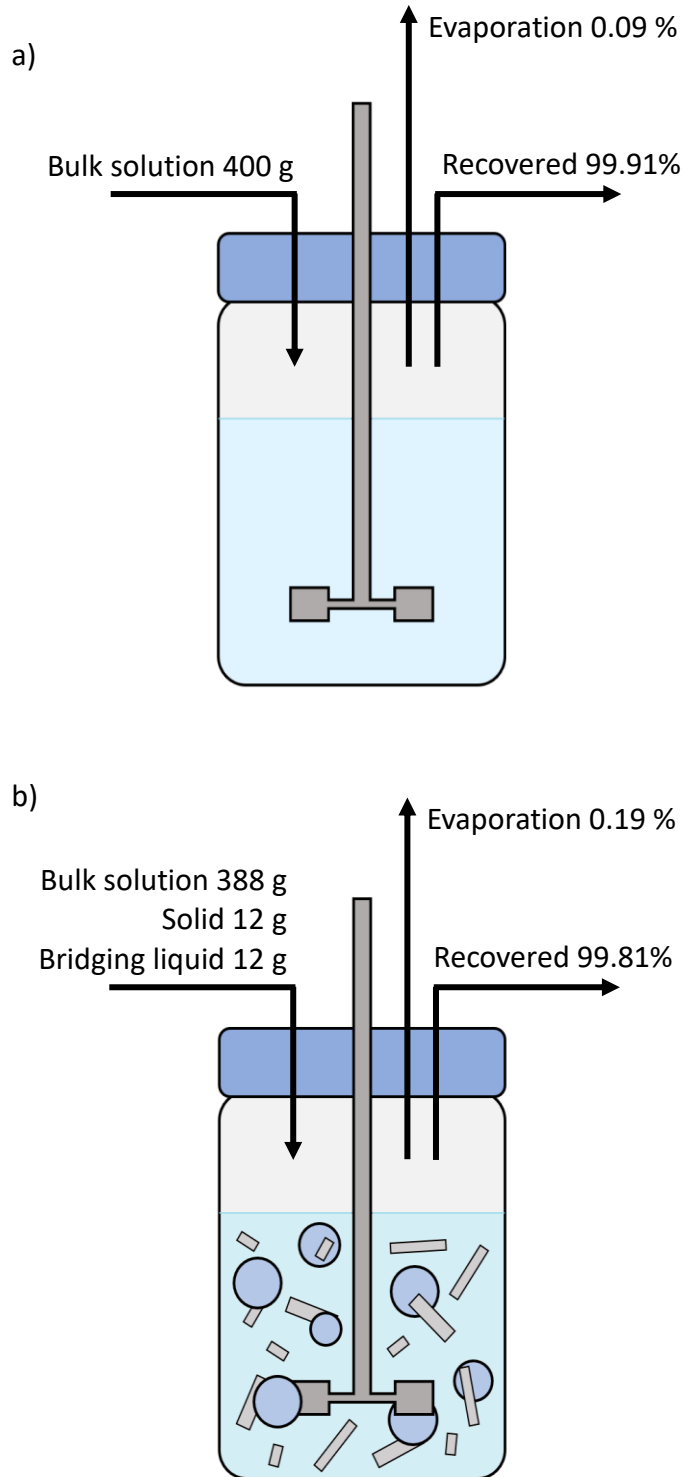


Figure 5.1. Testing of closed reactor experimental set-up for a) evaporation and b) dissolution and precipitation during spherical agglomeration experiments. Conditions replicating those of the validation experimental methodology were used here.

5.3 Experimental Design

TBSR values just above zero represent systems in which the bridging liquid miscibility within the bulk solution has only just been surpassed – that is, two distinct immiscible phases form spontaneously. These systems are of high interest in the spherical agglomeration context, as the distribution and immersion mechanisms may be investigated. Providing the relationship between the BSR and TBSR has been established, target TBSR values can be reached with ease. This involves examination of the system of interest and identifying the corresponding BSR value. This provides the volume of bridging liquid which should be added to the system to achieve the TBSR required *i.e.* the total volume of the bridging liquid rich phase. This volume is different if the bulk solution composition or bridging liquid is changed.

From the results presented in [Chapter 4](#), three bridging liquids were selected which have a wide range of interfacial tensions with acetone/water mixtures: butyl acetate; chloroform; methyl-isobutyl ketone (MIBK). These bridging liquids have been used extensively within the literature. All these bridging liquids were investigated with a bulk solution of 90 % w/w water, 10 % w/w acetone. From methodology developed in [Section 5.2](#), a TBSR of 0.5 formed a paste for all systems. Here, a range of different TBSR values were used, from 0.025 to 0.150 in increments of 0.025 to avoid the formation of a paste. The relationship between TBSR and BSR for the three systems is shown in [Figure 5.2](#). A TBSR equal to zero was also investigated as a control. In this condition, there is no bridging liquid rich phase, and thus any agglomeration or aggregation of crystals is not a result of the presence of bridging liquid. The particles studied were salicylic acid prepared to a sub-45 μm size. A solid loading of 3 % w/w was used throughout the calculations and validation experiments. [Table 5.1](#) provides the BSR and TBSR for the systems identified, and the relative mass fraction of each of the three solvent components within the system (not accounting for solid additions). Examples of the calculations are provided in [Appendix A](#).

Table 5.1. The bridging liquid addition volumes, BSR, TBSR and compositions (% w/w) of the bulk solutions, used in agglomeration validation experiments, prior to solid addition.

Mother Solution (% w/w)		Mass Fractions (% w/w)			BSR Values		Volume (ml)
Water	Acetone	Chloroform	Water	Acetone	TBSR	BSR	Chloroform
95	5	0.96	94.09	4.95	0.050	0.340	2.824
		1.03	94.02	4.95	0.100	0.388	3.225
		1.11	93.95	4.94	0.150	0.436	3.626
90	10	1.23	88.89	9.88	0.025	0.405	3.372
		1.30	88.83	9.87	0.050	0.429	3.569
		1.35	88.78	9.87	0.075	0.446	3.709
		1.40	88.74	9.86	0.100	0.462	3.838
		1.45	88.70	9.86	0.125	0.477	3.968
		1.51	88.64	9.85	0.150	0.499	4.148
85	15	1.44	83.77	14.78	0.025	0.477	3.965
		1.51	83.72	14.77	0.050	0.499	4.151
		1.58	83.66	14.76	0.075	0.522	4.337
		1.62	83.62	14.76	0.100	0.539	4.480
		1.67	83.58	14.75	0.125	0.553	4.600
		1.72	83.54	14.74	0.150	0.568	4.720
Water	Acetone	MIBK	Water	Acetone	TBSR	BSR	MIBK
95	5	2.76	92.38	4.86	0.050	1.664	14.262
		2.84	92.30	4.86	0.100	1.713	14.684
		2.92	92.23	4.85	0.150	1.762	15.105
90	10	3.05	87.26	9.70	0.025	1.841	15.786
		3.09	87.22	9.69	0.050	1.866	15.996
		3.13	87.19	9.69	0.075	1.890	16.205
		3.17	87.15	9.68	0.100	1.915	16.415
		3.20	87.12	9.68	0.125	1.939	16.625
		3.24	87.08	9.68	0.150	1.964	16.834
Water	Acetone	Butyl Acetate	Water	Acetone	TBSR	BSR	Butyl acetate
95	5	0.81	94.23	4.96	0.050	0.432	3.699
		0.90	94.14	4.95	0.100	0.481	4.120
		0.99	94.06	4.95	0.150	0.530	4.541
90	10	0.89	89.20	9.91	0.025	0.476	4.081
		0.94	89.16	9.91	0.050	0.500	4.290
		0.98	89.12	9.90	0.075	0.525	4.498
		1.03	89.07	9.90	0.100	0.549	4.707
		1.07	89.03	9.89	0.125	0.573	4.916
		1.12	88.99	9.89	0.150	0.598	5.124

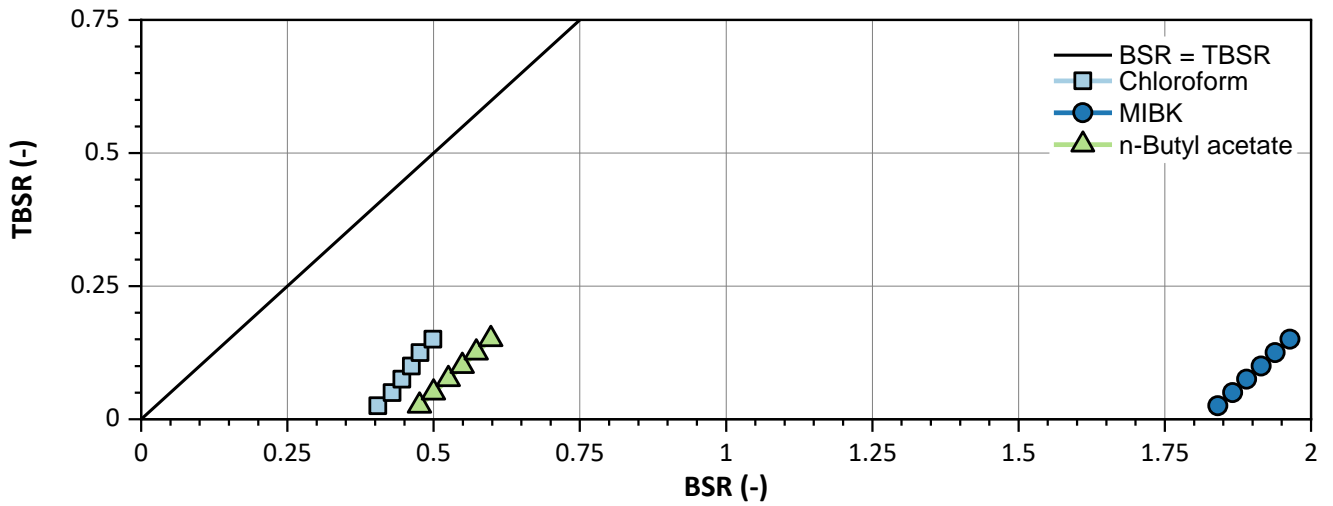


Figure 5.2. The identified agglomeration systems for three different bridging liquids with the same initial bulk solution composition (90 % w/w water, 10 % w/w acetone).

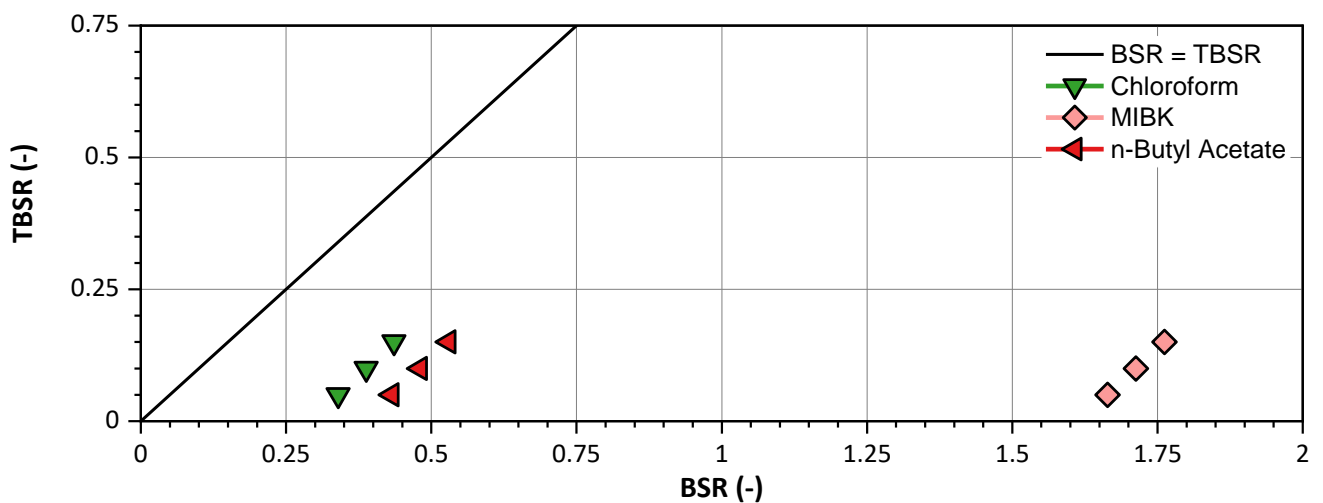


Figure 5.3. The identified agglomeration systems for three different bridging liquids with the same initial bulk solution composition (95 % w/w water, 5 % w/w acetone).

Three individual bulk solutions were also investigated for one bridging liquid, chloroform (95 % w/w water, 5 % w/w acetone; 90 % w/w water, 10 % w/w acetone; 85 % w/w water, 15 % w/w acetone). Bulk solutions with higher acetone mass fractions produce further deviation in the TBSR value from the BSR value. It should also be noted that, often, these systems failed to form two immiscible phases as the binodal curve of equilibrium was not reached. These systems represent a TBSR equal to zero and are not considered within this work.

As before, a range of different TBSR values were used, from TBSR equal to 0.025 through to TBSR equals 0.150 in increments of 0.025. These selections were chosen to investigate conditions below, within and above the proposed optimal range. A TBSR equal to zero was also investigated as a control. All these systems are displayed in Figure 5.2 to Figure 5.4.

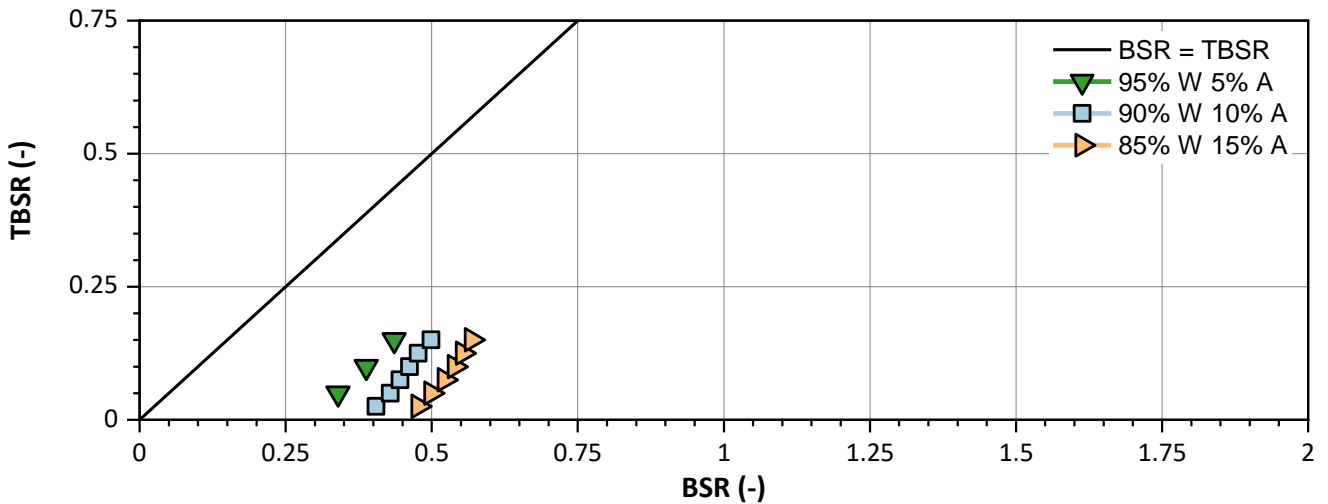


Figure 5.4. The identified agglomeration systems for chloroform with three different bulk solution concentrations.

5.4 Results & Discussion

5.4.1 The TBSR as a Comparison Tool

The rate processes of spherical agglomeration are sometimes considered as analogous to wet granulation systems. Figure 4.2a demonstrated that for a variety of wet granulation systems, regardless of the binder used, if the mean granule size is plotted against liquid pore saturation, the data collapses on to one smooth curve [90]. The bridging liquid volume (φ) was developed in a previous publication and defines the amount of bridging liquid within an agglomerate nuclei [12]. This is defined in Equation 5.1.

$$TBSR = \frac{\varphi}{1 - \varphi} \quad \text{Equation 5.1}$$

This parameter considers the volume of crystals within the nuclei, compared to the volume of the bridging liquid. Crystals which pack in the agglomerate nuclei effectively have a higher solids

fraction in the agglomerate, and thus φ becomes lower. For any system, the liquid volume fraction when the crystal are at their maximum solids fraction is called the critical packing liquid volume fraction φ_{cp} . Thus, Equation 5.1 with $\varphi = \varphi_{cp}$ should represent the minimum TBSR required for complete agglomeration. This relationship is shown in Figure 5.5 [12]. The strongly non-linear nature of the function demonstrates that care must be taken when estimating the optimal TBSR range.

If the results for percentage un-agglomerated (*i.e.* the normalised mass retained within the pan after sieving) are plotted for each different system as a function of the BSR, a wide variation is shown. However, plotting the same results against the TBSR of the system causes the systems to align much more closely together (see Figure 5.6 and Figure 5.7). This demonstrates that solvent miscibility is an important factor which must be considered when designing spherical agglomeration systems as, ultimately, the volume of the bridging liquid rich phase will dictate whether any agglomeration occurs. The systems could fall on a single curve, providing other factors were accounted for, namely the wettability of the bridging liquids. Previously, studies have highlighted the influence of having a high wetting bridging liquid for produced robust spherical agglomerates, as discussed in Section 2.4.3. Bridging liquids with lower contact angles, *i.e.* increased wetting, produce agglomerates which were larger and stronger [21].

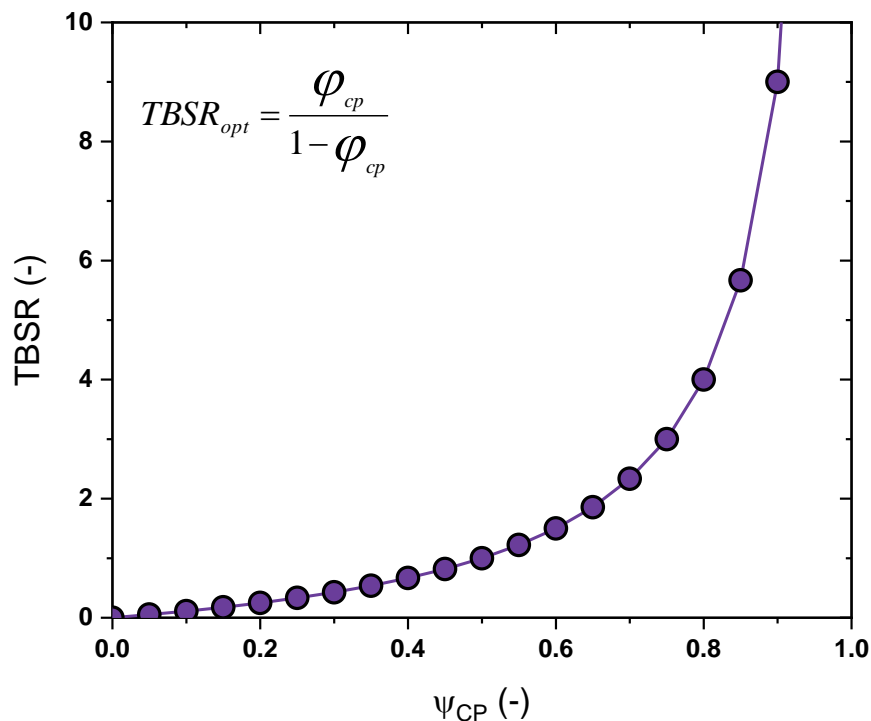


Figure 5.5. The relationship between critical packing bridging liquid volume (φ_{cp}) and the predicted minimum TBSR value, as developed by Arjmandi-Tash et al., [12].

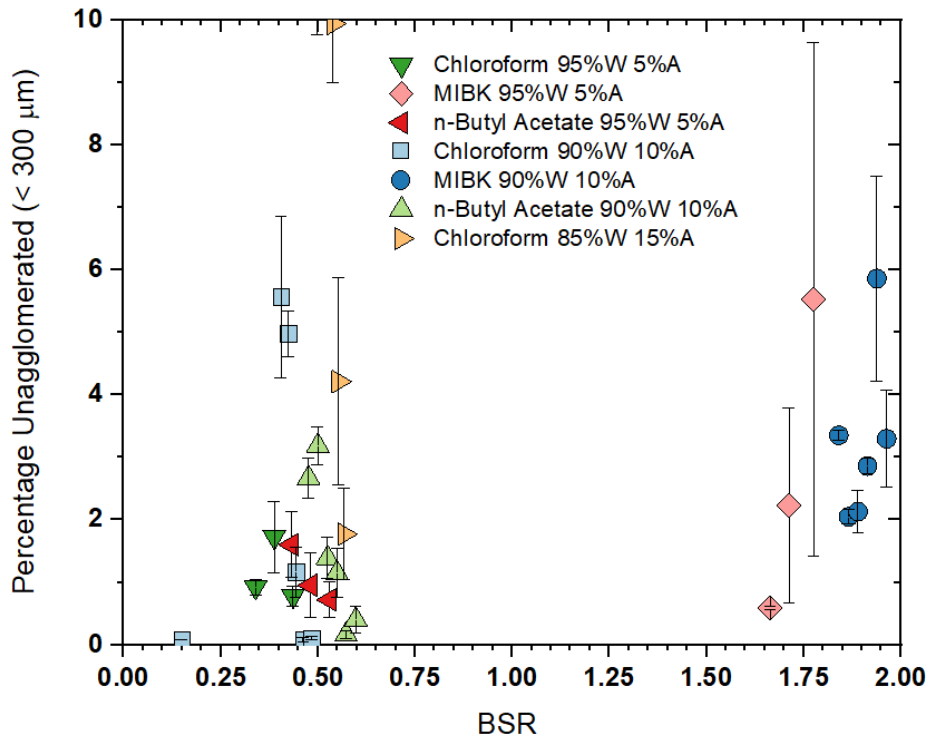


Figure 5.6. The relationship between the BSR and the percentage of fines observed for the systems investigated, including different bulk solutions, and bridging liquids.

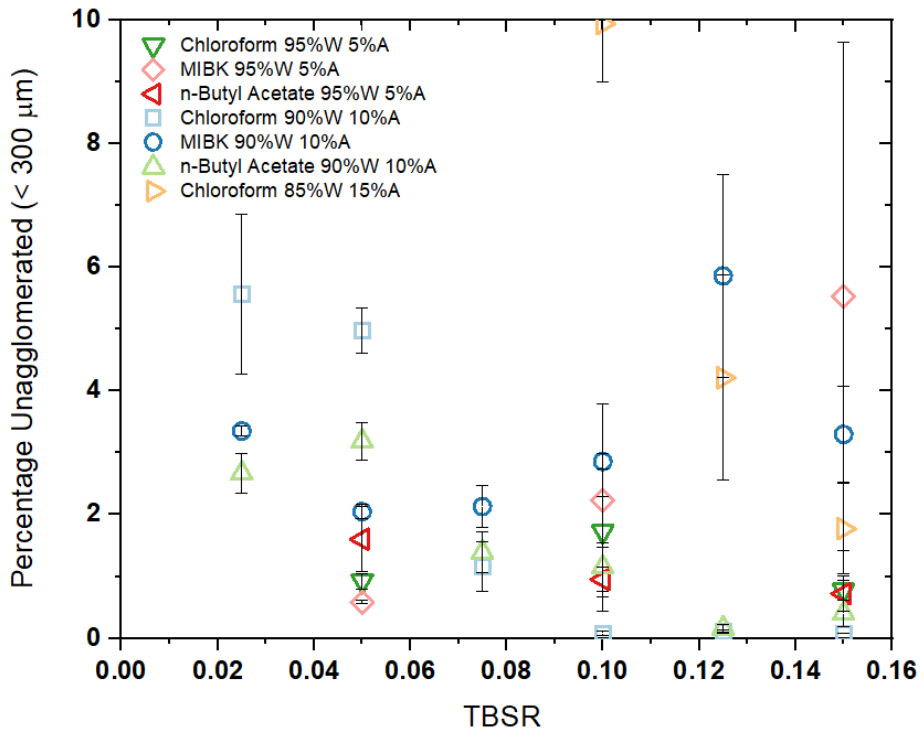


Figure 5.7. The relationship between the TBSR and the percentage of fines observed for the systems investigated, including different bulk solutions, and bridging liquids.

5.4.2 Effect of Bridging Liquid on Agglomerate Size Distribution

The mean agglomerate size from experimental validation of the TBSR is displayed in Figure 5.8 and Figure 5.9 for the BSR and TBSR definition respectively. Associated parameters are also provided in [Appendix B](#). Regardless of the bridging liquid used, the same trend can be identified: increasing the TBSR leads to increases in the agglomerate size. This is shown for both the BSR and TBSR. This is identified by a shift of the size distributions to the right. Regardless of the TBSR, a high level of suspended solid was incorporated into the agglomerates.

If [Figure 5.9](#), and indeed [Figure 5.7](#), is considered alongside the earlier presented results of Chapter 4, key relationships can be identified. As the BSR increases, the fraction of bridging liquid added available to agglomerate particles increases (see [Figure 4.4](#)). This in turn, leads to a direct increase in the average size of agglomerates, as well as a reduction in the number of fines left in solution. Note, that this latter reduction produces larger than expected gains in the agglomerate mean size. This indicates, although not directly measured, that the agglomerates form at higher BSR, and indeed TBSRs, tend to be less dense and more porous. This porosity arises due to a bridging liquid rich nuclei core, which upon drying, remains hollow.

For both chloroform and n-butyl acetate, increasing the TBSR results in a reduction in the percentage unagglomerated fraction, regardless of the bulk solution used. This trend is expected, as increasing the volume of available bridging liquid leads to the incorporation of a higher percentage of solids. MIBK does not follow this trend, and a much larger margin of error was calculated. For all bridging liquids, the TBSR required is much smaller than anticipated. If we assume that the particles are perfectly spherical, the physically closest packing can be achieved, which is approximately 64 %. From [Equation 5.1](#), a TBSR value of approximately 0.54 is required for this degree of packing. Thus, the expected TBSR value for these non-spherical particles should be higher than 0.54, and much higher than the observed behaviour.

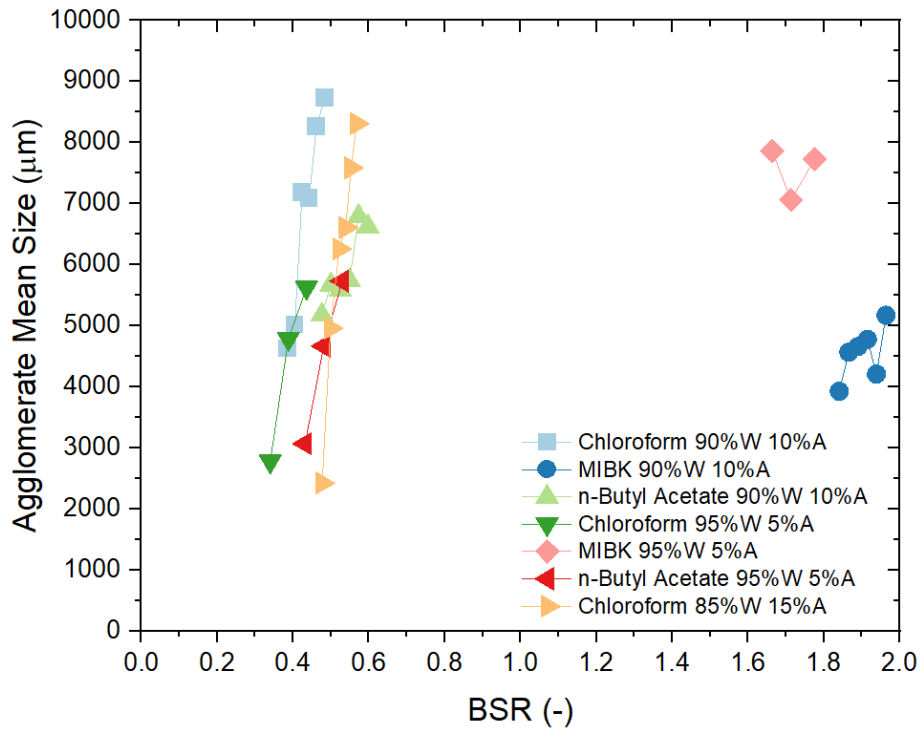


Figure 5.8. The relationship between the BSR and the agglomerate mean size for different bridging liquids and bulk solutions.

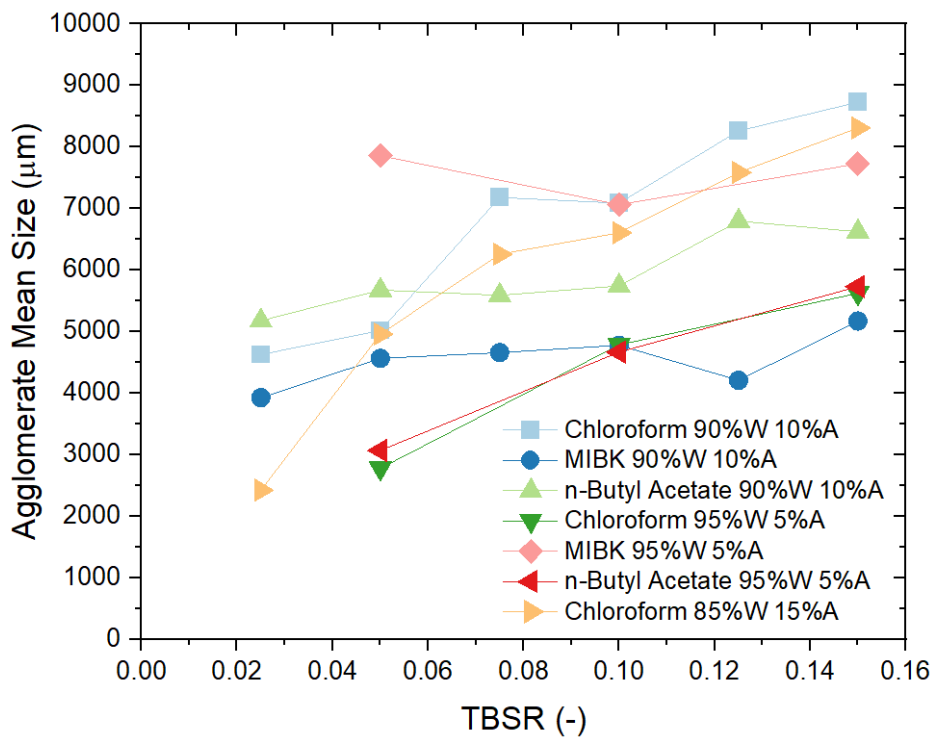


Figure 5.9. The relationship between the TBSR and the agglomerate mean size for different bridging liquids and bulk solutions.

There are several potential reasons for the observed behaviour. As [Section 5.2](#) details, the evaporation of solvent in-situ is unlikely. In a fully loaded system, the mass lost through evaporation

increases because of bridging liquid volatility. However, it is impossible to directly measure the degree of dissolution and precipitation that occurs through mass balance alone. Thus, it may be possible that salicylic acid is dissolving to a much greater degree than originally thought, especially when combined with a pre-saturated bulk solution. In this instance, the volume of the solid decreases, and thus the TBSR increases. This is a plausible explanation for the agglomeration behaviour observed, at what is thought to be an extremely low TBSR value. If the solubility of solid in the bridging liquid is known, this too could be incorporated into future TBSR calculations.

Differences in the agglomerate size distributions were observed across the different bridging liquids investigated, and this is mirrored by the changes seen in the mean size of agglomerates. These differences could be due to variations in the wettability of the solid by the bridging liquid, as the influence of bridging liquid miscibility is accounted for. Generally, chloroform and *n*-butyl acetate systems produced more mono-sized agglomerates of a much larger size. MIBK produced agglomerates with a high average size for one of the bulk solution compositions. However, it should be noted that there was a high level of fines left in solution. Figure 5.10 displays the size distribution data for the three bridging liquids at the 90 % w/w water, 10 % w/w acetone bulk solution. The size distributions for the other conditions can be found in [Appendix B](#).

Figure 5.10a displays the size distribution data for chloroform. Here, increases in the TBSR produce clear increases in the agglomerate size, whilst also reductions in the cumulative agglomerate frequency, *i.e.* the level of fines unincorporated into agglomerates. These trends are expected from the literature described within [Chapter 2](#). Similar trends to chloroform were observed for *n*-butyl acetate, although the differences between TBSR values were much smaller (see Figure 5.10c).

MIBK was noted for almost no variation in agglomeration profiles, regardless of the volume of bridging liquid added (see Figure 5.10b). MIBK has the highest miscibility in both water and acetone, and *n*-butyl acetate the second highest miscibility, out of the three bridging liquids investigated here. As such, the volume available to agglomerate particles is more likely to change with only minor variations in solvent composition. Bulk solutions not being completely homogenised may be a reason for variations in bulk composition. If the composition is different to the one upon which calculations are based, a different tie-line may be required and, thus, the TBSR value is different to the expected value.

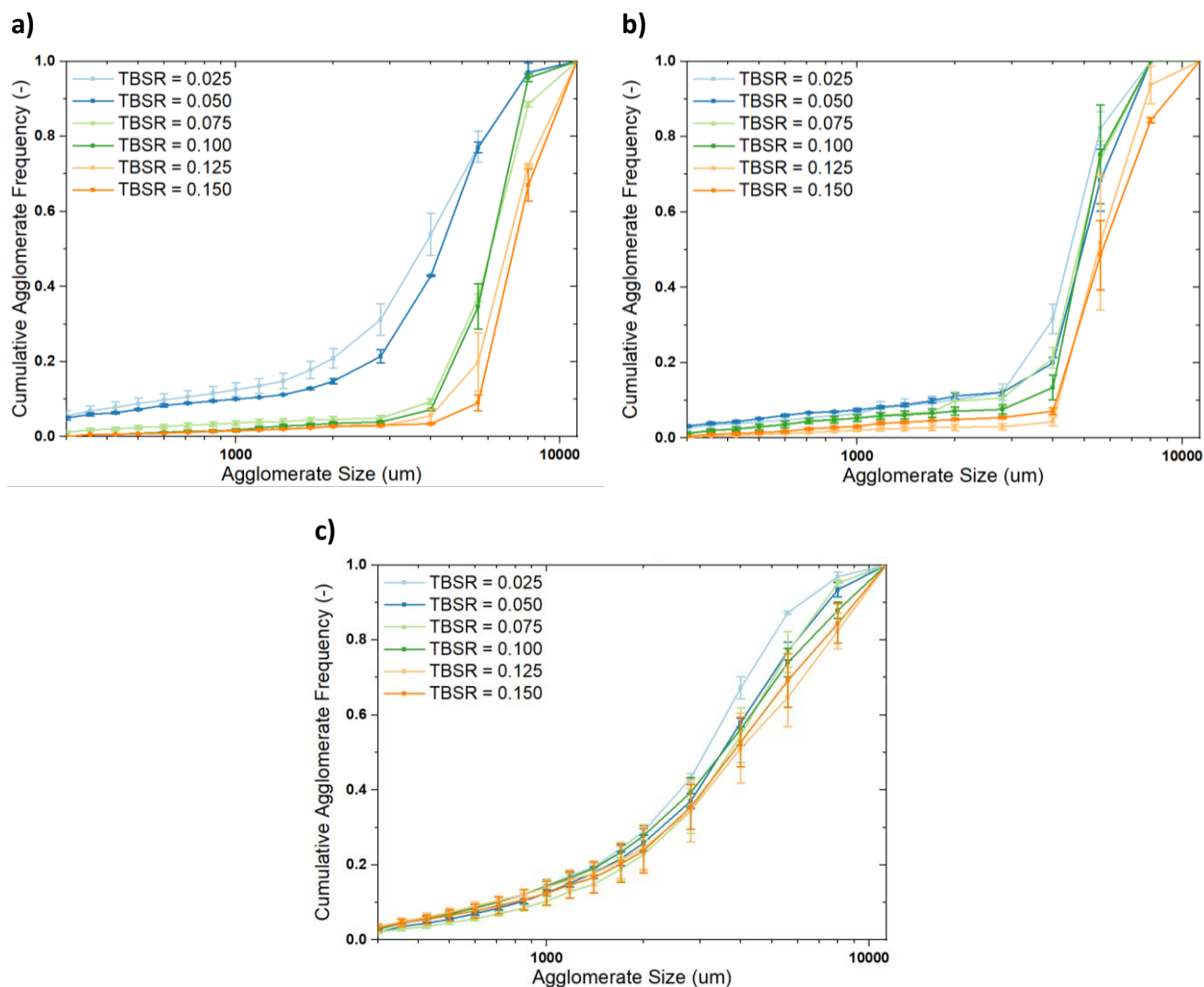


Figure 5.10. Agglomerate size distribution for salicylic acid-bridging liquid systems, a) chloroform, b) MIBK and c) *n*-butyl acetate, with an initial bulk solution of 90 % w/w water and 10 % w/w acetone. Error bars represent standard error of a least three repeats.

Generally, bridging liquids are accepted within the literature as being immiscible or slightly miscible. A relatively large degree of standard error was calculated for each condition, which reflects the high level of variability across repeats and, thus, the unsuitability of MIBK as a bridging liquid for salicylic acid. Whilst this does not explain the observed behaviour, these findings do further support the existing literature regarding bridging liquid immiscibility.

5.4.3 Bulk Solution Compositions

The experimental validation agglomeration profiles are displayed in Figure 5.11 for chloroform for the three different bulk solution compositions. Results for MIBK and n-butyl acetate can be found in [Appendix B](#). Associated parameters are also provided in [Appendix B](#).

For two of the water-acetone-chloroform systems with different initial solution compositions, there were some experiments with equal BSR values (see [Table 5.1](#)). For a BSR of 0.477, the TBSR is equal to 0.125 for 90 % w/w water, 10 % w/w acetone bulk solutions. The same BSR, however, equates to a TBSR of 0.025 for 85 % w/w water, 15 % w/w acetone bulk solutions. The traditional BSR definition would suggest that these systems produce roughly equal behaviour. Traditionally, it would be expected that the agglomerate size distribution is also relatively similar as the BSR is equal.

However, the TBSR definition demonstrates that the actual volume of bridging liquid available is different for both these systems. The experimental validation of the definition also shows very different agglomerate size distributions (see Figure 5.11). Similar observations were also found at a BSR of 0.499 in two further systems at 90 % w/w water, 10 % w/w acetone, and 85 % w/w water, 15 % w/w acetone composition (see [Table 5.1](#)).

If the new TBSR definition holds, it would also be expected to observe relatively similar agglomeration profiles. However, all three bridging liquids at this composition demonstrate different behaviour. Together, these results highlight that the TBSR definition is only partially validated within this work. Future works must be undertaken to further analyse the role of solid solubility within the bridging liquid, as well as the influence of changing the bulk solution composition. This further highlights the need for consideration of solvent system miscibility in spherical agglomeration processes.

5.5 Conclusions

For the first time, the influence of bridging liquid miscibility within the bulk solution has been accurately quantified. In this chapter, the definition of the True BSR proposed previously has also been partially validated experimentally. The agglomeration profiles of systems can be compared much more easily if the TBSR definition is used, rather than the BSR. Additional to this, key relationships between the fraction of bridging liquid available, compared to the added volume, the agglomerate mean size, and the agglomerate size distribution, have all been identified. This further exemplifies the necessity of the definition as a method of standardising bridging liquid volume reporting within

spherical agglomeration processes, as well as providing the basis for a regime map or dimensionless group.

The results from experimental validation of the TBSR definition has shown, largely, reproducible, and predictable spherical agglomeration processes, providing this definition is used rather than its traditional counterpart. Additionally, the TBSR has shown promise as an instant comparison tool across different bridging liquids and different bulk solution compositions. This has been achieved through the utilisation of the results presented in [Chapter 4](#).

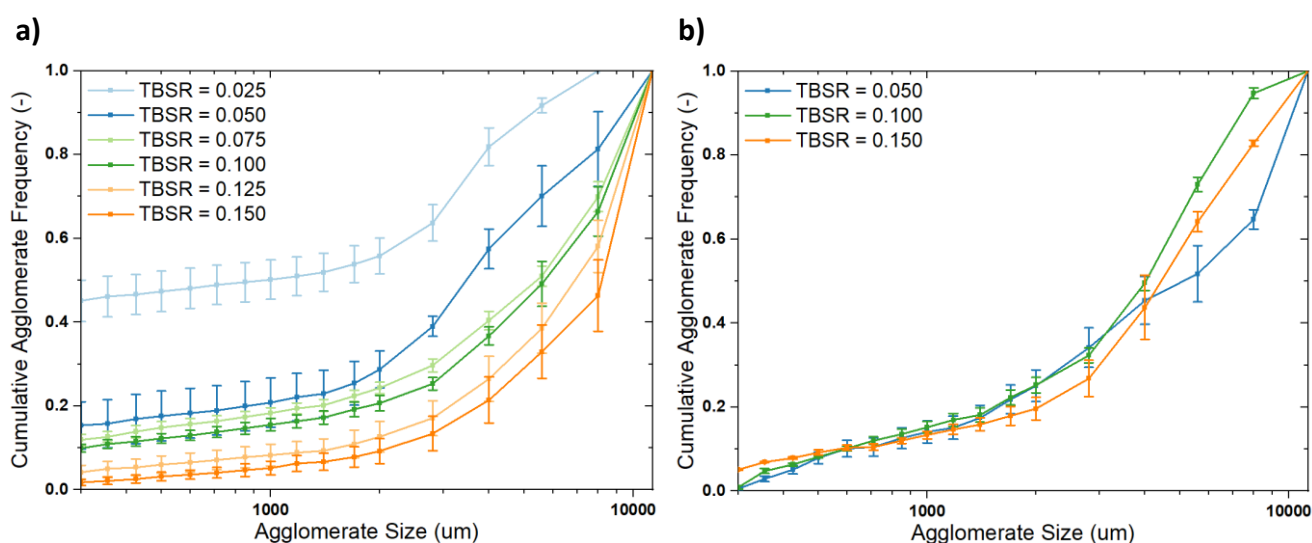


Figure 5.11. Agglomerate size distribution for salicylic acid-chloroform systems with an initial bulk solution of a) 85 % w/w water and 15 % w/w acetone, and b) 95 % w/w water and 5 % w/w acetone. Error bars represent standard error of a least three repeats.

Whilst evaluation of solvent miscibility allows prediction of process performance in spherical agglomeration, there is a need for other parameters to be considered. For example, within immersion nucleation, the volume of solid which can be packed into a defined bridging liquid droplet volume will ultimately dictate the amount of bridging liquid required. As a result, it is possible that the critical range may shift for particulate material with different morphologies. Additional to this, further tests should be undertaken which aim to identify the influence of solid solubility in the bridging liquid and, potentially, the bulk solutions utilised. This factor appears to have a much larger influence on the TBSR than initially thought.

**CHAPTER 6: A KINETIC
STUDY OF SPHERICAL
AGGLOMERATION
PROCESSES**

6.1 Introduction

The true bridging liquid-solid ratio (TBSR) was defined and partially validated in [Chapter 4](#) and [Chapter 5](#) respectively, as a means of quantifying and standardising bridging liquid volume reporting. TBSR has also shown promise as a process design tool. In this chapter, the definition is used to further mechanistic understanding within spherical agglomeration through a kinetic study which aims to identify relationships between rate processes and product outputs *i.e.* size, size distribution and density.

Within this chapter, results of paracetamol mechanistic studies are reported. This study was performed as part of a CMAC CORE Project (SPA 99) in collaboration with Dr Kate Pitt. While we worked as a team, Dr Pitt was primarily responsible for method development and experimental measurements, and I was primarily responsible for the data analysis and interpretation presented in [Section 6.2](#).

Paracetamol was used as the solid of interest. A robust system with good product outputs was initially identified. The influence of operating parameters on these product attributes was investigated, with the aim of elucidating the balance of mechanisms which arise in a '*perfect*' agglomeration system, *i.e.* all solids are incorporated and the time for paste formation is exceptionally long. The kinetics of these systems, where successful agglomeration occurs, is also studied within this section. The kinetics are evaluated as a means of identifying robust spherical agglomeration process performance. Systems such as these improve the likelihood of successful implementation. Paracetamol was chosen as it is one of the most widely available active pharmaceutical ingredients. Heptane was chosen as an anti-solvent to suspend the paracetamol, as paracetamol is almost insoluble in heptane. Water is used as a bridging liquid due to its immiscibility with heptane. Full materials and methods can be found in [Section 3.5](#).

Additionally, these results are compared to a previously developed mathematical model. This serves as the initial foundation for model validation, as well as furthering understanding of the mechanistic processes of spherical agglomeration. The kinetics have a large influence on the spherical agglomeration processes and should be adequately described through rate process understanding. Specifically, the immersion nucleation mechanism is isolated here in a novel methodology. A sensitivity analysis for the effect of TBSR, shear and solid loading is performed and compared to the experimental results.

6.2 Results & Discussion

Agglomerates formed through the immersion mechanism have been shown to be superior to those formed via the distribution mechanism. To aid comparison against immersion nucleation mathematical models, it was imperative to ensure the immersion mechanism occurred within the system of interest. To identify the dispersion of bridging liquid droplets and their initial interactions with paracetamol, water dyed with acid red IV was used. This allowed observation of the immersion mechanism in situ, as per the methods described in [Section 3.5](#). The experiment was performed at TBSR of 0.75 and a solids loading of 5 % w/w. [Figure 6.1](#) displays the agglomerates formed at different time points within the experiment. Here, agglomerate nuclei are clearly seen as red droplets with a surface covering of paracetamol. Flocs of paracetamol are also present although these are still white. This indicates these particles have not been wetted by the bridging liquid and the distribution mechanism is not occurring.

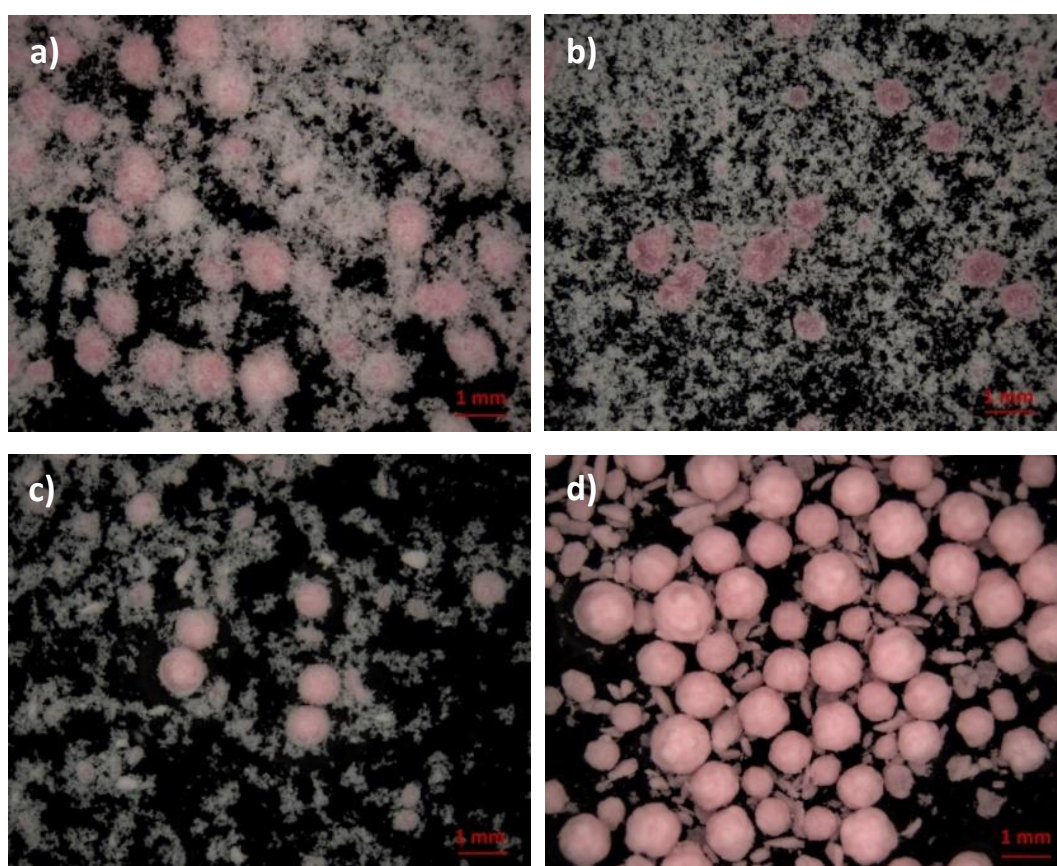


Figure 6.1. Agglomerates sampled at a) 20 minutes, b) 40 minutes, c) 60 minutes and d) 80 minutes with an Acid Red IV dyed bridging liquid (TBSR = 0.75; solids loading = 5 % w/w).

6.2.1 Influence of True Bridging Liquid-Solid Ratio

Incorporation of all material into spherical agglomerates is preferential as it promotes cost-efficiency and there is a reduced requirement for product recycling. Here, the role of the true bridging liquid-solid ratio and the time to paste is considered, as a means of further understanding the balance of mechanistic rate processes in spherical agglomeration. An optimum region where all solid material is incorporated without the formation of a paste is preferred.

It was expected that increasing the available bridging liquid volume will lead to the agglomeration of all solid particles in a shorter amount of time. As such, the time for a paste to form will be reduced compared to lower bridging liquid volumes. In some instances, this could lead to an immediate formation of a paste. Conversely, if the volume of bridging liquid available is less, then the time for all particles to be agglomerated would be longer. Here, the influence of the critical packing liquid volume fraction, ϕ_{cp} , becomes important. As this parameter quantifies the relationship of solid packing within a bridging liquid droplet, its value ultimately dictates the volume of bridging liquid necessary to agglomerate all particles (see [Section 5.4](#)).

The full method is described in [Section 3.5](#). A solid loading of 5 % w/w at 500 rpm was used. Values of TBSR over the range of 0.2 to 8 were investigated. For a TBSR value of 0.2, agglomerates formed slowly and not all suspended material was incorporated into agglomerates. The remaining material remains as flocs within the suspension. The solutions were left agitating for a total of four hours, but no significant changes in the agglomeration profile were observed (see [Figure 6.2](#)). These observations were mirrored for a TBSR value of 0.5, as shown in [Figure 6.3](#).

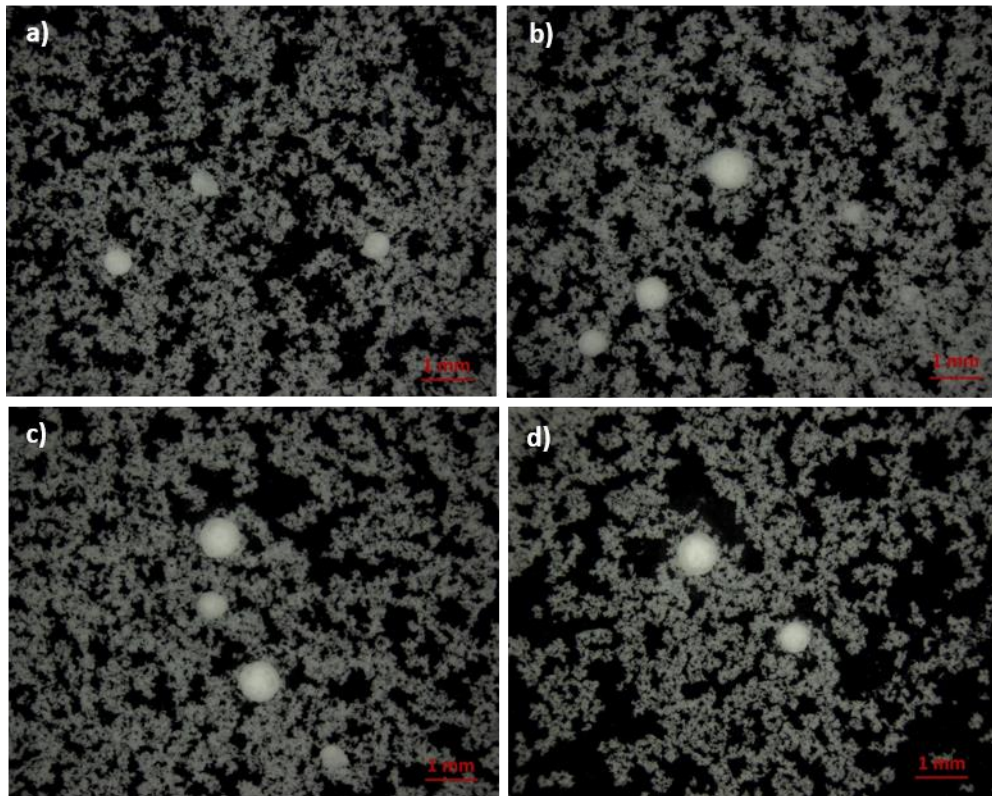


Figure 6.2. TBSR 0.2 produced agglomerates sampled at a) 60 minutes, b) 120 minutes, c) 180 minutes and d) 240 minutes.

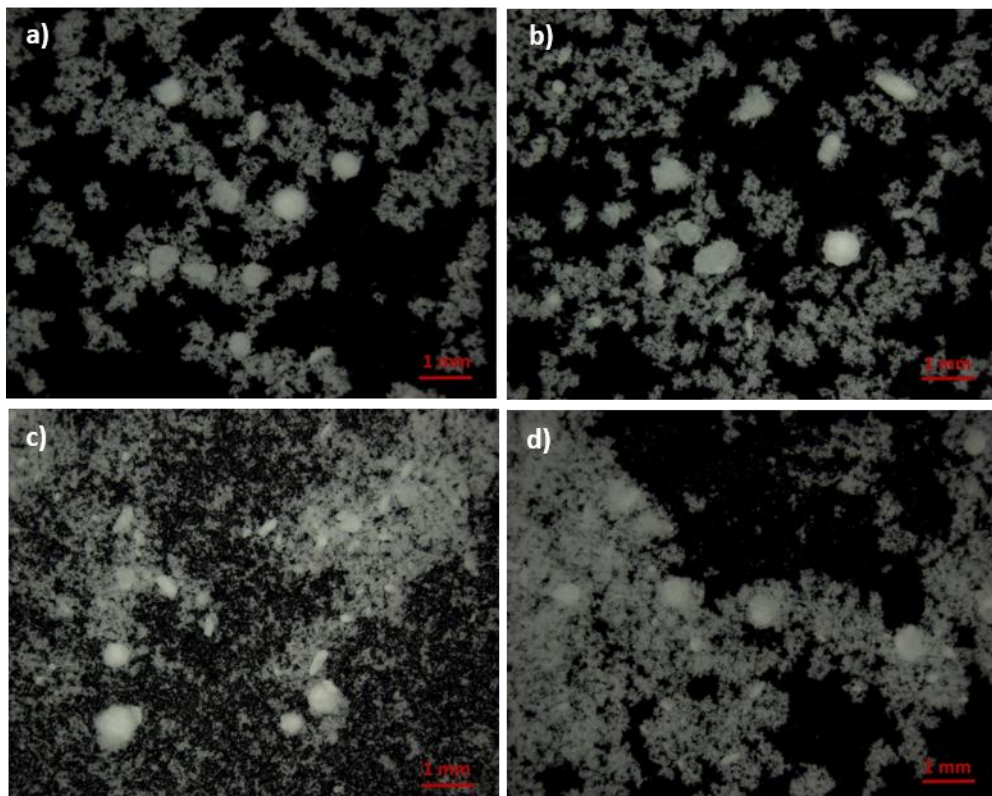


Figure 6.3. TBSR 0.5 produced agglomerates sampled at a) 60 minutes, b) 120 minutes, c) 180 minutes and d) 240 minutes.

At a TBSR of 0.7 and 0.8, in contrast to the behaviour of TBSRs of 0.2 and 0.5, agglomerates which are spherical and dense do form, with the recovery and drying of agglomerates found to be exceptionally quick. Importantly, agglomerates did not form a paste, even after prolonged periods of time under agitation. Here, the balance between the bridging liquid volume and the available solid is reached. These results are shown in [Figure 6.4](#) and [Figure 6.5](#).

A TBSR of 1.0 produced spherical agglomerates, which appear to be slightly weaker than those formed at lower TBSR values ([Figure 6.6](#)). Recovery and drying were possible. The time for complete agglomeration was 56 minutes, with the agglomerates remaining stable before forming a paste at 59 minutes. A TBSR of 1.5 produced agglomerates which also incorporated all of the suspended paracetamol. The agglomerates were spherical and fairly dense, and therefore able to survive filtration and drying ([Figure 6.7](#)). The time for formation of a paste was 39 minutes after the addition of bridging liquid, around one minute after all the solid had been incorporated into agglomerates.

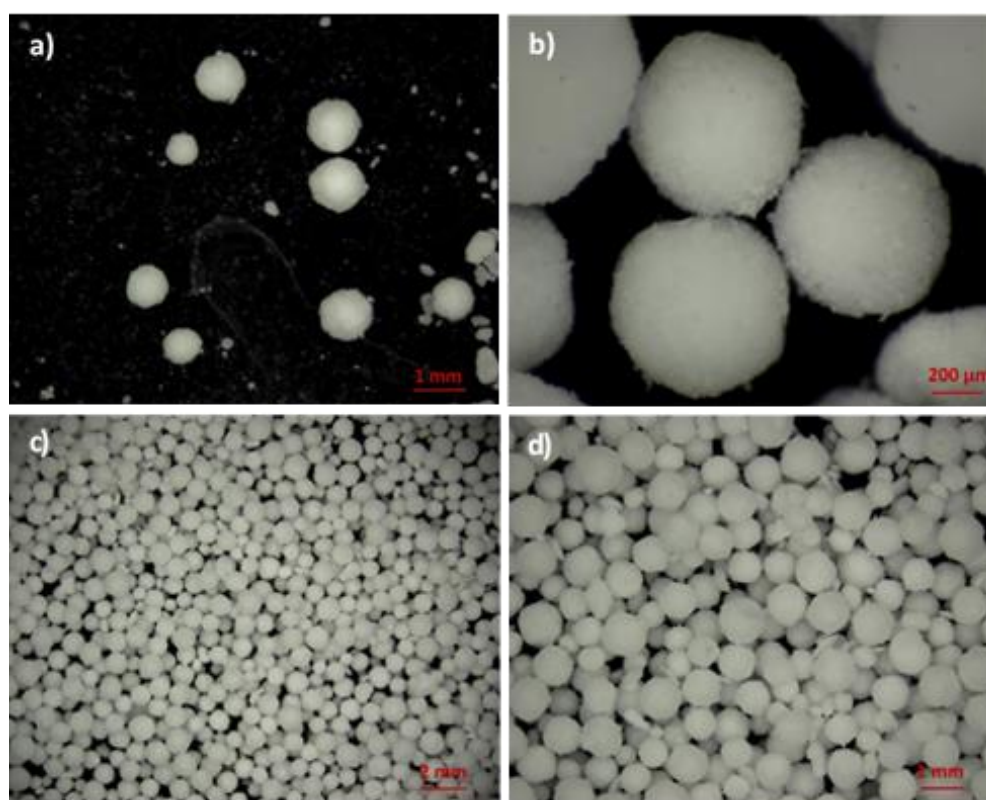


Figure 6.4. Agglomerates at 75 minutes after bridging liquid addition (TBSR = 0.7) with a) and b) isolated from the reactor and c) and d) filtered and dried.

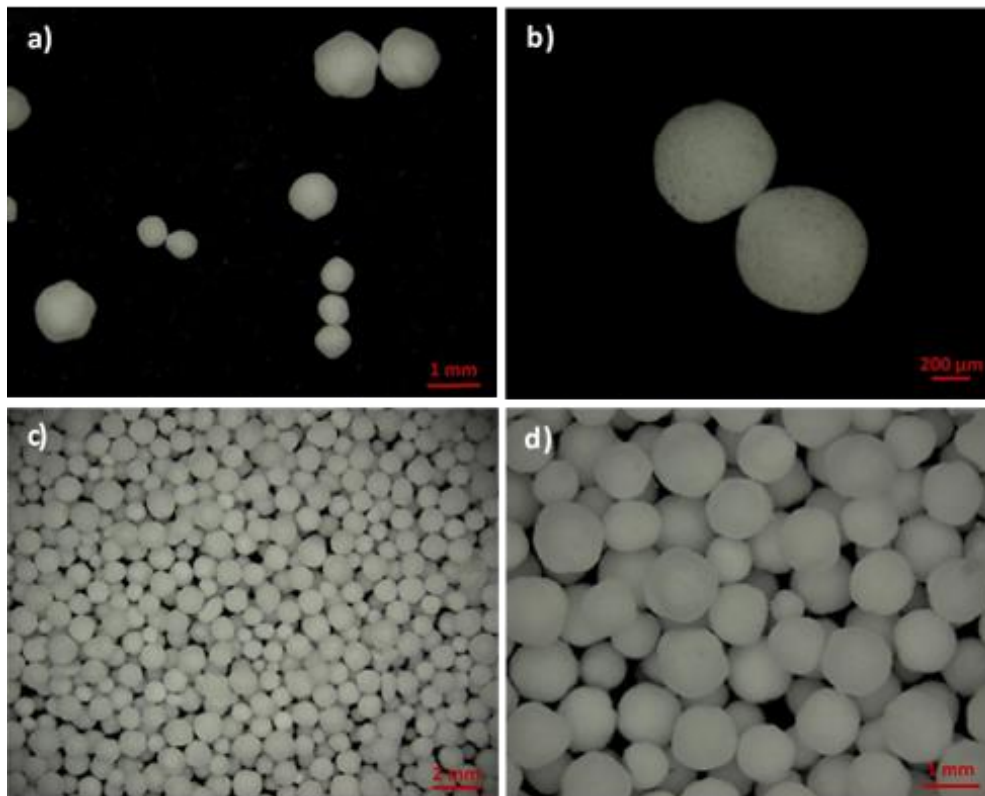


Figure 6.5. Agglomerates at 75 minutes after bridging liquid addition (TBSR = 0.8) with a) and b) isolated from the reactor and c) and d) filtered and dried.

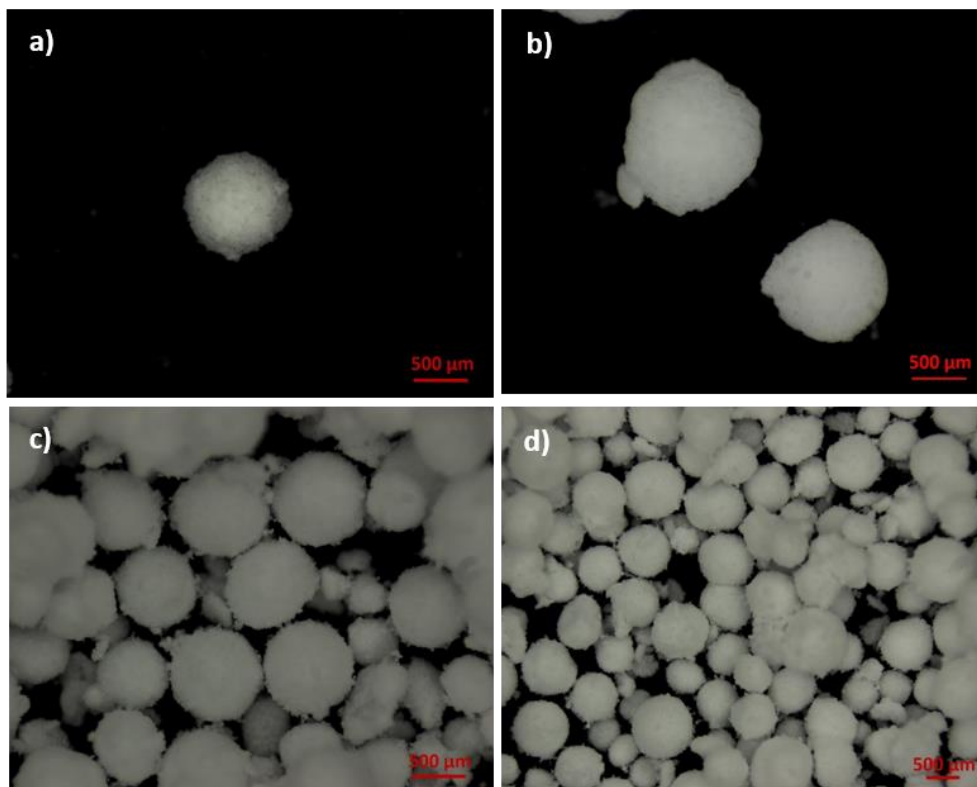


Figure 6.6. Agglomerates at 56 minutes after bridging liquid addition (TBSR = 1.0) with a) and b) isolated from the reactor and c) and d) filtered and dried.

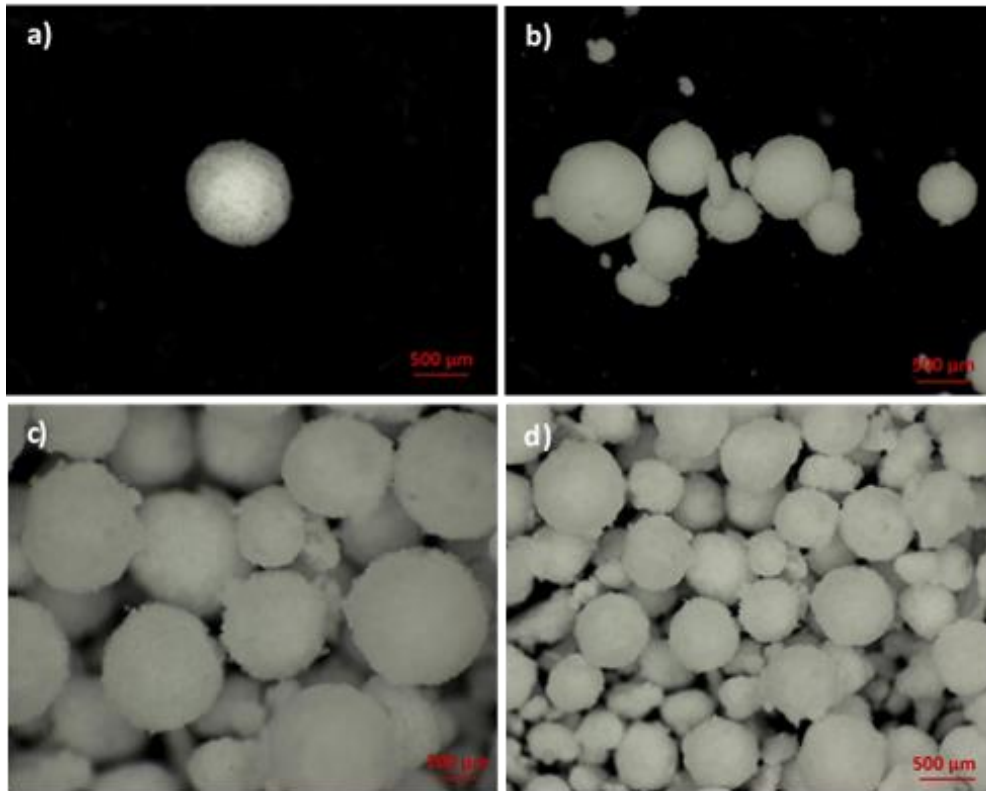


Figure 6.7. Agglomerates at 35 minutes after bridging liquid addition (TBSR = 1.5) with a) and b) isolated from the reactor and c) and d) filtered and dried.

At a TBSR of 2.0, another change in the agglomeration profile was observed. As before, 100 % agglomeration occurred, albeit on a much shorter timescale of approximately twenty-five minutes, with a paste forming soon after. Some agglomerates were spherical, but these were found to be weak and broke up during filtration and drying (Figure 6.8). A TBSR of 3.0 produces a paste at approximately fifteen minutes, with the recovery of preserved agglomerates being impossible. Upon filtration and drying, these agglomerates instantly form a brittle cake (Figure 6.9). Results for TBSR values of 0.9, 4, 6 and 8 are shown in Appendix C.

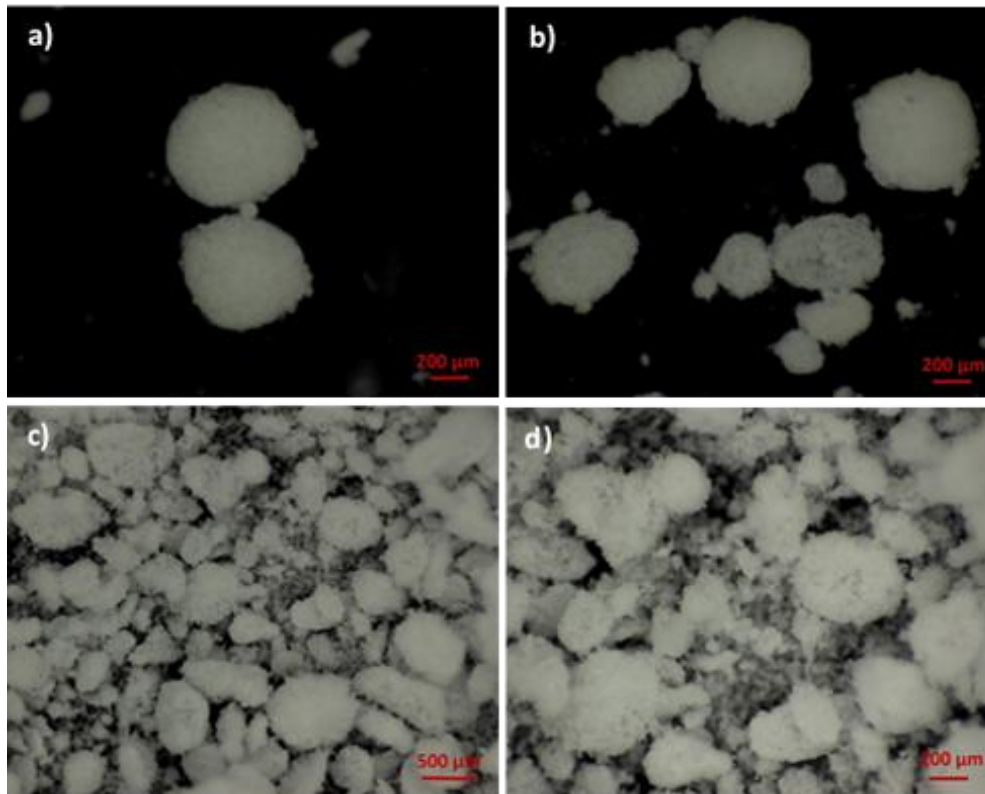


Figure 6.8. Agglomerates at 25 minutes after bridging liquid addition (TBSR = 2) with a) and b) isolated from the reactor and c) and d) filtered and dried.

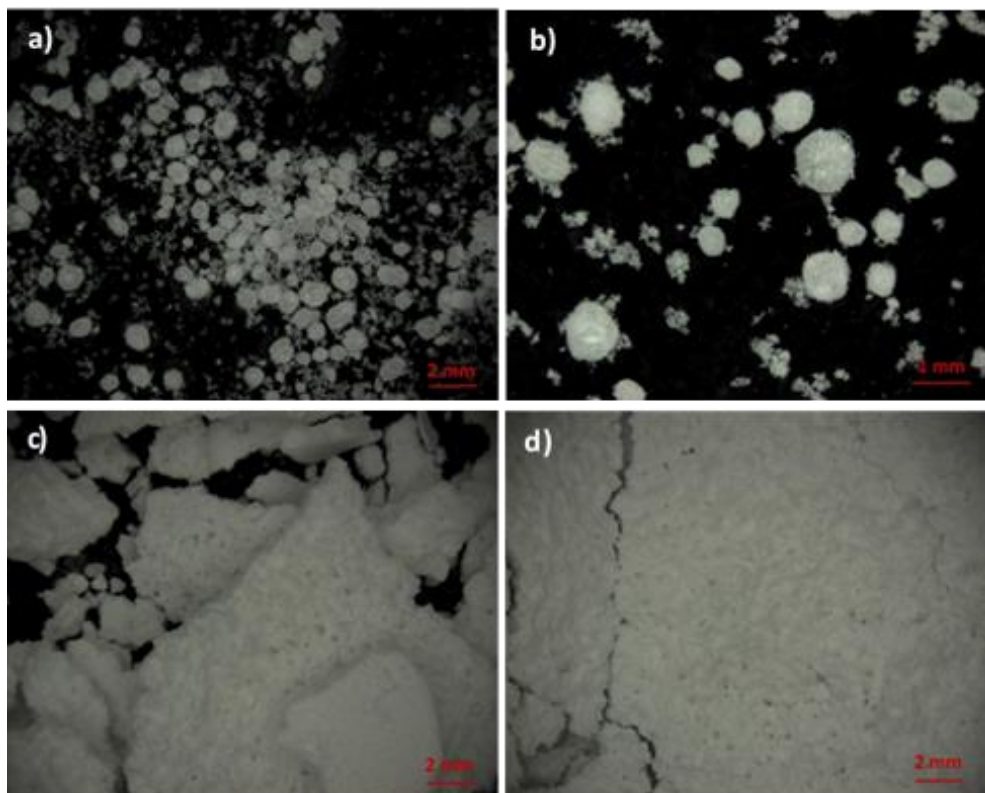


Figure 6.9. Agglomerates at 15 minutes after bridging liquid addition (TBSR = 3) with a) and b) isolated from the reactor and c) and d) filtered and dried.

Increasing TBSR reduced the time to paste overall. Additionally, agglomerates that did form were less dense. This would suggest that the increased number of bridging liquid droplets allowed a higher number of agglomerate shell nuclei to form. This rapid usage of the free material meant that densification of existing nuclei became impossible, explaining the low-density agglomerates observed here. If the time taken for paste formation is plotted against each TBSR value, the results follow a power law, as shown in [Figure 6.10](#). Five distinct agglomeration zones are observed, where each produces a different agglomeration profile.

These distinct zones provide an idea into the suitable operating region of the system under consideration. Zone E can immediately be discounted due to the instantaneous formation of a paste. Zone D produces agglomerates which are weak and do not survive filtration and drying. As such, these agglomerates are unsuitable for tableting as they are unlikely to be able to withstand the mechanical pressures involved. Zone A presents the converse: strong, robust agglomerates are formed but the yield of spherical agglomerates is low and primary particles remain in suspension; full agglomeration is never attained. This is generally undesirable in batch processes but could be beneficial in a continuous process, where the starting material can be recycled. Zone C represents the formation of strong, robust agglomerates, with a very high proportion of solid material incorporated, ideal for batch processes. These agglomerates are good candidates for downstream processing. As these conditions are time sensitive, it is important to recover the agglomerates as it is still possible to form a paste if the suspension is agitated for too long.

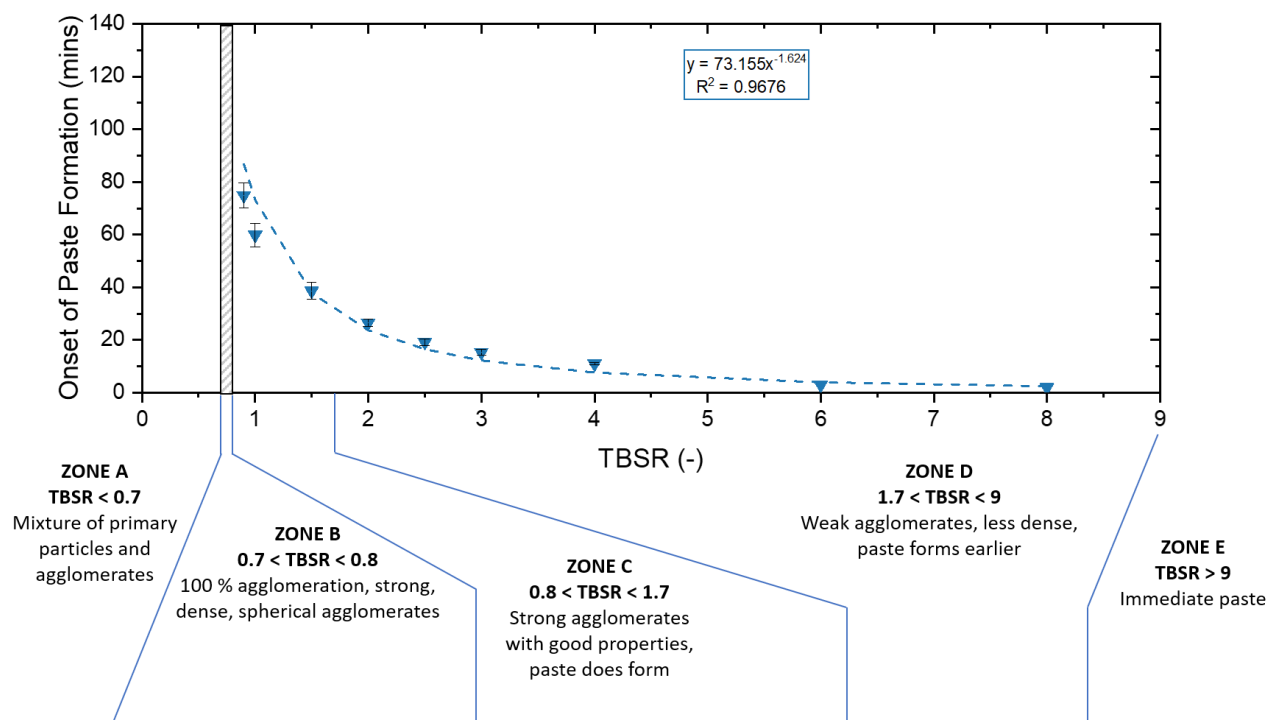


Figure 6.10. The influence of the TBSR value on the time required for paste formation in paracetamol-heptane-water spherical agglomeration experiments.

Zone B is the desired area of operation. Here, all the suspended product is incorporated which eliminates the need for product recycling. Additionally, there is an exceptionally long time required for the system to form a paste, which provides greater operational flexibility and stability: it may be possible to achieve adequate particle dispersion at low impeller speeds too. The agglomerates produced are also highly spherical and dense as desired. There is the potential for changes in the solid loading to have an influence on the agglomerate size distribution, which further enhances the desirability of operating within this region.

6.2.2 Influence of Solid Loading

Within spherical agglomeration literature, the influence and effect of solid loading is usually overlooked, with only two studies identified to date investigating this process parameter. Here, the authors found a decrease in porosity with increased loading, as well as an increase in agglomerate mean size [45,88]. Most studies reviewed in [Chapter 2](#) operate within 3 % w/w to 6 % w/w solid loading. Within the context of the pharmaceutical industry, higher solid loadings allow an increase product throughput and, therefore, a reduction in time to market of the finished product. Here, two

further solid loadings of 1 % w/w and 9 % w/w are investigated.

Interestingly, results from these experiments showed a degree of similarity for the time for paste formation, at different TBSR values as before, but there are some differences. These results are shown in Figure 6.11. The associated data is presented within Appendix C.

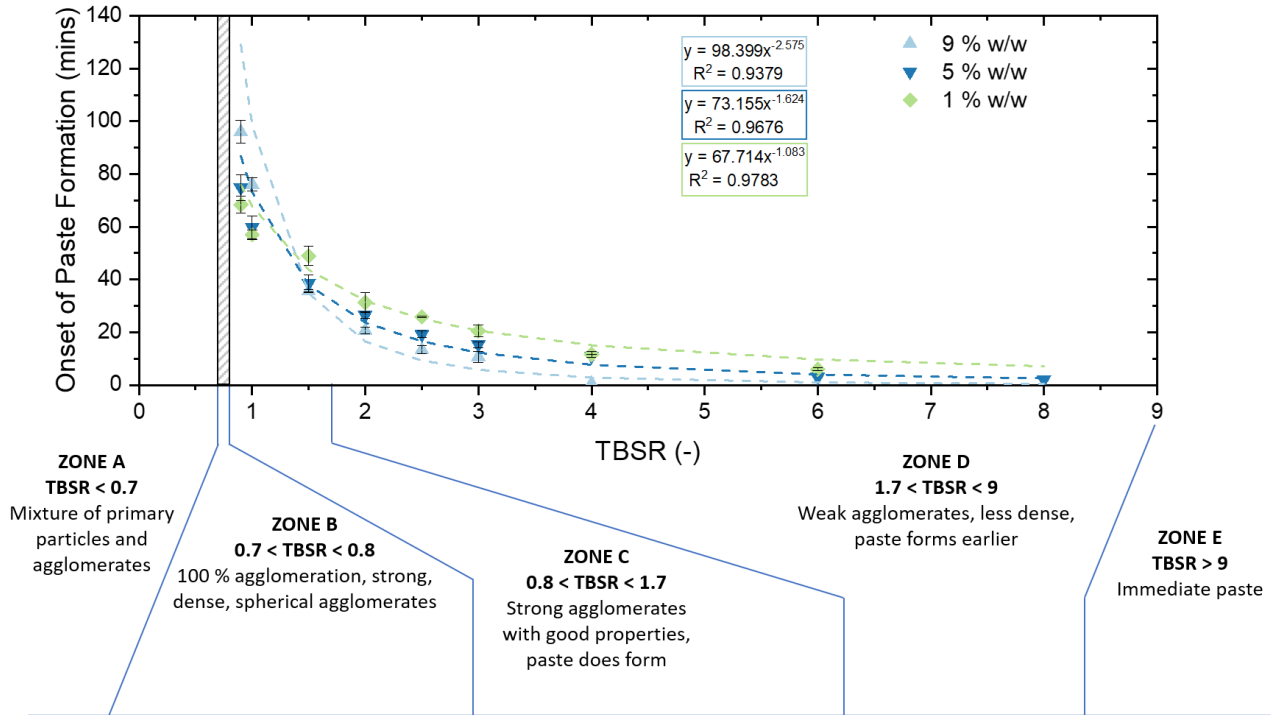


Figure 6.11. The influence of the TBSR value on the time required for paste formation in different solid loading conditions.

The results for agglomeration profiles are consistent across all solid loading conditions. The five demarcated zones previously identified are also still present, each with distinct product properties. The zones are separated at approximately the same TBSR value, regardless of the solid concentration used within the agglomeration vessel. Figure 6.11 shows an overlay of all three conditions, and the time to paste. At a TBSR of approximately 1.3, the three solid loading levels intersect. Below this TBSR, and above the optimal range, higher solid loadings take a longer time to form a paste. Above this TBSR, higher solid loadings take less time to form a paste. These results suggest that for TBSR values between 0.8 and 1.3, the agglomerate formation is limited by the volume of the bridging liquid available. As a result, it takes longer for all solid material to be incorporate into the fewer agglomerates formed. Conversely, above a value of 1.3, the process is not limited by this phenomenon. The bridging liquid is in excess, indicating particles are rapidly wetted and agglomerate growth begins almost instantaneously. This quick depletion of available solid results in agglomerate nuclei coalescence and the onset of paste formation.

The mean size of agglomerates was found to decrease with an increased solid loading, as shown in Figure 6.12. This also correlates with an overall decrease in agglomerate porosity (see Figure 6.13 and Equation 6.3). As the solid loading is increased, the available bridging liquid increases too, leading to an overall decrease in bridging liquid droplet sizes. This subsequently leads to a reduction in the agglomerate nuclei size and, eventually, the agglomerate size distribution. A larger number of collisions are also possible, which increases the compaction and consolidation of agglomerates. This is reflected by the noted increase in their density (reduction in their porosity).

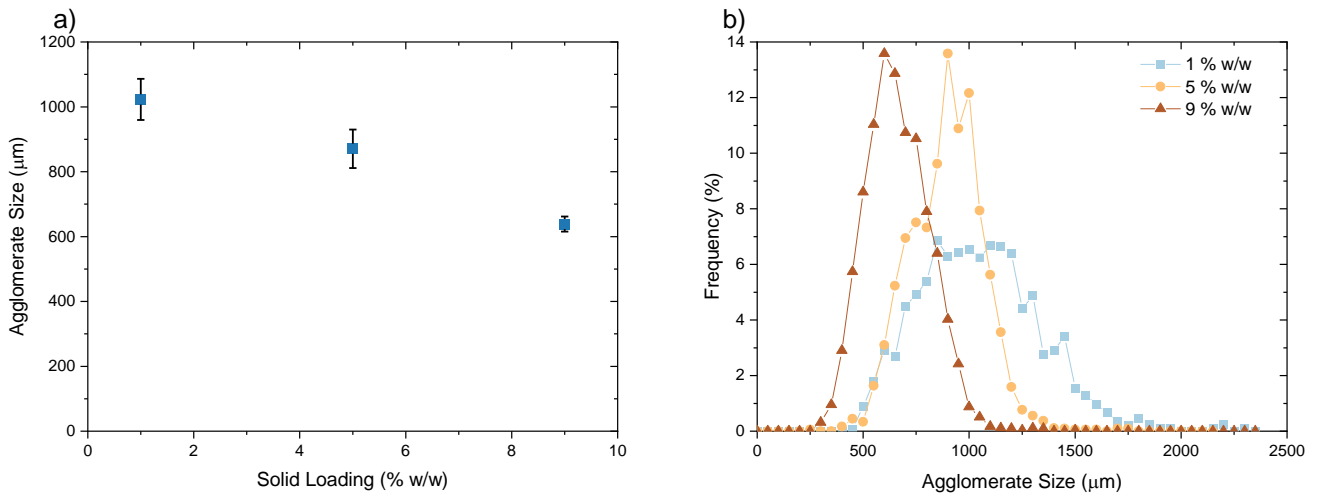


Figure 6.12. The mean size (a) and size distribution (b) of agglomerates as a function of solid loading, at a TBSR of 0.7. The recovery times are 100 mins for 1 % w/w loading, 160 mins for 5 % w/w loading and 320 mins for 9 % w/w loading.

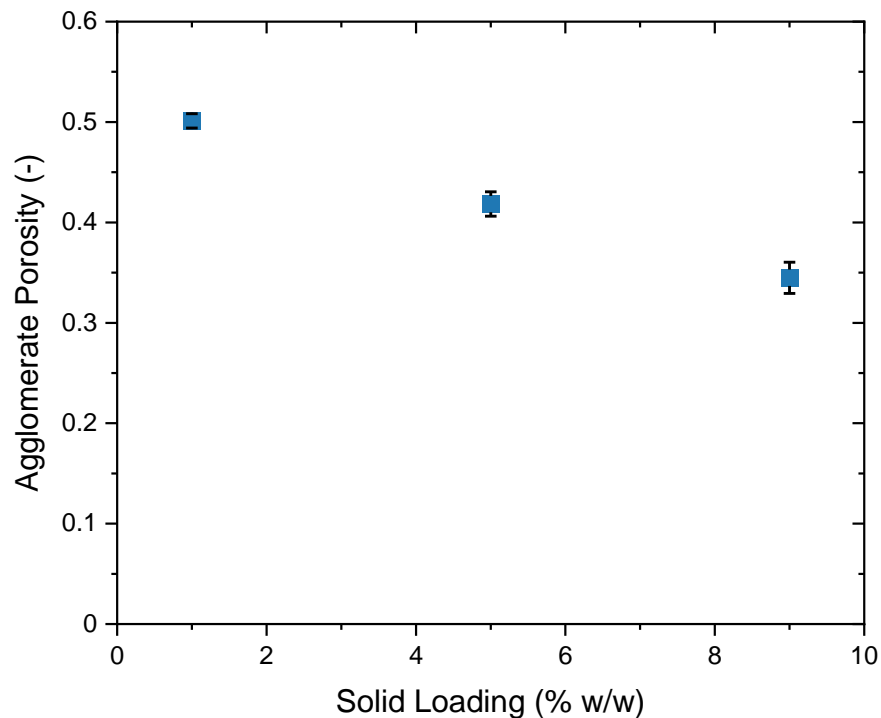


Figure 6.13. Agglomerate porosity as a function of solid loading. Error bars represent standard error of 20 measurements.

6.2.3 Influence of Impeller Speed

The investigation into the effect of shear rate was carried out in the optimum zone (TBSR = 0.75). Three different impeller speeds were used: 300 rpm, 500 rpm and 700 rpm. The energy dissipation rate can be estimated as:

$$\varepsilon = \frac{P \times D_{imp}^5 \times N^3}{V_{susp}} \quad \text{Equation 6.1}$$

Here, P is the power number, D_{imp} is the impeller diameter, N the speed of agitation, and V_{susp} the suspension volume. The Power Number is defined as:

$$P = \frac{Power}{\rho N^3 D_{imp}^5} \quad \text{Equation 6.2}$$

Table 6.1 shows the energy dissipation rates for this system ($P = 0.36$; $D_{imp} = 0.055$ m)[124].

Table 6.1. Calculated energy dissipations rates.

Speed of Agitation (rpm)	Calculated Energy Dissipation Rate (m ² s ⁻³)
300	0.453
500	2.097
700	5.754

Higher impeller speeds were shown to produce smaller agglomerates. The mean size of recovered agglomerates was 499 μm at an agitation speed of 700 rpm. At 500 rpm, this mean size increased to 723 μm. A speed of 300 rpm yields the largest agglomerates, with an average agglomerate size of 1182 μm. Figure 6.14 shows the recovered agglomerates, and Figure 6.15 shows the agglomerate size distribution, as measured through image analysis. This trend is expected as increasing the agitation speed reduces the size of bridging liquid droplets during infusion. It also promotes increased levels of consolidation through increased agglomerate-agglomerate and agglomerate-equipment collisions. The porosity of agglomerates can be calculated from the agglomerate density and the true density of paracetamol, as per Equation 6.3:

$$Porosity = 1 - \frac{\rho_{agg}}{\rho_{true}} \quad \text{Equation 6.3}$$

This finding is supported by a decrease in the porosity of agglomerates, as shown in Figure 6.16. Smoother, more spherical agglomerates were obtained at higher impeller speeds. It has been noted within the literature that these higher impeller speeds may promote breakage, which was also noted within the results here [6,23,45].



Figure 6.14. The influence of impeller speed on agglomerate size and morphology, at a TBSR of 0.75 with a 5 % solid loading. Conditions at a) 300 rpm, b) 500 rpm and c) 700 rpm.

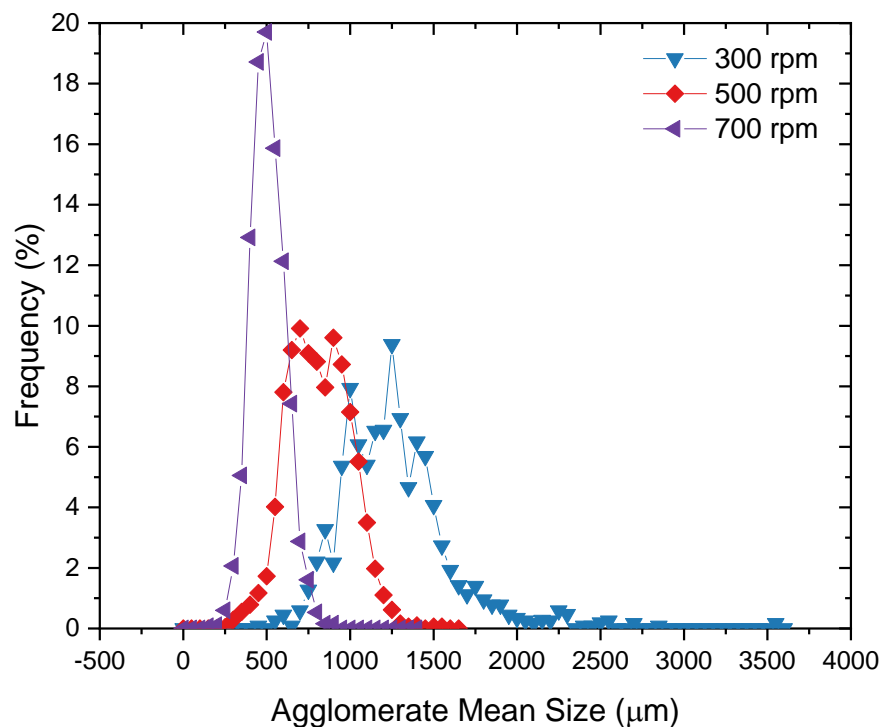


Figure 6.15. The influence of impeller speed on agglomerate size distribution at a TBSR of 0.75 with a 5 % solid loading.

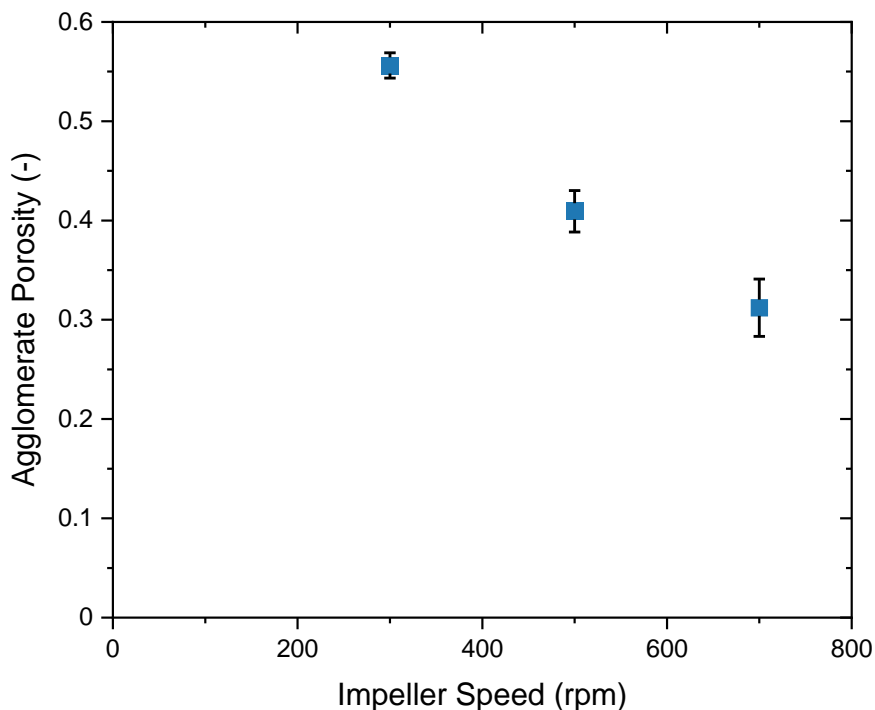


Figure 6.16. The influence of impeller speed on agglomerate porosity at a TBSR of 0.75 with a 5 % solid loading.

6.2.4 Agglomerate Structure Development

Agglomerate structure development was studied at TBSR = 0.75 with 5 % w/w solid loading. Here, the agglomeration profile remains within Zone B, where all material becomes fully incorporated without formation of a paste (see Figure 6.4 and Figure 6.5). Samples were taken at increasing time intervals from 10 min to 120 min after bridging liquid addition. Samples at 10 mins, 30 mins, 50 mins, 70 mins and 90 mins are shown in Appendix C. These results are displayed in Figure 6.17 to Figure 6.21.

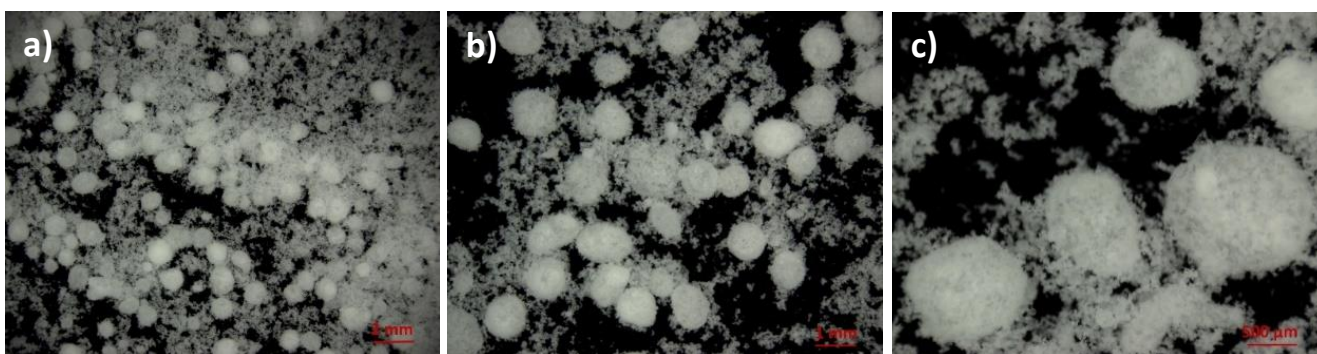


Figure 6.17. Observations of spherical agglomerate nuclei and paracetamol flocs 20 minutes after bridging liquid addition.

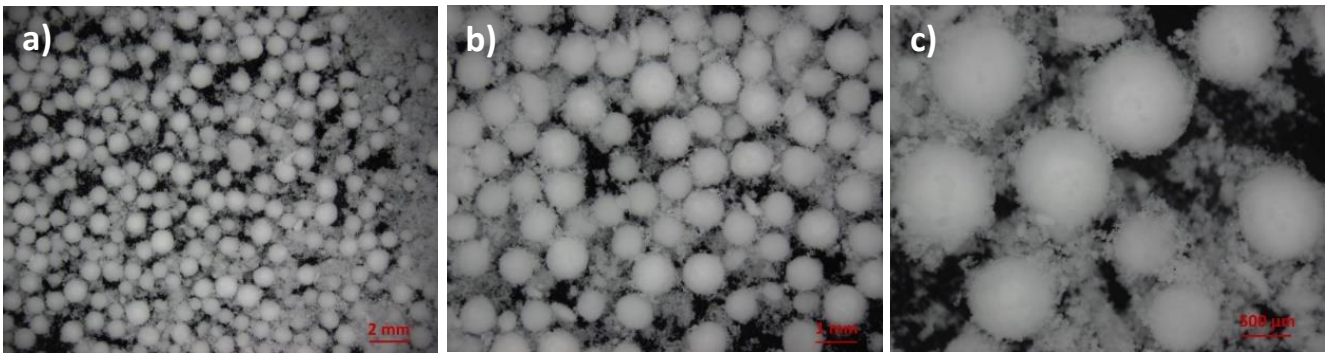


Figure 6.18. Observations of spherical agglomerates, nuclei and paracetamol flocs formed 40 minutes after bridging liquid addition.

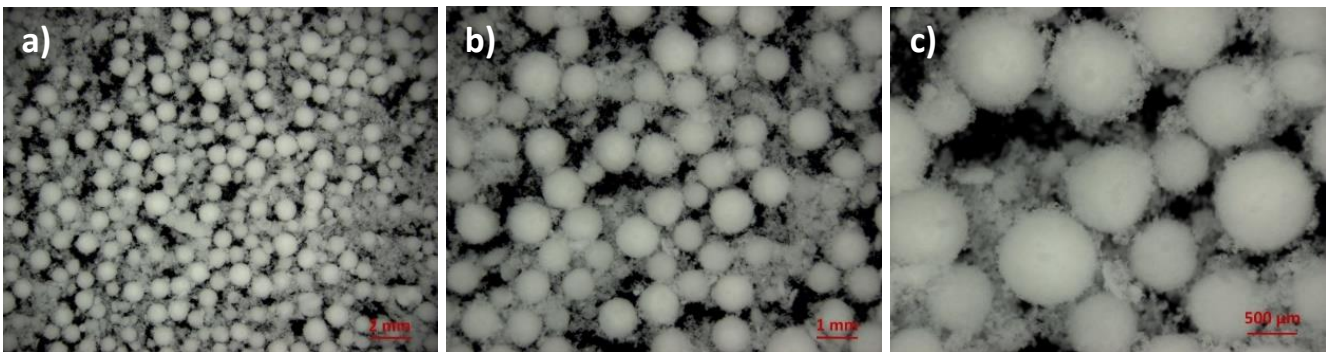


Figure 6.19. Observations of spherical agglomerates, and paracetamol flocs formed 60 minutes after bridging liquid addition.

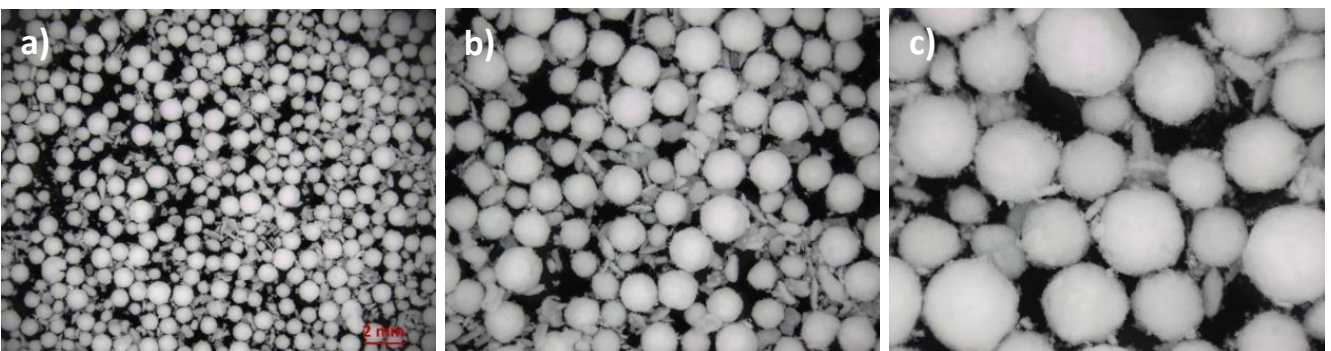


Figure 6.20. Observations of spherical agglomerates and fragments formed 80 minutes after bridging liquid addition.



Figure 6.21. Observations of spherical agglomerates and fragments formed 100 minutes after bridging liquid addition.

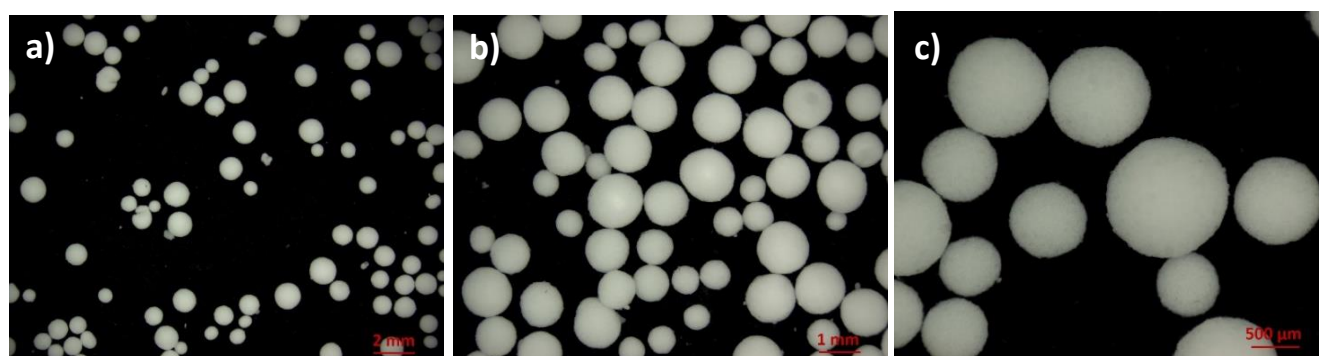


Figure 6.22. Observations of spherical agglomerates and fragments formed 120 minutes after bridging liquid addition.

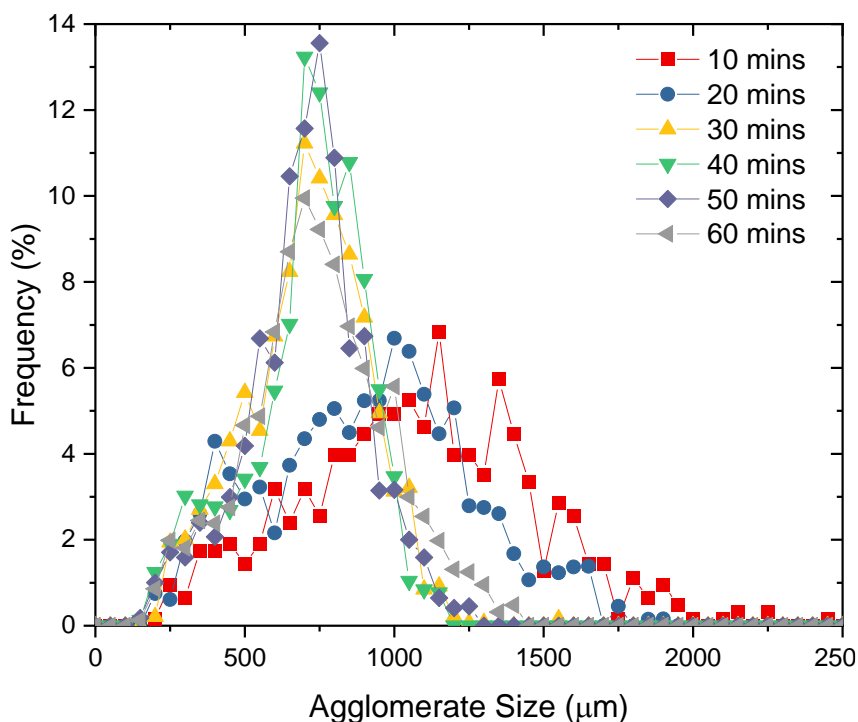
Over time, through compaction and consolidation, solid particles are pushed into the droplet which allows the nuclei to become much denser. This is reflected by the number of primary particles in solution reducing gradually over time, until all fines are incorporated at 80 minutes. This is mirrored by an increase in the number of distinct agglomerates formed, as well as agglomerates becoming smoother and more spherical with time.

There is some breakage or fragmentation of agglomerates at 80 minutes, as indicated in [Figure 6.20](#). However, this does not appear to lead to significant changes in the overall mean size of agglomerates. This suggests that the breakage which does occur happens at a rate equal to that of incorporation of material back into the agglomerate population. There appears, visually, to be a slight decrease in agglomerate sphericity and potentially a slight increase in agglomerate size. Fragments are still detected at 100 minutes, which suggests these rate processes are still occurring ([Figure 6.21](#)). After

120 minutes, highly spherical agglomerates are formed with only a very small amount of fragmented material remaining (see Figure 6.22). As identified in Section 6.2.1, there is no agglomerate coalescence at a TBSR of 0.75. Once all solid has been incorporated, there appears to be little to no free bridging liquid available. This absence of free bridging liquid is also a barrier to agglomerate coalescence.

The mean size of agglomerates was found to decrease within the first 30 minutes of the spherical agglomeration process. This is most likely due to consolidation and compaction, where young agglomerate nuclei become much more densified over time, as well as the breakage of large, weaker agglomerates. The finding is also supported by the increase in the percentage of solids agglomerated during spherical agglomeration experiments (see

Figure 6.23). The particle size distribution is also much wider at these earlier stages in the experiment (see Figure 6.24). These findings are mirrored in an immersion nucleation mathematical model of interest, where agglomeration processes limited by the collision rate of the particles and bridging liquid, showed an approximately linear growth of dimensionless agglomerate volume. This model is



discussed in more detail in subsequent sections.

Figure 6.23. The influence of residence time on the percentage of initial solid incorporated into agglomerates. A BSR of 0.75, 5 % w/w solid loading, and 500 rpm shear rate was used. Error bars represent standard error of three measurements.

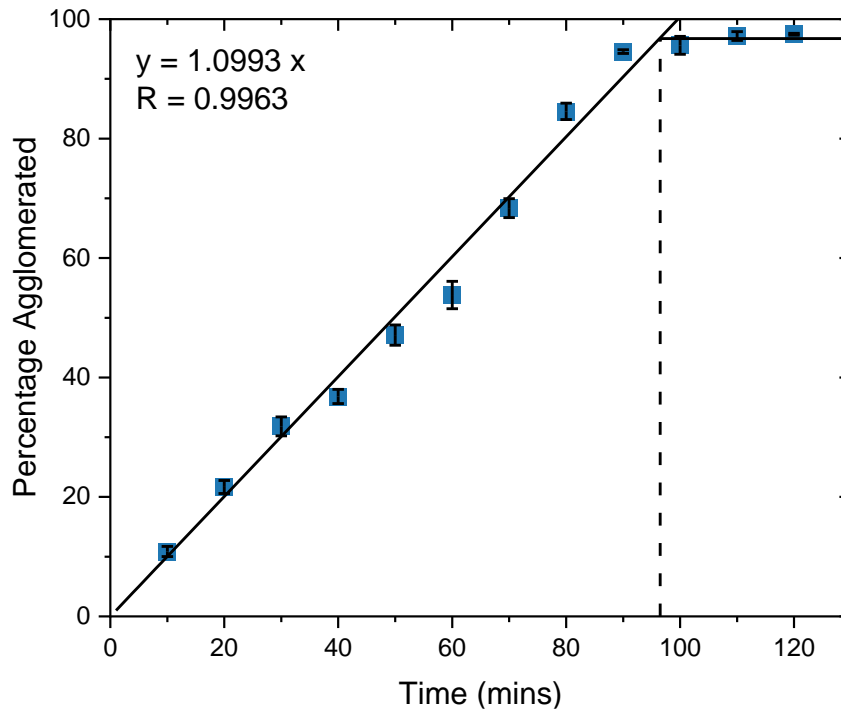


Figure 6.24. The influence of residence time on the agglomerate size distribution. A BSR of 0.75, 5 % w/w solid loading, and 500 rpm shear rate was used.

Figure 6.25 shows the relationship between agglomerate size and sphericity as a function of residence time. Critically, three distinct regions can be identified from the data and qualitative image analysis. Region A represents the formation of low-density agglomerates initially, which densify causing a decrease in their size. A sharp increase in sphericity mirrors a decrease in the average agglomerate size. Region B defines the formation of stronger and denser agglomerates, which are less susceptible to breakage. The sphericity increases slightly as agglomerates consolidate and become more well-formed. No significant change in the agglomerate size is detected, probably as a result of consolidation & growth and breakage & attrition rate processes being approximately equal. Finally, Region C represents dense agglomerates which are incorporating breakage fragments. This leads to zero change in density, but a decrease in sphericity. Through further shear force and consolidation, this decrease in sphericity is reversed as agglomerates become more rounded and smoother.

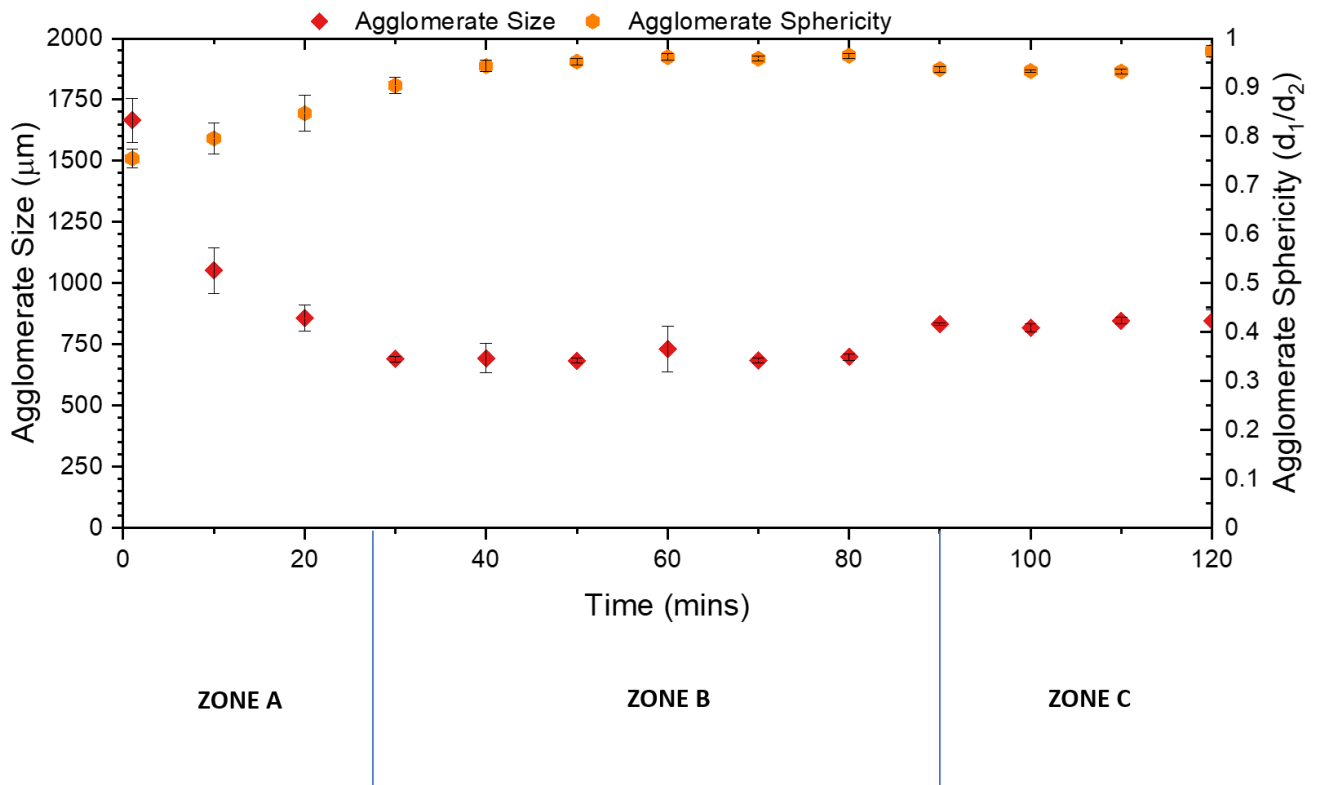


Figure 6.25. The influence of residence time on the agglomerate mean size and sphericity. Standard error bars represent standard deviation of two experiments.

Figure 6.26 shows that the agglomerate density increases with an increasing residence time. The relationship is linear until around a 100 minute residence time is reached. After this point, the density and porosity of agglomerates roughly remains constant. This time corresponds to complete agglomeration, as per percentage agglomeration plots (see

Figure 6.23). This agrees with visual observations of agglomerate formation, as all fines have been incorporated and a balance between breakage and consolidation is reached (Figure 6.21). This also aligns with

Figure 6.23, where, over multiple runs, all solid was deemed to have agglomerated just after 100 minutes. The final recorded density is 0.75 g cm^{-3} which corresponds to a final porosity of approximately 0.48. This aligns with results obtained for results in Section 6.2.2 and Section 6.2.3.

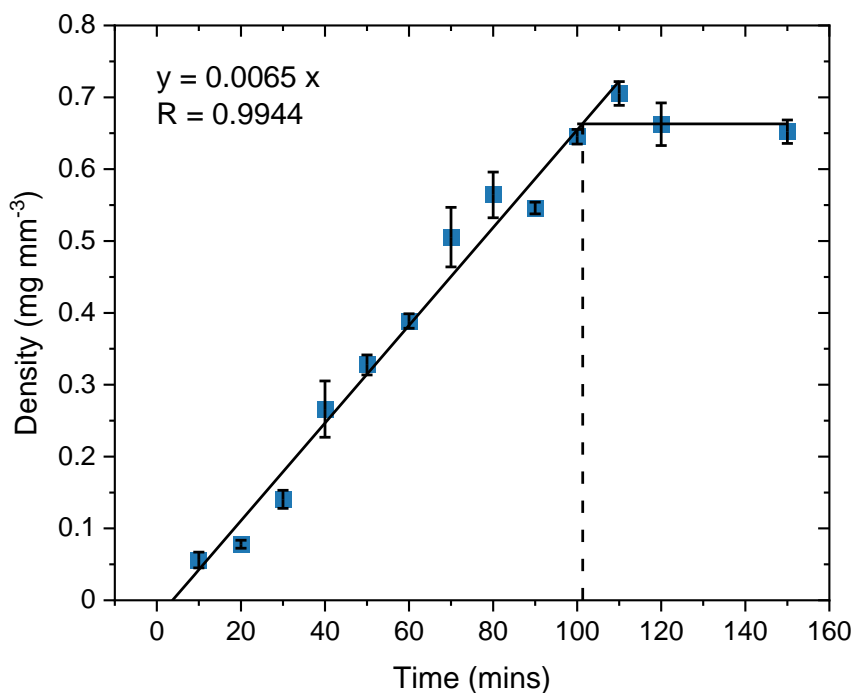


Figure 6.26. The influence of residence time on the agglomerate density. A BSR of 0.75, 5 % w/w solid loading and 500 rpm shear rate was used here. and

6.2.5 Mathematical Theory

Next a previously developed mathematical model is applied to further mechanistic understanding of the agglomerate nucleation kinetics of the immersion mechanism in the spherical agglomeration of paracetamol. This utilises observations made in the previous sections and should inform the direction of future studies into immersion nucleation.

The model provided a way of expressing the optimal TBSR range, providing that the critical packing liquid volume fraction of agglomerates is known. It should be noted that if the TBSR utilised is larger than $TBSR_{opt}$, there are not enough crystals within the bulk solution to reach a packing of φ_{cp} within bridging liquid droplets. Additionally, φ_{cp} may be difficult to calculate or estimate. From [Section 6.2](#), the optimal range for the TBSR of water-heptane-paracetamol system is between 0.70 and 0.80. Using these values produces φ_{cp} values of 0.412 and 0.444, respectively.

The mathematical model also identifies two key limiting regimes for the kinetics of agglomerate nucleation in the immersion mechanism. Both regimes consider conditions in which the particles are more wettable by the bridging liquid than the bulk solution. Here, the particles are able to penetrate and enter into the bridging liquid droplets through compressive forces, as opposed to the collision

velocities and surface tension forces involved. These forces only limit the kinetics of the immersion rate.

The *immersion rate limited* regime defines scenarios in which it is assumed a packed layer of particles is always available at the surface of the bridging liquid droplet [12]. Thus, the rate of agglomerate nucleation is controlled by the wetting action only, *i.e.* the rate at which particles can be incorporated into the young agglomerate nuclei. The *collision rate limited* regime assumes that nucleation is limited by the collision rate of particles and bridging liquid droplets, *i.e.* the availability of particles at the surface of the droplet. As such, this second regime occurs on a much faster timescale than the first. The agglomeration nucleation number is used to define these regions and is defined as the ratio between the timescales required for full agglomeration nucleation, limited by the immersion rate and the collision rate:

$$\frac{t_{imm}}{t_{coll_bat}} = AgNu \frac{TBSR \left(\frac{1 - \varphi_{cp}}{\varphi_{cp}} \right)}{\ln \left(\frac{1}{1 - TBSR \left(\frac{1 - \varphi_{cp}}{\varphi_{cp}} \right)} \right)} \quad \text{Equation 6.4}$$

In the case of the immersion rate limited model ($AgNu > 100$), the timescale for completion immersion of crystals inside the bridging liquid droplet is given by:

$$t_{imm} = \frac{15\mu_d D_d^2}{4\Psi D_p \gamma \cos\theta} \frac{(1 - \varphi_{cp})}{\varphi_{cp}^3} \quad \text{Equation 6.5}$$

where μ_d is the viscosity of the bridging liquid, D_d is the bridging liquid droplet diameter, Ψ is the sphericity factor, D_p the particle diameter, γ the interfacial tension of the bridging liquid in the suspension liquid, and θ the contact angle of the bridging liquid on the solid at the bulk solution-bridging liquid-solid interface. In the case of a collision rate limited regime ($AgNu < 1$), the timescale is given by:

$$t_{coll_bat} = \frac{D_d}{2\alpha \left[u(D_p)^2 + u(D_d)^2 \right]^{\frac{1}{2}} \varphi_{pb0} TBSR} \ln \left(\frac{1}{1 - TBSR \left(\frac{1 - \varphi_{cp}}{\varphi_{cp}} \right)} \right) \quad \text{Equation 6.6}$$

where α is the target efficiency, the target efficiency here defines the fraction of particles within the fluid volume displaced by the bridging liquid droplet, which successfully interact. Additionally, $u(D_p)$ and $u(D_d)$ represent the velocities of the particles and droplets, respectively. Instances during the immersion mechanism can occur, in which the system is limited by a combination of both the *immersion rate limited regime* and *collision rate limited regime* i.e., when the predicted *agglomeration nucleation number* is close to 1. This can be thought of as the *immersion rate limited* and *collision rate limited* timescales being approximately equal. This scenario is probable during several conditions, including a lack of crystal particles within the bulk solution. To assess the volume fraction of particles in the bulk mother solution over time for an immersion rate limited regime, the following equation can be used:

$$\varphi_{Pb}(t) = \varphi_{Pb0} \left(1 - \frac{2TBSR}{D_d} \left(\frac{\Psi D_p \gamma \cos\theta}{15\mu_d} (1 - \varphi_{cp}) \varphi_{cp} t \right)^{\frac{1}{2}} \right) \quad \text{Equation 6.7}$$

where φ_{Pb0} is the initial concentration of solid within the bulk solution. If we consider the kinetics of the time for paste formation of paracetamol (see [Section 6.2](#)), it can be assumed that the time for a paste to form is equal to when the solid concentration within the bulk solution is equal to zero ($\varphi_{Pb} = 0$). Using these parameters, the concentration of the solid within the solution at a given time t , can be calculated as follows:

$$\varphi_{Pb}(t) = \varphi_{Pb0} \exp \left(- \frac{2\alpha \left[u(D_p)^2 + u(D_d)^2 \right]^{\frac{1}{2}} \varphi_{Pb0} TBSR}{D_d} t \right) \quad \text{Equation 6.8}$$

The velocities of the particle-mother solution and droplet-mother solution can be calculated according to [Equation 6.9](#) and [Equation 6.10](#) respectively, and the target efficiency to [Equation 6.11](#). This is shown in [Figure 6.27](#).

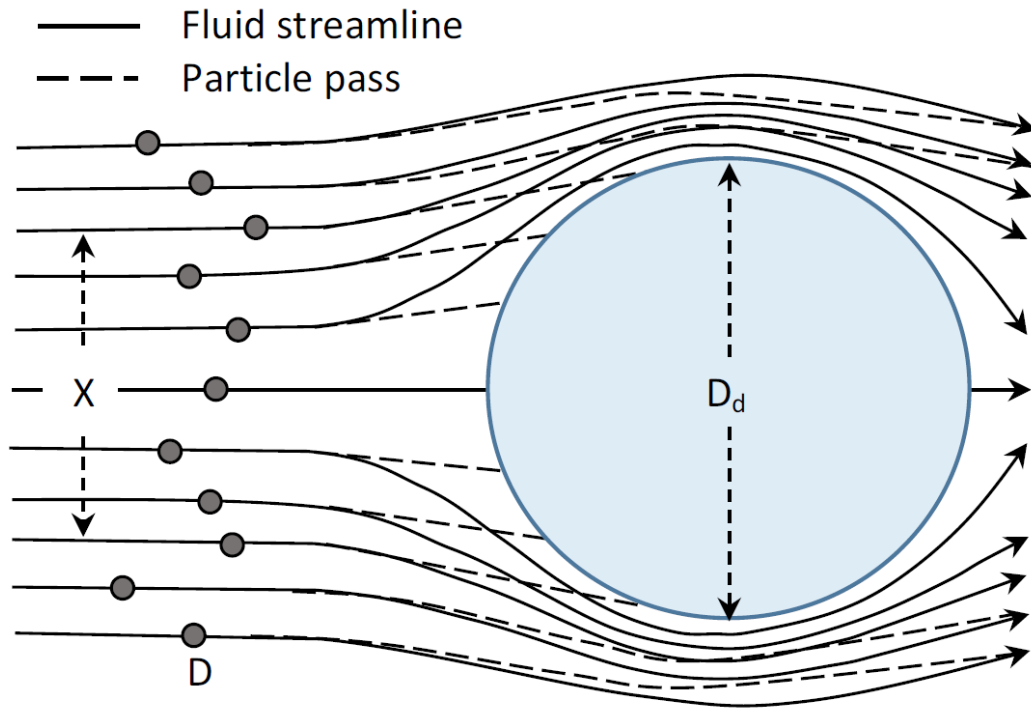


Figure 6.27. Bridging liquid droplet and particle interaction which defines the target efficiency. Reproduced from Arjmandi-Tash et al., [12].

$$u(D_p) = \left[\frac{(|\rho_p - \rho_l|)^3}{200\rho_l\mu_l(2\rho_p + \rho_l)} \right]^{\frac{1}{3}} D_p^{\frac{3}{5}} \varepsilon^{\frac{2}{5}} \quad \text{Equation 6.9}$$

$$u(D_d) = \left[\frac{(|\rho_d - \rho_l|)^3}{200\rho_l\mu_l(2\rho_d + \rho_l)} \right]^{\frac{1}{3}} D_d^{\frac{3}{5}} \varepsilon^{\frac{2}{5}} \quad \text{Equation 6.10}$$

$$\alpha = \left[\frac{32}{225} \frac{(\rho_p - \rho_l)^2 g^2}{\rho_l \mu_l} \right]^{\frac{1}{3}} \frac{D_p}{2gD_d} \left[u(D_p)^2 + u(D_d)^2 \right]^{\frac{1}{2}} \quad \text{Equation 6.11}$$

where ρ is density, μ is viscosity, D is diameter for the particles (p) and liquid (l).

6.2.6 Model Parameters & Assumptions

To evaluate the effect of TBSR on the concentration of paracetamol particles in the bulk solution during nucleation, the parameters use both known and assumed values. Table 6.2 displays the value for each of the parameters used in Equation 6.1 to Equation 6.11, for the experimental system used in Section 6.2. A TBSR of 0.75 is used, which represents a condition within the optimal region (see Figure 6.11). A value of 0.425 for φ_{cp} is calculated from this TBSR value. The sphericity Ψ , is assumed to be

0.5, and the bridging liquid droplet diameter D_d , is assumed to be 100 μm . Remaining parameters are calculated from the values shown in Table 6.2.

Table 6.2. Summary of parameters and values used for sensitivity analysis of a mechanistic model.

Parameter	Units	Value
D_p	m	2.1×10^{-5}
D_d	m	1×10^{-4}
μ_d	Pa s	8.9×10^{-4}
μ_L	Pa s	3.76×10^{-4}
γ	N m^{-1}	0.051
θ	°	45
ρ_p	kg m^{-3}	1260
ρ_d	kg m^{-3}	997
ρ_L	kg m^{-3}	684
ε	$\text{m}^2 \text{s}^{-3}$	2.097
ω	-	0.5
φ_{cp}	-	0.425
φ_{pb}	-	0.05
TBSR	-	0.75
α	-	
$u(D_p)$	m s^{-1}	
$u(D_d)$	m s^{-1}	
t_{imm}	s	
t_{coll}	s	

The following assumptions are also made, regardless of which regime the system falls in: crystal particles are assumed to be much more wettable by the bridging liquid, compared to the bulk solution of the system; immersion of particles into the bridging liquid droplet core occurs due to capillary force; a growing agglomerate nucleus contains a bridging liquid core and particle shell with liquid volume fractions of 1 and φ_{cp} respectively; a two-dimensional, planar geometry is used.

For the *immersion rate limited* regime only: a packed layer of particles is always available at the surface of bridging liquid droplets; the rate of nucleation is limited by the immersion of particles inside the bridging liquid droplets; the immersion rate is given by the rate of imbibition of bridging liquid in the packed layer through Darcy's law; permeability of the packed layer of particles is given by the Kozeny-Carman equation.

For the *collision rate limited* regime only: the immersion of particles inside the bridging liquid droplets is extremely fast; the rate of nucleation is limited by the collision rate between particles and

bridging liquid droplets; both the bridging liquid droplets and solid particles are larger than the Kolmogorov turbulent microscale; there is negligible change of the relative velocity of the bridging liquid droplet-bulk solution ($u(D_d)$) throughout the full nucleation time.

6.2.7 Model Prediction: Analysis & Discussion

Here, an insight into the relationship between the TBSR and the kinetics of agglomeration is provided. To do so, it can be assumed that the time required for the onset of paste formation is equal to when the solid concentration within the bulk solution is equal to zero. Experimentally, many systems formed a paste quickly (within a few minutes of all solids being incorporated into agglomerates), and therefore this assumption seems reasonable. Note that within the model, the onset time for nucleation is the parameter of most interest and is the one calculated, not the time for a paste to be formed. This nucleation time describes the time taken for droplets to ‘capture’ the particles of interest.

6.2.7.1 Effect of TBSR

If the immersion rate limited regime is first considered, using the appropriate values from [Table 6.2](#), [Figure 6.28](#) shows the results for various TBSR values. t_{imm} ([Equation 6.5](#)) was calculated to be a value of 0.00054 s. This corresponds to the complete filling of the droplets and depletion of solid within the bulk solution. For a TBSR of 0.7, the solid concentration within the bulk solution reaches zero to t_{imm} . This indicates there are not enough particles within the bulk solution to fill bridging liquid droplets to a value of $1 - \varphi_{cp}$. This model result was observed experimentally, with the disappearance fines for a TBSR of 0.7 after a certain period (see [Figure 6.20](#)). To reach the value of $1 - \varphi_{cp}$, the available solid would need to be increased. This indicates that the full packing was not reached. The model predictions for a TBSR of 0.4 and below show that t_{imm} is reached prior to the bulk solid concentration reaching zero. Here, there are enough particles for solids to reach $1 - \varphi_{cp}$. Experimentally, this is shown by particles remaining within solution (see [Figure 6.2](#) and [Figure 6.3](#)). It is unclear whether individual particles break off the agglomerates, whilst others are incorporated due to the shear forces.

If the collision rate limited regime is considered, again using appropriate values from [Table 6.2](#), [Figure 6.29](#) shows the results for various TBSR values. Here, the $1 - \varphi_{cp}$ condition of agglomerate formation is reached prior to the solids concentration within the solution reaching zero. This indicates

that there is an ample volume of solid available for the $1 - \phi_{cp}$ to be met. Experimentally, it would be expected that a large volume of fines are left in solution at a TBSR of 0.7, as the $1 - \phi_{cp}$ condition is satisfied. However, this was not observed experimentally, with all solid being incorporated into the agglomerates formed.

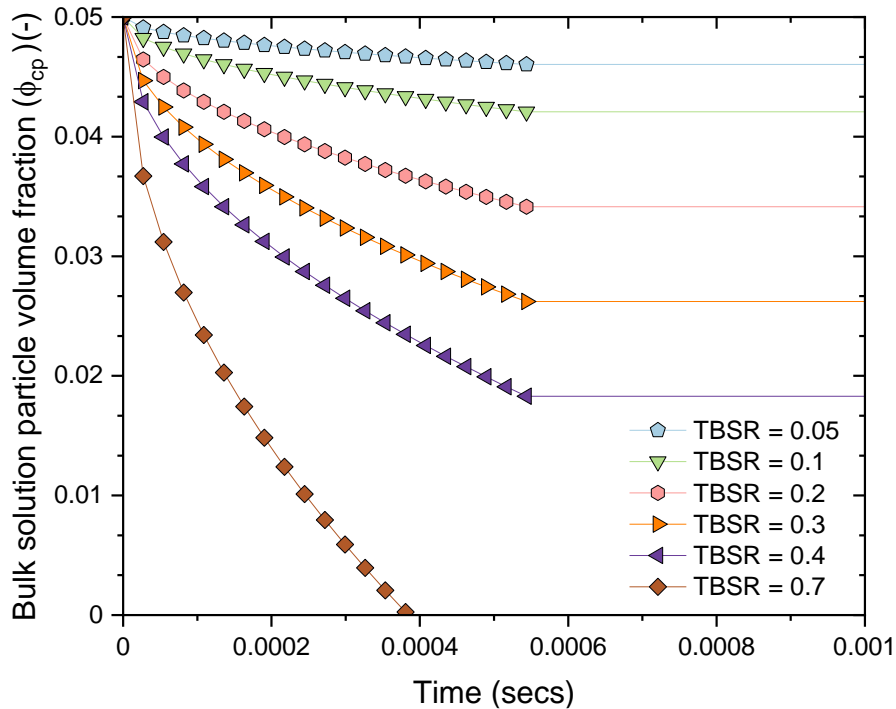


Figure 6.28. The time evolution of solid fraction within the bulk solution for the immersion rate limited regime, with variations in TBSR shown.

Figure 6.29. The time evolution of solid fraction within the bulk solution for the collision rate limited regime, with variations in TBSR shown.

6.2.7.2 Effect of Solid Loading

The influence of solid loading on the immersion rate and collision rate limited regimes was also considered through analysis of the ϕ_{cp} profiles. The solid loading, at 1 % w/w, 5 % w/w and 9 % w/w produced results contrasting to those when investigating varied TBSR values. In the immersion rate limited regime, changes in the solid loading of the system have no influence on the time taken for the bulk solids concentration to reach zero. This is shown in Figure 6.30, and occurs as the solid loading is not included in this parameter (see Equation 6.5). However, and as noted in Section 6.2.4 the solid loading does, in fact, play a role in the immersion nucleation kinetics.

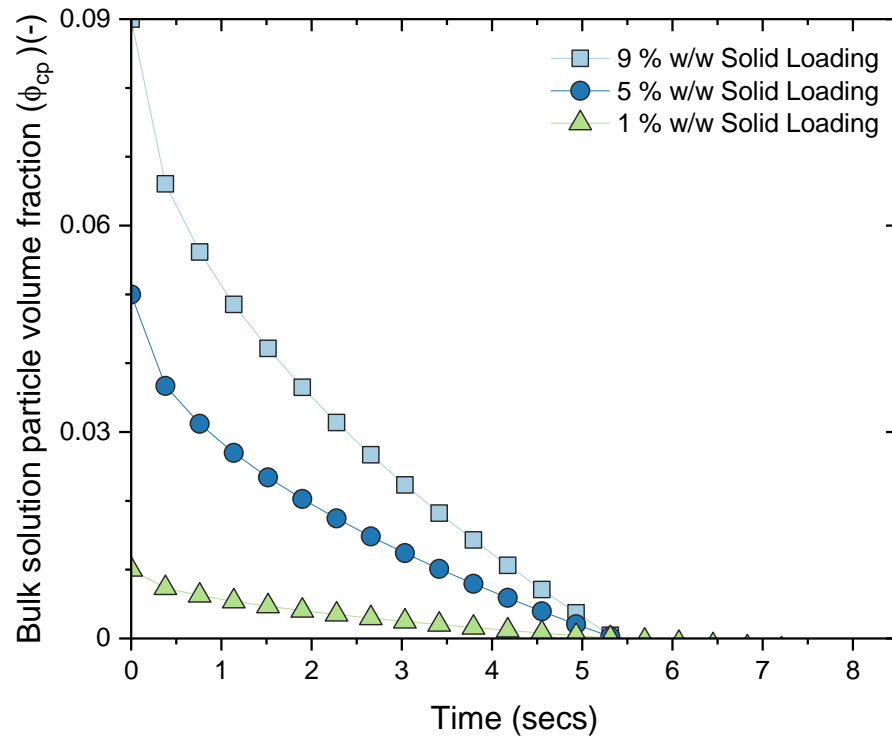


Figure 6.30. The time evolution of solid fraction within the bulk solution for the immersion rate limited regime, with variations in solid loading shown.

The collision rate limited regime predicts rapid decreases in the bulk solution solid concentration for systems with an increased level of solid loading. Systems with a 1 % w/w solid loading exhibited change over a much longer time frame (see Figure 6.31). There also appears to be cross-over point between all three solid loadings, although often the time t_{imm} is reached first. If present, this is a similar trend to that observed in Figure 6.11. Mechanistically, this result suggests that for higher solid loadings, particles are often wetted and incorporated into agglomerate nuclei exceptionally quickly, as more particle-nuclei collisions occur. As the particle concentration in the bulk solution decreases, the rate of collisions decreases, hence the slower rate seen later on. At higher solid loadings, the nuclei size becomes larger quicker. This is represented by the rate of reduction of the bulk solids concentration being higher in these conditions. For example, in Figure 6.31, at 0.2 seconds the rate of reduction in the bulk solids concentration is higher at 9 % loading, than both 5 % and 1 % conditions. As such, the time for a paste to form would expected to be lower at solids loadings of 9 %.

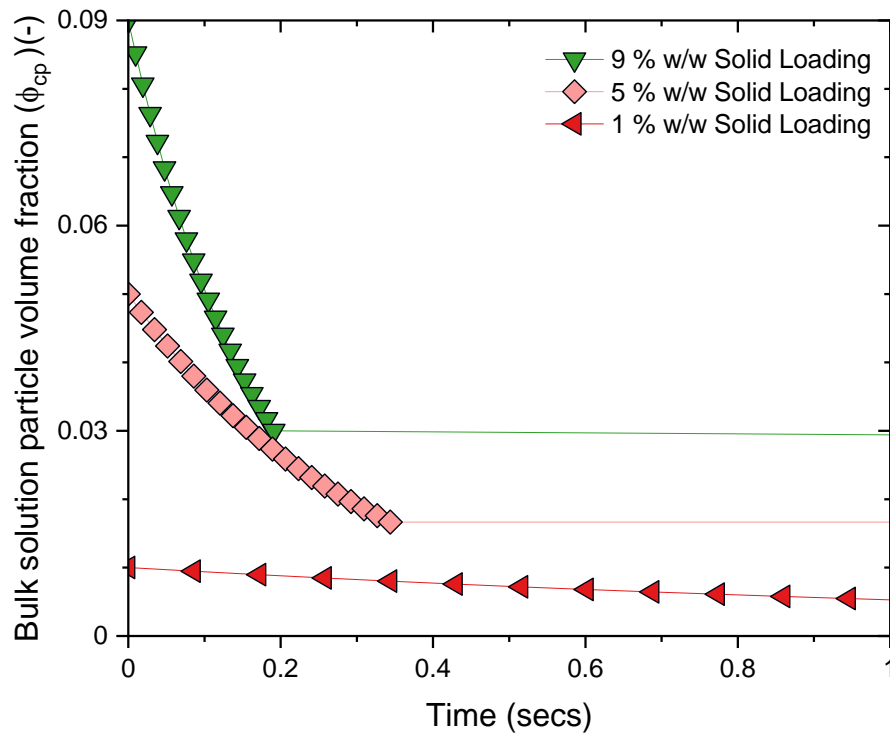


Figure 6.31. The time evolution of solid fraction within the bulk solution for the collision rate limited regime, with variations in solid loading shown.

6.2.8 Experimental vs Modelling Observations

In all model predictions, the predicted agglomeration times are several orders of magnitude different to those observed experimentally. This can be attributed to the direct result of the model considering the time for nucleation only, and not the time for the formation of a paste itself. Here, the time for nucleation describes the time required for particles to be captured by the bridging liquid droplet. Thus, the time taken for compaction and rearrangement of constituent crystals within an agglomerate nuclei is not considered. This process would allow further bridging liquid to become available at the nuclei surface, either to incorporate fines or un-agglomerated material from within the suspension or promote coalescence of individual agglomerate nuclei. Once the former of these processes has finished, then only agglomerate coalescence can occur, and thus, depending on the available bridging liquid at the surface of the nuclei, a paste is then formed. It should be noted that the time for the rearrangement and densification of nuclei takes a much longer time than anticipated in the case of paracetamol, most likely due to the needle-like morphology of primary particles.

However, the overall trends predicted by the model were observed experimentally. This indicates that the core theory of the model is correct and that, in the case of the paracetamol-heptane-water system, agglomeration is limited by the immersion rate of the solid inside bridging liquid

droplets. There are several possible reasons why the timescale for this rate process are experimentally different to the model prediction. The mathematical model here assumes that the solution is mono-dispersed – something which was not achieved experimentally. This was supported by the high degree of flocculation of paracetamol observed prior to the addition of bridging liquid. Additionally, the contact angle of water on paracetamol was found to be approximately 45° , much higher than literature values for other bridging liquid-solid systems. This is also much lower than the values measured for bridging liquids on salicylic acid, as used within [Chapter 5](#).

6.3 Conclusions

Paracetamol-heptane-water systems have been used to observe the immersion nucleation mechanism in-situ as a means of further developing mechanistic understanding. This includes the formation of agglomerate nuclei and their evolution into dense, spherical agglomerates. Here, a critical range of a TBSR of 0.7 – 0.8 was identified. This aligns with previously identified works, in which the optimal TBSR range and critical packing liquid volume fraction are directly related. This serves as an initial validation of the theory.

Four other distinct zones of operation were identified. These zones are separated by significant changes in the agglomerate properties, including their size, size distribution, porosity, and sphericity. These zones are also characterised by whether a paste forms and the time required for the onset of paste formation. Zone A represents systems where the TBSR is below the optimal range and is characterised by a high level of fines in solution ($\text{TBSR} < 0.7$). Here, the bridging liquid available is rapidly depleted and, thus, the formation of a paste was not observed, even at long residence times of 300 mins. Zone B represents the optimal range in which all particles are incorporated into spherical agglomerates. Here, agglomerates are more well-formed, reflected in their larger size, high sphericity, and density. When TBSR is higher than in Zone B, the agglomerate quality begins to decrease. A paste also forms providing the residence time is long enough.

Interestingly, these demarcated zones are still present and hold for changes in the solid loading of the system of interest. Slight differences in the time to paste were observed. At a TBSR of approximately 1.3, the time to paste curves intersect which provides further insights into the agglomeration kinetics of this study: between TBSR of 0.8 and 1.3, agglomeration is limited by the bridging liquid volume available; above this range, excess bridging liquid promotes nuclei coalescence

and the onset of a paste. Higher solid loading values were shown to reduce the average size of agglomerates from approximately 1050 μm to 700 μm , whilst increasing the density from approximately 0.63 g cm^{-3} to 0.82 g cm^{-3} . An increase in the shear of experiments was also found to promote similar changes in agglomerate characteristics.

A previously developed mathematical model was also used to evaluate the system of interest and draw comparison between the predicted and observed behaviours. Here, the general trends are the same for both, which serves as an initial validation of the model. However, the timescales predicted by the model are several magnitudes of order quicker. This can be attributed to the model only accounting for the nucleation time, and not the time for the compaction and rearrangement of constituent particles within agglomerate nuclei. Ultimately, the rate of this densification process will dictate the speed at which bridging liquid becomes available at the agglomerate surface, and thus, the time required for the formation of a paste. Further work characterising agglomerate nuclei at different residence times should be made, as a means of evaluating these compaction and rearrangement rate mechanisms.

CHAPTER 7:

CONCLUSIONS & FUTURE

WORK

7.1 Conclusions

Within this thesis, the influence of bridging liquid miscibility on the bridging liquid volume in spherical agglomeration processes has been identified. This influence has been quantitatively analysed through the use of simulations and experimental procedures. To account for this, a new process parameter, the true bridging liquid-solid ratio, has been developed and proposed. This definition is quantified as the total volume of the bridging liquid rich phase, which may be calculated by analysing solvent miscibility through ternary phase diagrams. As such, different bridging liquids and bulk solution compositions have no effect on this new process parameter, as their influence is accounted for within the calculations. This also extends to the solid loading concentration of the spherical agglomeration process under consideration.

As such, this new definition provides an instant comparison tool across different processes, regardless of these three aforementioned operating parameters. As the definition combines these three parameters together, and is indeed a dimensionless parameter, it should be used in subsequent future works as the beginnings of a regime map. The rationale of the definition has been supported through subsequent validation procedures within this body of work. The ease at which different systems can be compared has been demonstrated. Further results and analysis of the fraction of available bridging liquid, as a proportion of that originally added, has also been considered alongside agglomerate properties and size distributions. This provides further power in using the definition as a method of benchmarking spherical agglomeration processes.

The immersion nucleation mechanism has also been investigated within this thesis, using paracetamol as a model compound. From this investigation, a critical TBSR range was identified. Additional to this, distinct operating regimes were identified, all of which produced unique end agglomerate properties. The underlying mechanisms which govern these processes has been elucidated through identifying agglomeration formation, densification, and breakage over time. These kinetic results have been established through a novel sampling technique using aliquots and bridging liquid dyes. The results have also been compared to a mathematical model previously developed, which highlights that there is still much to learn. Whilst the model accurately predicts the overall trends occurring in immersion nucleation only spherical agglomeration processes, the timescales of such trends were found to be several orders of magnitudes slower than predicted by the model. This has identified a current limitation of this model, in which the time for the compaction and rearrangement of constituent particles within agglomerate nuclei is not accounted for.

7.2 Future Work

The recommendations for future work are as follows:

- Undertake experimental investigations for further ternary solvent systems and other particulates as means of further validating the TBSR definition proposed in this thesis.
- Investigate relaxing some of the assumptions in the TBSR definition to incorporate the degree of solid solubility within the bridging liquid rich phase during the spherical agglomeration processes.
- Further develop novel techniques, such as dyed bridging liquid, to promote and image the immersion mechanism in-situ to improve mechanistic understanding of wetting and nucleation in spherical agglomeration. Ideally, such studies should incorporate both bridging liquid droplet and particulate size control concurrently to ensure immersion nucleation.
- Study the timescales for the incorporation of crystalline particles into bridging liquid droplets and the compaction and rearrangement of constituent particles, paying particular attention to the influence of the solvent properties, for example, interfacial tension, wettability *etc.*

There are further areas within spherical agglomeration which also require further research. Whilst all studies may provide beneficial findings in spherical agglomeration as a whole, studies surrounding wetting and nucleation should be given priority. Ultimately, accurate control of this rate process will dictate how agglomerates form, grow and break, which determine the agglomerate properties themselves. Thus, wetting and nucleation may provide a crucial stepping-stone for the engineering of robust spherical agglomeration processes which produce superior spherical agglomerates.

Bibliography

-
- [1] P AGB, Shaping the future. Together., 2019.
- [2] K. Walshe, Education and debate The rise of regulation in the NHS, *Br. Med. J.* 324 (2002) 967–970.
- [3] K. Plumb, Continuous processing in the pharmaceutical industry: Changing the mind set, *Chem. Eng. Res. Des.* 83 (2005) 730–738.
- [4] J. Litster, *Design and processing of particulate products*, Cambridge University Press, 2016.
- [5] S.M. Iveson, J.D. Litster, K. Hapgood, B.J. Ennis, Nucleation, growth and breakage phenomena in agitated wet granulation processes: a review, *Powder Technol.* 117 (2001) 3–39.
- [6] M. Maghsoodi, A.S. Tajalli Bakhsh, Evaluation of physico-mechanical properties of drug-excipients agglomerates obtained by crystallization, *Pharm. Dev. Technol.* 16 (2011) 243–249.
- [7] K. Pitt, R. Peña, J.D. Tew, K. Pal, R. Smith, Z.K. Nagy, J.D. Litster, Particle design via spherical agglomeration: A critical review of controlling parameters, rate processes and modelling, *Powder Technol.* 326 (2018) 327–343.
- [8] J.H. Fincher, Particle size of drugs and its relationship to absorption and activity, *J. Pharm. Sci.* 57 (1968) 1825–1835.
- [9] Y. Kawashima, F. Cui, H. Takeuchi, T. Niwa, T. Hino, K. Kiuchi, Parameters determining the agglomeration behaviour and the micromeritic properties of spherically agglomerated crystals prepared by the spherical crystallization technique with miscible solvent systems, *Int. J. Pharm.* 119 (1995) 139–147.
- [10] Y. Kawashima, M. Okumura, H. Takenaka, Spherical crystallization: Direct spherical agglomeration of salicylic acid crystals during crystallization, *Science (80-.)*. 216 (1982) 1127–1128.
- [11] B. Kovačič, F. Vrečer, O. Planinšek, Spherical crystallization of drugs, *Acta Pharm.* 62 (2012) 1–14.
- [12] O. Arjmandi-Tash, J.D. Tew, K. Pitt, R. Smith, J.D. Litster, A new mathematical model for nucleation of spherical agglomerates by the immersion mechanism, *Chem. Eng. Sci.* (2019) 115258.
- [13] J.W. Mullin, *Crystallization*, 2001.
- [14] J.R. Farnand, H.M. Smith, I.E. Puddington, Spherical agglomeration of solids in liquid suspension, *Can. J. Chem. Eng.* 39 (1961) 94–97.
- [15] J.P. Sutherland, The agglomeration of aqueous suspensions, *Can. J. Chem. Eng.* (1962) 268–272.
- [16] A.F. Sirianni, C.E. Capes, J.E. Puddington, Recent experience with the spherical agglomeration process, *Can. J. Chem. Eng.* 47 (1969) 166–170.
- [17] A.M. Bailón-Salas, L.A. Ordaz-Díaz, I. Cháirez-Hernández, A. Alvarado-de la Peña, J.B. Proal-Nájera, Lead and copper removal from groundwater by spherical agglomeration using a biosurfactant extracted from *Yucca decipiens* Trel., *Chemosphere.* 207 (2018) 278–284.
- [18] Y. Kawashima, C.E. Capes, Further studies of the kinetics of spherical agglomeration in a stirred

- vessel, *Powder Technol.* 13 (1976) 279–288.
- [19] A. Lasagabaster, C. Martín, M.M. Goñi, Preparation of spherically agglomerated crystals of the 3,5-diglucoside of cyanidin (cyanin), *J. Chem. Technol. Biotechnol.* 60 (1994) 397–403.
- [20] A. Bausch, H. Leuenberger, Wet spherical agglomeration of proteins as a new method to prepare parenteral fast soluble dosage forms, *Int. J. Pharm.* 101 (1994) 63–70.
- [21] D. Amaro-González, B. Biscans, Spherical agglomeration during crystallization of an active pharmaceutical ingredient, *Powder Technol.* 128 (2002) 188–194.
- [22] S. Kumar, G. Chawla, A.K. Bansal, Spherical crystallization of mebendazole to improve processability, *Pharm. Dev. Technol.* 13 (2008) 559–568.
- [23] A.N. Usha, S. Mutalik, M.S. Reddy, A.K. Ranjith, P. Kushtagi, N. Udupa, Preparation and, in vitro, preclinical and clinical studies of aceclofenac spherical agglomerates, *Eur. J. Pharm. Biopharm.* 70 (2008) 674–683.
- [24] S. Bhadra, M. Kumar, S. Jain, S. Agrawal, G.P. Agrawal, Spherical crystallization of mefenamic acid, *Pharm. Technol.* 28 (2004) 66–76.
- [25] M. Ueda, Y. Nakamura, H. Makita, Y. Imasato, Y. Kawashima, Particle design of enoxacin by spherical crystallization technique. I. Principle of ammonia diffusion system (ADS), *Chem. Pharm. Bull.* 38 (1990) 2537–2541.
- [26] H.G. Puechagut, J. Bianchotti, C.A. Chiale, Preparation of norfloxacin spherical agglomerates using the ammonia diffusion system, *J. Pharm. Sci.* 87 (1998) 519–523.
- [27] Y. Kawashima, T. Niwa, T. Handa, H. Takeuchi, T. Iwamoto, K. Itoh, Preparation of controlled-release microspheres of ibuprofen with acrylic polymers by a novel quasi-emulsion solvent diffusion method, *J. Pharm. Sci.* 78 (1989) 68–72.
- [28] K. Chadwick, R.J. Davey, R. Mughal, I. Marziano, Crystallisation from water-in-oil emulsions as a route to spherical particulates: Glycine and the hydrochloride salts of glutamic acid and ephedrine, *Org. Process Res. Dev.* 13 (2009) 1284–1290.
- [29] F. Espitalier, B. Biscans, C. Laguérie, Particle design. Part A: Nucleation kinetics of ketoprofen, *Chem. Eng. J.* 68 (1997) 95–102.
- [30] Y. Kawashima, M. Imai, H. Takeuchi, H. Yamamoto, K. Kamiya, T. Hino, Improved flowability and compactibility of spherically agglomerated crystals of ascorbic acid for direct tableting designed by spherical crystallization process, *Powder Technol.* 130 (2003) 283–289.
- [31] M. Nocent, L. Bertocchi, F. Espitalier, M. Baron, G. Couarraze, Definition of a solvent system for spherical crystallization of salbutamol sulfate by quasi-emulsion solvent diffusion (QESD) method, *J. Pharm. Sci.* 90 (2001) 1620–1627.
- [32] R. Peña, Z.K. Nagy, Process Intensification through Continuous Spherical Crystallization Using a Two-Stage Mixed Suspension Mixed Product Removal (MSMPR) System, *Cryst. Growth Des.* 15 (2015) 4225–4236.
- [33] H.M. Smith, I.E. Puddington, Spherical Agglomeration of Barium Sulphate, 38 (1967).
- [34] A.Y. Huang, J.C. Berg, Gelation of liquid bridges in spherical agglomeration, *Colloids Surfaces A*

Physicochem. Eng. Asp. 215 (2003) 241–252.

- [35] Y. Kawashima, M. Okumura, H. Takenaka, The effects of temperature on the spherical crystallization of salicylic acid, *Powder Technol.* 39 (1984) 41–47.
- [36] S. Mahanty, J. Sruti, C.N. Patra, M.E.B. Rao, Particle Design of Drugs by Spherical Crystallization Techniques, *Int. J. Pharm. Sci. Nanotechnol.* 3 (2010) 912–918.
- [37] A. Sano, T. Kuriki, Y. Kawashima, H. Takeuchi, T. Hino, T. Niwa, Particle design of tolbutamide by the spherical crystallization technique. III. Micromeritic properties and dissolution rate of tolbutamide spherical agglomerates prepared by the quasi-emulsion solvent diffusion method and the solvent change method, *Chem. Pharm. Bull.* 38 (1990) 733–739.
- [38] Y. Kawashima, M. Okumura, H. Takenaka, A. Kojima, Direct preparation of spherically agglomerated salicylic acid crystals during crystallization, *J. Pharm. Sci.* 73 (1984) 1535–1538.
- [39] A. Sano, T. Kuriki, Y. Kawashima, H. Takeuchi, T. Hino, T. Niwa, Particle design of tolbutamide by the spherical crystallization technique. V. Improvement of dissolution and bioavailability of direct compressed tablets prepared using tolbutamide agglomerated crystals, *Chem. Pharm. Bull.* 40 (1992) 3030–3035.
- [40] K. Morishima, K. Yoshiaki, H. Takeuchi, T. Niwa, T. Hino, Y. Kawashima, Tableting properties of buccillamine agglomerates prepared by the spherical crystallization technique, *Int. J. Pharm.* 105 (1994) 11–18.
- [41] M. Müller, F. Löffler, Development of agglomerate size and structure during spherical agglomeration in suspension, *Part. Part. Syst. Charact.* 13 (1996) 322–326.
- [42] C. Subero-Couroyer, D. Mangin, A. Rivoire, A.F. Blandin, J.P. Klein, Agglomeration in suspension of salicylic acid fine particles: Analysis of the wetting period and effect of the binder injection mode on the final agglomerate size, *Powder Technol.* 161 (2006) 98–109.
- [43] D. Rossetti, S.J.R. Simons, A microscale investigation of liquid bridges in the spherical agglomeration process, *Powder Technol.* 130 (2003) 49–55.
- [44] D. Rossetti, X. Pepin, S.J.R. Simons, Rupture energy and wetting behavior of pendular liquid bridges in relation to the spherical agglomeration process, *J. Colloid Interface Sci.* 261 (2003) 161–169.
- [45] A.F. Blandin, D. Mangin, A. Rivoire, J.P. Klein, J.M. Bossoutrot, Agglomeration in suspension of salicylic acid fine particle: influence of some process parameters on kinetics and agglomerate final size, *Powder Technol.* 130 (2003) 316–323.
- [46] J. Thati, Å.C. Rasmuson, On the mechanisms of formation of spherical agglomerates, *Eur. J. Pharm. Sci.* 42 (2011) 365–379.
- [47] K. Morishima, Y. Kawashima, Y. Kawashima, H. Takeuchi, T. Niwa, T. Hino, Micromeritic characteristics and agglomeration mechanisms in the spherical crystallization of buccillamine by the spherical agglomeration and the emulsion solvent diffusion methods, *Powder Technol.* 76 (1993) 57–64.
- [48] Y. Kawashima, Experimental study of the kinetics sodium theophylline monohydrate, *Powder Technol.* 34 (1983) 255–260.

- [49] G.G. Bemer, *Agglomeration in Suspension: A Study of Mechanisms and Kinetics*, 1979.
- [50] A.F. Blandin, D. Mangin, C. Subero-Couroyer, A. Rivoire, J.P. Klein, J.M. Bossoutrot, Modelling of agglomeration in suspension: Application to salicylic acid microparticles, *Powder Technol.* 156 (2005) 19–33.
- [51] M. Maghsoodi, Z. Yari, Effect of drying phase on the agglomerates prepared by spherical crystallization, *Iran. J. Pharm. Res.* 14 (2015) 51–57.
- [52] T. Schaefer, C. Mathiesen, Melt pelletization in a high shearmixer. IX. Effects of binder particle size, *Int. J. Pharm.* 139 (1996) 139–148.
- [53] R. David, P. Marchal, J.P. Klein, J. Villermaux, Crystallization and precipitation engineering-III. A discrete formulation of the agglomeration rate of crystals in a crystallization process, *Chem. Eng. Sci.* 46 (1991) 205–213.
- [54] D.R. Ochsenbein, T. Vetter, S. Schorsch, M. Morari, M. Mazzotti, Agglomeration of needle-like crystals in suspension: I. Measurements, *Cryst. Growth Des.* 15 (2015) 1923–1933.
- [55] R. Peña, C.L. Burcham, D.J. Jarmer, D. Ramkrishna, Z.K. Nagy, Modeling and optimization of spherical agglomeration in suspension through a coupled population balance model, *Chem. Eng. Sci.* 167 (2017) 66–77.
- [56] K.P. Hapgood, J.D. Litster, R. Smith, Nucleation regime map for liquid bound granules, *AIChE J.* 49 (2003) 350–361.
- [57] S.M. Iveson, J.D. Luster, Growth regime map for liquid-bound granules, *AIChE J.* 44 (1998) 1510–1518.
- [58] A.H.L. Chow, M.W.M. Leung, A study of the mechanisms of wet spherical agglomeration of pharmaceutical powders, *Drug Dev. Ind. Pharm.* 22 (1996) 357–371.
- [59] P. Szabó-Révész, M. Hasznos-Nezdei, B. Farkas, H. Göcző, K. Pintye-Hódi, I. Erős, Crystal growth of drug materials by spherical crystallization, *J. Cryst. Growth.* 237–239 (2002) 2240–2245.
- [60] M.M. Gupta, B. Srivastava, Enhancement of flow property of poorly flowable Aceclofenac drug powder by preparation of spherical crystals using solvent change method and making drug powder suitable for direct compression, *Int. J. Curr. Pharm. Rev. Res.* 1 (2010) 12–23.
- [61] Y. Kawashima, S. Aoki, H. Takenaka, Y. Miyake, Preparation of spherically agglomerated crystals of aminophylline, *J. Pharm. Sci.* 73 (1984) 1407–1410.
- [62] R. Peña, D.J. Jarmer, C.L. Burcham, Z.K. Nagy, Further Understanding of Agglomeration Mechanisms in Spherical Crystallization Systems: Benzoic Acid Case Study, *Cryst. Growth Des.* 19 (2019) 1668–1679.
- [63] V.B. Yadav, A. V. Yadav, Comparative tableting behavior of carbamazepine granules with spherical agglomerated crystals prepared by spherical crystallization technique, *Int. J. ChemTech Res.* 1 (2009) 476–482.
- [64] V.R. GUPTA, S. MUTALIK, M.M. PATEL, G.K. JANI, Sferični kristali celekoksiba za poboljšanje topljivosti, osloba{anj}anja i mikromeričnih svojstava, *Acta Pharm.* 57 (2007) 173–184.
- [65] K. Kedia, S. Wairkar, Improved micromeritics, packing properties and compressibility of high

- dose drug, Cycloserine, by spherical crystallization, *Powder Technol.* 344 (2019) 665–672.
- [66] P. Di Martino, C. Barthélémy, F. Piva, E. Joiris, G.F. Palmieri, S. Martelli, Improved dissolution behavior of fenbufen by spherical crystallization, *Drug Dev. Ind. Pharm.* 25 (1999) 1073–1081.
- [67] M.K. Chourasia, N.K. Jain, S. Jain, N.K. Jain, S.K. Jain, Preparation and characterization of agglomerates of flurbiprofen by spherical crystallization technique, *Indian J. Pharm. Sci.* 65 (2003) 287–291.
- [68] S. Dwivedi, V.K. Mishra, P. Sakalle, G. Jain, D. Gupta, D. Gupta, Method development for spherical crystallization of glibenclamide and evaluation of micromeritic properties, *Drug Invent. Today.* 22 (2010) 119–122.
- [69] K. Dinesh, P.S. Kumar, W.A. P, D.A. S, I NTERNATIONAL J OURNAL OF P HARMACY & L IFE S CIENCES Spherical crystallization of glipizide for improvement of micrometric properties, 1 (2010) 463–466.
- [70] P. Subhash Chandra Bose, D. Saritha, M. Vimal Kumar Varma, S.K. Dathrika, Influence of various bridging liquids on spherical agglomeration of indomethacin, *Int. J. Res. Pharm. Sci.* 2 (2011) 147–157.
- [71] C.L. Viswanathan, S.K. Kulkarni, D.R. Kolwankar, Spherical agglomeration of mefenamic acid and nabumetone to improve micromeritics and solubility: a technical note., *AAPS PharmSciTech.* 7 (2006) E48.
- [72] M.S. Gordonx, Z.T. Chowhan, Manipulation of naproxen particle morphology via the spherical crystallization technique to achieve a directly compressible raw material, *Drug Dev. Ind. Pharm.* 16 (1990) 1279–1290.
- [73] P. Di Martino, R. Di Cristofaro, C. Barthélémy, E. Joiris, G. Palmieri Filippo, M. Sante, Improved compression properties of propyphenazone spherical crystals, *Int. J. Pharm.* 197 (2000) 95–106.
- [74] M.C. Deshpande, K.R. Mahadik, A.P. Pawar, A.R. Paradkar, Evaluation of spherical crystallization as a particle size enlargement technique for aspirin, *Indian J. Pharm. Sci.* 59 (1997) 32–34.
- [75] Y. Kawashima, T. Niwa, H. Takeuchi, T. Hino, Y. Itoh, S. Furuyama, Characterization of polymorphs of tranilast anhydrate and tranilast monohydrate when crystallized by two solvent change spherical crystallization techniques, *J. Pharm. Sci.* 80 (1991) 472–478.
- [76] D.R. Lide, *CRC Handbook of Chemistry and Physics 86th Edition 2005-2006*, 2005.
- [77] M. Chen, X. Liu, C. Yu, M. Yao, S. Xu, W. Tang, X. Song, W. Dong, G. Wang, J. Gong, Strategy of selecting solvent systems for spherical agglomeration by the Lifshitz-van der Waals acid-base approach, *Chem. Eng. Sci.* 220 (2020) 115613.
- [78] X. Cheng, F. Li, L. Luo, Z. Ding, L. Zeng, Y. Mao, X. Huang, H. Hao, On the selection of wetting liquid for spherical agglomeration of cefotaxime sodium, *Powder Technol.* 363 (2020) 593–601.
- [79] S. Jitkar, R. Thipparaboina, R.B. Chavan, N.R. Shastri, Spherical Agglomeration of Platy Crystals: Curious Case of Etodolac, *Cryst. Growth Des.* 16 (2016) 4034–4042.
- [80] A. Sano, T. Kuriki, T. Handa, H. Takeuchi, Y. Kawashima, Particle design of tolbutamide in the presence of soluble polymer or surfactant by the spherical crystallization technique:

- Improvement of dissolution rate, *J. Pharm. Sci.* 76 (1987) 471–474.
- [81] P.K. Kulkarni, M. Dixit, A. Jain, Spherical agglomeration of naproxan by solvent change method, *Stamford J. Pharm. Sci.* 4 (2011) 1–8.
- [82] J. Varshosaz, N. Tavakoli, F.A. Salamat, Enhanced dissolution rate of simvastatin using spherical crystallization technique, *Pharm. Dev. Technol.* 16 (2011) 529–535.
- [83] S.K. Pagire, S.A. Korde, B.R. Whiteside, J. Kendrick, A. Paradkar, Spherical crystallization of carbamazepine/saccharin co-crystals: Selective agglomeration and purification through surface interactions, *Cryst. Growth Des.* 13 (2013) 4162–4167.
- [84] Y. Kawashima, Y. Kurachi, H. Takenaka, Preparation of spherical wax matrices of sulfamethoxazole by wet spherical agglomeration technique using a CMSMPR agglomerator, *Powder Technol.* 32 (1982) 155–161.
- [85] W. Gardner, Note on the dynamics of capillary flow, *Phys. Rev.* 18 (1921) 206–209.
- [86] J. Thati, Å.C. Rasmuson, Particle engineering of benzoic acid by spherical agglomeration, *Eur. J. Pharm. Sci.* 45 (2012) 657–667.
- [87] R. Petela, Prediction of the product size in the agglomeration of coal particles in a water-oil emulsion, *Fuel.* 70 (1991) 509–517.
- [88] J. Katta, Å.C. Rasmuson, Spherical crystallization of benzoic acid, 2008.
- [89] R. Peña, J.A. Oliva, C.L. Burcham, D.J. Jarmer, Z.K. Nagy, Process Intensification through Continuous Spherical Crystallization Using an Oscillatory Flow Baffled Crystallizer, *Cryst. Growth Des.* 17 (2017) 4776–4784.
- [90] M. Ritala, P. Holm, T. Schaefer, H.G. Kristensen, Influence of liquid bonding strength on power consumption during granulation in a high shear mixer, *Drug Dev. Ind. Pharm.* 14 (1988) 1041–1060.
- [91] A.S. Bos, F.J. Zuiderweg, Kinetics of continuous agglomeration in suspension, *Powder Technol.* 44 (1985) 43–51.
- [92] S. Wu, K. Li, T. Zhang, J. Gong, Size Control of Atorvastatin Calcium Particles Based on Spherical Agglomeration, *Chem. Eng. Technol.* 38 (2015) 1081–1087.
- [93] L. Madec, H. Muhr, E. Plasari, Development of new methods to accelerate and improve the agglomeration of submicron particles by binding liquids, *Powder Technol.* 128 (2002) 236–241.
- [94] P.M. Orlewski, B. Ahn, M. Mazzotti, Tuning the particle sizes in spherical agglomeration, *Cryst. Growth Des.* 18 (2018) 6257–6265.
- [95] J. Gan, A. Yu, DEM study on the packing density and randomness for packing of ellipsoids, *Powder Technol.* 361 (2020) 424–434.
- [96] K. Ikegami, Y. Kawashima, H. Takeuchi, H. Yamamoto, N. Isshiki, D.I. Momose, K. Ouchi, Simultaneous particulate design of primary and agglomerated crystals of steroid by spherical agglomeration in liquid for dry powder inhalation, *Powder Technol.* 130 (2003) 290–297.
- [97] A.R. Paradkar, A.P. Pawar, J.K. Chordiya, V.B. Patil, A.R. Ketkar, Spherical crystallization of

- celecoxib, *Drug Dev. Ind. Pharm.* 28 (2002) 1213–1220.
- [98] K. Ikegami, Y. Kawashima, H. Takeuchi, H. Yamamoto, N. Isshiki, D.I. Momose, K. Ouchi, Primary crystal growth during spherical agglomeration in liquid: Designing an ideal dry powder inhalation system, *Powder Technol.* 126 (2002) 266–274.
- [99] H. Zhang, Y. Chen, J. Wang, J. Gong, Investigation on the spherical crystallization process of cefotaxime sodium, in: *Ind. Eng. Chem. Res.*, 2010: pp. 1402–1411.
- [100] R. Davey, J. Garside, *From Molecules to Crystallizers: An Introduction to Crystallization*, Oxford University Press, Oxford, 2000.
- [101] Y. Kawashima, S. Aoki, H. Takenaka, Spherical agglomeration of aminophylline crystals during reaction in liquid by the spherical crystallization technique, *Chem. Pharm. Bull.* 30 (1982) 1900–1902.
- [102] L. Madec, L. Falk, E. Plasari, Modelling of the agglomeration in suspension process with multidimensional kernels, *Powder Technol.* 130 (2003) 147–153.
- [103] R. David, P. Marchal, B. Marcant, Modelling of agglomeration in industrial crystallization from solution, *Chem. Eng. Technol.* 18 (1995) 302–309.
- [104] R. David, A.M. Paulaime, F. Espitalier, L. Rouleau, Modelling of multiple-mechanism agglomeration in a crystallization process, in: *Powder Technol.*, 2003: pp. 338–344.
- [105] M. Brunsteiner, A.G. Jones, F. Pratola, S.L. Price, S.J.R. Simons, Toward a molecular understanding of crystal agglomeration, *Cryst. Growth Des.* 5 (2005) 3–16.
- [106] D.R. Ochsenein, T. Vetter, M. Morari, M. Mazzotti, Agglomeration of Needle-like Crystals in Suspension. II. Modeling, *Cryst. Growth Des.* 15 (2015) 4296–4310.
- [107] L. Derdour, D. Skliar, A review of the effect of multiple conformers on crystallization from solution and strategies for crystallizing slow inter-converting conformers, *Chem. Eng. Sci.* 106 (2014) 275–292.
- [108] E. Simone, B. Szilagyi, Z.K. Nagy, Systematic model identification and optimization-based active polymorphic control of crystallization processes, *Chem. Eng. Sci.* 174 (2017) 374–386.
- [109] Y. Kawashima, T. Handa, H. Takeuchi, M. Okumura, H. Katou, O. Nagata, Crystal modification of phenytoin with polyethylene glycol for improving mechanical strength, dissolution rate and bioavailability by a spherical crystallization technique, *Chem. Pharm. Bull.* 34 (1986) 3376–3383.
- [110] Y. Kawashima, T. Handa, H. Takeuchi, M. Okumura, Effects of polyethylene glycol on the size of agglomerated crystals of phenytoin prepared by the spherical crystallization technique, *Chem. Pharm. Bull.* 34 (1986) 3403–3407.
- [111] N.G. Anderson, Practical use of continuous processing in developing and scaling up laboratory processes, *Org. Process Res. Dev.* 5 (2001) 613–621.
- [112] H. Thomas, Batch-to-continuous - Coming out of age, *Chem. Eng. Sci.* 805 (2008) 38–40.
- [113] D. Reay, C. Ramshaw, A. Harvey, Chapter 11 - Application Areas – the Built Environment, Electronics, and the Home, in: D. Reay, C. Ramshaw, A.B.T.-P.I. (Second E. Harvey (Eds.)), *Isot.*

Org. Chem., Butterworth-Heinemann, Oxford, 2013: pp. 393–435.

- [114] J.M. Vargas, S. Nielsen, V. Cárdenas, A. Gonzalez, E.Y. Aymat, E. Almodovar, G. Classe, Y. Colón, E. Sanchez, R.J. Romañach, Process analytical technology in continuous manufacturing of a commercial pharmaceutical product, *Int. J. Pharm.* 538 (2018) 167–178.
- [115] R. Pena, J.A. Oliva, C.L. Burcham, D.J. Jarmer, Z.K. Nagy, Process Intensification through Continuous Spherical Crystallization Using an Oscillatory Flow Baffled Crystallizer, *Cryst. Growth Des.* 17 (2017) 4776–4784.
- [116] K. Tahara, M. O'Mahony, A.S. Myerson, Continuous spherical crystallization of albuterol sulfate with solvent recycle system, *Cryst. Growth Des.* 15 (2015) 5155–5156.
- [117] H.M. Backes, M. Jing Jun, B. E., M. G., Interfacial tensions in binary and ternary liquid-liquid systems, *Chem. Eng. Sci.* 45 (1990) 275–286.
- [118] D.J. Donahue, F.E. Bartell, The Boundary Tension at Water-Organic Liquid Interfaces, *J. Phys. Chem.* 56 (1952) 480–484.
- [119] A.A. Freitas, F.H. Quina, F.A. Carroll, Estimation of Water–Organic Interfacial Tensions. A Linear Free Energy Relationship Analysis of Interfacial Adhesion, *J. Phys. Chem. B.* 101 (1997) 7488–7493.
- [120] F.U. Jufu, L.I. Buqiang, W. Zihao, Estimation of fluid-fluid interfacial tensions of multicomponent mixtures, *Chem. Eng. Sci.* 41 (1986) 2673–2679.
- [121] B. Li, J. Fu, Interfacial Tensions of Two-Liquid-Phase Ternary Systems, *J. Chem. Eng. Data.* 37 (1992) 172–174.
- [122] M.Z. Shahid, M.R. Usman, M.S. Akram, S.Y. Khawaja, W. Afzal, Initial Interfacial Tension for Various Organic-Water Systems and Study of the Effect of Solute Concentration and Temperature, *J. Chem. Eng. Data.* 62 (2017) 1198–1203.
- [123] A. Fredenslund, R.L. Jones, J.M. Prausnitz, Group-contribution estimation of activity coefficients in nonideal liquid mixtures, *AIChE J.* 21 (1975) 1086–1099.
- [124] J.H. Rushton, E.W. Costich, H.J. Everett, Power characteristics of mixing impellers, Parts 1 and 2, *Chem. Eng. Prog.* (1950).

Figure Acknowledgements

The following figures have been republished with kind permission from copyright.com CCC:

Figure 2.1 Y. Kawashima, M. Okumura, H. Takenaka, Spherical crystallization: Direct spherical agglomeration of salicylic acid crystals during crystallization, *Science* (80-.). 216 (1982) 1127–1128.

Figure 2.9, **Figure 2.10** and **Figure 2.21** S.M. Iveson, J.D. Litster, K. Hapgood, B.J. Ennis, Nucleation, growth and breakage phenomena in agitated wet granulation processes: a review, *Powder Technol.* 117 (2001) 3–39.

- Figure 2.11 M. Chen, X. Liu, C. Yu, M. Yao, S. Xu, W. Tang, X. Song, W. Dong, G. Wang, J. Gong, Strategy of selecting solvent systems for spherical agglomeration by the Lifshitz-van der Waals acid-base approach, *Chem. Eng. Sci.* 220 (2020) 115613.
- Figure 2.13 J. Thati, Å.C. Rasmuson, On the mechanisms of formation of spherical agglomerates, *Eur. J. Pharm. Sci.* 42 (2011) 365–379.
- Figure 2.23 and Figure 2.25 C. Subero-Couroyer, D. Mangin, A. Rivoire, A.F. Blandin, J.P. Klein, Agglomeration in suspension of salicylic acid fine particles: Analysis of the wetting period and effect of the binder injection mode on the final agglomerate size, *Powder Technol.* 161 (2006) 98–109.
- Figure 2.24 L. Madec, H. Muhr, E. Plasari, Development of new methods to accelerate and improve the agglomeration of submicron particles by binding liquids, *Powder Technol.* 128 (2002) 236–241.
- Figure 2.30 K. Morishima, Y. Kawashima, Y. Kawashima, H. Takeuchi, T. Niwa, T. Hino, Micromeritic characteristics and agglomeration mechanisms in the spherical crystallization of bucillamine by the spherical agglomeration and the emulsion solvent diffusion methods, *Powder Technol.* 76 (1993) 57–64.

Appendix A. The TBSR Theory

Titration Data

This part of **Appendix A** corresponds to **Section 4.3.1** in **Chapter 4**. The full results from titrations are presented in the following tables, bridging liquid by bridging liquid.

Table A.1. Titration data for water-acetone-chloroform systems.

WATER MASS (g)	ACETONE MASS (g)	BL MASS (g)	TOTAL MASS (g)	WATER w/w %	ACETONE w/w %	BL w/w%
0.760	1.060	20.000	21.820	0.035	0.049	0.917
0.140	1.070	18.850	20.060	0.007	0.053	0.940
0.240	1.090	19.010	20.340	0.012	0.054	0.935
0.450	1.980	18.220	20.650	0.022	0.096	0.882
0.280	2.010	18.040	20.330	0.014	0.099	0.887
0.340	1.990	18.420	20.750	0.016	0.096	0.888
0.410	2.920	18.380	21.710	0.019	0.135	0.847
0.540	3.010	17.690	21.240	0.025	0.142	0.833
0.410	2.960	18.780	22.150	0.019	0.134	0.848
0.350	4.000	16.380	20.730	0.017	0.193	0.790
0.280	4.020	16.880	21.180	0.013	0.190	0.797
0.350	4.000	15.920	20.270	0.017	0.197	0.785
0.460	5.340	15.790	21.590	0.021	0.247	0.731
0.410	5.130	15.120	20.660	0.020	0.248	0.732
0.420	5.010	16.820	22.250	0.019	0.225	0.756
0.290	6.000	14.410	20.700	0.014	0.290	0.696
0.380	6.130	14.100	20.610	0.018	0.297	0.684
0.480	6.180	14.250	20.910	0.023	0.296	0.681
0.550	7.100	13.150	20.800	0.026	0.341	0.632
0.590	7.130	13.490	21.210	0.028	0.336	0.636
0.690	7.030	13.390	21.110	0.033	0.333	0.634
0.760	8.070	12.380	21.210	0.036	0.380	0.584
0.790	8.100	12.730	21.620	0.037	0.375	0.589
0.560	7.950	12.130	20.640	0.027	0.385	0.588
0.860	8.920	11.550	21.330	0.040	0.418	0.541
0.850	9.340	11.020	21.210	0.040	0.440	0.520
0.770	9.030	11.810	21.610	0.036	0.418	0.547
1.370	10.240	10.270	21.880	0.063	0.468	0.469
1.140	10.230	10.200	21.570	0.053	0.474	0.473
0.990	10.060	10.010	21.060	0.047	0.478	0.475
1.310	11.230	9.080	21.620	0.061	0.519	0.420
1.260	11.050	9.010	21.320	0.059	0.518	0.423
1.240	11.150	9.550	21.940	0.057	0.508	0.435
1.800	11.990	8.720	22.510	0.080	0.533	0.387

Continued on the following page...

WATER MASS (g)	ACETONE MASS (g)	BL MASS (g)	TOTAL MASS (g)	WATER w/w %	ACETONE w/w %	BL w/w%
1.760	11.970	8.020	21.750	0.081	0.550	0.369
1.800	11.990	8.720	22.510	0.080	0.533	0.387
1.770	12.090	8.220	22.080	0.080	0.548	0.372
2.150	13.050	7.210	22.410	0.096	0.582	0.322
2.130	12.970	7.090	22.190	0.096	0.584	0.320
1.860	12.990	7.750	22.600	0.082	0.575	0.343
2.980	14.050	6.100	23.130	0.129	0.607	0.264
2.780	14.250	6.870	23.900	0.116	0.596	0.287
3.100	14.020	6.380	23.500	0.132	0.597	0.271
4.850	14.990	4.930	24.770	0.196	0.605	0.199
4.100	15.070	5.720	24.890	0.165	0.605	0.230
4.820	15.080	5.170	25.070	0.192	0.602	0.206
6.430	16.000	4.500	26.930	0.239	0.594	0.167
7.620	16.280	3.990	27.890	0.273	0.584	0.143
7.130	15.860	4.130	27.120	0.263	0.585	0.152
10.660	16.950	3.150	30.760	0.347	0.551	0.102
11.080	17.090	3.050	31.220	0.355	0.547	0.098
10.570	16.920	3.100	30.590	0.346	0.553	0.101
16.570	17.940	2.000	36.510	0.454	0.491	0.055
17.540	17.960	1.990	37.490	0.468	0.479	0.053
13.200	17.980	2.780	33.960	0.389	0.529	0.082
32.480	19.070	1.080	52.630	0.617	0.362	0.021
30.230	18.940	1.110	50.280	0.601	0.377	0.022
27.400	18.930	1.040	47.370	0.578	0.400	0.022
8.370	11.690	2.610	22.670	0.369	0.516	0.115
8.280	12.090	2.860	23.230	0.356	0.520	0.123
9.360	11.970	1.930	23.260	0.402	0.515	0.083
10.180	10.380	1.210	21.770	0.468	0.477	0.056
9.710	10.360	1.090	21.160	0.459	0.490	0.052
10.020	10.140	1.310	21.470	0.467	0.472	0.061
11.730	8.530	0.950	21.210	0.553	0.402	0.045
12.920	7.730	0.890	21.540	0.600	0.359	0.041
12.150	7.740	0.720	20.610	0.590	0.376	0.035
13.890	6.000	0.660	20.550	0.676	0.292	0.032
15.870	6.400	0.650	22.920	0.692	0.279	0.028
14.550	6.280	0.550	21.380	0.681	0.294	0.026
16.320	4.200	0.720	21.240	0.768	0.198	0.034
16.000	4.450	0.380	20.830	0.768	0.214	0.018
16.230	4.140	0.490	20.860	0.778	0.198	0.023
19.120	2.060	0.520	21.700	0.881	0.095	0.024
18.180	1.550	0.510	20.240	0.898	0.077	0.025
18.910	2.150	0.530	21.590	0.876	0.100	0.025

Table A.2. Titration data for water-acetone-heptane systems.

WATER MASS (g)	ACETONE MASS (g)	BL MASS (g)	TOTAL MASS (g)	WATER w/w %	ACETONE w/w %	BL w/w%
1.390	1.200	19.040	21.630	0.06	0.06	0.88
0.361	0.990	19.630	20.981	0.02	0.05	0.94
1.370	1.060	18.790	21.220	0.06	0.05	0.89
0.540	2.020	18.380	20.940	0.03	0.10	0.88
1.000	1.940	18.560	21.500	0.05	0.09	0.86
1.180	2.000	17.950	21.130	0.06	0.09	0.85
0.670	3.030	17.010	20.710	0.03	0.15	0.82
0.570	3.210	17.050	20.830	0.03	0.15	0.82
0.480	3.010	17.050	20.540	0.02	0.15	0.83
0.490	3.960	14.020	18.470	0.03	0.21	0.76
0.890	4.040	15.910	20.840	0.04	0.19	0.76
0.420	4.140	15.900	20.460	0.02	0.20	0.78
1.030	5.050	14.960	21.040	0.05	0.24	0.71
0.600	5.050	14.950	20.600	0.03	0.25	0.73
0.520	5.050	15.000	20.570	0.03	0.25	0.73
0.500	6.360	14.780	21.640	0.02	0.29	0.68
0.260	6.030	13.870	20.160	0.01	0.30	0.69
0.250	6.150	14.010	20.410	0.01	0.30	0.69
0.270	7.350	12.930	20.550	0.01	0.36	0.63
0.410	6.920	12.930	20.260	0.02	0.34	0.64
0.210	7.060	12.960	20.230	0.01	0.35	0.64
0.330	8.056	12.410	20.796	0.02	0.39	0.60
0.260	8.000	12.200	20.460	0.01	0.39	0.60
0.300	8.430	12.050	20.780	0.01	0.41	0.58
0.360	9.170	11.180	20.710	0.02	0.44	0.54
0.370	8.980	11.370	20.720	0.02	0.43	0.55
0.430	9.330	11.030	20.790	0.02	0.45	0.53
0.460	9.970	10.000	20.430	0.02	0.49	0.49
0.430	10.460	10.370	21.260	0.02	0.49	0.49
0.490	10.030	9.920	20.440	0.02	0.49	0.49
0.470	11.020	9.010	20.500	0.02	0.54	0.44
0.930	11.330	8.940	21.200	0.04	0.53	0.42
0.963	11.320	9.000	21.283	0.05	0.53	0.42
0.900	12.900	7.210	21.010	0.04	0.61	0.34
0.840	12.220	7.930	20.990	0.04	0.58	0.38
0.700	12.060	8.080	20.840	0.03	0.58	0.39
0.880	13.260	7.190	21.330	0.04	0.62	0.34
0.860	13.240	7.290	21.390	0.04	0.62	0.34
0.900	12.900	7.210	21.010	0.04	0.61	0.34
0.980	14.130	6.340	21.450	0.05	0.66	0.30

Continued on the following page...

WATER MASS (g)	ACETONE MASS (g)	BL MASS (g)	TOTAL MASS (g)	WATER w/w %	ACETONE w/w %	BL w/w%
1.240	14.010	6.050	21.300	0.06	0.66	0.28
1.070	14.000	5.950	21.020	0.05	0.67	0.28
1.480	15.380	5.000	21.860	0.07	0.70	0.23
1.420	15.330	4.980	21.730	0.07	0.71	0.23
1.320	14.780	4.990	21.090	0.06	0.70	0.24
1.770	15.970	4.170	21.910	0.08	0.73	0.19
1.880	15.990	3.840	21.710	0.09	0.74	0.18
2.080	16.370	4.060	22.510	0.09	0.73	0.18
2.540	17.070	3.060	22.670	0.11	0.75	0.13
2.800	17.000	3.030	22.830	0.12	0.74	0.13
2.680	17.360	3.170	23.210	0.12	0.75	0.14
7.230	18.160	1.550	26.940	0.27	0.67	0.06
4.730	18.260	1.940	24.930	0.19	0.73	0.08
4.790	18.090	1.880	24.760	0.19	0.73	0.08
10.320	19.120	0.880	30.320	0.34	0.63	0.03
6.520	19.130	1.310	26.960	0.24	0.71	0.05
9.340	19.480	1.130	29.950	0.31	0.65	0.04
8.490	12.310	0.860	21.660	0.39	0.57	0.04
8.730	11.550	0.530	20.810	0.42	0.56	0.03
8.400	12.370	0.590	21.360	0.39	0.58	0.03
10.490	10.200	0.550	21.240	0.49	0.48	0.03
9.840	10.390	0.670	20.900	0.47	0.50	0.03
10.400	10.220	0.470	21.090	0.49	0.48	0.02
12.160	7.860	0.450	20.470	0.59	0.38	0.02
13.170	8.310	0.590	22.070	0.60	0.38	0.03
12.080	7.960	0.590	20.630	0.59	0.39	0.03
14.210	5.980	0.450	20.640	0.69	0.29	0.02
14.740	6.480	0.370	21.590	0.68	0.30	0.02
14.360	6.190	0.340	20.890	0.69	0.30	0.02
16.330	3.960	0.330	20.620	0.79	0.19	0.02
16.530	4.010	0.370	20.910	0.79	0.19	0.02
16.640	4.060	0.410	21.110	0.79	0.19	0.02
18.460	1.880	0.510	20.850	0.89	0.09	0.02
18.320	2.160	0.350	20.830	0.88	0.10	0.02
18.200	2.120	0.360	20.680	0.88	0.10	0.02

Table A.3. Titration data for water-acetone-methyl isobutyl ketone systems.

WATER MASS (g)	ACETONE MASS (g)	BL MASS (g)	TOTAL MASS (g)	WATER w/w %	ACETONE w/w %	BL w/w%
0.750	1.030	19.220	21.000	0.04	0.05	0.92
0.570	1.010	18.870	20.450	0.03	0.05	0.92
0.890	1.120	19.070	21.080	0.04	0.05	0.90
0.910	2.050	18.010	20.970	0.04	0.10	0.86
0.870	2.180	18.140	21.190	0.04	0.10	0.86
0.950	2.130	17.930	21.010	0.05	0.10	0.85
0.710	3.100	17.020	20.830	0.03	0.15	0.82
0.470	3.010	18.340	21.820	0.02	0.14	0.84
0.530	3.010	17.080	20.620	0.03	0.15	0.83
0.730	3.920	16.540	21.190	0.03	0.18	0.78
0.860	0.960	16.450	18.270	0.05	0.05	0.90
0.630	4.020	16.460	21.110	0.03	0.19	0.78
0.960	5.290	15.090	21.340	0.04	0.25	0.71
0.940	4.960	15.010	20.910	0.04	0.24	0.72
0.940	5.090	15.120	21.150	0.04	0.24	0.71
1.400	6.080	14.040	21.520	0.07	0.28	0.65
1.000	6.050	14.100	21.150	0.05	0.29	0.67
1.020	6.150	14.030	21.200	0.05	0.29	0.66
1.190	7.150	13.230	21.570	0.06	0.33	0.61
1.570	7.510	13.000	22.080	0.07	0.34	0.59
1.690	7.080	13.150	21.920	0.08	0.32	0.60
1.540	8.380	12.320	22.240	0.07	0.38	0.55
1.690	8.070	12.300	22.060	0.08	0.37	0.56
1.410	8.150	12.020	21.580	0.07	0.38	0.56
1.760	8.930	10.960	21.650	0.08	0.41	0.51
2.100	9.260	11.330	22.690	0.09	0.41	0.50
1.880	9.530	10.980	22.390	0.08	0.43	0.49
2.270	9.990	10.130	22.390	0.10	0.45	0.45
2.140	9.990	10.910	23.040	0.09	0.43	0.47
2.650	10.150	9.860	22.660	0.12	0.45	0.44
3.910	11.370	9.240	24.520	0.16	0.46	0.38
3.170	11.050	9.030	23.250	0.14	0.48	0.39
3.020	10.910	8.930	22.860	0.13	0.48	0.39
3.490	12.390	10.120	26.000	0.13	0.48	0.39
4.560	11.900	8.320	24.780	0.18	0.48	0.34
4.460	12.030	7.930	24.420	0.18	0.49	0.32
5.950	12.940	7.150	26.040	0.23	0.50	0.27
6.100	13.130	7.280	26.510	0.23	0.50	0.27
6.260	13.030	7.130	26.420	0.24	0.49	0.27
8.910	14.130	6.180	29.220	0.30	0.48	0.21

Continued on the following page...

WATER MASS (g)	ACETONE MASS (g)	BL MASS (g)	TOTAL MASS (g)	WATER w/w %	ACETONE w/w %	BL w/w%
7.960	14.030	6.690	28.680	0.28	0.49	0.23
8.600	14.080	6.250	28.930	0.30	0.49	0.22
13.160	15.250	5.020	33.430	0.39	0.46	0.15
12.610	15.080	5.040	32.730	0.39	0.46	0.15
12.610	15.510	5.440	33.560	0.38	0.46	0.16
18.900	16.220	3.980	39.100	0.48	0.41	0.10
17.600	15.880	4.120	37.600	0.47	0.42	0.11
18.320	16.060	4.130	38.510	0.48	0.42	0.11
29.490	17.370	3.410	50.270	0.59	0.35	0.07
29.820	17.250	3.160	50.230	0.59	0.34	0.06
30.520	17.220	3.020	50.760	0.60	0.34	0.06
7.750	11.810	5.610	25.170	0.31	0.47	0.22
8.330	12.110	5.250	25.690	0.32	0.47	0.20
7.930	12.240	5.380	25.550	0.31	0.48	0.21
10.190	10.120	3.420	23.730	0.43	0.43	0.14
9.950	9.710	2.980	22.640	0.44	0.43	0.13
10.000	10.250	3.100	23.350	0.43	0.44	0.13
12.240	8.170	2.100	22.510	0.54	0.36	0.09
12.170	7.900	2.040	22.110	0.55	0.36	0.09
12.170	8.100	1.790	22.060	0.55	0.37	0.08
14.200	6.400	1.370	21.970	0.65	0.29	0.06
14.460	6.060	1.100	21.620	0.67	0.28	0.05
14.180	6.110	1.070	21.360	0.66	0.29	0.05
15.980	4.110	0.910	21.000	0.76	0.20	0.04
16.620	4.170	1.140	21.930	0.76	0.19	0.05
16.370	3.700	0.780	20.850	0.79	0.18	0.04
18.300	2.100	0.800	21.200	0.86	0.10	0.04
18.110	2.040	0.930	21.080	0.86	0.10	0.04
18.440	2.190	1.020	21.650	0.85	0.10	0.05
16.320	4.200	0.720	21.240	0.77	0.20	0.03
16.000	4.450	0.380	20.830	0.77	0.21	0.02
16.230	4.140	0.490	20.860	0.78	0.20	0.02
19.120	2.060	0.520	21.700	0.88	0.09	0.02
18.180	1.550	0.510	20.240	0.90	0.08	0.03
18.910	2.150	0.530	21.590	0.88	0.10	0.02

Table A.4. Titration data for water-acetone-n-butyl acetate systems.

WATER MASS (g)	ACETONE MASS (g)	BL MASS (g)	TOTAL MASS (g)	WATER w/w %	ACETONE w/w %	BL w/w%
1.250	1.440	20.900	23.590	0.05	0.06	0.89
0.490	0.990	19.090	20.570	0.02	0.05	0.93
0.480	1.200	19.110	20.790	0.02	0.06	0.92
0.690	2.110	18.320	21.120	0.03	0.10	0.87
0.240	2.100	18.040	20.380	0.01	0.10	0.89
0.280	1.950	17.900	20.130	0.01	0.10	0.89
0.210	3.110	16.900	20.220	0.01	0.15	0.84
0.390	3.040	17.010	20.440	0.02	0.15	0.83
0.470	3.180	16.990	20.640	0.02	0.15	0.82
0.580	3.980	15.980	20.540	0.03	0.19	0.78
0.660	4.060	16.710	21.430	0.03	0.19	0.78
0.600	3.960	15.960	20.520	0.03	0.19	0.78
0.440	5.120	14.960	20.520	0.02	0.25	0.73
0.630	5.000	15.150	20.780	0.03	0.24	0.73
0.560	5.190	14.960	20.710	0.03	0.25	0.72
0.800	6.330	14.130	21.260	0.04	0.30	0.66
0.970	6.000	14.040	21.010	0.05	0.29	0.67
0.950	6.010	13.980	20.940	0.05	0.29	0.67
1.150	7.380	13.120	21.650	0.05	0.34	0.61
1.160	6.960	13.710	21.830	0.05	0.32	0.63
0.980	6.980	13.260	21.220	0.05	0.33	0.62
1.310	8.400	12.250	21.960	0.06	0.38	0.56
1.370	8.230	12.000	21.600	0.06	0.38	0.56
1.230	8.110	12.020	21.360	0.06	0.38	0.56
1.440	8.940	10.980	21.360	0.07	0.42	0.51
1.640	9.130	10.960	21.730	0.08	0.42	0.50
1.270	8.990	12.250	22.510	0.06	0.40	0.54
1.840	10.220	9.940	22.000	0.08	0.46	0.45
1.950	10.190	9.800	21.940	0.09	0.46	0.45
2.030	9.940	9.870	21.840	0.09	0.46	0.45
2.390	11.010	8.900	22.300	0.11	0.49	0.40
2.320	11.300	9.050	22.670	0.10	0.50	0.40
2.070	10.950	9.040	22.060	0.09	0.50	0.41
3.050	12.020	7.880	22.950	0.13	0.52	0.34
2.880	11.950	8.160	22.990	0.13	0.52	0.35
3.260	12.350	7.910	23.520	0.14	0.53	0.34
4.810	13.250	7.170	25.230	0.19	0.53	0.28
4.030	12.900	7.860	24.790	0.16	0.52	0.32
4.490	13.020	7.010	24.520	0.18	0.53	0.29
5.200	13.810	7.000	26.010	0.20	0.53	0.27

Continued on the following page...

WATER MASS (g)	ACETONE MASS (g)	BL MASS (g)	TOTAL MASS (g)	WATER w/w %	ACETONE w/w %	BL w/w%
6.580	14.260	6.150	26.990	0.24	0.53	0.23
5.970	14.260	6.070	26.300	0.23	0.54	0.23
8.170	14.970	5.440	28.580	0.29	0.52	0.19
9.080	15.390	5.140	29.610	0.31	0.52	0.17
8.960	14.860	4.930	28.750	0.31	0.52	0.17
11.310	15.830	4.310	31.450	0.36	0.50	0.14
8.320	16.010	7.330	31.660	0.26	0.51	0.23
10.460	16.060	4.040	30.560	0.34	0.53	0.13
15.100	17.430	3.900	36.430	0.41	0.48	0.11
15.150	17.140	3.430	35.720	0.42	0.48	0.10
15.000	17.000	3.300	35.300	0.42	0.48	0.09
21.060	18.270	2.610	41.940	0.50	0.44	0.06
22.750	18.010	1.860	42.620	0.53	0.42	0.04
20.100	17.780	2.556	40.436	0.50	0.44	0.06
38.500	19.410	0.880	58.790	0.65	0.33	0.01
33.200	19.660	1.260	54.120	0.61	0.36	0.02
38.960	18.820	1.760	59.540	0.65	0.32	0.03
7.990	12.310	4.150	24.450	0.33	0.50	0.17
8.200	12.190	4.060	24.450	0.34	0.50	0.17
8.740	12.100	3.410	24.250	0.36	0.50	0.14
10.120	9.850	1.850	21.820	0.46	0.45	0.08
10.140	9.700	1.690	21.530	0.47	0.45	0.08
10.290	9.920	1.970	22.180	0.46	0.45	0.09
12.040	8.480	1.170	21.690	0.56	0.39	0.05
12.210	7.970	1.220	21.400	0.57	0.37	0.06
11.760	8.270	1.050	21.080	0.56	0.39	0.05
14.126	5.930	0.870	20.926	0.68	0.28	0.04
14.060	6.030	0.970	21.060	0.67	0.29	0.05
14.410	6.100	0.850	21.360	0.67	0.29	0.04
16.440	4.100	0.590	21.130	0.78	0.19	0.03
16.570	3.930	0.690	21.190	0.78	0.19	0.03
16.350	3.660	0.560	20.570	0.79	0.18	0.03
19.190	2.010	0.810	22.010	0.87	0.09	0.04
18.650	2.170	0.530	21.350	0.87	0.10	0.02
18.270	2.690	0.630	21.590	0.85	0.12	0.03

Table A.5. Titration data for water-acetone-toluene systems.

WATER MASS (g)	ACETONE MASS (g)	BL MASS (g)	TOTAL MASS (g)	WATER w/w %	ACETONE w/w %	BL w/w%
0.600	0.930	19.150	20.680	0.03	0.04	0.93
0.570	1.300	19.040	20.910	0.03	0.06	0.91
0.500	1.010	18.870	20.380	0.02	0.05	0.93
0.370	2.030	17.950	20.350	0.02	0.10	0.88
0.320	1.980	18.180	20.480	0.02	0.10	0.89
0.220	2.040	18.100	20.360	0.01	0.10	0.89
0.480	3.000	16.990	20.470	0.02	0.15	0.83
0.580	2.970	17.540	21.090	0.03	0.14	0.83
0.730	3.080	16.990	20.800	0.04	0.15	0.82
0.210	3.930	16.140	20.280	0.01	0.19	0.80
0.016	4.200	16.060	20.276	0.00	0.21	0.79
0.180	4.070	16.040	20.290	0.01	0.20	0.79
0.220	4.950	14.900	20.070	0.01	0.25	0.74
0.130	5.160	15.120	20.410	0.01	0.25	0.74
0.130	5.200	15.350	20.680	0.01	0.25	0.74
0.170	6.160	13.920	20.250	0.01	0.30	0.69
0.150	5.820	14.270	20.240	0.01	0.29	0.71
0.220	5.930	13.980	20.130	0.01	0.29	0.69
0.230	7.020	13.230	20.480	0.01	0.34	0.65
0.230	7.100	13.080	20.410	0.01	0.35	0.64
0.520	6.910	12.960	20.390	0.03	0.34	0.64
0.750	8.060	11.860	20.670	0.04	0.39	0.57
0.580	8.080	12.550	21.210	0.03	0.38	0.59
0.650	7.920	12.250	20.820	0.03	0.38	0.59
0.600	9.040	11.120	20.760	0.03	0.44	0.54
0.600	8.840	11.990	21.430	0.03	0.41	0.56
0.780	8.840	10.940	20.560	0.04	0.43	0.53
0.900	9.870	9.990	20.760	0.04	0.48	0.48
0.700	9.990	9.980	20.670	0.03	0.48	0.48
0.800	10.100	10.250	21.150	0.04	0.48	0.48
0.850	10.970	9.040	20.860	0.04	0.53	0.43
0.940	10.910	9.220	21.070	0.04	0.52	0.44
0.870	10.920	9.040	20.830	0.04	0.52	0.43
1.150	12.080	8.090	21.320	0.05	0.57	0.38
1.180	12.100	8.020	21.300	0.06	0.57	0.38
1.280	12.120	8.000	21.400	0.06	0.57	0.37
1.480	13.090	7.520	22.090	0.07	0.59	0.34
1.420	13.110	7.850	22.380	0.06	0.59	0.35
1.470	13.050	6.980	21.500	0.07	0.61	0.32
2.090	14.090	6.050	22.230	0.09	0.63	0.27

Continued on the following page...

WATER MASS (g)	ACETONE MASS (g)	BL MASS (g)	TOTAL MASS (g)	WATER w/w %	ACETONE w/w %	BL w/w%
2.070	14.080	6.100	22.250	0.09	0.63	0.27
1.970	14.020	6.260	22.250	0.09	0.63	0.28
2.893	15.080	5.080	23.053	0.13	0.65	0.22
3.250	14.970	5.000	23.220	0.14	0.64	0.22
2.940	14.980	5.100	23.020	0.13	0.65	0.22
4.870	15.980	3.840	24.690	0.20	0.65	0.16
4.270	15.970	4.200	24.440	0.17	0.65	0.17
4.873	16.410	4.010	25.293	0.19	0.65	0.16
7.060	16.954	2.990	27.004	0.26	0.63	0.11
7.270	17.350	2.970	27.590	0.26	0.63	0.11
6.610	16.870	3.040	26.520	0.25	0.64	0.11
10.140	17.910	2.140	30.190	0.34	0.59	0.07
12.840	18.250	1.970	33.060	0.39	0.55	0.06
10.890	18.330	2.000	31.220	0.35	0.59	0.06
18.560	19.130	1.000	38.690	0.48	0.49	0.03
17.430	18.990	1.100	37.520	0.46	0.51	0.03
17.080	19.060	1.014	37.154	0.46	0.51	0.03
9.340	11.930	0.930	22.200	0.42	0.54	0.04
7.720	11.910	1.130	20.760	0.37	0.57	0.05
8.510	12.090	1.040	21.640	0.39	0.56	0.05
9.930	9.650	0.860	20.440	0.49	0.47	0.04
9.860	9.620	0.850	20.330	0.48	0.47	0.04
10.090	9.990	0.720	20.800	0.49	0.48	0.03
12.120	8.770	0.760	21.650	0.56	0.41	0.04
13.440	8.330	0.880	22.650	0.59	0.37	0.04
12.840	8.270	0.670	21.780	0.59	0.38	0.03
13.790	6.400	0.290	20.480	0.67	0.31	0.01
13.900	6.470	0.270	20.640	0.67	0.31	0.01
13.910	5.930	0.220	20.060	0.69	0.30	0.01
15.910	4.100	0.480	20.490	0.78	0.20	0.02
16.550	4.000	0.210	20.760	0.80	0.19	0.01
16.160	4.130	0.250	20.540	0.79	0.20	0.01
18.680	1.860	0.240	20.780	0.90	0.09	0.01
19.260	2.100	0.220	21.580	0.89	0.10	0.01
18.860	2.230	0.230	21.320	0.88	0.10	0.01

Aspen Data

This part of [Appendix A](#) corresponds to [Section 4.2](#) in [Chapter 4](#). Here, the raw data from Aspen models is presented for each bridging liquid in-turn. Note, Aspen does not produce results in mass fractions, but mole fractions. The data was extracted and then converted into mass fractions. The values of molecular weight to do this can be found in [Table A.6](#).

Table A.6. Standard properties of solvents used at 1 atmosphere and 25 °C [76].

Solvent	Molecular Formula (-)	Molecular Weight (g mol ⁻¹)	Density (g cm ⁻³)
Acetone	C ₃ H ₆ O	58.079	0.7845
Chloroform	CHCl ₃	119.378	1.4788
Heptane	C ₇ H ₁₆	100.202	0.6795
MIBK	C ₆ H ₁₂ O	100.158	0.7965
<i>n</i> -Butyl acetate	C ₆ H ₁₂ O ₂	116.158	0.8825 ^a
Toluene	C ₇ H ₈	92.139	0.8668 ^a
Water	H ₂ O	18.015	0.9970

Table A.7. Raw data from Aspen for the phase envelope of chloroform ternary phase diagrams from UNIF-LL. Mass fractions were calculated from the molecular weight of each component.

Mole Fraction			Mass Fraction		
Water	Acetone	Chloroform	Water	Acetone	Chloroform
0.999	0.000	0.001	0.993	0.000	0.007
0.970	0.029	0.002	0.903	0.086	0.011
0.951	0.047	0.002	0.850	0.136	0.013
0.933	0.064	0.003	0.806	0.178	0.016
0.914	0.082	0.003	0.761	0.220	0.019
0.890	0.106	0.004	0.706	0.271	0.022
0.852	0.143	0.006	0.630	0.340	0.029
0.791	0.199	0.010	0.528	0.429	0.043
0.675	0.303	0.022	0.376	0.543	0.081
0.606	0.360	0.034	0.304	0.584	0.112
0.606	0.361	0.032	0.305	0.587	0.108
0.609	0.360	0.030	0.309	0.589	0.102
0.591	0.375	0.034	0.292	0.598	0.110
0.578	0.385	0.038	0.280	0.600	0.120
0.542	0.411	0.047	0.249	0.609	0.142
0.536	0.416	0.048	0.244	0.612	0.144
0.235	0.598	0.167	0.072	0.590	0.338
0.112	0.607	0.281	0.029	0.498	0.473
0.067	0.547	0.386	0.015	0.402	0.583
0.043	0.464	0.493	0.009	0.311	0.680
0.028	0.367	0.604	0.005	0.227	0.768
0.018	0.260	0.721	0.003	0.149	0.848
0.011	0.144	0.845	0.002	0.076	0.922

Table A.8. Raw data from Aspen for the tie-lines of the UNIF-LL chloroform prediction.

LEFT SIDE POINT (Mole Frac.)			RIGHT SIDE POINT (Mole Frac.)		
Water	Acetone	Chloroform	Water	Acetone	Chloroform
0.005	0.000	0.995	0.999	0.000	0.001
0.006	0.025	0.969	0.993	0.006	0.001
0.007	0.050	0.943	0.988	0.011	0.001
0.008	0.076	0.916	0.982	0.016	0.001
0.009	0.103	0.888	0.977	0.021	0.002
0.010	0.131	0.859	0.972	0.026	0.002
0.012	0.159	0.829	0.967	0.031	0.002
0.013	0.188	0.798	0.962	0.036	0.002
0.015	0.218	0.767	0.957	0.041	0.002
0.017	0.249	0.734	0.952	0.045	0.002
0.020	0.280	0.700	0.947	0.050	0.002
0.023	0.312	0.665	0.942	0.055	0.002
0.026	0.344	0.630	0.937	0.060	0.003
0.030	0.377	0.593	0.931	0.066	0.003
0.034	0.411	0.555	0.925	0.072	0.003
0.040	0.444	0.516	0.919	0.078	0.003
0.046	0.478	0.476	0.911	0.085	0.003
0.055	0.511	0.435	0.902	0.094	0.004
0.065	0.543	0.392	0.892	0.104	0.004
0.079	0.572	0.348	0.878	0.117	0.005
0.100	0.598	0.303	0.861	0.133	0.005
0.131	0.615	0.254	0.839	0.155	0.007
0.187	0.613	0.199	0.808	0.183	0.009
0.309	0.564	0.127	0.773	0.216	0.011

Table A.9. Processed data from Aspen for the tie-lines of the UNIF-LL chloroform prediction.

LEFT SIDE POINT (% w/w)			RIGHT SIDE POINT (% w/w)		
Water	Acetone	Chloroform	Water	Acetone	Chloroform
0.001	0.000	0.999	0.993	0.000	0.007
0.001	0.012	0.987	0.974	0.018	0.008
0.001	0.025	0.974	0.957	0.034	0.009
0.001	0.039	0.960	0.941	0.050	0.009
0.001	0.053	0.945	0.925	0.065	0.010
0.002	0.069	0.930	0.910	0.079	0.011
0.002	0.085	0.913	0.896	0.093	0.011
0.002	0.103	0.895	0.882	0.106	0.012
0.003	0.121	0.876	0.869	0.119	0.012
0.003	0.141	0.856	0.855	0.132	0.013
0.004	0.162	0.834	0.842	0.144	0.014
0.004	0.185	0.811	0.829	0.156	0.015
0.005	0.209	0.786	0.816	0.169	0.015
0.006	0.235	0.759	0.802	0.182	0.016
0.007	0.263	0.730	0.787	0.196	0.017
0.008	0.293	0.699	0.771	0.211	0.018
0.010	0.325	0.665	0.753	0.228	0.019
0.012	0.359	0.629	0.733	0.246	0.020
0.015	0.396	0.589	0.710	0.268	0.022
0.019	0.436	0.545	0.683	0.293	0.024
0.025	0.478	0.498	0.649	0.324	0.027
0.034	0.522	0.444	0.607	0.361	0.032
0.054	0.567	0.379	0.555	0.406	0.039
0.104	0.612	0.284	0.500	0.451	0.048

Table A.10. Raw data from Aspen for the phase envelope of heptane ternary phase diagrams from UNIFAC. Mass fractions were calculated from the molecular weight of each component.

Mole Fraction			Mass Fraction		
Water	Acetone	Heptane	Water	Acetone	Heptane
0.001	0.000	0.999	0.000	0.000	1.000
0.004	0.168	0.828	0.001	0.105	0.894
0.006	0.228	0.767	0.001	0.147	0.852
0.008	0.278	0.714	0.002	0.184	0.815
0.011	0.338	0.652	0.002	0.230	0.767
0.013	0.371	0.616	0.003	0.258	0.739
0.016	0.410	0.574	0.003	0.292	0.705
0.020	0.459	0.521	0.005	0.337	0.659
0.040	0.577	0.383	0.010	0.461	0.529
0.039	0.594	0.367	0.010	0.479	0.511
0.047	0.621	0.333	0.012	0.513	0.475
0.057	0.629	0.314	0.015	0.529	0.456
0.111	0.685	0.204	0.032	0.639	0.328
0.173	0.687	0.140	0.055	0.700	0.246
0.239	0.664	0.097	0.082	0.733	0.186
0.309	0.624	0.067	0.115	0.747	0.138
0.384	0.572	0.045	0.155	0.745	0.100
0.463	0.509	0.028	0.205	0.726	0.069
0.548	0.436	0.016	0.268	0.688	0.043
0.639	0.353	0.008	0.351	0.625	0.024
0.738	0.259	0.003	0.464	0.526	0.011
0.839	0.161	0.001	0.616	0.381	0.003
0.925	0.074	0.000	0.793	0.206	0.001

Table A.11. Raw data from Aspen for the tie-lines of the UNIFAC heptane prediction.

LEFT SIDE POINT (Mole Frac.)			RIGHT SIDE POINT (Mole Frac.)		
Water	Acetone	Heptane	Water	Acetone	Heptane
0.001	0.000	0.999	1.000	0.000	0.000
0.001	0.032	0.967	0.982	0.018	0.000
0.001	0.062	0.936	0.962	0.038	0.000
0.002	0.090	0.908	0.940	0.060	0.000
0.002	0.116	0.882	0.916	0.084	0.000
0.003	0.139	0.858	0.888	0.112	0.000
0.003	0.159	0.838	0.856	0.143	0.001
0.004	0.176	0.820	0.820	0.179	0.001
0.004	0.190	0.805	0.780	0.218	0.002
0.005	0.203	0.793	0.738	0.259	0.003
0.005	0.214	0.781	0.693	0.302	0.005
0.006	0.225	0.769	0.648	0.345	0.007
0.006	0.237	0.757	0.603	0.387	0.011
0.006	0.249	0.744	0.557	0.428	0.015
0.007	0.262	0.731	0.512	0.467	0.020
0.008	0.277	0.716	0.467	0.505	0.027
0.008	0.292	0.700	0.422	0.542	0.036
0.009	0.309	0.682	0.377	0.576	0.046
0.010	0.327	0.663	0.332	0.608	0.059
0.011	0.347	0.641	0.287	0.637	0.075
0.013	0.370	0.617	0.242	0.662	0.096
0.015	0.396	0.589	0.195	0.681	0.124
0.017	0.428	0.555	0.147	0.690	0.162
0.022	0.473	0.505	0.097	0.678	0.225

Table A.12. Processed data from Aspen for the tie-lines of the UNIFAC heptane prediction.

LEFT SIDE POINT (% w/w)			RIGHT SIDE POINT (% w/w)		
Water	Acetone	Heptane	Water	Acetone	Heptane
0.000	0.000	1.000	1.000	0.000	0.000
0.000	0.019	0.981	0.943	0.056	0.000
0.000	0.037	0.963	0.887	0.113	0.000
0.000	0.055	0.945	0.830	0.170	0.001
0.000	0.071	0.929	0.771	0.228	0.001
0.001	0.086	0.914	0.711	0.288	0.002
0.001	0.099	0.900	0.648	0.349	0.003
0.001	0.110	0.889	0.585	0.411	0.004
0.001	0.120	0.879	0.523	0.470	0.007
0.001	0.129	0.870	0.464	0.526	0.011
0.001	0.137	0.862	0.409	0.575	0.016
0.001	0.145	0.854	0.360	0.617	0.022
0.001	0.153	0.845	0.316	0.653	0.031
0.001	0.162	0.836	0.276	0.683	0.041
0.001	0.172	0.827	0.240	0.706	0.053
0.002	0.183	0.816	0.208	0.725	0.068
0.002	0.194	0.804	0.178	0.738	0.084
0.002	0.207	0.791	0.151	0.745	0.103
0.002	0.222	0.776	0.127	0.748	0.125
0.002	0.238	0.759	0.104	0.744	0.152
0.003	0.257	0.740	0.083	0.734	0.184
0.003	0.280	0.717	0.063	0.714	0.223
0.004	0.308	0.688	0.045	0.679	0.276
0.005	0.350	0.645	0.028	0.619	0.354

Table A.13. Raw data from Aspen for the phase envelope of MIBK ternary phase diagrams from UNIFAC. Mass fractions were calculated from the molecular weight of each component.

Mole Fraction			Mass Fraction		
Water	Acetone	MIBK	Water	Acetone	MIBK
0.087	0.000	0.913	0.017	0.000	0.983
0.109	0.220	0.671	0.024	0.156	0.820
0.122	0.299	0.579	0.028	0.224	0.748
0.154	0.417	0.429	0.040	0.346	0.614
0.173	0.458	0.369	0.047	0.399	0.554
0.246	0.521	0.233	0.077	0.521	0.402
0.278	0.524	0.198	0.091	0.550	0.359
0.335	0.510	0.155	0.118	0.578	0.304
0.353	0.511	0.136	0.128	0.597	0.275
0.349	0.513	0.138	0.126	0.598	0.276
0.369	0.503	0.127	0.137	0.601	0.262
0.375	0.500	0.125	0.140	0.601	0.259
0.403	0.483	0.114	0.155	0.601	0.244
0.447	0.456	0.097	0.182	0.599	0.219
0.489	0.428	0.083	0.210	0.592	0.198
0.545	0.389	0.066	0.251	0.578	0.170
0.604	0.344	0.052	0.301	0.554	0.144
0.663	0.297	0.040	0.360	0.520	0.120
0.724	0.247	0.030	0.430	0.473	0.097
0.783	0.196	0.021	0.510	0.412	0.077
0.838	0.147	0.015	0.600	0.340	0.060
0.887	0.103	0.011	0.694	0.259	0.047
0.928	0.064	0.008	0.788	0.175	0.037

Table A.14. Raw data from Aspen for the tie-lines of the UNIFAC MIBK prediction.

LEFT SIDE POINT (Mole Frac.)			RIGHT SIDE POINT (Mole Frac.)		
Water	Acetone	MIBK	Water	Acetone	MIBK
0.087	0.000	0.913	0.996	0.000	0.004
0.090	0.034	0.876	0.988	0.007	0.005
0.092	0.068	0.840	0.980	0.015	0.005
0.095	0.100	0.805	0.971	0.024	0.005
0.098	0.131	0.770	0.961	0.033	0.006
0.102	0.162	0.737	0.951	0.042	0.006
0.105	0.191	0.704	0.940	0.053	0.007
0.109	0.219	0.672	0.928	0.064	0.008
0.113	0.247	0.640	0.915	0.076	0.009
0.117	0.273	0.609	0.902	0.089	0.010
0.122	0.299	0.579	0.886	0.103	0.011
0.127	0.324	0.550	0.870	0.118	0.012
0.132	0.347	0.521	0.852	0.134	0.014
0.138	0.370	0.492	0.833	0.152	0.016
0.145	0.392	0.464	0.812	0.171	0.018
0.152	0.412	0.436	0.788	0.191	0.021
0.160	0.432	0.408	0.763	0.213	0.024
0.169	0.451	0.380	0.736	0.237	0.028
0.179	0.469	0.352	0.705	0.262	0.032
0.191	0.485	0.324	0.672	0.290	0.038
0.206	0.499	0.295	0.635	0.320	0.045
0.224	0.512	0.264	0.592	0.353	0.055
0.248	0.521	0.231	0.542	0.391	0.067
0.286	0.523	0.191	0.477	0.436	0.087

Table A.15. Processed data from Aspen for the tie-lines of the UNIFAC prediction.

LEFT SIDE POINT (% w/w)			RIGHT SIDE POINT (% w/w)		
Water	Acetone	MIBK	Water	Acetone	MIBK
0.017	0.000	0.983	0.977	0.000	0.023
0.018	0.022	0.961	0.952	0.023	0.025
0.019	0.044	0.938	0.927	0.047	0.026
0.019	0.066	0.915	0.901	0.071	0.028
0.020	0.088	0.891	0.874	0.096	0.030
0.022	0.110	0.868	0.847	0.122	0.032
0.023	0.133	0.844	0.818	0.148	0.034
0.024	0.155	0.821	0.788	0.175	0.037
0.025	0.178	0.797	0.758	0.203	0.040
0.027	0.201	0.772	0.726	0.231	0.043
0.028	0.224	0.748	0.694	0.259	0.047
0.030	0.247	0.723	0.660	0.288	0.051
0.032	0.270	0.698	0.626	0.318	0.056
0.034	0.293	0.673	0.591	0.347	0.062
0.036	0.317	0.647	0.555	0.376	0.068
0.039	0.341	0.620	0.519	0.405	0.075
0.042	0.365	0.593	0.482	0.434	0.084
0.045	0.389	0.566	0.445	0.462	0.093
0.049	0.414	0.537	0.407	0.489	0.104
0.054	0.440	0.507	0.369	0.514	0.117
0.060	0.466	0.474	0.331	0.538	0.131
0.067	0.493	0.440	0.291	0.560	0.149
0.077	0.523	0.400	0.249	0.579	0.172
0.094	0.556	0.350	0.202	0.594	0.204

Table A.16. Raw data from Aspen for the phase envelope of *n*-butyl acetate ternary phase diagrams from UNIQUAC. Mass fractions were calculated from the molecular weight of each component.

Mole Fraction			Mass Fraction		
Water	Acetone	NBA	Water	Acetone	NBA
0.074	0.000	0.926	0.012	0.000	0.988
0.089	0.125	0.786	0.016	0.073	0.911
0.118	0.295	0.587	0.024	0.196	0.780
0.135	0.361	0.504	0.030	0.256	0.714
0.155	0.416	0.430	0.036	0.314	0.650
0.177	0.459	0.364	0.044	0.369	0.586
0.202	0.491	0.307	0.054	0.421	0.526
0.230	0.513	0.256	0.065	0.468	0.467
0.264	0.525	0.211	0.080	0.510	0.410
0.302	0.527	0.172	0.097	0.546	0.357
0.369	0.514	0.117	0.133	0.596	0.272
0.386	0.504	0.111	0.142	0.596	0.262
0.440	0.474	0.087	0.174	0.604	0.222
0.509	0.430	0.061	0.222	0.606	0.172
0.569	0.387	0.044	0.271	0.593	0.136
0.627	0.342	0.032	0.324	0.570	0.106
0.683	0.295	0.022	0.385	0.535	0.080
0.738	0.247	0.015	0.453	0.488	0.059
0.790	0.200	0.010	0.528	0.430	0.042
0.839	0.154	0.006	0.610	0.361	0.029
0.884	0.112	0.004	0.697	0.284	0.020
0.925	0.073	0.002	0.788	0.199	0.013
0.961	0.037	0.001	0.881	0.110	0.009

Table A.17. Raw data from Aspen for the tie-lines of the UNIQUAC *n*-butyl acetate prediction.

LEFT SIDE POINT (Mole Frac.)			RIGHT SIDE POINT (Mole Frac.)		
Water	Acetone	NBA	Water	Acetone	NBA
0.074	0.000	0.926	0.999	0.000	0.001
0.078	0.034	0.888	0.990	0.009	0.001
0.082	0.067	0.851	0.980	0.019	0.001
0.085	0.100	0.815	0.970	0.029	0.001
0.089	0.131	0.780	0.959	0.039	0.002
0.094	0.162	0.745	0.948	0.050	0.002
0.098	0.191	0.711	0.936	0.062	0.002
0.103	0.220	0.677	0.923	0.074	0.002
0.108	0.248	0.644	0.910	0.087	0.003
0.114	0.275	0.612	0.896	0.101	0.003
0.119	0.301	0.580	0.881	0.115	0.004
0.126	0.326	0.548	0.865	0.131	0.005
0.132	0.351	0.517	0.847	0.147	0.006
0.139	0.374	0.487	0.829	0.164	0.007
0.147	0.397	0.456	0.809	0.183	0.008
0.156	0.418	0.426	0.788	0.202	0.010
0.165	0.438	0.396	0.765	0.223	0.012
0.176	0.458	0.366	0.740	0.245	0.015
0.188	0.476	0.336	0.712	0.270	0.018
0.202	0.492	0.306	0.682	0.296	0.022
0.219	0.506	0.274	0.648	0.324	0.028
0.240	0.518	0.242	0.608	0.356	0.035
0.268	0.526	0.206	0.561	0.393	0.046
0.312	0.525	0.163	0.496	0.439	0.065

Table A.18. Processed data from Aspen for the tie-lines of the UNIQUAC *n*-butyl acetate prediction.

LEFT SIDE POINT (% w/w)			RIGHT SIDE POINT (% w/w)		
Water	Acetone	NBA	Water	Acetone	NBA
0.012	0.000	0.988	0.995	0.000	0.005
0.013	0.019	0.968	0.965	0.029	0.006
0.014	0.037	0.948	0.936	0.057	0.007
0.015	0.057	0.928	0.906	0.086	0.008
0.016	0.076	0.908	0.876	0.115	0.009
0.017	0.096	0.887	0.845	0.144	0.010
0.019	0.116	0.865	0.815	0.174	0.012
0.020	0.137	0.843	0.784	0.203	0.013
0.021	0.158	0.821	0.752	0.232	0.015
0.023	0.179	0.798	0.721	0.262	0.018
0.025	0.201	0.774	0.689	0.291	0.020
0.027	0.223	0.750	0.657	0.320	0.024
0.029	0.246	0.725	0.624	0.349	0.027
0.031	0.269	0.700	0.591	0.377	0.032
0.034	0.293	0.674	0.558	0.406	0.037
0.037	0.317	0.646	0.524	0.433	0.043
0.040	0.342	0.618	0.490	0.460	0.050
0.044	0.368	0.588	0.455	0.487	0.058
0.048	0.394	0.557	0.420	0.512	0.068
0.054	0.422	0.524	0.383	0.536	0.081
0.061	0.451	0.489	0.346	0.558	0.096
0.069	0.482	0.449	0.307	0.579	0.115
0.081	0.515	0.403	0.264	0.596	0.141
0.102	0.554	0.344	0.212	0.607	0.181

Table A.19. Raw data from Aspen for the phase envelope of toluene ternary phase diagrams from UNIQUAC. Mass fractions were calculated from the molecular weight of each component.

Mole Fraction			Mass Fraction		
Water	Acetone	Toluene	Water	Acetone	Toluene
0.005	0.124	0.871	0.001	0.082	0.917
0.008	0.220	0.771	0.002	0.152	0.846
0.013	0.306	0.681	0.003	0.220	0.777
0.020	0.380	0.599	0.005	0.284	0.711
0.029	0.445	0.526	0.007	0.345	0.648
0.053	0.544	0.402	0.014	0.454	0.532
0.070	0.580	0.350	0.019	0.501	0.480
0.112	0.626	0.262	0.032	0.582	0.386
0.138	0.637	0.225	0.041	0.615	0.344
0.170	0.640	0.191	0.053	0.643	0.304
0.226	0.627	0.147	0.076	0.674	0.250
0.229	0.627	0.144	0.077	0.677	0.246
0.242	0.622	0.135	0.082	0.682	0.236
0.283	0.603	0.114	0.100	0.691	0.208
0.352	0.564	0.084	0.136	0.700	0.165
0.406	0.528	0.065	0.166	0.697	0.137
0.463	0.488	0.049	0.202	0.687	0.110
0.519	0.445	0.037	0.243	0.670	0.087
0.576	0.398	0.026	0.289	0.644	0.067
0.688	0.300	0.012	0.401	0.564	0.035
0.743	0.250	0.007	0.468	0.509	0.023
0.795	0.200	0.004	0.544	0.442	0.014
0.847	0.151	0.002	0.630	0.362	0.008
0.945	0.055	0.000	0.841	0.157	0.002

Table A.20. Raw data from Aspen for the tie-lines of the UNIQUAC toluene prediction.

LEFT SIDE POINT (Mole Frac.)			RIGHT SIDE POINT (Mole Frac.)		
Water	Acetone	Toluene	Water	Acetone	Toluene
0.002	0.000	0.998	1.000	0.000	0.000
0.003	0.036	0.961	0.984	0.015	0.000
0.003	0.072	0.925	0.969	0.031	0.000
0.004	0.107	0.889	0.953	0.047	0.000
0.005	0.141	0.853	0.937	0.063	0.000
0.006	0.175	0.818	0.920	0.079	0.001
0.008	0.208	0.784	0.903	0.096	0.001
0.009	0.241	0.750	0.885	0.114	0.001
0.011	0.273	0.716	0.867	0.132	0.002
0.013	0.304	0.682	0.848	0.150	0.002
0.016	0.335	0.649	0.828	0.169	0.003
0.019	0.365	0.617	0.807	0.189	0.004
0.022	0.394	0.584	0.785	0.210	0.005
0.026	0.422	0.553	0.762	0.232	0.006
0.030	0.449	0.521	0.738	0.254	0.007
0.035	0.476	0.489	0.713	0.278	0.009
0.041	0.502	0.458	0.685	0.303	0.012
0.047	0.526	0.426	0.656	0.329	0.015
0.056	0.550	0.395	0.625	0.357	0.019
0.065	0.572	0.363	0.590	0.386	0.024
0.077	0.593	0.330	0.552	0.418	0.030
0.092	0.611	0.296	0.509	0.452	0.039
0.113	0.627	0.260	0.460	0.490	0.050
0.143	0.638	0.219	0.398	0.534	0.068

Table A.21. Processed data from Aspen for the tie-lines of the UNIQUAC toluene prediction.

LEFT SIDE POINT (% w/w)			RIGHT SIDE POINT (% w/w)		
Water	Acetone	Toluene	Water	Acetone	Toluene
0.000	0.000	1.000	0.999	0.000	0.001
0.001	0.023	0.976	0.951	0.048	0.001
0.001	0.047	0.953	0.906	0.093	0.001
0.001	0.070	0.929	0.862	0.136	0.002
0.001	0.094	0.905	0.820	0.178	0.002
0.001	0.119	0.880	0.780	0.217	0.003
0.002	0.143	0.855	0.741	0.255	0.004
0.002	0.168	0.830	0.704	0.292	0.005
0.002	0.193	0.804	0.667	0.327	0.006
0.003	0.219	0.778	0.631	0.361	0.008
0.004	0.244	0.752	0.596	0.394	0.010
0.004	0.270	0.725	0.562	0.425	0.013
0.005	0.296	0.698	0.528	0.456	0.016
0.006	0.323	0.671	0.495	0.485	0.019
0.007	0.350	0.643	0.463	0.514	0.024
0.009	0.377	0.615	0.430	0.541	0.029
0.010	0.404	0.586	0.398	0.567	0.035
0.012	0.432	0.556	0.366	0.591	0.043
0.014	0.461	0.525	0.334	0.615	0.051
0.017	0.490	0.493	0.302	0.636	0.062
0.021	0.520	0.459	0.269	0.656	0.075
0.026	0.551	0.423	0.235	0.673	0.091
0.033	0.584	0.384	0.200	0.688	0.112
0.043	0.620	0.337	0.161	0.698	0.141

TBSR Calculation

For more accurate calculation of the composition of both immiscible phases, a higher number of tie-lines was required. For each tie-line, the compositions at both the start and end point were known, as provided within Aspen. The change in height and width between the first two tie-lines was evaluated. The difference was divided by twenty and this value was added to the first tie-line values. This produced an additional tie-line. The process was repeated for each subsequent twentieth, to produce a further nineteen tie-lines. This process was repeated for each pair of adjacent tie-lines, up to the twenty-third and twenty-fourth tie-line. It should be noted that the twenty-fifth tie-line produced within Aspen was always along the X component axis. To improve accuracy, this tie-line was discarded. As such, the methods discussed here produced a total of four-hundred and eighty tie-lines. The equation of the line for each tie-line was calculated. These equations are required later.

An Exemplar TBSR Calculation

In this section, an exemplar calculation of the True BSR is presented. This calculation shows answers to 2 decimal places only, for simplicity. Common properties of the species involved are given in Table A.22.

Table A.22. Standard properties of solvents used at 1 atmosphere and 25 °C [76].

Chemical Species	Molecular Formula	Molecular Weight (g mol ⁻¹)	Density (g cm ⁻³)
Acetone	C ₃ H ₆ O	58.079	0.7845
Chloroform	CHCl ₃	119.378	1.4788
Water	H ₂ O	18.015	0.9970

4.3 g of a solid active pharmaceutical ingredient is dissolved in 60 g of acetone, before the solution is added to 140 g of water. 18 ml of bridging liquid (chloroform) is then added to agglomerate the particles.

BSR

$$= \frac{\text{volume of bridging liquid}}{\text{volume of solid}} = \frac{18}{4.3} = 4.19$$

Equation A.1

The following calculations are used in the calculation of the True BSR.

$$\text{Acetone Mass Fraction} = \frac{60}{60 + 140 + \frac{18}{1.48}} \sim 26.5 \% \quad \text{Equation A.2}$$

$$\text{Water Mass Fraction} = \frac{140}{60 + 140 + \frac{18}{1.48}} \sim 61.8 \% \quad \text{Equation A.3}$$

$$\text{Chloroform Mass Fraction} = \frac{\frac{18}{1.48}}{60 + 140 + \frac{18}{1.48}} \sim 11.7 \% \quad \text{Equation A.4}$$

Next, identify the closest tie-line to the agglomeration system (Figure A.1) and determine the co-ordinates of the tie-line start and end point.

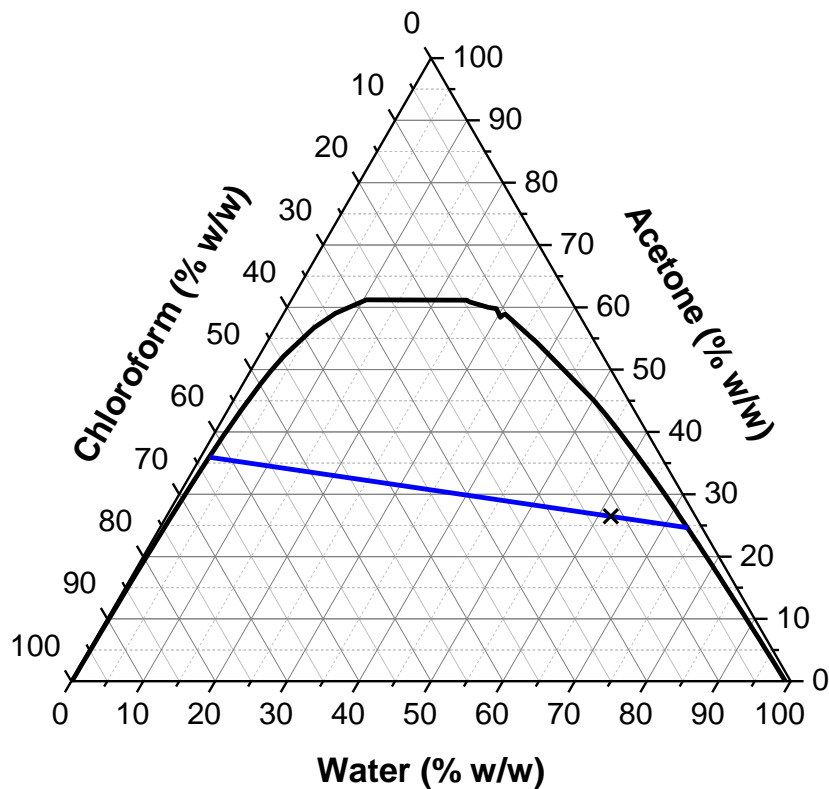


Figure A.1. An example Aspen ternary phase diagram plotted in Origin Pro. The blue line indicates the boundary between miscible (above) and immiscible (below) regions. Dashed lines show the tie-lines of the system.

These are given as:

$$x_1 = 0.733 ; y_1 = 0.246 \quad \text{Equation A.5}$$

$$x_2 = 0.011 ; y_2 = 0.359 \quad \text{Equation A.6}$$

From the co-ordinates, the equation of the line for the selected tie-line could be calculated:

$$m = \frac{0.246 - 0.359}{0.733 - 0.011} = -0.157 \quad \text{Equation A.7}$$

$$y = -0.157 x + 0.361 \quad \text{Equation A.8}$$

If the mass fraction of water (**Equation A.3**) is substituted into **Equation A.8**, the answer calculated is equal to the mass fraction of acetone (**Equation A.2**). The total length of the tie-line was calculated according to Pythagoras Theorem, using the co-ordinates specified in **Equation A.6**:

$$\text{Distance} = \sqrt{(0.733 - 0.011)^2 + (0.246 - 0.359)^2} = 0.731 \quad \text{Equation A.9}$$

The location of the system of interest along the tie-line could also be calculated by evaluating the distance between its co-ordinates and those of **Equation A.6**:

$$\text{Distance} = \sqrt{(0.618 - 0.011)^2 + (0.265 - 0.359)^2} = 0.614 \quad \text{Equation A.10}$$

Through the inverse lever rule, the mass fraction of the bridging liquid poor phase is initially given and, thus, the bridging liquid rich phase:

$$\text{Mass Fraction of BL poor} = \frac{0.614}{0.731} \sim 0.86 \quad \text{Equation A.11}$$

$$\text{Mass Fraction of BL rich} = 1 - \left(\frac{0.614}{0.731}\right) \sim 0.14 \quad \text{Equation A.12}$$

Resultantly, the masses of each phase are then calculated:

$$\text{Mass of BL poor} = 0.86 \times 226.6 = 194.88 \text{ g} \quad \text{Equation A.13}$$

$$\text{Mass of BL rich} = 0.14 \times 226.6 = 31.72 \text{ g} \quad \text{Equation A.14}$$

As the tie-line co-ordinates provide the relative compositions of each phase (**Equation A.5** and **Equation A.6**), the masses of each component within each phase could be calculated. If the bridging liquid poor phase is considered initially:

$$\text{Acetone Mass} = 194.88 \times 0.246 = 47.94 \text{ g} \quad \text{Equation A.15}$$

$$\text{Water Mass} = 194.88 \times 0.733 = 142.85 \text{ g} \quad \text{Equation A.16}$$

$$\text{Chloroform Mass} = 194.88 \times 0.021 = 3.91 \text{ g} \quad \text{Equation A.17}$$

And the chloroform rich phase is calculated as containing:

$$\text{Acetone Mass} = 31.72 \times 0.359 = 11.39 \text{ g} \quad \text{Equation A.18}$$

$$\text{Water Mass} = 31.72 \times 0.011 = 0.35 \text{ g} \quad \text{Equation A.19}$$

$$\text{Chloroform Mass} = 31.72 \times 0.021 = 19.95 \text{ g} \quad \text{Equation A.20}$$

To check the accuracy, a mass balance across both immiscible phases can be performed, and the error in calculations evaluated.

$$\text{Acetone Mass Balance: } 47.94 \text{ g} + 11.39 \text{ g} = 59.33 \text{ g} \quad \text{Equation A.21}$$

$$\text{Water Mass Balance: } 142.85 \text{ g} + 0.35 \text{ g} = 143.10 \text{ g} \quad \text{Equation A.22}$$

$$\text{Chloroform Mass Balance: } 3.90 \text{ g} + 19.95 \text{ g} = 23.85 \text{ g} \quad \text{Equation A.23}$$

Note that the chloroform mass equates to 16.11 ml approximately. The errors are given as approximately 1.2 %, 2.2 % and 0.7 % for acetone, water and chloroform respectively. As the TBSR is defined as the total volume of the bridging liquid rich phase, this can then be calculated:

$$TBSR = \frac{\left(\frac{11.39}{0.78}\right) + \left(\frac{0.35}{1}\right) + \left(\frac{19.95}{1.48}\right)}{4.3} = 6.61 \quad \text{Equation A.24}$$

If these calculations are repeated, a BSR vs TBSR graph can be yielded for the system in question. From this, the graph can be used to calculate the bridging liquid volume required, for any desired TBSR. In this example:

$$TBSR = 0.5 ; BSR = 0.9 \quad \text{Equation A.25}$$

$$\text{Volume Required} = 0.9 \times 4.3 = 3.87 \text{ ml} \quad \text{Equation A.26}$$

Appendix B. Validation of the TBSR

Common Properties of Agglomerates

This section lists the common size properties of the agglomerates yielded from TBSR validation experiments. Here, all values are calculated from the mean of a minimum of three repeats.

Table B.1. A variety of different parameters describing the agglomerate profile of salicylic acid-bridging liquid experiments, with a 90 % w/w water and 10 % w/w bulk solution.

Bulk Solution Composition	TBSR	Parameter (μm)					
		D10	D50	D90	Span	D32	D43
Butyl Acetate	0.025	1702	5177	6653	0.96	6302	6622
	0.050	1700	5675	7231	0.97	6842	7102
	0.075	2001	5590	7078	0.98	6638	6919
	0.100	2830	5744	7028	0.73	6595	6842
	0.125	4094	6797	7501	0.50	7785	8235
	0.150	4050	6623	7482	0.51	7721	8165
Chloroform	0.025	600	4629	6943	1.37	7134	7900
	0.050	850	5021	6956	1.22	7026	7701
	0.075	5423	7181	8400	0.41	8420	8861
	0.100	5427	7089	7633	0.31	7913	8198
	0.125	5431	8263	10104	0.57	9402	9796
	0.150	7736	8730	10299	0.29	9655	9974
MIBK	0.025	698	3928	6112	1.38	6800	7870
	0.050	835	4566	6955	1.34	7756	8713
	0.075	984	4661	6965	1.28	7441	8312
	0.100	834	4779	7078	1.33	8566	9510
	0.125	697	4211	8264	1.80	8664	9619
	0.150	698	5173	9182	1.64	8905	9769

Table B.2. A variety of different parameters describing the agglomerate profile of salicylic acid-chloroform experiments, with variations in bulk solution composition.

Bulk Solution Composition	TBSR	Parameter (μm)					
		D10	D50	D90	Span	D32	D43
95 % W, 5 % A	0.050	600	2782	6943	2.28	8765	9850
	0.100	502	4788	7110	1.38	7634	8399
	0.150	500	5624	9379	1.58	8957	9730
90 % W, 10 % A	0.025	600	4629	6943	1.37	7134	7900
	0.050	850	5021	6956	1.22	7026	7701
	0.075	5423	7181	8400	0.41	8420	8861
	0.100	5427	7089	7633	0.31	7913	8198
	0.125	5431	8263	10104	0.57	9402	9796
	0.150	7736	8730	10299	0.29	9655	9974
85 % W, 15 % A	0.025	-	2424	5110	-	6047	6653
	0.050	-	4959	9533	-	9318	10129
	0.075	-	6260	10202	-	9928	10423
	0.100	301	6608	10316	1.52	10022	10502
	0.125	712	7587	10512	1.13	10210	10610
	0.150	1693	8310	10685	1.08	10545	10853

Agglomerate Size Distributions

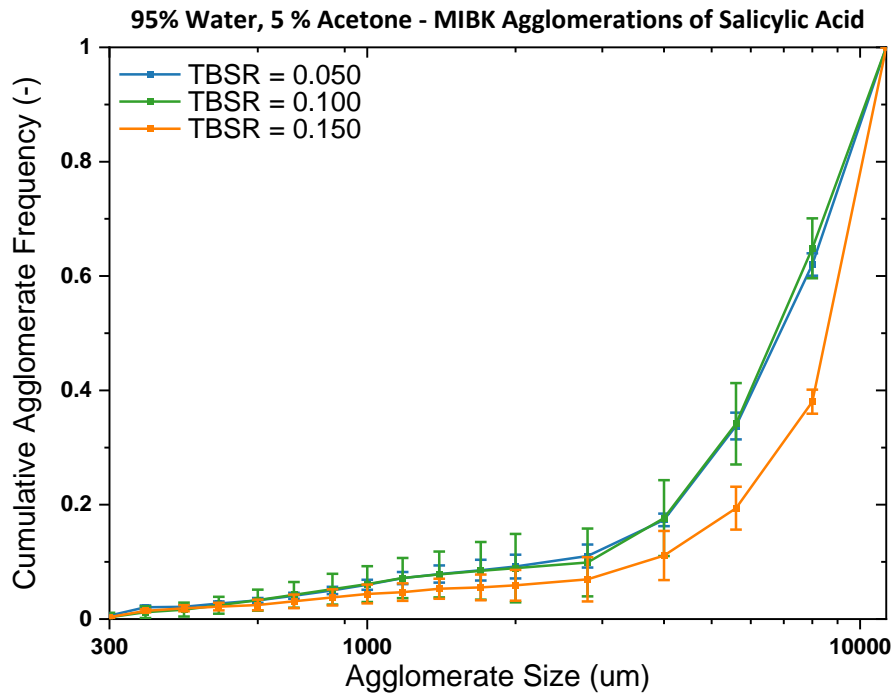


Figure A.1. Agglomerate size distribution for salicylic acid-MIBK systems with an initial bulk solution of 95 % w/w water and 5 % w/w acetone. Error bars represent standard error of a least three repeats.

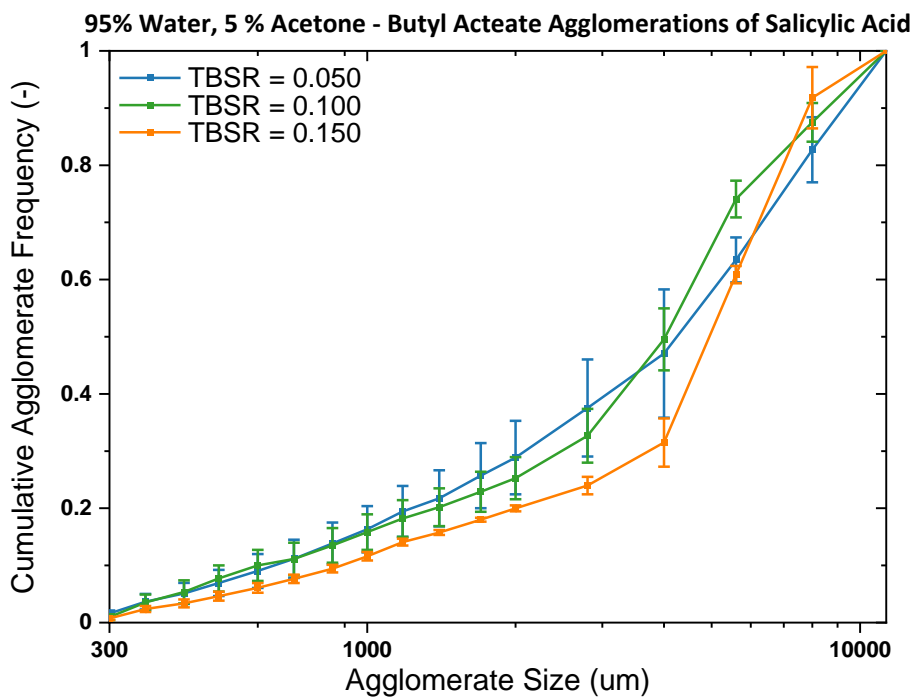


Figure A.2. Agglomerate size distribution for salicylic acid-butyl acetate systems with an initial bulk solution of 95 % w/w water and 5 % w/w acetone. Error bars represent standard error of a least three repeats.

Appendix C. Kinetic Studies of Paracetamol

TBSR Influence on Agglomerate Properties

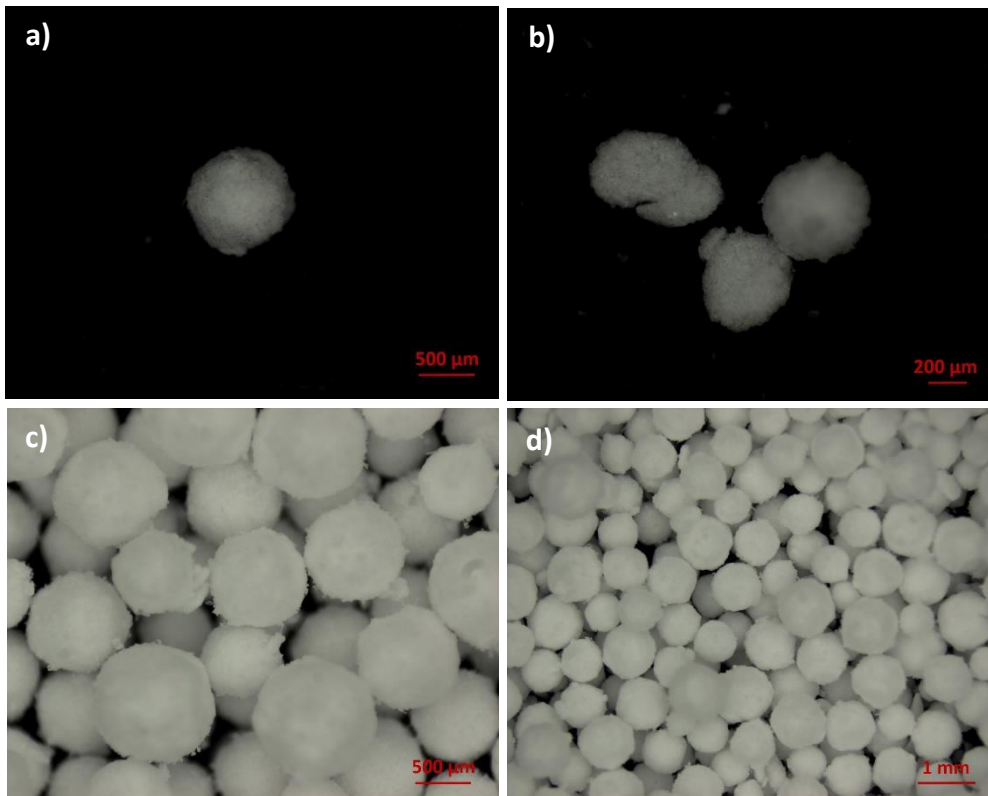


Figure C.1. Agglomerates at 56 minutes after bridging liquid addition (TBSR = 0.9) with a) and b) isolated from the reactor and c) and d) filtered and dried.

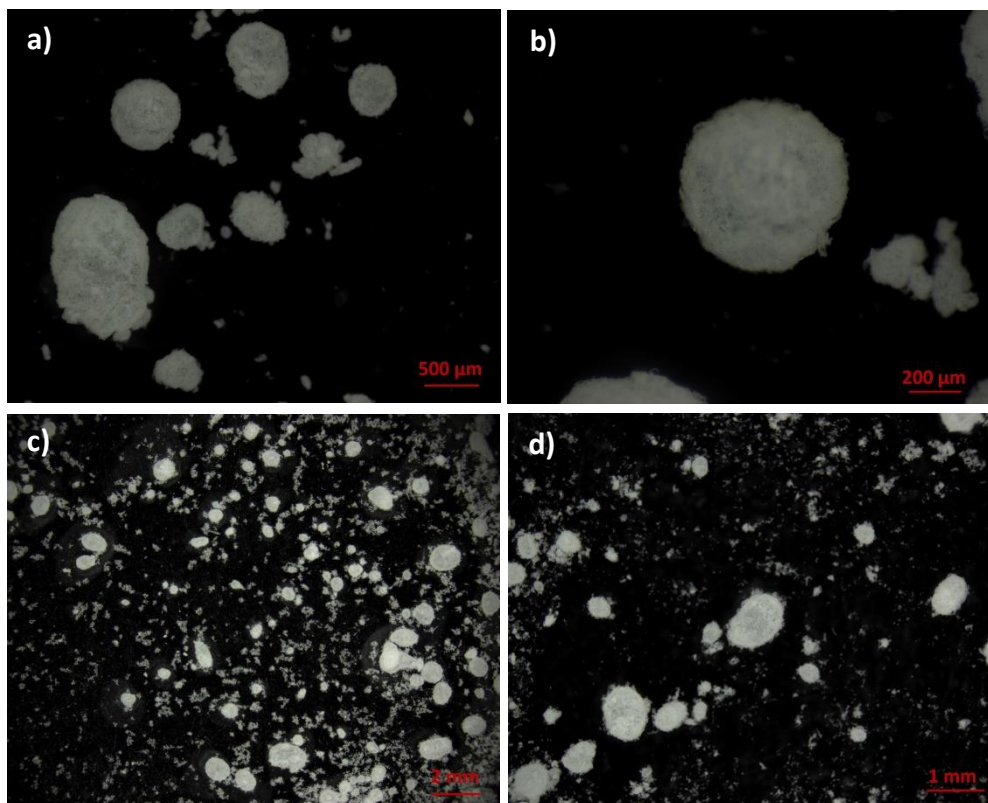


Figure C.2. Agglomerates at 11 minutes after bridging liquid addition (TBSR = 4), all sampled from the reactor.

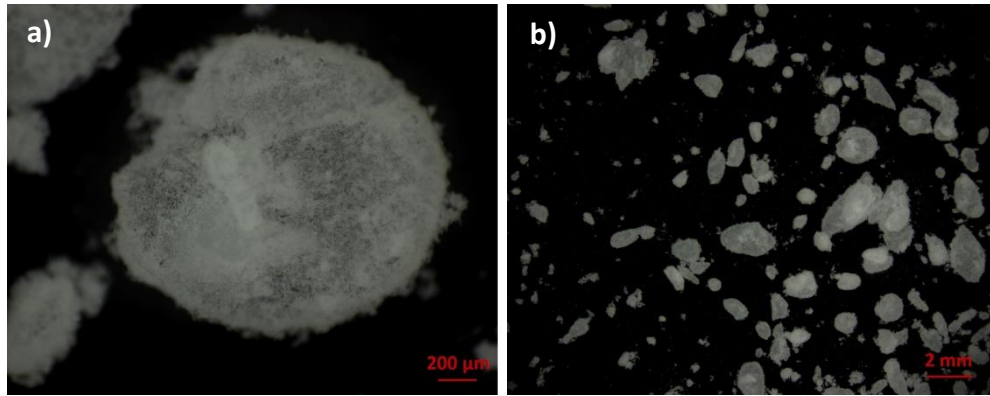


Figure C.3. Agglomerates at 3 minutes after bridging liquid addition (TBSR = 6), all sampled from the reactor.

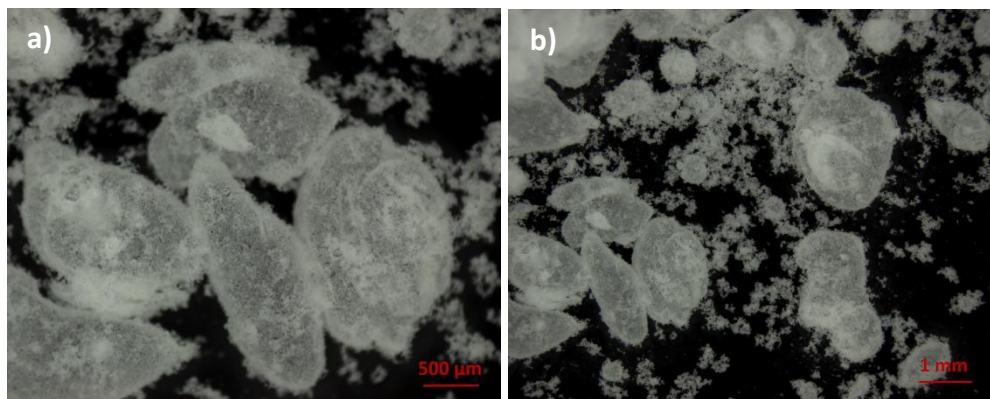


Figure C.4. Agglomerates at 2 minutes after bridging liquid addition (TBSR = 8), all sampled from the reactor.

Table C.1. Summary of the time to paste in minutes, for different TBSR values and different solid loading percentages. Standard deviations are given in brackets

TBSR Value (-)	Solid Loading (% w/w)		
	1 % (SD)	5 % (SD)	9 % (SD)
0.20	-	-	-
0.50	-	-	-
0.70	-	-	-
0.75	-	-	-
0.80	-	-	-
0.90	68.33 (3.21)	74.83 (4.80)	96.00 (4.36)
1.00	57.00 (1.73)	59.83 (4.37)	76.00 (2.52)
1.50	49.00 (3.61)	38.67 (3.21)	35.67 (0.58)
2.00	31.33 (3.69)	26.50 (1.32)	20.67 (1.15)
2.50	25.83 (0.29)	19.17 (1.25)	13.33 (1.53)
3.00	20.50 (2.29)	15.33 (1.15)	10.67 (2.08)
4.00	-	11.00 (0.50)	-
6.00	11.67 (1.15)	3.00	0.50
8.00	6.00 (0.50)	2.00	-

Agglomerate Structure Development

Agglomerate structure development was studied at TBSR = 0.75 with 5 % w/w solid loading. Samples at 10 mins, 30 mins, 50 mins, 70 mins and 90 mins are shown here, whilst remaining data is shown in [Section 6.2.4](#).

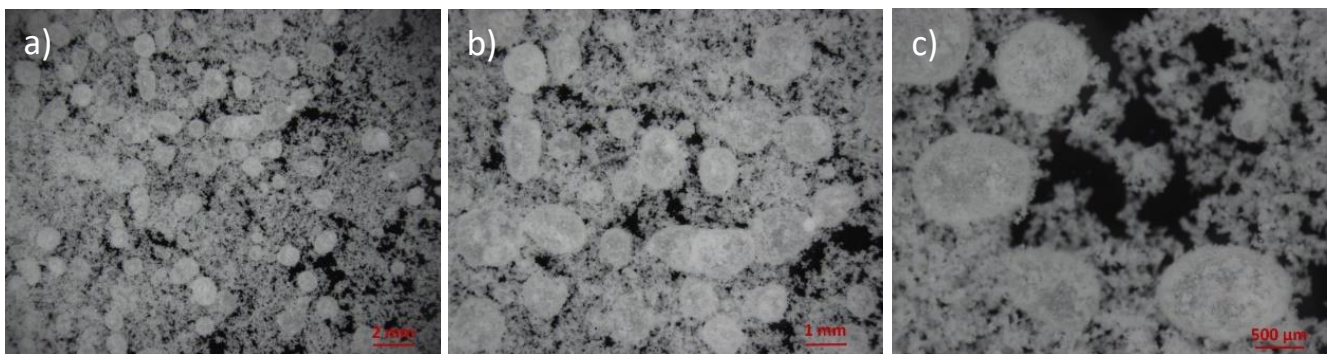


Figure C.5. Observations of spherical agglomerates, nuclei and paracetamol flocs formed 10 minutes after bridging liquid addition.

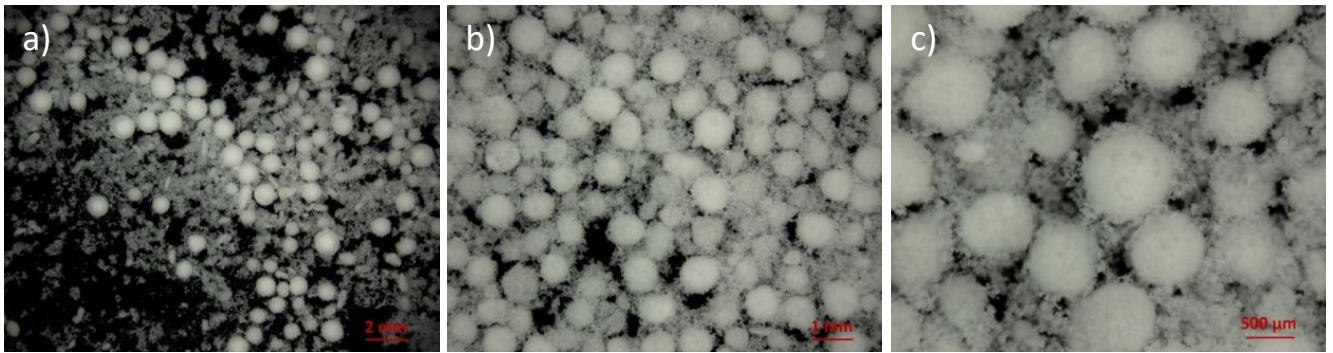


Figure C.6. Observations of spherical agglomerates, nuclei and paracetamol flocs formed 30 minutes after bridging liquid addition.

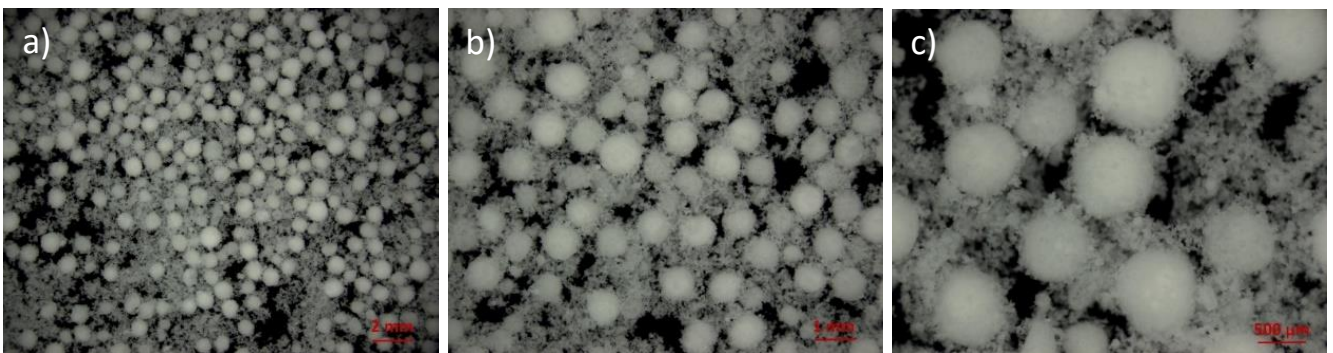


Figure C.7. Observations of spherical agglomerates, nuclei and paracetamol flocs formed 50 minutes after bridging liquid addition.

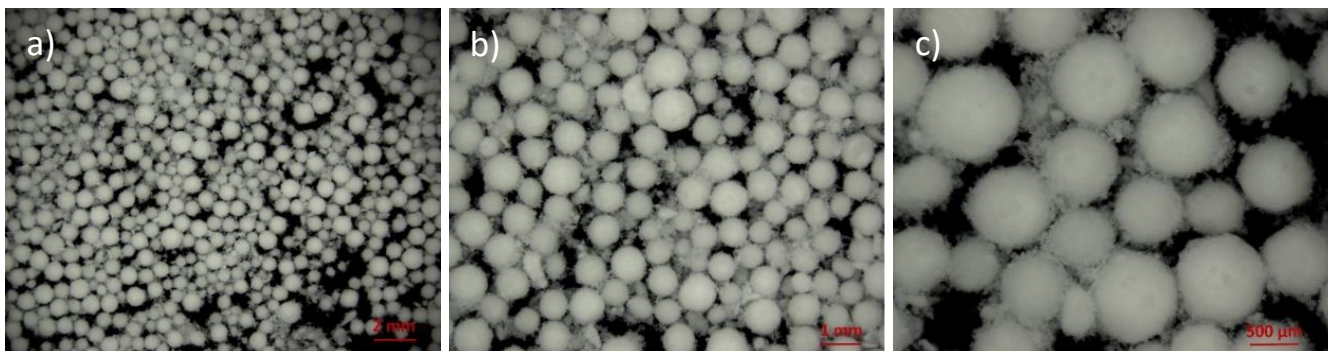


Figure C.8. Observations of spherical agglomerates, nuclei and paracetamol flocs formed 70 minutes after bridging liquid addition.

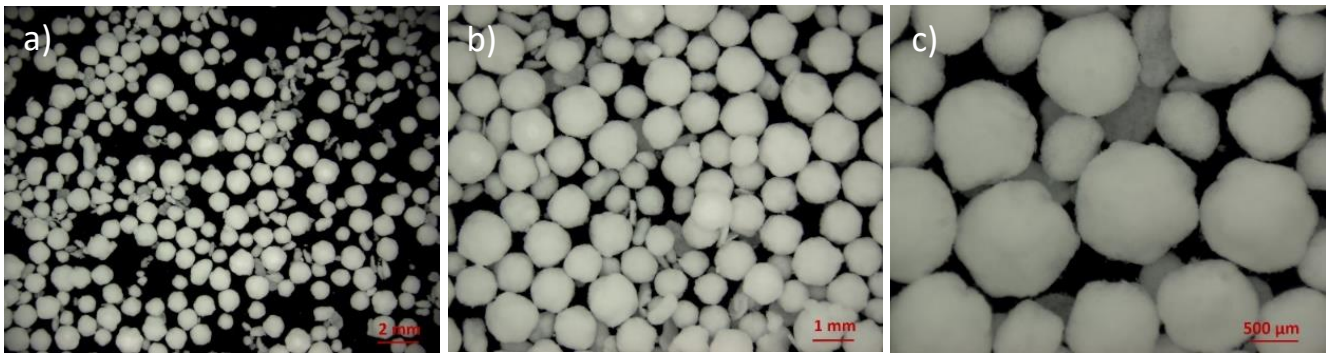


Figure C.9. Observations of spherical agglomerates, nuclei and paracetamol flocs formed 90 minutes after bridging liquid addition.